Tarr, David (2012) *Imaging the effects of acute hyperglycaemia on early ischaemic injury using MRI in an experimental stroke model.* PhD thesis.

http://theses.gla.ac.uk/3757/

Copyright and moral rights for this thesis are retained by the author

A copy can be downloaded for personal non-commercial research or study, without prior permission or charge

This thesis cannot be reproduced or quoted extensively from without first obtaining permission in writing from the Author

The content must not be changed in any way or sold commercially in any format or medium without the formal permission of the Author

When referring to this work, full bibliographic details including the author, title, awarding institution and date of the thesis must be given

Glasgow Theses Service
http://theses.gla.ac.uk/
theses@gla.ac.uk

Imaging the effects of acute hyperglycaemia on early ischaemic injury using MRI in an experimental stroke model.

David Tarr

BSc (Hons)

Submitted in fulfilment of the requirements for the degree of Doctor of Philosophy to the Institute of Neuroscience and Psychology, College of Medical, Veterinary and Life Sciences, University of Glasgow

August, 2012

Abstract

In the UK, stroke is the third most common cause of death after heart disease and cancer. Importantly, most strokes are not fatal meaning stroke is the leading cause of adult disability, with one third of survivors still functionally dependent after one year.

Post stroke hyperglycaemia (PSH) predicts poor outcome independent of age, stroke type or severity and occurs in over 60% of patients without a diagnosis of diabetes and in more than 90% of diabetic patients. Around 56% of hyperglycaemic acute stroke patients are subsequently diagnosed with insulin resistance, manifesting as impaired glucose tolerance, impaired fasting glucose or the "metabolic syndrome." Clinical guidelines recommend routine blood glucose monitoring, and intervention with insulin for hyperglycaemia. However, there is currently no clinical evidence of benefit from insulin use, and recent findings raise concerns about the safety of insulin use in predominantly non-diabetic acute stroke populations. Hyperglycaemia in animal models of cerebral ischaemia is associated with increased infarct size. However, a recent systematic review highlighted uncertainties about the relevance of many previously published preclinical studies to the typical clinical picture of PSH with respect to whether clinically relevant elevations in blood glucose exacerbate ischaemic brain damage in models other than those of type I diabetes, or whether responses are different in animals with and without features of metabolic syndrome.

The aim of this thesis was to investigate the differential effects of clinically relevant hyperglycaemia on the acute evolution of damage in animals with and without features of the metabolic syndrome and to investigate the potential mechanistic role of oxidative stress in glucose mediated ischaemic damage. I hypothesised that hyperglycaemia would exacerbate acute lesion evolution and final infarct volume in animals with and without features of the metabolic syndrome and that oxidative stress mechanisms would be involved.

Developing suitable animal models for investigating post stroke hyperglycaemia and metabolic syndrome

The first aim of this thesis was to develop a series of animal models for the investigation of clinically relevant PSH, metabolic syndrome in the presence and absence of PSH, and an appropriate focal cerebral ischaemia model. A previously described model of metabolic syndrome using the spontaneously hypertensive stroke-prone rat (SHRSP) fed on a 60% fructose diet for two weeks was set up in the laboratory and glucose tolerance, adiposity, plasma insulin, plasma triglycerides, cholesterol were measured and compared to the SHRSP reference strain, the Wistar-Kyoto (WKY). Fructose fed-SHRSP rats exhibited glucose intolerance, hypertriglyceridaemia, hyperinsulinaemia, increase adiposity and reduced HDL cholesterol compared to the WKY controls. This suitably modelled the features of the metabolic syndrome. Clinically relevant levels of PSH were achieved using a bolus intraperitoneal injection of 15% glucose (10ml/kg) 10 minutes prior to permanent middle cerebral artery occlusion (MCAO). Two methods of MCAO were compared; intraluminal filament (ILF) model and a distal diathermy MCAO model. The ILF method produced expansive lesions incorporating the majority of the ipsilateral hemisphere whereas the distal diathermy occlusion produced smaller cortical infarcts which were shown to produce a large volume of penumbra. The diathermy model was selected for all future experiments.

Investigating the effects of hyperglycaemia on acute lesion growth after focal cerebral ischaemia in rats with and without components of the metabolic syndrome

The second aim of this thesis was to determine the effects of hyperglycaemia on acute ischaemic lesion evolution and infarct volume in rats with and without features of the metabolic syndrome. Hyperglycaemia was induced in WKY or fructose-fed SHRSP rats 10 minutes prior to permanent MCAO. Magnetic resonance imaging (MRI) was used to quantify the expansion of the lesion using ADC maps calculated from diffusion weighted imaging (DWI) carried out over the first 4 hours after MCAO. Acute hyperglycaemia, at clinically relevant levels, exacerbated early ischaemic damage in both normal and metabolic syndrome rats. Hyperglycaemia worsened infarct volume at 24h in normal but not

metabolic syndrome rats. These data suggest that management of hyperglycaemia may be most beneficial in the absence of an underlying dysglycaemia. Using a marker of oxidative stress to probe the tissue sections suggested that perhaps hyperglycaemic effects were mediated through oxidative stress mechanisms.

Investigation of oxidative stress mechanisms in hyperglycaemia-dependant ischaemic damage.

Based on the potential involvement of oxidative stress mechanisms in hyperglycaemia-associated ischaemic damage this was investigated in a proof of concept study using pre-treatment with a SOD/catalase mimetic, EUK-134. The rationale for this study was based on the involvement of increased superoxide production in chronic hyperglycaemia and diabetic complications. Sprague-Dawley rats received the same dose of glucose previously used 10 minutes prior to MCAO by distal diathermy. EUK-134 (2.5mg/kg) or vehicle (saline) was administered 20 minutes prior to MCAO. Infarct volume, calculated from RARE T2-weighted MR images and neurological scoring was measured 24 hours post MCAO. Arterial superoxide levels were measured along with the lipid peroxidation marker malondialdehyde in cerebral tissue. Hyperglycaemia increased infarct volume although no effect of high blood glucose on tissue lipid peroxidation was observed. EUK-134 failed to reduce infarct volume. EUK-134 reduced lipid peroxidation in ipsilateral cortex of normoglycaemic rats but not in hyperglycaemic rats. Thus, hyperglycaemia associated damage was not reduced by attenuating oxidative stress.

Generating a threshold for quantitative T2 maps

Using the data generated in the previous Chapter a study was carried out to determine if improvements could be made in the analysis of MRI data in pre-clinical rat studies. RARE T2-weighted images, where T_2 relaxation time denotes contrast, have been used for infarct quantification 24 hours post MCAO. Generating a lesion volume from these images requires manual tracing of the visually defined infarct from the images. A degree of error is associated with this methodology either as inter-investigator reproducibility or in repeats conducted by the same investigator. The RARE T_2 images are not quantifiable as arbitrary

values denote contrast and this prevents direct comparison of T_2 relaxation times for a particular structure between subjects. Using a MSME T2 sequence, quantitative T_2 maps can be generated which calculate absolute T_2 relaxation times for each voxel.

Using quantitative maps an attempt was made to establish a threshold to discriminate between normal and ischaemically damaged tissue in animals that had undergone MCAO using the distal diathermy model. This threshold aimed to minimise inter- or intra-investigator error. A T2 threshold of abnormality for the quantitative T_2 maps was established from the RARE T2 weighted images. Tissue that had a T_2 relaxation time of 76 ms or more was deemed to be infarct according to the derived threshold. The suitability of the threshold was then assessed in a separate cohort and was found to produce similar infarct volumes to the manual delineation of RARE T_2-weighted images. The 76ms threshold was also applied to animals that had undergone MCAO using the intraluminal filament model. However, the calculated threshold was not suitable for the intraluminal filament model due to interferences from cerebrospinal fluid signal. A more selective method for determining infarct volume in animals subjected to intraluminal filament MCAO needs to be established.

Conclusions

The studies presented in this thesis highlight that acute hyperglycaemia increases the rate of ischaemic lesion growth and final infarct volume in rats lacking insulin resistance and associated cardiovascular co-morbidities. The mechanism by which hyperglycaemia exacerbates ischaemic damage remains elusive. Oxidative stress may be involved, although from the investigations conducted in this thesis, it is not a primary mechanism of hyperglycaemia associated ischaemic damage following permanent MCAO.

Table of Contents

Table of Figures

List of Tables

Acknowledgements

Firstly, I would like to thank my principal supervisor, Dr Debbie Dewar for her encouragement and guidance over the past 4 years. I'd also like to thank Professor Mhairi Macrae, for her invaluable input and support.

Secondly I'd like to say thank you to all the staff at the Wellcome Surgical Institute; Lindsay Gallagher, for experimental assistance and for passing on her surgical skills; Linda Carberry and George Graham for their help with many different experiments; Dr Chris McCabe for MRI support and Jim Mullin, for his technical and practical input.

I'd also like to thank Dr Delyth Graham from the BHF Glasgow Cardiovascular Research Centre for showing me how to perform the tail cuff method and the glucose tolerance test and Dr Lorraine Work for her help with lipid peroxidation assays.

A big thank you to all my fellow students at the Wellcome Surgical Institute for keeping spirits high and making this such an enjoyable experience; Craig, Emma R, Adriana and especially to Lisa, Emma B, Ashleigh and Emma M for the invention of Disco Friday.

Lastly I would like to extend my thanks to my parents, Jane and Victor, who have provided unrivalled support throughout my life at university. They have always been there for me through good times and bad, believing in me and supporting me to achieve my goals. This thesis is dedicated to them.

Declaration

I declare that, except where explicit reference is made to the contribution of others, this dissertation is the result of my own work and has not been submitted for any other degree at the University of Glasgow or any other institution

David Tarr

List of Abbreviations

^{1}H	hydrogen nuclei
7T	seven tesla
ADC	apparent diffusion coefficient
AMPA	alpha-amino-3-hydroxy-5-methyl-4-isoxazolepropionate
ANOVA	analysis of variance
APAF1	apoptosis-activating factor
ASL	arterial spin labelling
ATLANTIS	Alteplase Thrombolysis for Acute Noninterventional Therapy in Ischemic Stroke
ATP	adenosine triphosphate
BOLD	blood oxygen level dependent
BP	blood pressure
Ca^{2+}	calcium ion
CASL	continuous arterial spin labelling
CBF	cerebral blood flow
CBV	cerebral blood volume
CI	confidence interval
Cl^{-}	chlorine ion
CMRglc	cerebral glucose utilisation rate
$CMRO_2$	cerebral metabolic rate of oxygen
CNS	central nervous system
CO_2	carbon dioxide
CSD	cortical spreading depolarisations
CSF	cerebrospinal fluid
CT	computed tomography
CTP	computed tomography perfusion
dATP	deoxyadenosine triphosphate
DEFUSE	diffusion and perfusion imaging evaluation for understanding stroke evolution study
DNA	deoxyribonucleic acid
DNase	DNA-degrading enzyme
DSC	dynamic susceptibility contrast

DWI	diffusion-weighted imaging
DWI/PWI mismatch	diffusion-perfusion mismatch
ECA	external carotid artery
ECASS III	third European Cooperative Acute Stroke Study
ECG	electrocardiogram
EPI	echo planar imaging
EPITHET	Echoplanar Imaging Thrombolytic Evaluation Trial
FLAIR	fluid-attenuated inversion recovery
fMRI	functional magnetic resonance imaging
GKI	Glucose, potassium and insulin
GLUT	glucose transporter
GTT	glucose tolerance test
H&E	haematoxylin and eosin
ICA	internal carotid artery
ICH	intracranial haemorrhage
ILF	intraluminal filament
i.v.	intravenous
K^+	potassium ion
LCBF	local cerebral blood flow
L-NAME	NG-nitro-L-arginine methyl ester
LPO	lipid peroxidation
MABP	mean arterial blood pressure
MCA	middle cerebral artery
MCAO	middle cerebral artery occlusion
MDA	malondialdehyde
MRI	magnetic resonance imaging
mRS	modified Rankin Scale
MRS	magnetic resonance spectroscopy
MTT	mean transit time
Na^+	sodium ion
NIH	National Institute of Health
NIHSS	National Institute of Health stroke scale
NINDS	National Institute of Neurological Disorders and Stroke
NMDA	N-methyl-D-aspartate
NO	nitric oxide

NOS	nitric oxide synthase
O_2	oxygen
OEF	oxygen extraction fraction
OTT	onset to start of treatment
$PaCO_2$	arterial partial pressure of carbon dioxide
PAM	paraformaldehyde in phosphate buffered saline
PaO_2	arterial partial pressure of oxygen
PET	positron emission tomography
PID	peri-infarct depolarisations
PKC	protein kinase C
PSH	post stroke hyperglycaemia
PWI	perfusion-weighted imaging
RARE	rapid acquisition with refocused echoes
RBC	red blood cell
rCBF	relative cerebral blood flow
RF	radio frequency
ROI	region of interest
ROS	reactive oxygen species
rT-PA	recombinant tissue plasminogen activator
SD	standard deviation
SELESTIAL	Spectroscopic Evaluation of Lesion Evolution in Stroke: Trial of Insulin for Acute Lactic acidosis
SOD	superoxide dismutase
SPECT	single photon emission computed tomography
SUTC	Stroke Unit Trialists' Collaboration
T_1	longitudinal relaxation time
T_2	transverse relaxation time
TE	echo time
TR	repetition time
TTC	2,3,5-triphenyltetrazolium chloride
TTP	time to peak

Chapter 1 - Introduction

1.1 Stroke

1.1.1 Stroke Incidence

Stroke is the second commonest cause of death worldwide behind ischaemic heart disease, accounting for around 51,000 deaths in the UK each year (Donnan *et al* 2008). The rate of stroke deaths varies geographically, with parts of Scotland having the highest rates in the UK, around 50% higher than in London (http://www.heartstats.org, Stroke Statistics 2009). Age is a major risk factor with 75% of all strokes occurring after the age of 65 (Sudlow and Warlow 1997). The aged population continues to grow in the UK and it has been suggested that the incidence of stroke death will increase exponentially in the next 20 years (Mackay and Mensah 2004).

Most strokes are not fatal and therefore the condition represents the greatest cause of severe adult disability worldwide with nearly half of stroke patients requiring constant care and 30% expected to die within the first year of stroke-onset (Donnan *et al* 2008; Warlow *et al* 2003). In the UK around 20% of all acute NHS hospital beds and 25% of long-term beds are occupied by stroke patients, and this is expected to rise with the growing aged population so further increasing the health and economic burden (Department of Health, 2005). In 2007 the total economic cost of stroke was £4.5 billion, of which, £1.1 billion was devoted to inpatient hospital care and £900 million for residential care (http://www.heartstats.org Stroke Statistics 2009).

Despite the scale of the economic and social burden of stroke only thrombolytic therapy (recombinant tissue plasminogen activator, rt-PA) is currently licensed for treatment of stroke patients in the UK. Since fewer than 10% of patients can receive thrombolysis (Cocho *et al* 2005) experimental research is invaluable for understanding the extensive pathological mechanisms of stroke to help identify new therapies and provide better management of patients.

1.1.2 Classification of Stroke

Stroke results from a severe reduction in cerebral blood flow (CBF) that leads to tissue loss and functional impairments. The brain receives around 15% of total cardiac output even though it only equates to 2-3% of body weight. This is because the brain has a limited capacity to store energy and requires a constant nutritive supply to maintain normal metabolic function. The brain utilises around 20% of the total oxygen consumption and 25% of total glucose consumption by the body and this high metabolic demand exemplifies how damaging a reduction in CBF could be to brain tissue. Reductions in CBF associated with stroke can occur from either the occlusion or haemorrhage of a cerebral artery (Figure 1.1)

Haemorrhagic stroke accounts for a small proportion of cases (~20%) and commonly occurs due to the presence of an arterial aneurysm, arteriovenous malformation or as a result of persistent hypertension (Warlow *et al* 2003). This type of stroke can be sub classified into intracerebral haemorrhage and subarachnoid haemorrhage, which account for 25% and 75% of all haemorrhagic strokes, respectively.

The majority of strokes are ischaemic, accounting for approximately 80-87% of all cases (Chen *et al* 2010; Donnan *et al* 2008; Rothwell *et al* 2005). Ischaemic stroke often arises either from atherosclerotic plaques, or from a displaced embolus such as a blood clot that travels from the heart to the brain and becomes lodged in a cerebral artery (Figure 1.1). Atherosclerotic plaques result from endothelial disruption, extracellular lipid deposits, smooth muscle cell migration and proliferation, and thickening of the intima, which causes the lumen of the affected blood vessel to become narrowed. Complicated atherosclerotic plaques may rupture exposing the extremely thrombogenic fatty component of the lesion to flowing blood leading to thrombus formation and occlusion of the artery (Zaman *et al* 2000). Atherosclerosis is associated with approximately 50% of all ischaemic strokes whereas emboli originating from the heart, commonly as a result of atrial fibrillation, accounts for 20% of cerebral artery occlusions. The remainder are as a result of occlusions in small intracranial vessels and lacunar strokes, which affect small arterioles, often caused by hypertension leading to morphological changes.

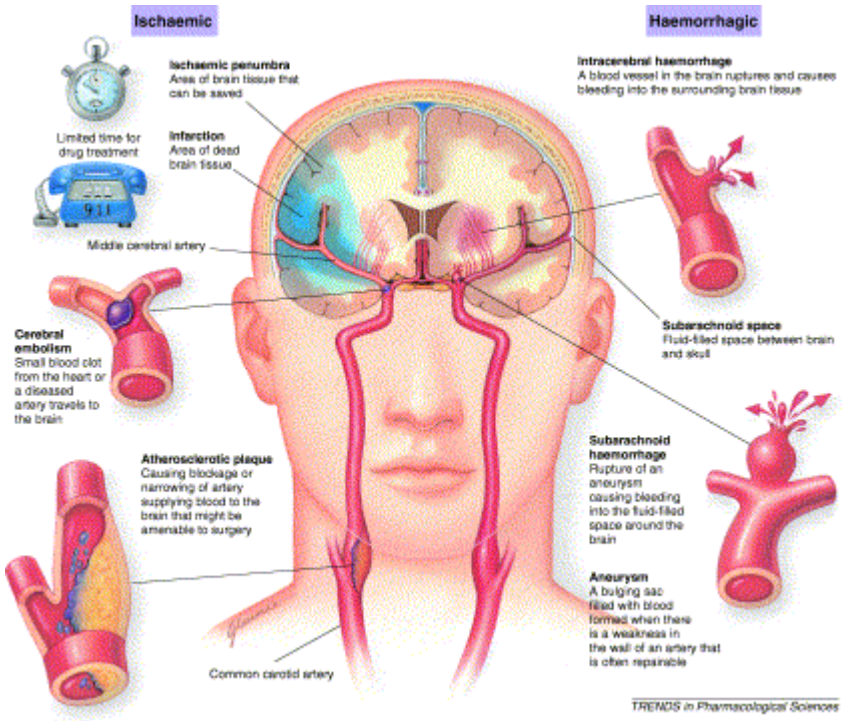

Figure 1.1: The major types of ischaemic and haemorrhagic stroke. Reproduced from Richard Green *et al* (2003).

1.2 The rat as a stroke model

Ischaemic stroke has been modelled in a variety of animal species enabling an extensive understanding of the mechanisms and pathways associated with cerebrovascular occlusion. However concerns have been raised over the animal models used due to the number of neuroprotective compounds that have failed to show benefit in clinical trials after promising results in animal models (Savitz and Fisher 2007). There are a number of species that have been used to generate models of human stroke including non-human primates, cats, rabbits and rodents (Tamura et al, 1996). The greatest relevance to the human condition is undoubtedly from the study of non-human primates due to their gyrencephalic brains and their behavioural similarities to humans, in particular manual dexterity which is lacking in lower mammals. However there are a number of problems associated with the use of primates in animal research, in particular economical and ethical considerations due to the lower social acceptance of using these animals (Carmichael 2005).

Rodent models of cerebral ischaemia have become the most widely used in pre-clinical research primarily using young male rats and mice, due to the availability of transgenic lines (Cenci *et al* 2002; Hunter *et al* 1995; Mhairi Macrae 1992). The relevance of the rat as an animal model of ischaemic stroke is still debated due to the lack of success of neuroprotective drugs tested in clinical trials however there are a number of similarities between humans and rats including the mechanisms of ischaemic damage and the sensorimotor deficits observed following middle cerebral artery (MCA) occlusion (Cenci *et al* 2002), and the similarities in the structure and organisation of the cerebral vasculature, with both species possessing a circle of Willis (Figure 1.2). Studies in rats are also economically viable due to low maintenance costs and the availability of inbred strains bred for genetic homology mean that infarction size and distribution is relatively reproducible.

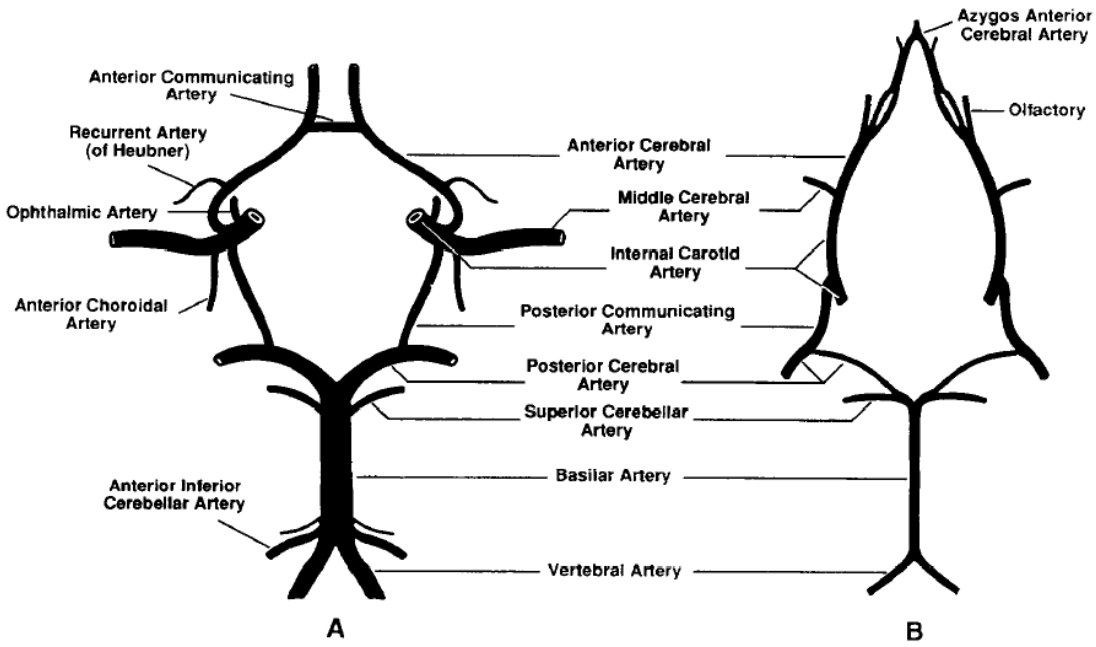

Figure 1.2: Organisation of blood vessels in the brain for A) Human, and B) Rat (taken from Lee, 1995)

1.2.1 Rodent models of focal ischaemia

Most human strokes involve the middle cerebral artery (MCA) territory (Barnett, Mohr, Stein et al, 1992, Figure 1.3). MCA occlusions account for approximately 80% of cases in Caucasians (Derouesne et al, 1993; Warlow et al, 2003), and because of this the majority of animal models of focal ischaemia that have been developed involve occlusion of the MCA (McAuley 1995) (Figure 1.4).

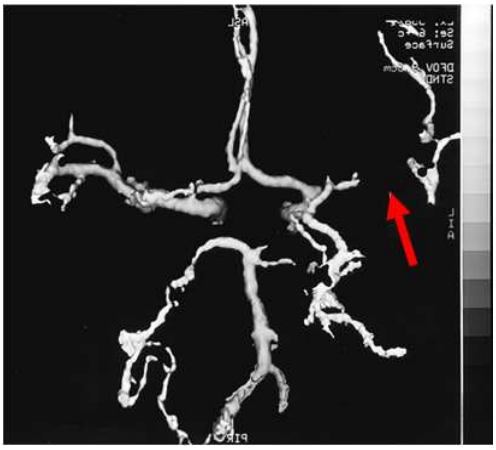

Figure 1.3: CT angiography displaying MCA occlusion (red arrow) in a stroke patient. Modified from Wong et al (1996)

1.2.1.1 Intraluminal filament model (ILF)

The most commonly used method of inducing permanent or transient focal ischaemia is the intraluminal filament (ILF) model (Koizumi *et al* 1986). This involves the insertion of a silicon rubber-coated monofilament into the external carotid artery, where it is introduced into the internal carotid artery and advanced to block the origin of the MCA. The filament can remain in this position permanently, or be retracted and removed to allow tissue reperfusion. The ILF model is advantageous because it does not require a craniotomy, although adherence of the filament to the blood vessel walls may cause mechanical endothelial damage. Additionally, the infarcts tend to be more variable than with some other MCA occlusion (MCAO) models, with higher mortality often reported (Minematsu *et al* 1992). A typical pattern of ischaemic damage using the ILF method is shown with Magnetic Resonance Imaging (MRI) (Figure 1.5).

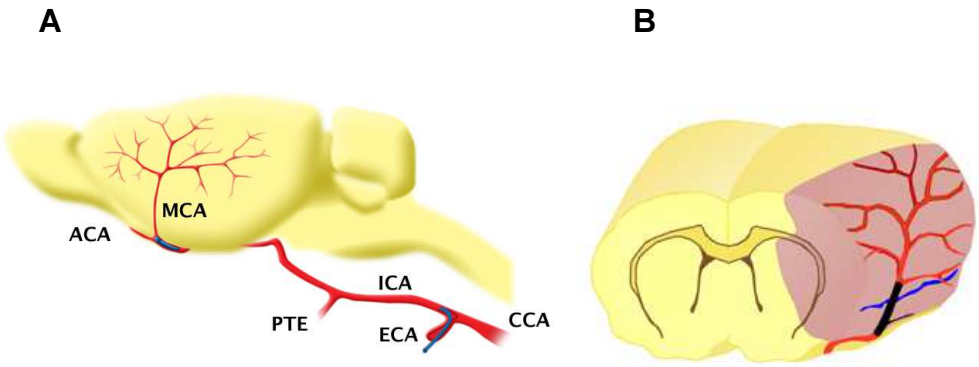

Figure 1.4: Two commonly used rodent MCAO models. A. Sagittal representation of the intraluminal filament method of MCAO, where the bulbed monofilament is introduced through the external and internal carotid arteries to block the origin of the MCA, thus precluding flow and inducing ischaemia, and B. Coronal representation of the electrocoagulation method of MCAO, in which the MCA occluded by electrocoagulation is coloured black. The pink shading represents the ischaemic territory following MCA occlusion. Illustration A courtesy of C Stock, University of Manchester. Illustration B courtesy of J Sharkey, University of Glasgow

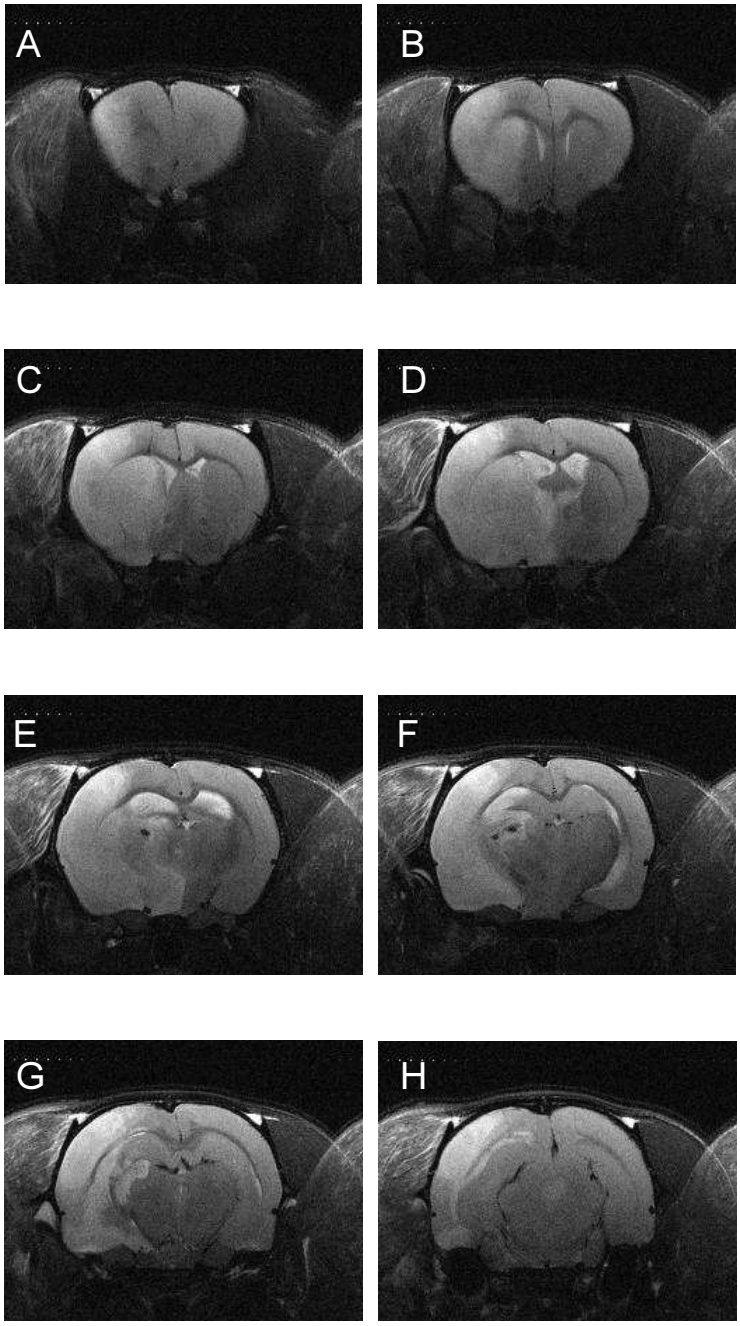

Figure 1.5: T_2-weighted coronal rat brain images at 24 hours following the intraluminal filament model of permanent MCAO (rostral (A) to caudal (H)). On T_2 images, ischaemic tissue appears hyperintense due to its high water content. Similarly the cerebrospinal fluid (CSF) in the ventricles also appears bright. Considerable brain swelling is evident in the ipsilateral hemisphere at this time point due to cerebral oedema, and this accounts for the midline shift. Small haemorrhages are also common in this model, for example in the caudate nucleus (dark structures) on Images (E) & (F). Courtesy of C. Robertson, University of Glasgow.

1.2.1.2 Electrocoagulation model

A second MCAO model involves electrocoagulation of the MCA with diathermy forceps, following a craniotomy, which was developed by Robinson and colleagues (1975) and further modified by Tamura and colleagues (1981). The method described by Tamura involves direct ligation of the MCA proximal to the lenticulostriate artery inducing both cortical and striatal damage, whereas the technique by Robinson and colleagues involves electrocoagulation of a more distal region of the MCA at the rhinal fissure of the rat which induces cortical damage only. Thus, the extent of ischaemic damage is dependent upon the position and length of the occlusion. A more distal occlusion produces more variability in the extent of the ischaemic lesion and occlusion of only a small segment (1-2 mm) can lead to low rates of infarction. Increasing the length of vessel occluded can greatly improve the reproducibility of the lesion (Bederson *et al* 1986b). The craniotomy diminishes the deleterious consequences of brain swelling following ischaemia, making this method popular due to the low post surgical mortality rate; however, it cannot be used to study transient focal ischaemia. A typical pattern of ischaemic damage using the distal diathermy model is shown with MRI (Figure 1.6).

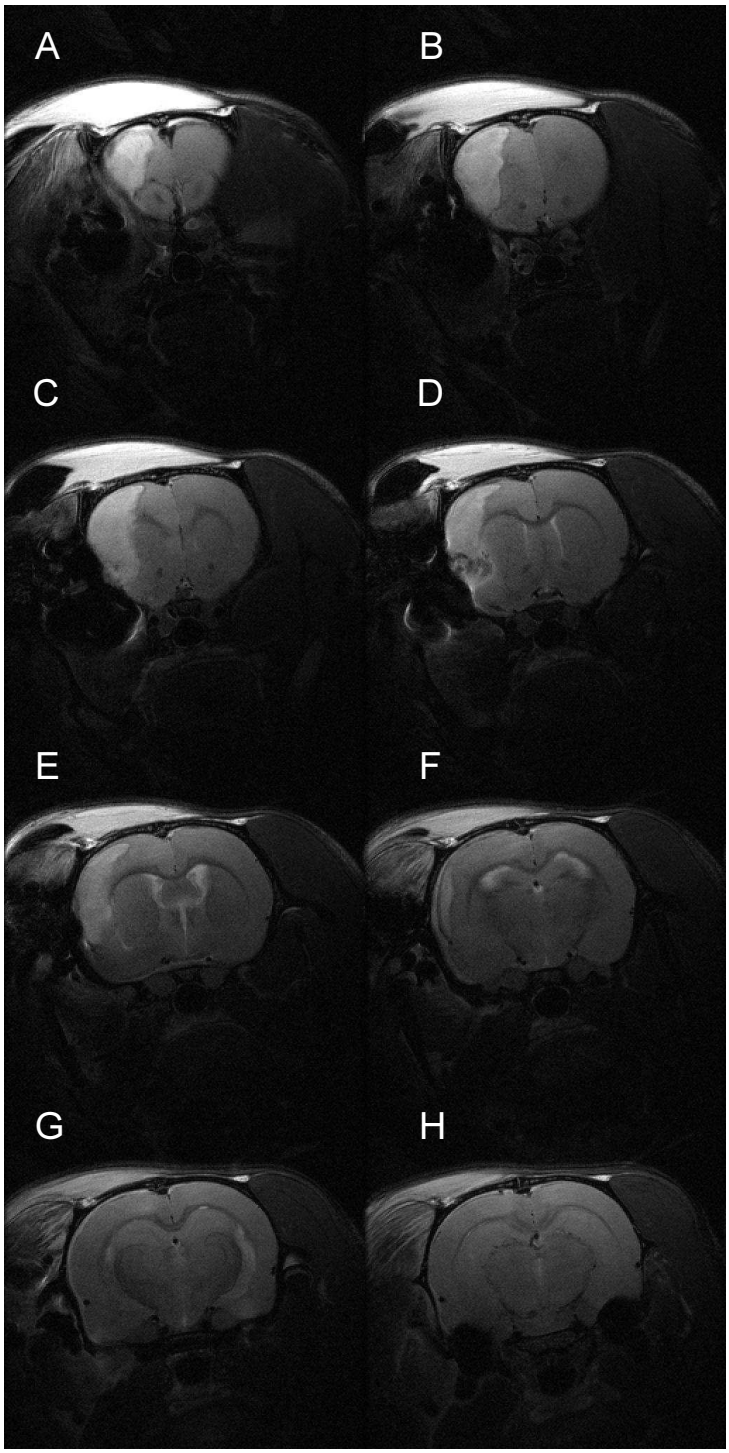

Figure 1.6: T_2-weighted coronal rat brain images at 24 hours following the distal diathermy model of permanent MCAO (rostral (A) to caudal (H)). On T_2 images, ischaemic tissue appears hyperintense. The lesion is primarily restricted to the cortex and spatial profile is much smaller compared to the intraluminal filament model. Mechanic damage to the brain can occur due to the diathermy of the MCA which is apparent in (D).

1.2.2 Pathophysiology of Ischaemic Stroke

Ischaemic stroke initiates a constellation of pathophysiological processes, including energy failure, increased intracellular calcium, excitotoxicity, necrosis and secondary pathogenic mechanisms, inflammation and apoptosis that develop for hours and even days after the initial occlusion (Figure 1.7).

1.2.2.1 Energy Failure

A reduction in cerebral blood flow due to an occlusion of a cerebral artery prevents the necessary substrates for energy production, namely glucose and oxygen from reaching the supplied tissue. The brain relies almost solely on oxidative phosphorylation to generate energy and therefore insufficient delivery of glucose and oxygen leads to energy failure within the tissue through a loss of adenosine triphopshate (ATP)(Martin *et al* 1994). Consequently neuronal membrane potentials are lost as the Na^+-K^+ pump Na^+/K^+-ATPase and Ca^{2+}/H-ATPase pumps, as well as the reversal of the Na^+-Ca^{2+} exchanger cannot maintain ionic gradients (Lipton 1999). This results in an elevation of intracellular Na^+, Ca^{2+}, and Cl^- causing cytotoxic oedema and events triggered by excess intracellular Ca^{2+} (Durukan, and Tatlisumak, 2007).

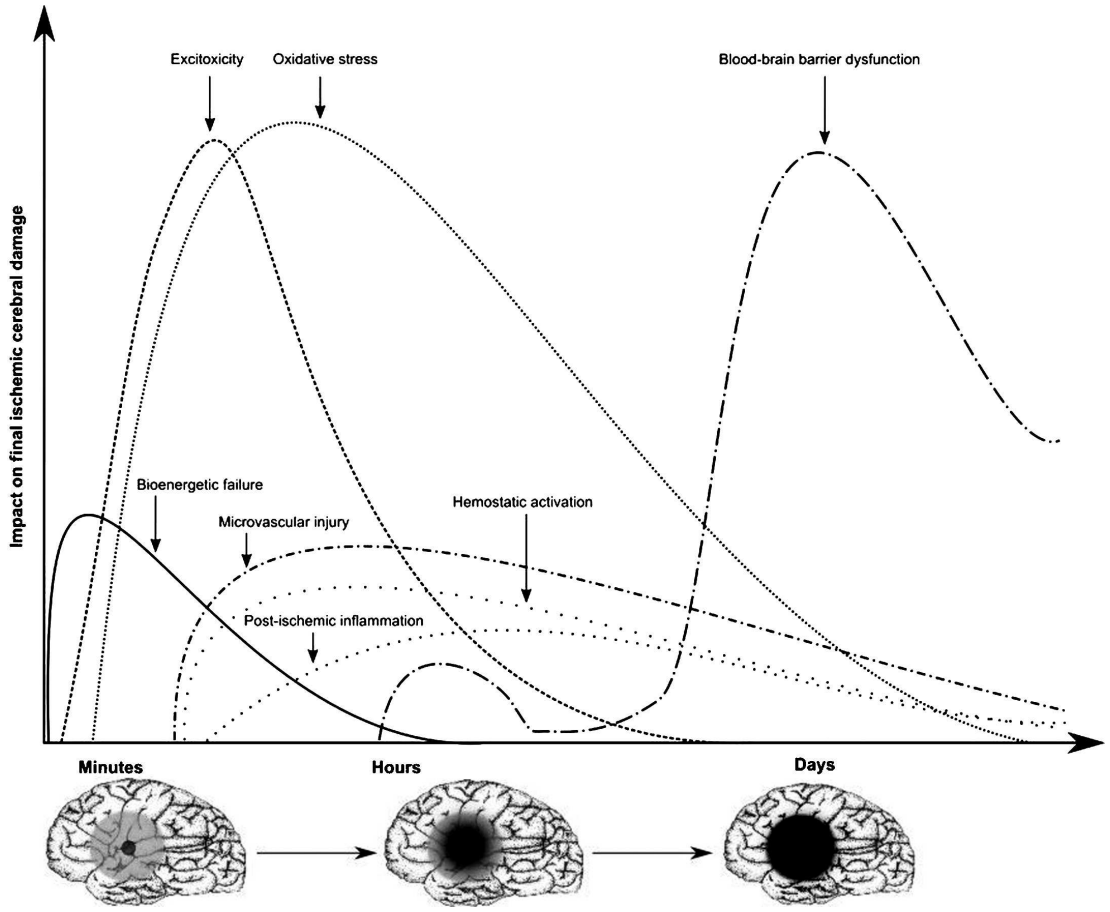

Figure 1.7: The time course and impact of the pathophysiological cascade following cerebral ischaemia. (Brouns and De Deyn 2009).

1.2.2.2 Elevation of intracellular Calcium

The excessive accumulation of intracellular Ca^{2+} is thought to initiate many downstream mechanisms that can cause cell damage and even death via apoptotic pathways and necrosis. Depolarisation of neurones and glia, caused by the diminished energy production, leads to the activation of presynaptic and postsynaptic voltage gated Ca^{2+} channels and the influx of Ca^{2+}. Free calcium is also released from the mitochondria and the endoplasmic reticulum further increasing the concentration of Ca^{2+} in the cytosol.

The rise in intracellular Ca^{+2} ions can induce the proteolytic degradation of cytoskeletal proteins (actin and spectrin) and the extracellular protein laminin (Chen and Strickland 1997; Furukawa *et al* 1997). Ca^{2+} is also known to stimulate phospholipase A and C which break down membrane phospholipids, resulting in the release of free arachidonic acid which directly increases membrane permeability and also has profound secondary metabolic events. It is presumed

that cellular oedema occurs as an almost immediate consequence of cerebral ischaemia.

1.2.2.3 Excitotoxicity

Excitotoxicity is the pathological process triggered by the excessive release of glutamate and other excitatory neurotransmitters, as a result of cellular energy failure, which causes nerve cell damage and death. Diminished energy production and failure of ion pumps leads to the activation of presynaptic and postsynaptic voltage gated Ca^{2+} channels and the depolarisation of neurones and glia and the release of glutamate into the extracellular space (Dirnagl *et al* 1999). Normal glutamate re-uptake into the presynaptic cell is impeded by lack of available energy which maintains a high level of extracellular glutamate. This increase in extracellular glutamate has been demonstrated in an experimental model of stroke (Shimizu-Sasamata *et al* 1998). The excessive extracellular glutamate triggers a rise in intracellular [Ca^{2+}] by binding to glutamate receptors: N-methyl-D-aspartate (NMDA), -amino-3-hydroxy-5-methyl-4-isoxazole propionic acid (AMPA) and metabotropic glutamate receptors (mGluRs). Group I mGluRs facilitate this by releasing Ca^{2+} from its intracellular stores via phospholipase C and IP_3 (inositol 1,4,5-triphosphate) signalling (Abe *et al* 1992; Aramori and Nakanishi 1992). Na^+ ions enter cells via AMPA (α-amino-3-hydroxy-5-methyl-4-isoxazole propionic acid) receptors which creates an osmotic gradient due to slower K^+ efflux. Water can then diffuse into cells and the ensuing oedema can affect perfusion in surrounding areas as well as causing secondary problems such as increasing intracranial pressure and compressing cerebral vessels (Dirnagl *et al* 1999).

1.2.2.4 Free Radical Generation

Ischaemia leads to the production of various free radicals and reactive oxygen species (ROS) via a number of mechanisms (Figure 1.8). The activation of the enzyme phospholipase A_2 triggers the generation of arachidonic acid from the breakdown of membrane phospholipids. Ischaemic neurones are known to express the enzyme COX2 which is capable of producing ROS and neurotoxic prostanoids

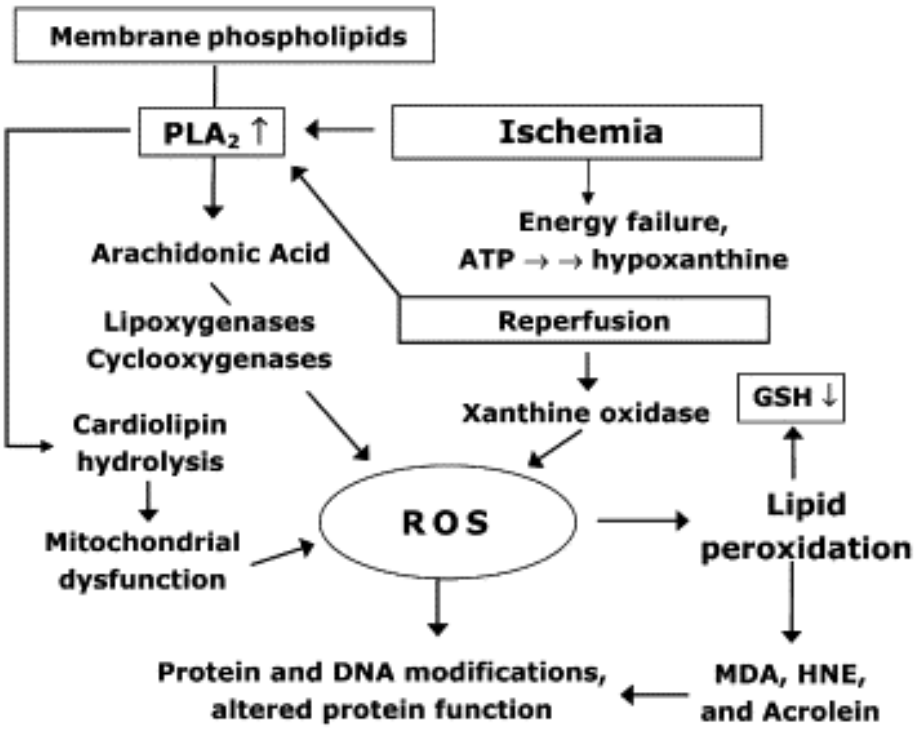

Figure 1.8: Reactive oxygen species generation during ischaemia. (Muralikrishna Adibhatla and Hatcher 2006)

from arachidonic acid (Nogawa *et al* 1997). The phospholipase A_2 pathway involves a positive feedback cycle, as free radical production further stimulates phospholipase A_2 activity and consequently augments the further production of free radicals. Free radicals may also be generated as a result of hypoxanthine oxidation. Hypoxanthine accumulates under hypoxic conditions due to the breakdown of adenine nucleotides. Xanthine dehydrogenase is converted to xanthine oxidase which is capable of producing superoxide during the metabolism of hypoxanthine. This has been shown in Long-Evans rats where the fraction of xanthine dehydrogenase present as the superoxide producing xanthine oxidase rose from 23% to 30% following ischaemia although this is not thought to be a major contributor to ROS generation in cerebral ischaemia (Lindsay *et al* 1991).

ROS are proposed to play important roles in coordinating and regulating a number of cellular signalling pathways (redox signalling) (Taylor and Crack 2004). These systems depend on a balance between ROS and the endogenous defences capable of detoxifying ROS, including superoxide dismutase (SOD), catalase and glutathione. Oxidative stress results when the formation of ROS exceeds the capacity of the antioxidant defence systems. Neurons may be particularly vulnerable to free radical damage since they contain low levels of glutathione (Taylor and Crack 2004). Mice and rats overexpressing SOD1 showed significantly smaller infarcts compared to their respective wildtypes following transient focal cerebral ischaemia supporting the role of ROS in ischaemic damage (Chan *et al* 1998; Wang *et al* 1998).

Nitric oxide (NO) production increases during ischaemia due to increased activation of nitric oxide synthase (NOS), the enzyme which catalyzes the synthesis of NO from its precursor, L-arginine (Zhang *et al* 1993). Under normal physiological conditions, NO functions as a neurotransmitter and has a role in synaptic plasticity as well as in the control of cerebral blood flow, where it acts as a vasodilator (Pacher *et al* 2007). Under ischaemic conditions, NO reacts with superoxide to form peroxynitrite, which is a highly reactive oxidant. Peroxynitrite is extremely cytotoxic and causes extensive tissue damage via inhibition of DNA synthesis, nucleic acid damage and lipid peroxidation leading to membrane breakdown. The neutralisation of NO by increased levels of superoxide can potentially lead to the loss of NO-dependant vasodilation (Didion

and Faraci 2002), causing a reduction in cerebral blood flow further extending the perfusion deficit following occlusion in addition to the detrimental effects of peroxynitrite.

Under ischaemic conditions the brain is particularly susceptible to oxidative stress due to the limited antioxidant capabilities of the tissue (Adibhatla & Hatcher, 2010). The extensive production of ROS and other free radicals overwhelms the limited endogenous free radical scavengers and cause widespread cellular damage mediated via enzyme inactivation, release of calcium ions from intracellular stores, protein denaturation, lipid peroxidation and damage to DNA and RNA, in addition to cytoskeletal component breakdown (Brouns and De Deyn 2009). Free radicals also act as signalling molecules to induce an inflammatory response and trigger apoptosis (Brouns and De Deyn 2009). Free radicals have detrimental effects on mitochondria, where they disrupt the inner mitochondrial membrane via lipid peroxidation and oxidise electron transport chain proteins, causing impairments in ATP production (Dugan and Choi 1994). Overall, free radicals result in severe mitochondrial dysfunction and mediate cellular damage via numerous actions within the cell.

1.2.2.5 Peri-infarct Depolarisations

Secondary mechanisms can contribute to the expansion of the ischaemic lesion into the surrounding tissue. These include spreading depolarisations which are waves of neuronal depolarisations caused as a result of the primary cellular energy failure in the core area of the ischaemic damage and the high extracellular glutamate and K^+ ion concentration. These depolarisations propagate out with the ischaemic core in to the tissue at risk, i.e. moderately hypoperfused tissue deemed the ischaemic penumbra (explained in more detail below). The short supply of ATP means that further depolarisations can exhaust energy supply and lead to further cell death and therefore expand the infarct. These repetitive depolarisations are known as peri-infarct depolarisations and have been detected in many animal models of stroke (Dirnagl *et al* 1999; Hossmann 1996). They have been found to occur several times per hour and the number of these depolarisations is proportional to infarct size (Mies *et al* 1993). Unfortunately peri-infarct depolarisations have not been observed in human ischaemic stroke therefore the significance of these findings is unclear with

regards to the human disease. Interestingly however, in traumatic brain injury and aneurysmal subarachnoid haemorrhage spreading cortical depolarisations have been identified as mechanisms of ischaemic damage suggesting that these may still be observed in the future (Dreier *et al* 2009; Fabricius *et al* 2006)

1.2.2.6 Inflammation

Many pro-inflammatory genes are expressed in response to the increase in free radical production and activation of Ca^{2+}-dependant pathways initiated by excitotoxicity. Tumour necrosis factor α (TNF-α) and interleukin 1ß (Il-1ß) and platelet activating factor which are known mediators of inflammation are produced by damaged cells in the brain (Rothwell and Hopkins 1995). This promotes expression of various adhesion molecules allowing neutrophil infiltration followed by monocytes and macrophages with further inflammatory cells being recruited to the ischaemic area by the release of chemokines (Yamasaki *et al* 1995). Preceding this infiltration, microglial cells become activated particularly in the ischaemic penumbra where they are thought to contribute to brain injury (Schilling *et al* 2003).

This post-ischaemic inflammation is thought to exacerbate ischaemic brain injury via a multitude of mechanisms. Studies have shown that preventing infiltration of neutrophils can reduce ischaemic damage (Dirnagl *et al* 1999). Also blocking the binding of adhesion molecules to their receptors has proved beneficial. One study has shown that in null ICAM-1 mice infarct volume was significantly attenuated (Connolly *et al* 1996). Neutrophils are thought to evoke cell damage by producing excessive amounts of NO via inducible NOS (Forster *et al* 1999). This can lead to peroxynitrite formation, from NO reacting with superoxide, which is a highly reactive ROS that causes cell damage. Secondly neutrophils are also thought to have a physical role in exacerbating ischaemia by occluding the microvasculature and this has been shown in baboons (del Zoppo *et al* 1991). In addition the activated microglia found in the penumbra and to a lesser extent the ischaemic core can produce deleterious compounds such as ROS adding to cell damage (Giulian *et al* 1994). TNF-α is also produced by these neurones but some studies have suggested that TNF-α has a beneficial role by inducing antioxidant enzymes (Barone *et al* 1997; Bruce *et al* 1996).

1.2.2.7 Necrosis and Apoptosis

Under ischaemic conditions in the brain, cells die either by necrosis or apoptotic pathways. These pathways are highly conserved biochemical pathways that signal and execute cell death. The mechanism of cell death for a cell is dependant on the severity of ischaemia, the excitotoxic stimulus and the cell type (Leist and Nicotera 1998). Necrosis is the most common mechanism of cell death in severe ischaemia, especially within the ischaemic core of the insult (Dirnagl *et al* 1999). The process of cellular necrosis involves disruption of membrane structural and functional integrity, rapid influx of Ca^{2+} and water, and subsequently, dissolution of the cell. Therefore, cellular necrosis results from abrupt environmental changes and a loss of normal physiological conditions. When cells die via the necrotic pathway, they release more glutamate and toxic mediators into the surrounding environment affecting neighbouring cells (Brouns and De Deyn 2009).

Apoptosis is a programmed mechanism that orchestrates cell death in cells that are affected by milder injury such as in the ischaemic penumbra (Dirnagl *et al* 1999). These apoptotic pathways can be either caspase dependant or independent although caspase dependant pathways are primarily involved in neuronal cell death following focal cerebral ischaemia. Caspases are a family of protein cleaving enzymes that are constitutively expressed in neurones and other brain cells. These enzymes can cleave numerous proteins leading to protein activation or inactivation, both of which may promote cell death. Caspases 1 and 3 are thought to be primarily involved in ischaemia-mediated apoptosis. Caspase 3 has been found to be present in the ischaemic core and the penumbra following reperfusion in a mouse model of temporary MCA occlusion (Namura *et al* 1998) and caspase 1 knockout mice elicit a reduced lesion size following focal MCA occlusion (Schielke *et al* 1998). The exact nature of the upstream mechanism that leads to the activation of these caspases following ischaemia is still not well understood. However, it has been found that cytochrome C release from mitochondria, which occurs during excitotoxicity, forms part of an apoptosome complex which can activate the various executioner caspases and induce apoptosis (Green and Reed 1998).

1.3 The Ischaemic Penumbra

1.3.1 Cerebral Blood Flow

Following stroke, there is a heterogeneous reduction in cerebral blood flow (CBF) across the affected vascular territory. Tissue in end artery territory has the greatest severity of ischaemia where complete or profound loss of CBF represents tissue that will progress to an infarct and this is deemed the ischaemic core.

The brain has a complex network of anastomosing vessels which means perfusion of the adjacent region to the core is partially achieved by collateral supply and thus the hypoperfusion is less severe. Following vascular occlusion this tissue will have functional impairment but will not immediately undergo irreversible morphological changes and is termed the ischaemic penumbra (Figure 1.9).

The concept of the penumbra was first described in a series of experiments conducted in the 1970s into the effects of progressive reductions in cerebral blood flow on the baboon cortex which found that different cerebral blood flow thresholds existed in the pathogenesis of stroke relating to tissue function and survival (Astrup *et al* 1977; Branston *et al* 1974; Branston *et al* 1977; Symon *et al* 1974). These studies examined cortical-evoked responses at varying thresholds of blood flow and found that there was an area of hypoperfused tissue with cellular dysfunction but not death and that full restoration of blood flow had the potential to reverse cellular dysfunction in this region. It was established from examining cortical-evoked responses that there were three blood flow thresholds; one threshold that determines morphological damage (ischaemic core), a less severe threshold for functional impairment (ischaemic penumbra) and finally normal tissue thought to include some benign oligaemia. Benign oligaemic tissue refers to tissue that has suffered a modest reduction in blood flow which is not severe enough to threaten its survival. In primates, following blockage of a cerebral vessel the end artery territory (ischaemic core) has CBF of <10 mL/100 g per min within which irreversible cell damage takes place within minutes. The intermediate tissue around the periphery of this core (ischaemic penumbra) experiences a more modest reduction in CBF, where flow

is ~15% to 40% of normal levels. Unless blood flow is restored, this penumbral tissue will progressively become incorporated into the infarct, and this process can take a number of hours (Pulsinelli, 1992). There are often some areas of modest hypoperfusion which are not expected to become incorporated into the infarct under normal circumstances. This benign oligaemic tissue and its blood flow can range from normal CBF values down to ~20 mL/100g/min (Baron et al, 2001). It is expected that this region enters a less severely hypoperfused state (above 30 mL/100g/min), which prevents the tissue undergoing infarction (Linskey et al, 1994). However, benign oligaemic regions are not completely safe from infarction as factors such as hyperglycaemia, fever and hypotension, present in conjunction with small reductions in CBF, may induce progressive damage.

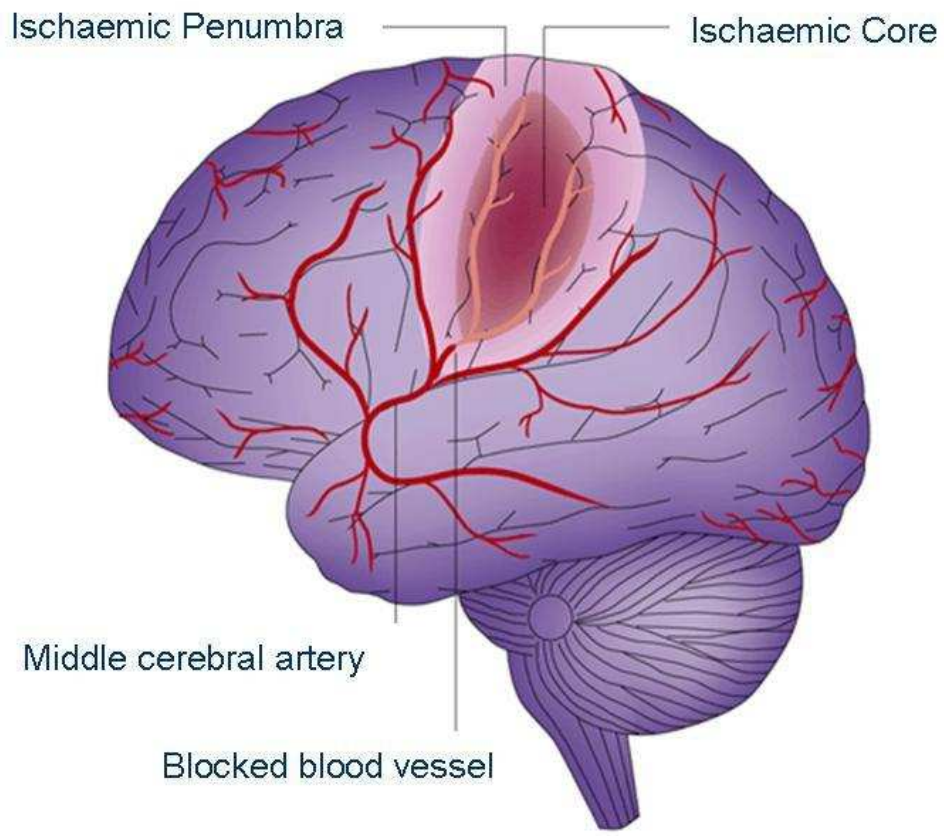

Figure 1.9: Depiction of the nature of ischaemic injury, with penumbral tissue surrounding an ischaemic core following blockage of a cerebral artery. Adapted from Allan and Rothwell (2001)

1.3.2 Imaging the ischaemic penumbra

There are several imaging modalities available to visualise the ischaemic penumbra following cerebral artery occlusion both clinically and experimentally. In the clinical setting the rapid detection of penumbral tissue will improve patient selection for treatment with thrombolysis. It may also provide the potential to group similar patients in distinct cohorts in clinical trials. It is thought that a lack of efficacy in both thrombolysis and neuroprotection trials may have arisen from treating patients who lacked a significant volume of the potentially salvageable penumbral tissue even within the conventional time windows (Muir 2002). The possible improvement in selection for thrombolysis safety based on more advanced penumbral imaging has been suggested (Schellinger *et al* 2003).

1.3.3 Computed tomography

Computed tomography (CT) is currently the most accessible clinical technique for identification of the ischaemic penumbra due to its widespread availability in hospitals, speed of image acquisition and its relative cost-effectiveness. Non contrast CT scans cannot identify the penumbra reliably with acute hypoperfused regions often appearing as normal (Ebinger *et al* 2009). However, CT perfusion (CTP) techniques using injection of an iodinated contrast agent are useful in predicting the fate of ischaemic tissue (Parsons *et al* 2007). CT perfusion imaging defines penumbra based on changes in cerebral blood volume (CBV), CBF and the contrast mean transit time (MTT). Using these methods, the ischaemic core has been defined as a region with CBV below 2 mL/100g and a relative MTT above or equal to 145% of the contralateral value (Tan *et al* 2007). CTP defines penumbral tissue as a region with increased cerebral blood volume (relative to the ischaemic core due to local vasodilatation, where autoregulatory processes compensate for reduced relative (rCBF)), as well as reduced CBF and increased MTT. Xenon-enhanced CT has also been used to identify ischaemic core and penumbra. Xenon crosses the blood-brain barrier after inhalation and due to its high atomic number can be measured on the CT scanner. This technique has been shown to give a high resolution and sensitivity (Yonas and Jungreis 1995). However, these CT techniques suffer from a lack of validation

for visualisation of the penumbra. The software provided with each different system varies in the post-processing algorithms and whole brain scanning is still very limited. Radiation exposure may prevent serial scanning, and iodinated contrast agent administration may cause nephropathy (Ebinger et al, 2009).

1.3.4 Positron Emission Tomography (PET)

PET is widely regarded as the gold standard for clinical assessment of penumbra as it can quantifiably measure CBF, cerebral oxygen metabolism ($CMRO_2$) and oxygen extraction fraction (OEF). PET relies on the intravenous administration of a positron emitting radioisotope bound to a tracer ligand. The gamma rays emitted by the tracer are detected and reconstructed to produce a tomographic image. Multi-tracer PET using ^{15}O or $H_2{}^{15}O$ as tracers has been used to identify the penumbra as tissue with reduced CBF, preserved $CMRO_2$ and an increased OEF (Baron 1999; Ebinger *et al* 2009)(Figure 1.10). This signature of penumbral tissue was termed 'misery perfusion' by Baron and colleagues (1981). In humans, oxygen metabolism and CBF thresholds of irreversibly damaged tissue have been defined as 65 µmol/100g/min and 12 mL/100g/min, respectively (Heiss 2003).

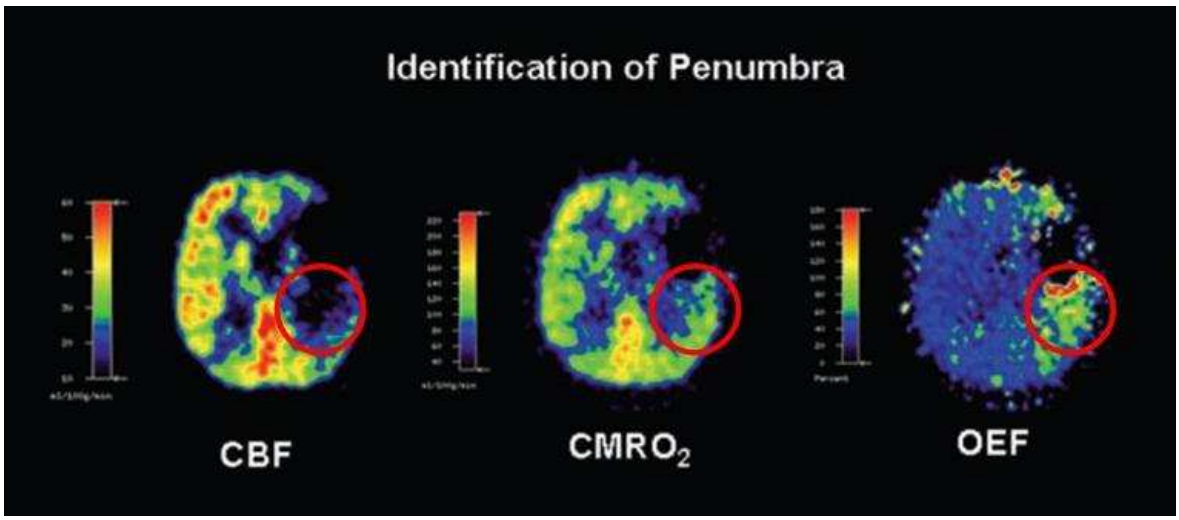

Figure 1.10: Multimodal imaging 5 hours post-stroke in a human patient. Penumbra is defined as a region with reduced CBF, preserved CMRO2 and increased OEF circled in red. Adapted from Heiss et al (2004)

Modern PET tracers like the hypoxic ligand [^{18}F]-fluromisonidazole (FMISO) and the neuronal receptor ligand, [^{11}C]-flumazenil (FMZ) can also identify penumbral tissue. FMZ is a central benzodiazepine receptor ligand which is a marker of neuronal integrity capable of detecting neuronal damage within the first few hours of stroke onset. FMISO is a tracer of hypoxic viable tissue and is therefore useful in the detection of penumbra where increased areas of tracer are detected (Heiss 2003). The use of these ligands was supported by Takasawa and colleagues (2007), who reported increased FMISO uptake in the first hours in a MCAO rat model in the absence of reperfusion when the tissue was not yet irreversibly damaged. However, increased FMISO uptake has been shown 20 hours post-stroke despite reperfusion in the rat (Saita *et al* 2004). It was suggested that the persistent hypoxia may have occurred due to peri-infarct oedema, small vessel occlusion, or the 'no-reflow' phenomenon where removal of the intraluminal filament fails to recanalise the previously occluded vessel.

Although PET is an accurate means of physiological monitoring which permits quantitative measurements, it is impractical for clinical use (Muir and Santosh 2005; Schellinger *et al* 2003). It necessitates arterial catheterisation for blood sampling, and it is prohibited when the administration of thrombolytics is planned (Heiss *et al* 1998). Additionally, although serial PET scanning has been done pre-clinically to assess the temporal evolution of the penumbra, multiple scans cannot be performed in humans due to the radiation dose administered. It is also expensive, technically challenging and of limited availability in stroke units (Muir and Santosh 2005; Schellinger *et al* 2003). As such, MRI and CTP are preferred for penumbral imaging in the clinical research domain.

1.3.5 Magnetic Resonance Imaging (MRI)

MRI is a non-invasive imaging modality that is based upon the electromagnetic activity of atomic nuclei, namely hydrogen atoms, since they are the most abundant in the body. MRI is capable of producing high resolution anatomical images as well as imaging pathological processes, organ function and even neural activity which means it is an extremely useful technique with regards to, but not limited to, diseases of the central nervous system. The presence of a strong

external magnetic field takes advantage of the intrinsic characteristics of the hydrogen nuclei in the body. Each hydrogen nucleus consists of a single positively charged proton which rotates around its own axis. Each proton generates its own magnetic field on the basis of their spin and the positive charge these protons possess. This magnetic field is known as a magnetic moment. When a subject is placed in a magnetic field such as created by an MRI scanner, the protons are forced to align in one of two possible positions; either parallel or anti-parallel with the magnetic field. In order to generate a magnetic resonance signal the protons must be excited from a low to high energy state by exposure to electromagnetic radiation of radio frequency (RF). When radio waves are sent toward these hydrogen atoms, the alignment of the magnetisation (magnetisation vector) is altered. This causes the emittance of a weak radio signal that can be amplified and detected by the scanner. The magnetisation vector is altered by either 90° or 180° by exposure to specific radio frequencies know as RF 90° and RF 180°. Following the excitation of protons and the changes imposed on the magnetisation vector, the protons return to magnetic equilibrium within the scanner. The time taken for the magnetic resonance signal to fade and equilibrium to be reached is known as the relaxation time which can be measured. This relaxation time is reliant on two independent processes that almost happen simultaneously. The first known as spin-lattice interaction (T_1 relaxation) involves the dissipation of energy into the surroundings in order to regain equilibrium. Spin-spin interaction (T_2 relaxation) is where the MR signal fades as the magnetic fields from adjacent protons interfere with each other. Different types of tissues send back different signals, allowing differentiation between internal structures, which leads to a reconstruction of the image of the subject. MRI images can be 'weighted' to allow one factor to determine the contrast of the image. T_1 relaxation time can be used to primarily determine the image contrast and these are known as T_1-weighted images. Similarly T_2-weighted images can be generated by using T_2 relaxation to determine the contrast.

1.3.6 T_2-weighted imaging

T_2-weighted imaging has been used in clinical and preclinical studies to assess ischaemic brain tissue 12 to 24 hours following stroke but in the critical period

regarding the ischaemic penumbra (up to 12 hours post stroke) this imaging modality is unable to adequately determine the extent of ischaemically damaged tissue (Baird and Warach 1998). Ischaemically damaged tissue has a longer T_2 relaxation time than normal parenchymal tissue meaning that it has a higher signal intensity on T_2-weighted images. Some T_2-weigted sequences can be converted to quantitative T_2 maps which enable the comparison of T_2 relaxation times of different tissue compartments between subjects. There is also the potential to derive a threshold of abnormality to distinguish between ischaemically damaged tissue and unaffected tissue.

Different MRI sequences have been developed to allow the penumbra to be visualised based on the use of diffusion and perfusion weighted imaging.

1.3.7 Diffusion weighted imaging

Diffusion-weighted imaging utilises signal changes, which are dependant on the diffusion of water protons within tissues. DWI is based on the sensitivity of MR to motion, which shows the signal intensity changes that are due to the movement of water by diffusion. Water molecules have isotropic diffusion properties which mean they are free to move in all directions. However the rate of water diffusion within a voxel is determined by cellular structures such as cell membranes which act as diffusion barriers and therefore increase anisotropic diffusion, i.e. diffusion in a particular direction. Within brain tissue under normal conditions, extracellular water molecules diffuse relatively freely which results in a low signal on DWI images. Following energy failure associated with ischaemia, the loss of ion pump function leads to the shift of water from the extracellular space to the intracellular space resulting in cytotoxic oedema, cell swelling and the restriction of water molecule diffusion (Moseley *et al* 1990a). This reduced mobility of protons leads to an increase in the diffusion constant and a high signal intensity on DWI images. The diffusion constants can be used to generate a quantitative measure of diffusion for a particular voxel, which is known as the apparent diffusion coefficient (ADC). These ADC values can be used to generate ADC maps where a higher intensity represents areas of free diffusion of water and lower intensity represents restrictive diffusion, which is the opposite of DWI images. A decrease in the ADC of the ischaemic brain tissue has

been shown to coincide with the onset of cytotoxic oedema and so ADC has been taken as an indicator of irreversibly damaged tissue (Davis et al, 1994). DWI can detect ischaemic injury within minutes of MCA occlusion in animal models of stroke (Moseley *et al* 1990b) which has similarly been observed in humans (Yoneda *et al* 1999). This is far quicker than can be achieved with CT scans and T_2-weighted MRI scans where ischaemic damage can only be detected between 3 and 12 hours post-stroke, respectively (Roberts et al, 2002). Although reduced ADC is thought to represent irreversibly damaged tissue there is evidence that shows following rapid reperfusion some of the ADC-defined lesion can be reversed suggesting that the ADC-defined ischaemic damage may overestimate the extent of ischaemic injury (Hasegawa *et al* 1994). However clinically relevant reversal of the ADC-defined lesion has been found to be uncommon and often transient (Campbell *et al* 2012)

1.3.8 Perfusion weighted imaging (PWI)

Cerebral blood flow can be quantified using perfusion based MR imaging by monitoring the signal changes induced by a tracer entering the brain. One commonly used MR technique for perfusion imaging is known as contrast agent bolus tracking which involves the intravenous administration of a gadolinium-based contrast agent into the circulation. These agents are paramagnetic which results in magnetic inhomogeneity. This results in a decrease in signal intensity as the contrast agent passes through the cerebral vasculature. As the contrast agent passes away from the detection plane the homogeneity of the magnetic field is restored and the signal returns to normal. This change in signal intensity enables the contrast agent to be tracked throughout the brain and identify areas of low perfusion. However, CBF values generated with this technique tend to overestimate the region of perfusion deficit when compared with the gold standard PET techniques (Zaro-Weber *et al* 2009).

Another MR based technique for CBF quantification, called Arterial Spin Labelling (ASL), uses electromagnetically labelled arterial blood as an endogenous tracer rather than relying on the introduction of a contrast agent (Figure 1.11). The technique involves using a specific RF pulse sequence that inverts the spin of protons in an artery supplying an area of interest (labelled

slice). A coronal image is acquired at the region of interest and the signal intensity is measured (imaging slice). The signal intensity for a pixel is dependant on the number of labelled protons that have travelled to that particular pixel which is proportional to the amount of inflowing blood. This is known as the labelled image. A second image, the non-labelled image, is acquired without the labelling of protons so that a simple mathematical equation will produce qualitative CBF maps. Quantitative CBF maps can be generated subsequently by taking into account the T_1 relaxation time. ASL sequences have been widely used in rodent models of cerebral ischaemia (McCabe *et al* 2009; Meng *et al* 2004; Robertson *et al* 2011) as well as in humans (Chalela *et al* 2000), and provide a non-invasive, multi-slice perfusion measure that can be repeated for serial analysis of CBF without the need for exogenous contrast agents.

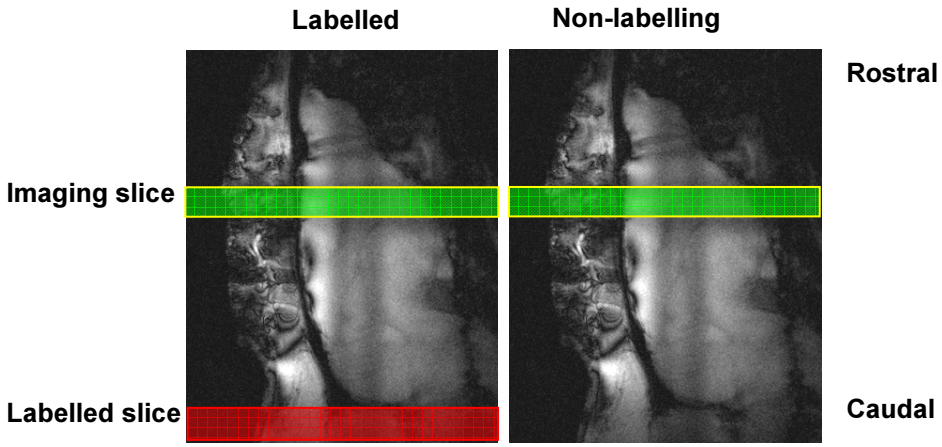

Figure 1.11: Concept of arterial spin labelling, shown on a sagittal scan of a rat brain

1.3.9 MRI Perfusion-Diffusion Mismatch

The combination of DWI and PWI in stroke has enabled an MRI based identification of suspected penumbral tissue (Baird and Warach 1998). In this method the DWI based ADC maps are used to identify the region of ischaemic injury that is thought to be irreversibly damaged, i.e. the ischaemic core. This area of ischaemic injury is overlaid onto a CBF map generated from PWI which indicates the hypoperfused area resulting from cerebral vascular occlusion (Figure 1.12).

Acutely after occlusion, the area of hypoperfusion usually incorporates a greater area than the ADC-derived ischaemic lesion, and this difference, known as the diffusion-perfusion mismatch (DWI/PWI mismatch) approximately represents the ischaemic penumbra (Schlaug *et al* 1999). The DWI/PWI mismatch was used in the phase II Desmoteplase in Acute Ischaemic Stroke (DIAS) Trial as part of the patient selection criteria for thrombolysis. All patients that were recruited had at least a 20% PWI/DWI mismatch and patients who received desmoteplase within 9 hours of stroke symptom onset demonstrated a higher rate of reperfusion and improved clinical outcome compared with patients treated with placebo (Hacke *et al* 2005). The diffusion and perfusion imaging evaluation for understanding stroke evolution (DEFUSE) study also supported the validity of the DWI/PWI mismatch hypothesis in patients treated with thrombolysis therapy in the 3 to 6 hour time window (Albers *et al* 2006). This study showed that patients who presented with a DWI/PWI mismatch (perfusion deficit 120% of ADC-derived ischaemic injury) were associated with a more favourable clinical outcome after early reperfusion, with thrombolysis, than patients where no mismatch was present (Albers *et al* 2006). Similar findings were observed in the Echoplanar Imaging Thrombolytic Evaluation Trial (EPITHET) where thrombolysis treatment was given between 3 and 6 hours following stroke symptom onset. Patients who presented with mismatch again showed improved functional outcome, which was associated with reduced infarct growth and increased reperfusion (Davis *et al* 2008).

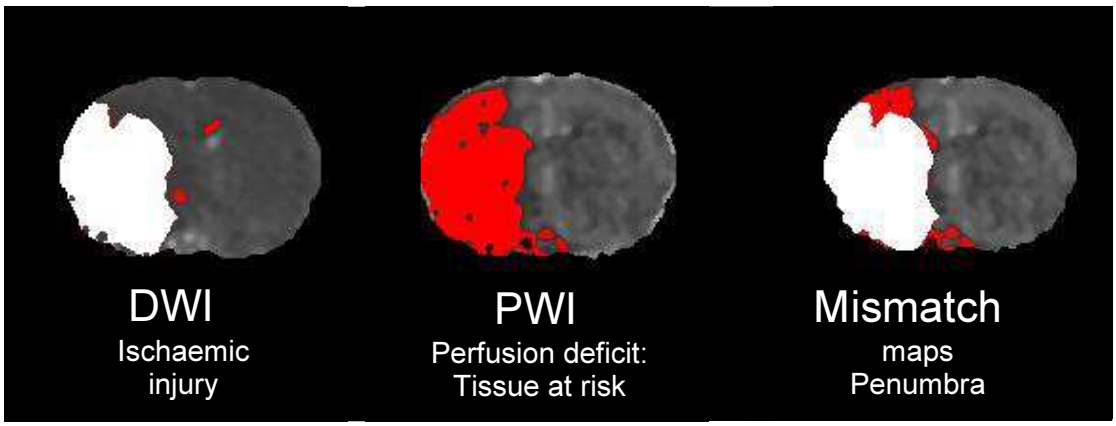

Figure 1.12: Coronal images of rat brain obtained 1 hour after permanent MCAO. The thresholded PWI (57% reduction of mean contralateral CBF values) illustrates the perfusion deficit, whilst the thresholded DWI (16.5% reduction in mean contralateral ADC values) is an indication of ischaemic damage. The thresholded area on the DWI is subtracted from the region of hypoperfusion, the mismatch corresponding to the ischaemic penumbra.

The DWI/PWI mismatch has been used in pre-clinical research to assess the temporal evolution of the penumbra. It has been shown that following permanent MCAO in Sprague Dawley rats the diffusion lesion expands temporally to encompass the perfusion deficit, reducing the amount of penumbral tissue over time (Meng *et al* 2004). This mismatch has been demonstrated in spontaneously hypertensive stroke-prone rats (SHRSP) and their normotensive control strain Wistar-Kyoto (WKY) where a reduction in mismatch was observed in the SHRSP compared to the WKY (McCabe *et al* 2009; Reid *et al* 2012).

There are a few disadvantages to the DWI/PWI mismatch which include the inability to differentiate between penumbral tissue and benign oligaemia, the partial or full reversibility of the DWI-defined ischaemic injury (Kidwell *et al* 2000) and the lack of standardised viability thresholds for both DWI and PWI (Butcher *et al* 2005; Guadagno *et al* 2004).

1.3.10 Salvaging the ischaemic penumbra

The nature of the ischaemic penumbra has made it the primary focus for treatment of acute ischaemic stroke. As it is known that the penumbra is hypoperfused yet still metabolically active, it represents tissue that is at risk of infarction if restoration of blood flow or attenuation of the ischaemic cascade is not achieved. This means that the penumbra is tissue that can be potentially salvaged and its rescue has been associated with improvements in both neurological function and recovery (Molina and Saver 2005).

Using animal models of stroke, a vast quantity of potential neuroprotective agents have been investigated that pharmacologically target aspects of the ischaemic cascade and the pathophysiology of cerebral ischaemia. Many of these agents showed preclinical efficacy by reducing infarct size and functional deficits. However the translation of these neuroprotectants to the human condition has proved extremely difficult (Howells *et al* 2010) Preclinical data from 1026 potential stroke treatments in acute cerebral ischaemia were evaluated and showed that out of these potential neuroprotectants 603 were tested in models of focal cerebral ischaemia, of which 374 were found to show efficacy. Of these, 97 were assessed in clinical trials but only a single treatment was found to be effective in human stroke (O'Collins *et al* 2006). This treatment was thrombolysis using recombinant tissue plasminogen activator (rt-PA). rt-PA is an enzyme that catalyses the conversion of plasminogen to plasmin, which can break down the blood clot responsible for the blood vessel occlusion, reperfusing the territory of the artery and potentially rescuing the penumbra (Figure 1.13).

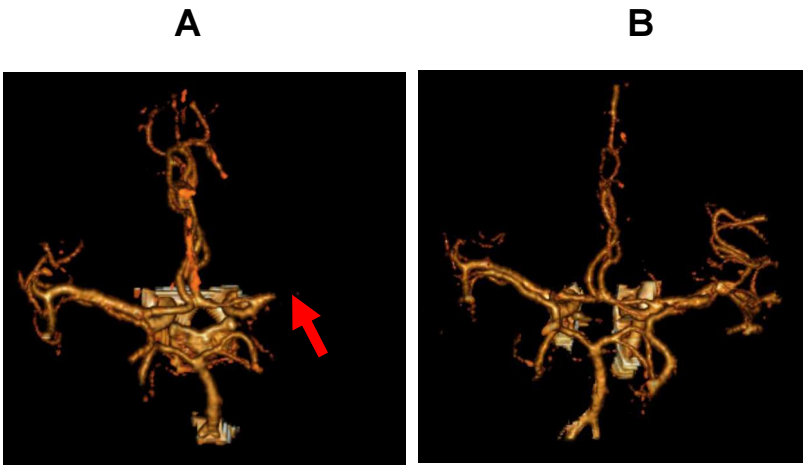

Figure 1.13: 3D CT image of the Circle of Willis of an acute stroke patient with an occluded middle cerebral artery identified by the missing vessel (red arrow) (A) and following thrombolysis (B), where flow is restored to previously ischaemic regions (Images provided by Professor K Muir, Southern General Hospital)

The National Institute of Neurological Disorders and Stroke (NINDS) trial of rt-PA found that intravenous administration up to 3 hours after stroke symptom onset improved clinical outcome and patients that received rt-PA were 30% more likely to have little or no disability after 3 months compared to placebo treated patients(1995). This trial led to the recommendation for use within this short time window (Adams *et al* 1996). The European Cooperative Acute Stroke Study (ECASS) investigated extending the time window for treatment with rt-PA up to 6 hours from stroke symptom onset. ECASS found that although functional outcome was improved in patients with a moderate to severe neurological deficit following thrombolysis, the mortality rate was higher at 30 days post stroke than the placebo treated group (Hacke *et al* 1995). This increase in mortality was partially attributed to an increased frequency of parenchymal haemorrhage and these factors led to the conclusion that rt-PA should not be administered up to 6 hours post stroke onset in an unselected population. This trial was followed by a second (ECASS II) which failed to show any neurological improvement with treatment up to 6 hours following stroke onset, similarly reporting increased risk of haemorrhage after thrombolysis (Hacke *et al* 1998). The third ECASS trial (ECASS III) reported that improvements in clinical outcome were observed in patients treated with rt-PA between 3 and 4.5 hours following

symptom onset (Hacke *et al* 2008), and subsequently the guidelines for rt-PA were adjusted to allow treatment within 4.5 hours of stroke onset (Saver *et al* 2009).

However, even with the extended time window for treatment many patients are ineligible for thrombolytic therapy, with less than 10% of stroke patients receiving rt-PA (Cocho et al, 2005; Molina and Saver, 2005). The low treatment rates are due to a number of factors including, presenting outside the time window, and lack of rapid medical assessment (Katzan et al, 2004, Kahn et al, 2005). In addition, patients are excluded if they are experiencing mild or rapidly improving symptoms, if the time of onset is unclear (due to waking with symptoms) and the concern over potential haemorrhage (Barber, 2001).The Stroke Association ran a campaign recently to raise awareness of the symptoms of stroke and the importance of getting to hospital quickly for timely treatment (Figure 1.14). The Department of Health reported that in the 2 months following the Act F.A.S.T campaign 16% of patients were arriving at hospital quicker which is imperative to increase the thrombolysis therapy rate. (http://www.dh.gov.uk/health/2012/02/act-fast/).

Figure 1.14: Example of a poster produced by the NHS to promote the Act F.A.S.T campaign which aimed to raise awareness of the common symptoms of stroke and the need to be treated quickly in hospital.

It is widely appreciated in preclinical research that physiological parameters can affect the amount of ischaemic damage resulting from MCAO. Blood gases, including PaO_2 and $PaCO_2$, and blood pressure outside the normal limits for CBF autoregulation can cause a significant decrease in global CBF which in turn can affect consequential ischaemia. Core body temperature changes have also been associated with alterations in neuronal injury (as reviewed by Macrae, 1992). Plasma glucose concentrations have also been implicated in altering ischaemic injury and this is potentially a target for managing stroke patients.

1.4 Hyperglycaemia and Stroke

Hyperglycaemia is a condition of abnormally high levels of circulating glucose dissolved in the plasma as a result of an imbalance in normal glucose homeostasis. A rise in blood sugar stimulates the release of insulin from the ß-cells of the pancreas into the circulation. Insulin acts on insulin receptors in the liver to stimulate glycogen synthesis. Insulin also stimulates glucose uptake through glucose transporters into insulin sensitive tissues, such as skeletal muscle and adipose tissue maintaining the level of glucose at a physiological level. Hyperglycaemia occurs when either the secretion of insulin is perturbed or the sensitivity to insulin of various tissues is lost.

Hyperglycaemia following ischaemic stroke is common, occurring in 60% of patients who are not diagnosed with diabetes and in 90% of diabetic patients following acute stroke (Muir *et al* 2011). Post-stroke hyperglycaemia (PSH) is a predictor of mortality and disability which is independent of age, stroke type or severity from clinical studies (Capes *et al* 2001; Weir *et al* 1997).There has been much debate about the origin of hyperglycaemia in stroke. Many initial studies proposed that the mechanism of hyperglycaemia was the result of a stress response following more severe stroke (Murros *et al* 1992; O'Neill *et al* 1991; Tracey and Stout 1994) but later larger studies failed to correlate hyperglycaemia with stress response mechanisms, anatomical location or stroke severity suggesting that this was not the case (Christensen 2005; Moreton *et al* 2007). It has been found that around 56% of patients who present with hyperglycaemia following acute stroke have an unrecognised dysglycaemic state such as impaired glucose tolerance, metabolic syndrome or diabetes (Gray *et al* 2004b).

The availability of neuroimaging techniques has provided information on the fate of the penumbra under hyperglycaemic conditions. Using the MRI based DWI/PWI mismatch for defining penumbra, blood glucose was shown to correlate with reduced penumbral salvage, greater infarct size and worse functional outcome (Parsons *et al* 2002).

Hyperglycaemia at hospital admission has also been found to be deleterious in patients treated with rt-PA. A small study (47 patients) showed that patients who experienced hyperglycaemia (blood glucose >7.7 mmol/l) prior to recanalisation, led to the DWI-defined ischaemic lesion growing 2.7 times faster than in normoglycaemic patients (Ribo *et al* 2007). Baird et al. (2003) used a similar continuous measurement of blood glucose to Ribo et al (2007) and identified persistent hyperglycaemia as an independent determinant of infarct expansion and also correlated it with reduced functional outcome (Baird *et al* 2003). Data from the NINDS rt-PA stoke trial found that admission plasma glucose levels were not associated with altered effectiveness of thrombolysis but increasing glucose levels in the blood did predict worse outcome and increased risk of intracerebral haemorrhage (Bruno *et al* 2002). The risk of haemorrhage following rt-PA, regardless of glycaemic state, is significant and has been a major factor for not extending the treatment time window of thrombolysis. Patients suffering from symptomatic or asymptomatic intracerebral haemorrhage following rt-PA treatment were found to have a higher serum glucose concentration, further suggesting that hyperglycaemia increases the rt-PA associated risk of intracerebral haemorrhage (Tanne *et al* 2002). This potentially means that in the presence of hyperglycaemia the time window for effective rt-PA could actually be much shorter than the 4.5 hours recommended currently.

1.4.1 Preclinical research into post stroke hyperglycaemia

The research investigating hyperglycaemia in animal models of stroke is extensive and generally supports the findings of clinical observations. Hyperglycaemia has been associated with increases in infarct size, brain oedema and worsening neurological scores (de Courten-Myers *et al* 1988; Kamada *et al* 2007; Lin *et al* 1998; Warner *et al* 1995). Preclinical data (de Courten-Myers *et al* 1994; Zhu and Auer 2004), indicated that hypoglycaemia is potentially as detrimental as hyperglycaemia with an optimal blood glucose level of 6-7 mmol/l in rats being suggested for minimal damage(Zhu and Auer 2004). There are a number of models of hyperglycaemia which commonly feature in the literature and these will be discussed in the subsequent sections.

1.4.1.1 Streptozotocin-induced hyperglycaemia

Streptozotocin was first identified as an agent to create a model of type 1 diabetes mellitus in the early sixties (Karunanayake *et al* 1974; Like and Rossini 1976; Rakieten *et al* 1963). Streptozotocin causes pancreatic islet cell destruction resulting in an insulin deficiency which mimics human type 1 diabetes mellitus and the severity of the ensuing diabetes is dose dependent (Junod *et al* 1969). This model of hyperglycaemia has been used in combination with focal, both transient and permanent, and global cerebral ischaemia models. In rats, using a permanent MCAO model, streptozotocin-induced hyperglycaemia (blood glucose ~30.8 mmol/l) led to a significant increase in infarct volume compared to controls (blood glucose <11.1 mmol/l) measured 48 hours post MCAO (Bomont and MacKenzie 1995). This study supported previous findings in rats using a 48 hour permanent focal ischaemia model, where severe hyperglycaemia (blood glucose ~25.3 mmol/l) induced by streptozotocin resulted in a more substantial lesion volume than control rats (Duverger and MacKenzie 1988). Nedergaard & Diemer (1987) found acute administration of streptozotocin (2 days) was not sufficient to increase infarct volume compared to normoglycaemic controls, but chronic (4 months) administration exacerbated cerebral infarction compared to control rats showing that the length of the dosing period is important. The effect of streptozotocin-induced hyperglycaemia on ischaemic injury has been seen far earlier than 48 hours after MCAO. Using serial DWI and T_2-weighted MRI from 20 minutes to 6 hours post MCAO, the rate of incorporation of tissue into the ADC-defined ischaemic lesion has been shown to be increased in hyperglycaemic animals compared to controls (Huang *et al* 1996). Quast et al (1997) also utilised MRI using single slice DWI for ischaemic damage determination and also relative CBF and CBV measurements using different MR sequences. They failed to show any difference in ischaemic injury following a 4 hour MCAO, although it seemed that the perfusion deficit changes correlated to ischaemic damage (Quast *et al* 1997). It was suggested that the effect of hyperglycaemia on cerebral ischaemia perhaps relied on the presence of collateral vessels. A study using the spontaneously hypertensive (SHR) rats, which are known to suffer from poor collateral flow, showed that chronic hyperglycaemia induced by streptozotocin had no effect on infarct volume using a two vessel (MCA and ipsilateral CCA) focal ischaemia model (Slivka 1991).

The use of transient MCAO has also been studied in streptozotocin-induced hyperglycaemic rats and has complemented the research conducted in permanent MCAO models. Nedergaard (1987) found that following temporary occlusion of the MCA proximal to the lenticulostriate branches, for 10 or 15 minutes, hyperglycaemic animals (plasma glucose >20 mmol/l) exhibited significantly larger infarcts than control animals, when assessed histologically 4 days post MCAO. Streptozotocin administration only began two days before MCAO which in a permanent model failed to exacerbate infarct volume, even though blood glucose was elevated considerably (Nedergaard and Diemer 1987). Utilising MRI to assess the potential acceleration of damage in the acute phase of cerebral ischaemia it has been shown that streptozotocin-mediated hyperglycaemia augments DWI-defined ischaemic injury compared to controls following 1 hour of MCAO and subsequent reperfusion (Huang *et al* 1996). Interestingly the damage in hyperglycaemic animals following transient MCAO was more pronounced than after permanent MCAO up to 3 hours post occlusion suggesting that hyperglycaemia may stimulate or enhance reperfusion injury mechanisms. Similarly, following 1 hour of MCAO and reperfusion, streptozotocin-mediated hyperglycaemia increased final infarct volume by 41% compared to control rats. This was associated with a diminished restoration of CBF in hyperglycaemic rats compared to controls potentially caused by a downregulation in cerebral vessel t-PA expression (Kittaka *et al* 1996). Quast et al (1997) utilised single-slice DWI to investigate hyperglycaemia mediated damage following transient MCAO. They observed that after a 2 hour MCAO followed by 2 hours of reperfusion DWI-defined ischaemic injury was increased by 118% in hyperglycaemic animals compared to controls, yet in a permanent MCAO model hyperglycaemia failed to have any effect (Quast *et al* 1997). Another study utilising MRI showed that 5 hours after MCAO (2 hour occlusion followed by 3 hours reperfusion) DWI-defined ischaemic injury was significantly augmented compared to controls and this was associated with a larger area of no-reflow similar to what Kittaka et al (1996) had reported (Wei and Quast 1998). A high frequency of seizures following streptozotocin-induced hyperglycaemia has been observed following transient MCAO, occurring in up to 40 % of the hyperglycaemic animals (Li *et al* 1998). The effect of streptozotocin-induced hyperglycaemia in transient MCAO consistently produces a greater effect on the expansion of ischaemic injury and infarction than following

permanent MCAO. A recent meta-analysis highlighted that the effect estimate for infarct volume was 55.2 in permanent MCAO compared to 319.1 for transient MCAO for streptozotocin induced hyperglycaemia (MacDougall and Muir 2010).

1.4.1.2 D-glucose administration mediated hyperglycaemia

D-glucose administration has been used widely to model the effects of hyperglycaemia on cerebral ischaemia. Many different protocols have been used with differences in route of administration (intraperitoneal or intravenous), the dose used and the frequency of dosing. The majority of studies have administered glucose prior to induction of MCAO which has resulted in hyperglycaemia levels of between 13 mmol/l and 31 mmol/l with an average of ~23 mmol/l. A number of early studies were conducted in cats using both permanent and transient MCAO models. Infusion with glucose 1 hour prior to MCAO followed by either 8 hours of saline infusion or 6 further hours of glucose and 2 hours of saline infusion cause a marked increase in infarct size, assessed 2 weeks post MCAO, compared to controls infused with saline only (de Courten-Myers *et al* 1988). A quarter of hyperglycaemic animals receiving pre and post occlusion glucose died within 24 hours highlighting that prolonged hyperglycaemia is more detrimental and that hyperglycaemia-dependant damage is dose dependant. Further studies by de Courten-Myers et al highlighted that using insulin to reduce hyperglycaemia had a detrimental, not beneficial, effect on infarct size in animals that became hypoglycaemic following the treatment (de Courten-Myers *et al* 1994). Transient (8 hours) MCAO in the presence of hyperglycaemia was also responsible for a 10 fold increase in infarct volume compared to normoglycaemic controls with permanent MCAO. Transient (4 hour) MCAO in cats mirrored what had been seen in streptozotocin treated rats with a greater effect observed on outcome than in permanent MCAO. Although infarct volume following transient MCAO was considerably smaller in both normoglycaemic and hyperglycaemic cats than after permanent MCAO, approximately 50% of cats died prior to the experimental end point as a result of infarct expansion, haemorrhagic transformation and MCA territory oedema (de Courten-Myers *et al* 1989). However, hyperglycaemia in cats has been shown to lessen the extent of neuronal injury 6 hours after permanent MCAO compared to normoglycaemic controls (Zasslow *et al* 1989). Combs et al (1990) failed to reproduce any differences between hyperglycaemic cats, in the presence or

absence of raised plasma insulin, and normoglycaemic cats following an 8 hour permanent MCAO although a greater variability was present in the hyperglycaemic groups. This lack of consistency in the literature could be due to: the nature of the animal model; genetic heterogeneity and the use of both sexes in these studies.

The D-glucose model has also been applied to rats in conjunction with permanent or transient MCAO to investigate the effects of acute hyperglycaemic on ischaemic injury. Permanent MCAO in rats treated with D-glucose prior to ischaemia caused more extensive tissue infarction, two days post MCAO, compared to controls administered with saline (Bomont and MacKenzie 1995). However the effect of glucose loading in other studies using permanent models of MCAO have not produced the same level of evidence gathered from streptozotocin-induced hyperglycaemia in rats, with a number of studies failing to show any changes in infarct volume. Diemer (1987) found that following a permanent MCAO occlusion acute hyperglycaemia, induced by intravenous administration of 50% glucose solution 5 minutes after MCAO and the repeated intraperitoneally 2 hours post MCAO, failed to have any effect on infarct volume measured four days after MCAO. Similarly in SHR rats, no difference in ischaemic damage was seen between hyperglycaemic and control rats after permanent MCAO, although this mirrored what was seen with streptozotocin in this rat model (Slivka 1991).

Transient MCAO models have provided more consistent evidence of the detrimental effect of D-glucose-mediated hyperglycaemia in focal ischaemia. Serial DWI scanning protocols have demonstrated that after 1 hour of ischaemia followed by reperfusion the rate of DWI-defined ischaemic injury growth in hyperglycaemic rats was increased compared to normoglycaemic rats leading to a significantly greater volume of ischaemically damaged tissue (Wei *et al* 2003). This effect was attenuated by the introduction of 2-deoxyglucose which competitively inhibits glucose metabolism and reduces the level of brain lactate, the latter thought to be a primary mediator of damage under hyperglycaemic conditions (see later). Intraperitoneal injection of D-glucose 30 minutes prior to 1 hour MCAO caused an almost 3 fold increase in infarct volume compared to vehicle-treated controls which was associated with a worsening of neurological scores (Martin *et al* 2006). Liu et al (2007) investigated the acute damage

following induction of hyperglycaemia with an intraperitoneal injection of 10% D-glucose. They found that following permanent MCAO, the resulting ischaemic damage, as measured by TTC 4 hours post MCAO, was significantly more widespread that in normoglycaemic controls. However the extent of ischaemic injury following transient MCAO was again more substantial than the permanent occlusion (Liu *et al* 2007).

1.4.1.3 Limitations to the preclinical literature

Streptozotocin-induced hyperglycaemia is a model of type 1 diabetes which does not accurately reflect the pathophysiology of PSH and studies that induce hyperglycaemia using pre-ischaemic D-glucose injections or infusions may have greater clinical relevance. Generally the levels of hyperglycaemia achieved in D-glucose injection studies, which are similar to those following streptozotocin treatment, are very severe and are grossly misrepresentative of the blood glucose levels experienced by the majority of patients following stroke.

Around 56% of hyperglycaemic acute stroke patients are subsequently diagnosed with insulin resistance, manifesting as impaired glucose tolerance, impaired fasting glucose or the “metabolic syndrome,” a phenotype comprising combinations of insulin resistance, hypertension, hypertriglyceridaemia and obesity that is a significant risk factor for cardiovascular disease. The current literature assessing both PSH and insulin treatments have seldom incorporated this phenotype into the design of experiments, even though the incidence of some form of insulin resistance pathology is extremely frequent in the human disease. Models of metabolic syndrome could potentially replicate the pathophysiology more closely than has been achieved until now as the majority of human patients with PSH do not have type-1 diabetes mellitus yet 60% have insulin resistance manifesting commonly as type-2 diabetes or metabolic syndrome.

1.4.1.4 Models of the metabolic syndrome

The fatty Zucker rat was first described in 1961(Zucker and Zucker 1961). The Zucker rat strain has a spontaneous mutation (*fa* or fatty) that affects the action of the adipocyte peptide hormone leptin. Leptin is a key element in the

regulation of food intake through the inhibition of the release of hypothalamic neuropeptide Y. The Zucker rat also has a degree of glucose intolerance, variable hyperglycaemia, hyperinsulinaemia, insulin resistance and a potent tendency to obesity (Berthiaume and Zinker 2002; Ionescu *et al* 1985). These features are only seen in the homozygous *fa/fa* animals and are not seen the lean heterozygous *Fa/fa* or the homozygous *Fa/Fa* Zucker rats(Russell and Proctor 2006). The Zucker rat may be more representative of the average human stroke patient and may be a better model for post-stroke hyperglycaemia than animals treated with streptozotocin or dextrose infusions.

The spontaneously hypertensive stroke-prone (SHRSP) rat is a well characterised model of hypertension compared to its reference Wistar-Kyoto (WKY) strain. Feeding SHRSP rats on a fructose rich diet for 2 weeks has been shown to induce insulin resistance, hypertriglyceridaemia, reduced HDL and increased adiposity in addition to the known hypertension compared to the reference WKY strain (Strahorn *et al* 2005).

1.4.2 Mechanisms of hyperglycaemia-induced harm

The mechanisms by which hyperglycaemia can possibly exacerbate ischaemic brain injury have been investigated using various animal models of stroke and through clinical observations.

1.4.2.1 Reduction in CBF

In rats, induction of hyperglycaemia (plasma glucose, 39mmol/L) by intraperitoneal D-glucose injection caused a 24% reduction in regional blood flow compared to controls receiving saline (Duckrow *et al* 1985). This reduction in blood flow could not be explained purely by the increase in plasma osmolality caused by increased blood glucose since administration of mannitol, leading to a similar blood osmolality, only reduced blood flow by 10% (Duckrow *et al* 1985). Similarly in cats, but using an intravenous infusion of glucose, at 3 hours post MCAO, hyperglycaemic animals (plasma glucose, 20mmol/L) showed at 70% reduction in blood flow compared to a 34% reduction in normoglycaemic controls (Wagner *et al* 1992). The ability of glucose to reduce cerebral perfusion could therefore increase the volume of hypoperfused tissue and lead to substantially larger infarcts and greater penumbral loss. The ability of glucose to reduce

regional cerebral blood flow in this manner is comparable to the effect of diabetes on cerebral blood flow regulation. A 5% CO_2 challenge following normocapnia is known to increase cerebral blood flow in non-diabetic patients, but this effect is markedly attenuated in diabetics suggesting a loss cerebrovascular reactivity (Dandona *et al* 1978). Nitric oxide mediates cerebral vasodilation induced by CO_2 and in diabetics it has been shown that NO production is reduced (Brownlee 2001). Glucose-induced reactive oxygen species can neutralise NO, further reducing its availability for NO dependant vasodilation (Frank *et al* 2005). This suggests that post-stroke hyperglycaemia may reduce cerebral perfusion by impairing NO production or diminishing its availability.

1.4.2.2 Lactic Acidosis

In the penumbra where tissue is hypoperfused yet still viable, changes in the cerebral metabolism occur, which can lead to deleterious effects and it is postulated that hyperglycaemia can augment this, further exacerbating damage. Oxygen delivery is not adequately maintained, due to the reduction in cerebral blood flow to the penumbra, which causes a shift from aerobic to anaerobic metabolism. This leads to the production of lactic acid. Increasing the availability of glucose for metabolism causes excessive production of lactic acid and intracellular acidosis within the ischaemic tissue (Kagansky *et al* 2001). In a study on cats, normoglycaemia prevented rises in lactate due to depletion of tissue glucose (Wagner *et al* 1992). Acidosis was not markedly increased in this study until 4 hours suggesting that the effect of H^+ ions is successfully buffered in the early stages of ischaemia (Wagner *et al* 1992). Tissue acidosis may lead to more extensive ischaemic damage by enhancing production of free-radicals, activation of endonucleases leading to DNA fragmentation and altering gene expression or protein synthesis (Siesjo *et al* 1996). A clinical study using MR spectroscopy to measure lactate and choline peaks has supported this hypothesis concluding that increases in acute-subacute lactate-to-choline ratios were predicted by higher acute blood glucose concentration and a doubling of plasma glucose concentration from 5 mmol/L to 10 mmol/L almost tripled the acute-subacute lactate-to-choline ratio (Parsons *et al* 2002). This study also reported that doubling plasma glucose concentration from 5 mmol/L to 10 mmol/L increased infarct size on average by 56 $cm^3$and led to a 60% reduction in

penumbra salvage (Parsons *et al* 2002). Similar results have been found in cats following MCAO. Hyperglycaemic cats (plasma glucose, 11-17 mmol/L) had elevated lactic acid as well as reduced cerebral high energy phosphates, such as ATP, and larger infarcts compared to controls in the occluded MCA territory (Chew *et al* 1991). Mitochondria within the ischaemic penumbra may also be directly affected by hyperglycaemia leading to intracellular acidosis in the brain. In hyperglycaemic rabbits (plasma glucose, >28 mmol/L), intracellular pH was substantially reduced and NADH regeneration, a measure of the redox state, was diminished compared to controls in the ischaemic penumbra (Anderson *et al* 1999). This acidosis led to the incorporation of penumbra into the ischaemic core.

1.4.2.3 Enhancing excitotoxicity

Excitotoxicity is a major pathological mechanism in the expansion of ischaemic damage. The initiation of excitotoxicity is dependant on an excessive increase in extracellular glutamate concentration so that postsynaptic NMDA receptors and other glutamate receptors can be activated (Dirnagl *et al* 1999). This facilitates the rise in intracellular [Ca^{2+}] that precedes organelle failure and eventually cell death. In a model of forebrain ischaemia the rise in extracellular glutamate observed in the cerebral cortex following an insult was significantly larger in hyperglycaemic rats (plasma glucose, 21 mmol/L) compared with controls suggesting raised blood glucose may increase ischaemic damage by facilitating the excitotoxic mechanism (Li *et al* 2000).

1.4.2.4 Oxidative stress and Inflammation

Hyperglycaemia is known to be involved in oxidative stress and inflammation and can contribute to these pathological processes through a number of mechanisms. Firstly, hyperglycaemia can increase the production of reactive oxygen species (ROS), such as superoxide. Using a global transient ischaemic model with a glucose infusion prior to ischaemia, hyperglycaemia (plasma glucose, 20 mmol/L) caused around a 2-fold increase in neuronal superoxide production compared to normoglycaemic animals and this rise in superoxide preceded an exacerbation of cell death in CA1 hippocampal neurons (Muranyi and Li 2006). Moreover a simple glucose challenge has shown in humans to increase the

production of ROS from leukocytes as well as increase the expression of $p47^{phox}$, the key protein component in the formation of NADPH oxidase (Mohanty *et al* 2000). NADPH oxidase is the enzyme responsible for the conversion of O_2 to the superoxide anion. This rise in $p47^{phox}$ potentially could be due to glucose modulating the $p47^{phox}$ gene. Superoxide has been shown to significantly disrupt the blood-brain barrier (BBB) and increase brain oedema (Kamada *et al* 2007). During reperfusion, elevated blood glucose levels are thought to enhance ROS production, which are known to be detrimental to the BBB (Muranyi and Li 2006; Weir *et al* 1997). Kamada et al. (2007) recently demonstrated that hyperglycaemia increased production of superoxide ions as well as increasing expression of COX2 and NADPH oxidase, which are both enzymes responsible for superoxide production in the later stages of ischaemic reperfusion. Matrix metalloproteinase-9 (MMP-9) is also implicated in the proteolytic degradation of the BBB following focal cerebral ischaemia and superoxide is known to be involved in MMP-9 activation (Asahi *et al* 2001; Jian Liu and Rosenberg 2005). Hyperglycaemia therefore can exacerbate BBB dysfunction and brain oedema by augmenting oxidative stress and activity of MMP-9 (Kamada *et al* 2007).

1.4.3 Management of Hyperglycaemia

Hyperglycaemia has been associated with poorer outcome after stroke in a number of human studies and this has led to the production of international guidelines that recommend hyperglycaemia following acute stroke should be treated with insulin therapy to reduce blood glucose (Adams *et al* 2007; 2009). These guidelines have not been supported by evidence from clinical trials and there is huge variation in the protocols that stroke units and hospitals are using. Preclinical animal data are partially responsible for introduction of the guidelines suggesting tight glycaemic control is beneficial in acute stroke patients, however these data are very heterogeneous. In streptozotocin treated rats, pre-ischaemic dosing (from 2 days prior to MCAO) with glucose and insulin produced similar infarct sizes, measured 1 week after MCAO, supporting the use of insulin (Hamilton *et al* 1995). In streptozotocin treated rats, pre-ischaemic dosing (from 2 days prior to MCAO) with insulin resulted in a marked decrease in infarct volume, measured 2 days after MCAO (Bomont and MacKenzie 1995). However, more recently, no benefit was reported from insulin use in hyperglycaemic animals. This

was attributed to insulin-induced hypoglycaemia which seems to be as potentially detrimental as hyperglycaemia with the preferred blood glucose level for minimal damage lying between 6 and 7 mmol/l (Zhu and Auer 2004). In rats with transient MCAO reducing blood glucose from 8-9 mmol/l to around 3-4 mmol/l with insulin dramatically reduced subsequent cerebral infarction which contradicts the finding of Zhu et al (2004)(Hamilton *et al* 1995). However the study by Hamilton et al (1995) was conducted in rats previously absent of hyperglycaemia, which is similar to the study conducted by Izumi et al (1992) where insulin significantly attenuated lesion expansion compared to controls and this reduction was also achieved in the absence of prior hyperglycaemia. The relevance of this to PSH is unknown as subsequent clinical trials have failed to reproduce the beneficial effects of insulin.

The UK Glucose-Insulin Stroke Trial (GIST-UK) is the largest clinical trial in acute stroke addressing the management of blood glucose (Gray *et al* 2007). GIST-UK failed to produce conclusive evidence of beneficial effects of tight glycaemic control in the acute period following stroke onset. The trial used a glucose-potassium-insulin (GKI) infusion in patients presenting within 24 hours of stroke onset with blood glucose level between 6.0 – 17 mmol/l. Although a significant reduction in blood glucose was observed (mean glucose 0.57mmol/L less than controls) there was no change in mortality or secondary outcomes after 3 months. In fact patients in the GKI treatment group with the greatest reduction in plasma glucose concentration had a higher mortality rate and the infusion of saline alone was able to reduce plasma glucose (Gray *et al* 2007). The results from the GIST-UK trial are difficult to interpret due to the much smaller sample size recruited (only ~30% of intended sample size) and only minor reductions in blood glucose achieved compared to controls. The SELESTIAL (Spectroscopic Evaluation of Lesion Evolution in Stroke: Trial of Insulin for Acute Lacticacidosis) (McCormick *et al* 2010), aimed to assess the effects of GKI infusion on brain lactate levels using MRI and MR spectroscopy. The rationale for SELESTIAL was based on a previous clinical study which reported that lactic acidosis, in anaerobically metabolising tissue, is a potential mechanism for hyperglycaemia-mediated ischaemic injury acceleration following stroke (Parsons *et al* 2002). The SELESTIAL trial found that although GKI infusion significantly reduced blood glucose for around 12 hours after the start of the treatment compared to controls and attenuated the increase in brain lactate, there was no difference in

infarct volume between GKI and control groups at any time point. In addition to this there was a significant incidence of hypoglycaemia in the GKI groups even with frequent monitoring. A relationship was also discovered between the GKI treatment and intracranial artery patency which highlights a safety issue with using insulin (McCormick *et al* 2010).

Hyperglycaemia is a common finding in myocardial infarction and similar trials to those conducted in acute stroke have been conducted targeting plasma glucose. One trial found that in diabetic patients with acute myocardial infarction, an insulin-glucose infusion and subsequent insulin-based therapy reduced mortality by 52% (Malmberg *et al* 1995). Studies in patients in medical and surgical intensive care units have also shown positive effects of insulin based glycaemic control (van den Berghe *et al* 2001; Van den Berghe *et al* 2006). Van den Berghe et al. (2006) showed that intensive insulin treatment reduced mortality by 32% in patients staying more than 5 days in a surgical intensive care unit. More recent trials have failed to reproduce these results with some even reporting negative effects of intense insulin treatment (Griesdale *et al* 2009; Malmberg *et al* 2005). These findings with regards to myocardial infarction and stroke suggest that the use of insulin therapy needs further investigation before it can be recommended clinically (Gray *et al* 2007; Griesdale *et al* 2009).

1.4.4 Summary

In light of the potential risk of hypoglycaemia with insulin regimes in stroke, it is important to question whether the harmful effects of acute hyperglycaemia pertain to all stroke patients, or whether they differ in those with and without pre-existing insulin resistance. Addressing this question could potentially improve the effectiveness of glycaemic control by selecting those patients who are likely to benefit most from glucose lowering therapies.

The hyperglycaemia preclinical literature on experimental stroke reports increased infarct size which is consistent with the clinical observations from stroke patients. However, the recent systematic review by MacDougall et al (2011) highlighted the uncertain relevance of preclinical studies to the typical clinical picture of PSH with respect to whether *clinically relevant* elevations in blood glucose exacerbate ischaemic brain damage in models other than those of

type I diabetes, or whether responses are different in animals with and without features of metabolic syndrome.

1.5 Study Aims

1. To characterise and optimise rodent models for investigations of post stroke hyperglycaemia. Firstly, establish a previously described model of insulin resistance and metabolic syndrome in the lab (Strahorn *et al* 2005). Secondly, optimise a method of inducing acute hyperglycaemia in rats that led to a level of blood glucose that reflects what has been found in hyperglycaemic stroke patients by the GIST-UK clinical trial (Gray *et al* 2004b). Finally, compare two different methods of middle cerebral artery occlusion (MCAO) to decide which one should be carried forward to future experiments.

2. To determine the effects of clinically relevant levels of hyperglycaemia and insulin resistance with associated cardiovascular co-morbidities on acute ischaemic damage following MCAO using DWI and PWI MR imaging. Assess whether hyperglycaemia, in the presence and absence of insulin resistance and associated co-morbidities leads to any changes in infarct volume. Finally, to address the potential role of oxidative stress mechanisms in hyperglycaemia-mediated damage following permanent MCAO.

3. To investigate the potential mechanistic role of oxidative stress in hyperglycaemia mediated damage following experimental stroke using the SOD/catalase mimetic EUK-134.

4. Calculate thresholds for a new quantitative T_2-weighted MRI sequence for future infarct analysis.

Chapter 2 - Methods

2.1 Animals

All experiments and procedures were carried out under license from the UK Home Office (Personal Licence number 60/11925, working under Project Licence numbers 60/3759 and 60/3618) and in accordance with the Animals (Scientific Procedures) Act, 1986. Male SHRSP and WKY rats were obtained from inbred colonies in the Division of Cardiovascular and Medical Sciences at the University of Glasgow. Sprague Dawley rats were obtained from Harlan Laboratories UK. All rats were allowed a 1 week acclimatisation period before any experimentation. Rats were doubly housed in standard laboratory cages with sizzle nest and cardboard tubing. All animals were maintained on a 12:12 h light/dark cycle. Water and food were available *ad libitum*. All surgical procedures were carried out by David Tarr.

2.2 Animal preparation

On the day of surgery rats were transferred from the animal housing unit to the operating theatre. Animals were then weighed prior to induction of anaesthesia. Reproducible cerebral lesions were achieved by occluding the left middle cerebral artery (MCA). Two models of permanent focal ischaemia were used to achieve suitable lesion sizes; the intraluminal thread model (Koizumi *et al* 1986) and a distal MCA diathermy model modified from Tamura *et al* (1981).

Rats were initially anaesthetised in an anaesthetic chamber using 5% isoflurane (Baxter Healthcare Ltd, UK) in an oxygen-nitrous oxide mixture (30:70). The depth of anaesthesia was assessed by means of the withdrawal reflex, where the footpad of a hindlimb is tightly squeezed to evoke withdrawal of the foot. Once the rat showed no foot reflex upon pinching it was considered to be deeply anaesthetised and therefore safe to proceed with the surgery. Tracheotomy

A surgical tracheotomy was performed on all non-recovery animals for mechanical ventilation. The rat was transferred from the anaesthetic chamber and positioned on its back where a face mask was used to continue the delivery of anaesthetic at 2.5% – 3% isoflurane in the same gas mixture used for the initial anaesthesia. The neck area was shaved using electric clippers (Wahl, UK) and

70% alcohol was used to clean the exposed area. A small incision using blunt ended scissors was made through the skin and fascia of the neck and the trachea was exposed and isolated from connective tissue using blunt dissection techniques. Two ligatures of 2-0 thread (Sofsilk, Tyco Healthcare, USA) were loosely tied around the proximal and distal ends of the trachea approximately 1.5 cm apart. The area was dried using triangular absorbent sponge to prevent fluid entering the trachea. An incision was made between rings of cartilage using micro scissors and a catheter (Linton Instruments, UK) was quickly inserted 20 mm into the trachea. Care was taken not to advance any further than this to prevent the tube blocking off one of the bronchi. The catheter was then connected to a ventilator (Ugo Basile, Linton Instruments, UK) where the stroke volume was set to ~3 ml at a frequency of 45 strokes per minute. The lower tie and the upper tie were then both tied firmly around the trachea and catheter before the neck was stitched using 4-0 silk suture (Sofsilk, Tyco Healthcare, USA).

In experiments where the animal was allowed to recover following surgery, artificial ventilation was maintained by intubation where the tube can be removed without trauma to the trachea. The animal was removed from anaesthetic chamber and transferred to a cork board. A loop of thread, which was pinned to the board, was attached around the incisors of the rat and the board was lifted into a vertical position. A fibre optic light (Meiji Techno) was applied to the neck of the rat and the tongue was pulled to one side to allow visualization of the vocal cords and the trachea. A 16 gauge catheter (MillPledge Veterinary, UK) attached to a guide wire was then advanced into the trachea before the guide wire was removed. The catheter was attached to a ventilator at a stroke volume of ~3 ml and a frequency of 60 strokes per minute. Chest expansion was examined to confirm the intubation tube was correctly positioned in the trachea. The tube was secured by stitching it to the side of the mouth using 4-0 silk suture to prevent it being pulled out whilst manipulating the position of the rat.

Femoral artery cannulation was performed to monitor mean arterial blood pressure and blood gases. The upper part of the right hind limb was shaved using electric clippers and wiped clean using 70% alcohol. A small incision using blunt ended scissors was made through the skin and fascia and a ~15 mm section

femoral artery was isolated from the femoral vein. Two ligatures (4-0 silk suture) were loosely tied around the distal and proximal ends of the isolated artery. The ligatures were pulled tight and secured to the cork board using sticky tape and a small incision was made in the artery using micro scissors. With the aid of right-angled sharp forceps a polythene catheter (Portex, UK) was inserted into the vessel and advanced approximately 2-3 cm along the vessel. Both ligatures were secured tightly around the vessel and the inserted catheter. Excess thread was removed before closing the wound with 4-0 thread to prevent the tissue drying out. The catheter was connected to transducer linked to a computer where physiological parameters including heart rate and blood pressure were recorded.

The femoral cannulation procedure was also performed on the femoral vein for drug administration in Chapter 5.

2.3 Focal cerebral ischaemia

2.3.1 Intraluminal filament model of MCAO

Occlusion of the middle cerebral artery (MCA) using the intraluminal filament was performed according to the method first described by Koizumi et al (1986) with subsequent modifications (Longa *et al* 1989)(Figure 2.1). All of the surgery was performed under a light microscope. The common carotid artery (CCA) was isolated through the same site used for the tracheotomy. If the animals were intubated the neck area was similarly prepared and an incision was made through the skin and fascia. A 4-0 thread ligature was fastened around the CCA at the bifurcation of the external carotid artery (ECA) and the internal carotid artery (ICA). The ECA was then tied off using a 4-0 silk suture at an intermediate point between the ascending pharyngeal artery and the lingual and maxillary branches. The three branches from the ECA were cauterised and then cut with microscissors. The ECA was then sealed off using diathermy forceps distal from ligature and then cut with micro scissors to allow manipulation of the vessel. Connective tissue was dissected bluntly from around the area of CCA bifurcation and the ICA. The occipital artery branching from the ICA was cauterised using diathermy forceps and then cut using micro scissors. A loose tie (4-0 silk thread)

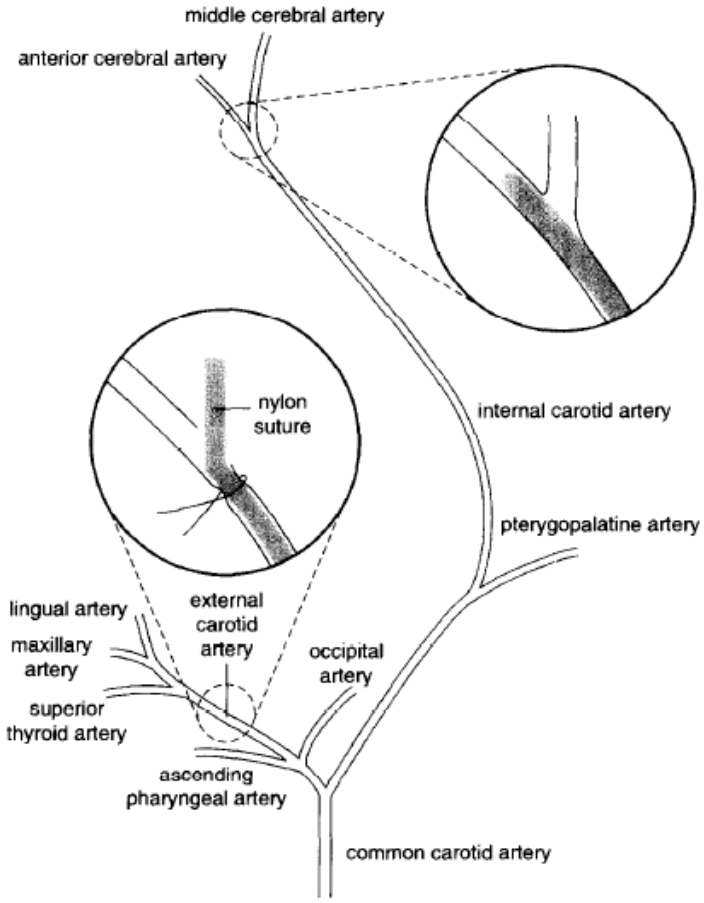

Figure 2.1: Diagram of the intraluminal thread model of MCAO. The external carotid artery is ligated and all branches are transected to allow the artery to be manipulated for ease of passage of the nylon monofilament. The pterygopalatine artery is ligated and the monofilament is introduced into the internal carotid artery. The filament is advanced along the internal carotid until it lodges in the narrow proximal anterior cerebral artery, where it blocks the origin of the middle cerebral artery. This method of MCAO can be transient or permanent. Image reproduced from Hunter et al (1995).

was then placed around the ICA and secured with enough tension to prevent flow. The pterygopalatine artery was identified and a suture (4-0 silk thread) secured around the origin of the artery where it meets the ICA. Tension was applied to both the ECA tie and the CCA tie to create a triangle with the ICA. A small incision was made near the base of the ECA using micro scissors and a filament was introduced through the incision. The filament was then advanced into the ICA and before continuing to advance the filament 22 mm up the ICA. Once inserted 22mm the incision site was electrocoagulated closed and the loose ICA tie was tied firmly. Excess thread was removed before closing the wound with 4-0 silk thread to prevent drying out.

2.3.2 Distal MCA Diathermy Model of MCA occlusion

The animal was positioned laterally with the side of head in clear view. The left eye was sutured closed (4-0 thread, Sofsilk, Tyco Healthcare, USA) to prevent it from drying out during surgery. The skin between the left eye and auditory canal was shaved using electric clippers and wiped clean using alcohol wipes. A small incision was made at the midpoint between the auditory canal and the left orbit above the longest whisker at the side of the face. Using sharp-ended scissors the underlying connective tissue and muscle were dissected until the skull was clearly visible. Retractors were used to pull the muscle back to create a large enough working area for the exposure of the MCA. The surrounding connective tissue and muscle was further removed from area and protected from drilling using pieces of absorbent sponge (Surgiswabs, John Weiss International). A dental drill (Volvere Vmax, Nakanishi Inc) was used to perform a craniectomy of the exposed area. Drilling was conducted in an up and down manner over the surface of the skull with little pressure to prevent premature puncturing of the skull and damage to the brain. The drilling process continued until the MCA and inferior cerebral vein (ICV) were visible through the skull. The remaining thin layer of skull and the dura were then removed carefully using a dural hook. If bleeding occurred from small vessels of the dura or those surrounding the MCA sterile saline (0.9%, Baxter Healthcare Ltd) was applied to the area to help cease the bleeding. If this failed then absorbent sponge was used to apply gentle pressure or the vessels were electrocoagulated using diathermy forceps. The point at which the MCA crossed the ICV was identified and the MCA was

electrocoagulated with diathermy forceps 2 mm distally from this point. Following this the MCA was cut with microscissors to confirm a complete occlusion. The absorbent sponges and retractors were then removed from working area and haemostatic sponge (Spongostan™, Ferrosan UK) was used to cover the craniectomy site. The muscle was then allowed to close over and the skin was sutured together (4-0 thread, Sofsilk, Tyco Healthcare, USA).

2.3.3 Physiological monitoring

Whilst under anaesthesia a number of physiological variables were monitored. Temperature was monitored using a rectal thermocouple and was maintained at 37±0.5°C using a heat lamp. Blood gases were measured immediately after the femoral artery was cannulated and each hour after this point until the end of anaesthesia. Blood gases and pH were maintained within a defined range [$PaCO_2$ 35-45 mmHg, pH 7.35-7.45]. PaO_2 remained outside the normal physiological range of 80-100 mmHg due to the high percentage of oxygen ventilating the animals. For this reason PaO_2 was recorded to confirm no group differences being observed. The blood gases and pH were maintained by altering the output parameters of the ventilator. Blood pressure was monitored using a pressure transducer in combination with an MP150 Biopac system and AcqKnowledge software (Linton). Mean arterial blood pressure was maintained within the range of 85-95 mmHg in Sprague Dawley and WKY rats and within the range of 105-115 mmHg for SHRSP rats.

2.3.4 Recovery of animals from anaesthesia

In animals that were recovered from surgery once the experimental protocol was completed, including the removal of the femoral artery cannula, the isoflurane concentration was reduced before being discontinued completely. The animals would then be ventilated with 50-50 oxygen-nitrous oxide mixture until responsiveness to foot pinching was observed and that the animal had started to breathe without the ventilator. At this point the animal was disconnected from the ventilator and subsequently the intubation tube was removed. A face mask was then applied to the animal (50-50 oxygen-nitrous oxide) until some motor function had been restored. The animal was then transferred to a clean cage

with soft bedding, softened rat chow and water available *ad libitum*. The cage was transferred to a recovery room maintained at ~ 25 ºC where it remained until the animal was killed. The animal was checked every hour post-operatively for the next 3 hours and details of its recovery were recorded on animal recovery sheets.

2.4 Brain Processing

2.4.1 Perfusion fixation

Rats were transcardially perfused with fixative to allow histological examination of the brain following focal cerebral ischaemia. Animals were deeply anaesthetised in an anaesthetic chamber with 5% isoflurane in an oxygen-nitrous oxide (30:70) mixture before being transferred to an absorbent tray and placed on a face mask for continuation of anaesthesia. An incision was made at sternum using blunt ended scissors. The rib cage and diaphragm was subsequently cut and the rib cage retracted to expose the chest cavity. Once cleared of connective tissue the heart was grasped with forceps and a blunt-ended 16 gauge needle, attached to a perfusion fixation set-up, was inserted into the base of the heart through the left ventricle and advanced into the aorta. The needle was secured in place with a clamp and the right atrium was cut to allow drainage of blood. Perfusion was started with heparinised (5 ml/litre) saline (0.9 %, 300 ml) at a pressure of approximately 100-150 mmHg. When the blood was cleared from the body, paraformaldehyde (PAM) (4 % in 50mM phosphate buffer, 300 ml) was perfused at the same pressure. Spontaneous movement and a lightened colour of the liver were indicative of a successful perfusion fixation. After fixation rats were decapitated and the heads immersed in 4 % PAM for 24h – 48h before removing the brains. The brains were kept in 4 % PAM for a minimum of 24h prior to further processing.

2.4.2 Tissue Processing

Following perfusion fixation brains were transferred to an automatic processor (Tissue-Tek VIP, Miles Scientific) which cycled through alcohols to allow dehydration and then into xylene which acts as a clearing reagent. Brains were

then submerged in liquid paraffin wax at 60°C. The entire process takes 59 hours to complete (Table 2.1). Brains were then submerged in liquid paraffin wax at 60°C.

Station	Solution	Temperature	Time
1	70% Alcohol	35°C	2 hours
2	80% Alcohol	35°C	3 hours
3	96% Alcohol	35°C	4 hours
4	Absolute Alcohol	35°C	4 hours
5	Absolute Alcohol	35°C	5 hours
6	Absolute Alcohol	35°C	5 hours
7	Absolute Alcohol	35°C	6 hours
8	Xylene/ Abs Al	35°C	4 hours
9	Xylene 1	35°C	5 hours
10	Xylene 2	35°C	5 hours
11	Paraffin wax 1	60°C	5 hours
12	Paraffin wax 2	60°C	5 hours
13	Paraffin wax 3	60°C	6 hours

Table 2.1: The tissue processing procedure

2.4.3 Tissue embedding and sectioning

The brains are then removed from the processor and individually housed in small containers where they were embedded in liquid paraffin wax and left to cool. Once the paraffin had set the embedded brains were removed from their containers and mounted onto wooden blocks. Each brain was cut coronally into 6 µm sections using a microtome (leica) and mounted onto poly-l-lysine coated glass slides.

2.4.4 Haematoxylin and eosin histological staining

Brain sections from each of the eight pre-determined coronal levels were stained with haematoxylin and eosin (Surgipath, UK) and assessed for lesion size (Table 2.2). Sides were placed in a rack and submerged in 100% Histoclear (National Diagnostics) for 30 minutes with regular agitation. The sections were then rehydrated by being immersed in 100 % alcohol for 2 minutes followed by 90 % alcohol and 70 % alcohol for 2 minutes each. Thereafter the slides were immersed in running water for 5 minutes before being stained in haematoxylin for 4 minutes. The slides were returned to running water for 2-3 minutes or until the water ran clear. Slides were differentiated in acid alcohol for 2-3 seconds before being immersed in running water again. Slides were then transferred to Scots Tap Water Substitute (STWS) for 2 minutes then back into running water for a further 5 minutes. The sections were the dehydrated by placing in 70 % alcohol and 90 % alcohol for 2 minutes each before being stained in eosin for 4 minutes. Slides were then washed in 3 different 100 % alcohol baths for 4 minutes each and then transferred to Histoclear for 5 minutes. Coverslips were then mounted on slides using DPX mounting medium.

Solution	Time
Histoclear 1	4-5 mins
Histoclear 2	4-5 mins
Histoclear 3	4-5 mins
Absolute Alcohol 1	3 mins
Absolute Alcohol 2	3 mins
90% Alcohol	3 mins
70% Alcohol	3 mins
Wash in running water	4 mins
Haematoxylin	4 mins
Wash in running water	1-2 mins
Differentiate in acid alcohol	A few dips
Wash well in running water	3 mins
Scott's Tap Water Substitute	2 mins
Wash in running water	2 mins
Dehydrate in 70% Alcohol	2 mins
Dehydrate in 90% Alcohol	2 mins
Stain in Alcoholic Eosin (95%)	4 mins
Dehydrate in Absolute Alcohol 1	4 mins
Dehydrate in Absolute Alcohol 2	4 mins
Dehydrate in Absolute Alcohol 3	4 mins
Clear in Histoclear 1	4 mins
Clear in Histoclear 2	4 mins
Clear in Histoclear 3	4 mins

Table 2.2: Chronological list of agents used for the staining procedure

2.4.5 Determination of ischaemic damage and quantification of infarct size

The haematoxylin and eosin stained sections were viewed under a light microscope at a range of magnifications (x5, x10, x20 and x40) to accurately determine the boundary of the infarct. Morphological characteristics of ischaemic neurons compared to non-ischaemic neurons, and pallor/vacuolisation of the neuropil were identified on stained sections to delineate areas of infarction. Ischaemic neurons were identified as pyknotic (shrunken and triangular in shape) with cellular incrustations most evident at x20 magnification. Pyknotic neurons also showed an eosinphilic cytoplasm and the surrounding neuropil was disrupted and displayed pallor. Identification of the boundaries between infarcted tissue and unaffected tissue was achieved by studying the neuronal morphology combined with changes in the neuropil in the form of pallor of staining and microvacuolation. Regions of interest (ROIs) representing the ischaemic core (where the majority of cells and neuropil showed the irreversible features of ischaemic cell change, Figure 2.2B), border zone (mixed population of cells with abnormal and normal morphology, Figure 2.2C) and adjacent normal zone (normal cell morphology and neuropil, Figure 2.2A) are shown in Figure 2.2.

Areas of infarct were transcribed onto line diagrams of 8 pre-determined coronal levels with known stereotaxic coordinates (Figure 2.3, Paxinos & Watson, 1998) throughout the MCA territory and quantified using image (Image J) based on the original method by Osborne and co-workers (1987). The stereotaxic coordinates of the coronal levels were between 2.64-12.24mm anterior to the interaural line. The total lesion volume was calculated in graphical software (GraphPad Prism 4) by integration of the areas with the known distance between each coronal level, using stereotaxic endpoints of 13.20mm and 0.50mm.

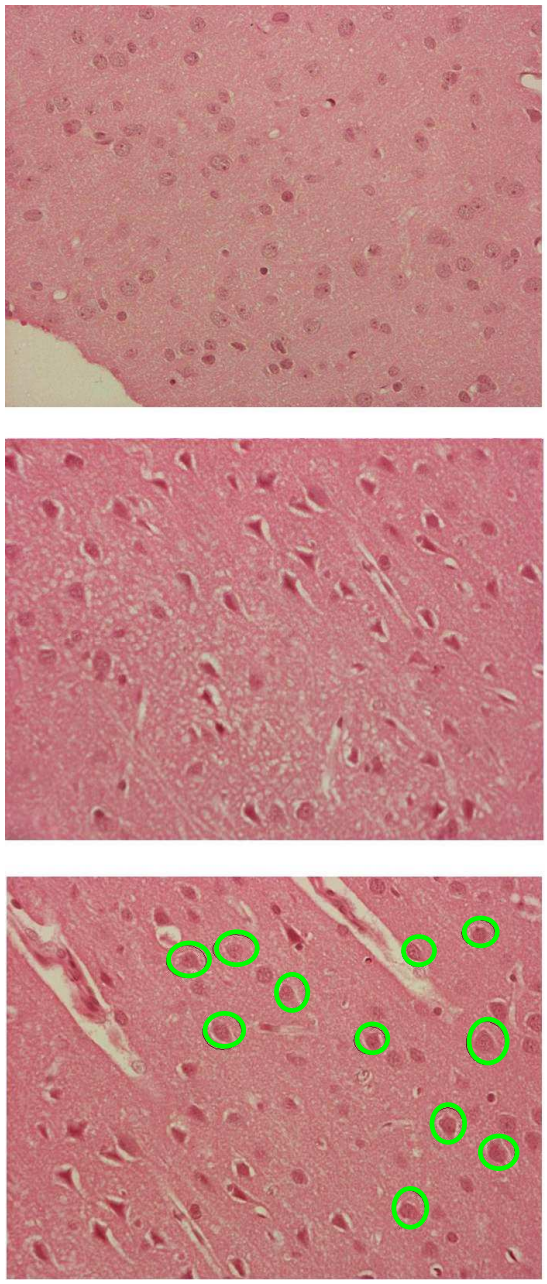

Figure 2.2: Haematoxylin and Eosin stained sections used for infarct quantification. A) shows the morphology of normal tissue, B) exhibits neurons with and C) border zone. Histological photomicrographs of ROI in dorso-lateral cortex ipsilateral to permanent MCAO from a representative animal. Pictures from haematoxylin & eosin stained sections have been captured at x 40 magnification:

a) Normal Cortex. Neurons display normal morphology;

b) Ischaemic Core. Note darkly stained triangular neurons that have the features of the ischaemic cell process within microvacuolated, pale stained neuropil;

c) Border Zone. Scattered throughout the ischaemic cortex are normal neurons (circled) which display a normal morphology

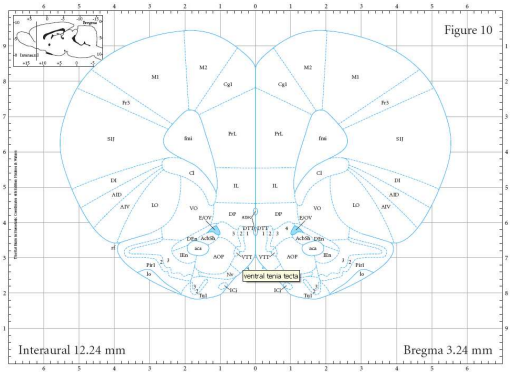

Level 1. Interaural = 12.24 mm

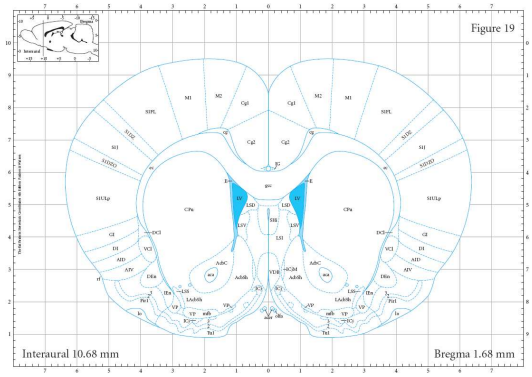

Level 2. Interaural = 10.68 mm

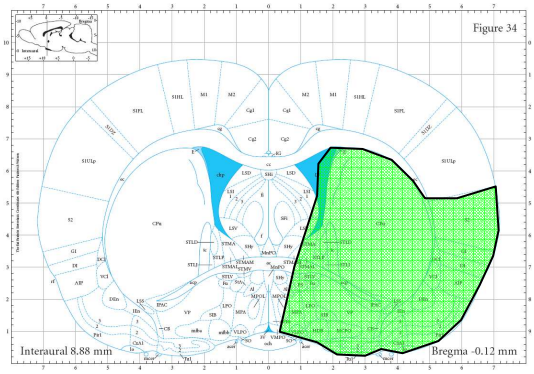

Level 3. Interaural = 8.88 mm

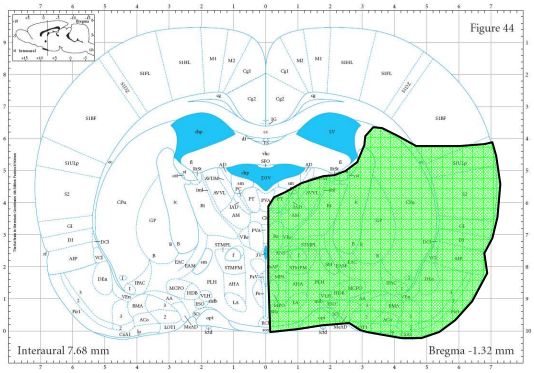

Level 4. Interaural = 7.68 mm

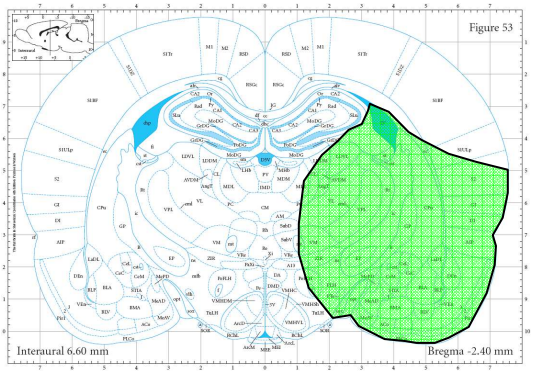

Level 5. Interaural = 6.60 mm

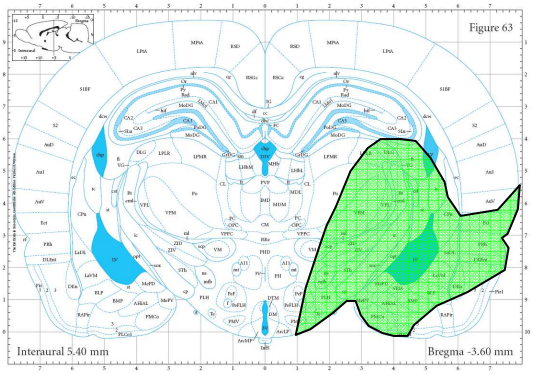

Level 6. Interaural = 5.40 mm

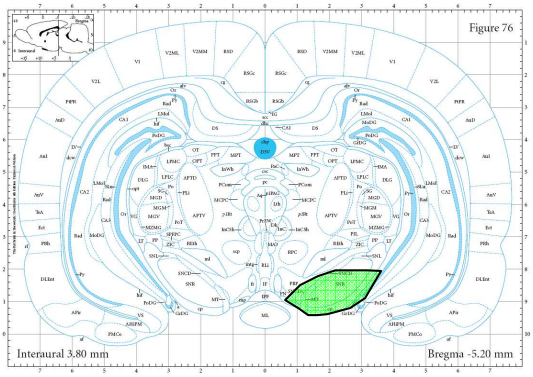

Level 7. Interaural = 3.80 mm

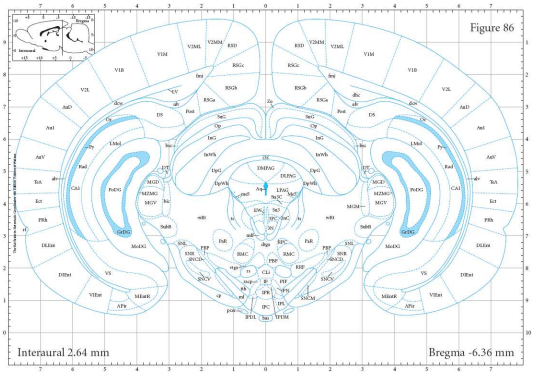

Level 8. Interaural = 2.64 mm

Figure 2.3: Line diagram comprising 8 pre-determined coronal levels with the distance from interaural of each level adjacent to it. Brain sections were collected at these levels and areas of infarct (in green) were transcribed onto the diagram (Paxinos and Watson 1998)

2.4.6 Triphenyltetrazolium chloride (TTC) staining and quantifying damage

2,3,5-triphenyltetrazolium chloride (TTC) is a colourless, water-soluble salt which is oxidised by mitochondrial dehygrogenases, to a lipid soluble bright red formazan. In undamaged tissue, TTC is reduced to formazan which stains a deep red. The intensity of the stain reflects the functional activity of the mitochondria. In infarcted tissue, where the mitochondrial systems are non-functional, TTC is remains colourless and so no staining is observed (Figure 2.4). TTC is effective in assessing infarct volume at 24 hours after cerebral ischaemia.

The animal was anaesthetised with 5% isoflurane and decapitated for brain removal. The brain was then transferred to a freezer for around twenty minutes to make it easier to slice. Previously a rat brain matrix (World Precision Instruments, Hertfordshire, UK) had been used to slice the brain coronally with razor blades positioned 2mm apart, although this proved troublesome as the fragile slices were difficult to remove intact. The brain instead was removed from the freezer and using the matrix as a guide the brain was sliced, one slice at a time, using a single razor blade. The slices were then incubated in 2% TTC at 37^{o}C for 15 minutes. TTC staining after 24 hours of focal ischaemia displays deep red staining of normal brain tissue and white non-staining of ischaemically-injured tissue with a distinct border. The slices were stored in 4 % PAM for 24 h before quantifying the volume of ischaemic damage. Digital photographs of both sides of the slices were taken with a Canon Camcoder Mv750i. The photographs were analysed using ImageJ v1.39

Figure 2.4: TTC stained coronal slice of tissue from an animal 4 hours after permanent MCAO. The white area represents ischaemic damage

(http://rsb.info.nih.gov/ij/). The white areas corresponding to the ischaemic damage were measured from both sides of each slice and added together to give the total volume of ischaemic damage. This only works due to the slice thickness being 2 mm. TTC has been validated for use 24 hours after injury (Bederson *et al* 1986a), but it cannot accurately delineate areas of infarcted tissue as early as 4 hours after permanent MCAO. However, after 36 hours of ischaemia, infiltration of macrophages and microglia, neovasculisation and astrocytic reactions occur, which can obscure the margin of ischaemic damage (Hudgins and Garcia 1970). Also, although the extent of ischaemic damage can be assessed using this technique, there is no differentiation of grey and white matter structures, or the ability to study the consequences of ischaemia on individual cells.

2.5 Magnetic resonance imaging

2.5.1 Magnet specifications

All animals were scanned in a Bruker Biospin Avance 7T (300MHz) Magnetic Resonance Imaging (MRI) system, equipped with an inserted gradient coil (121 mm ID, 400mT/m) and a 72 mm birdcage resonator.

2.5.2 Physiological monitoring during MRI scans

Following surgery to induce MCAO, animals were placed prone in a Perspex cradle, with the head restrained using ear and tooth bars to limit movement. A linear surface receiver coil (2 cm diameter) was placed above the head of the animal. The base of the cradle, and a cover placed over the rat's body, contained water channels with circulating warm water connected to a temperature controlled combined heater and water pump. This could be pre-set for a given temperature to maintain body temperature at 37ºC. Physiological variables including core body temperature, electrocardiogram (ECG) and respiration rate were monitored with a BioTrig system (Bruker, BioSpin) which had both a command and acquisition module. Physiological input was acquired by attaching electrocardiogram leads (3M innovation) to the rat with conductive electrode gel (Sigma) and electrode adhesive pads; two were attached to the

animal's chest and a third to the inner right thigh. A rectal thermocouple was reinserted for continual temperature monitoring. The system was connected to a laptop and AcqKnowledge software used to display the cardiac and respiratory waveforms. Stability of physiological variables was determined from the waveform patterns and temperature readout, and manual control of anaesthetic levels and water heater temperature ensured maintenance of variables within the physiological range. MABP was monitored via the femoral artery cannula attached to a blood pressure transducer, which was in turn connected to Biopac (Bruker, Biospin) software.

2.5.3 Diffusion-weighted scans

2.5.3.1 Technical Specifications

Spin Echo planar (EPI) diffusion-weighted scans consisted of eight contiguous coronal slices of 1.5 mm thickness which were generated with an in-plane resolution of 260 μm. The field of view was 25 x 25 mm^2 and the matrix size was 96 x 96 mm. The gradient strengths (B values) were 0 and 1000 s/mm^2 and gradient directions were x, y and z. The repetition time (TR) was 4000.3 ms and the echo time (TE) was 43 ms. A DWI scan over the whole brain takes approximately 3 minutes.

2.5.3.2 Post processing

ADC maps were generated for each of the 8 coronal slices acquired throughout the brain (Figure 2.5). Raw datasets were initially processed using Paravision v5 (Bruker Biospin). Subsequent analysis of ADC maps was carried out using ImageJ (http://rsb.info.nih.gov.ij) software.

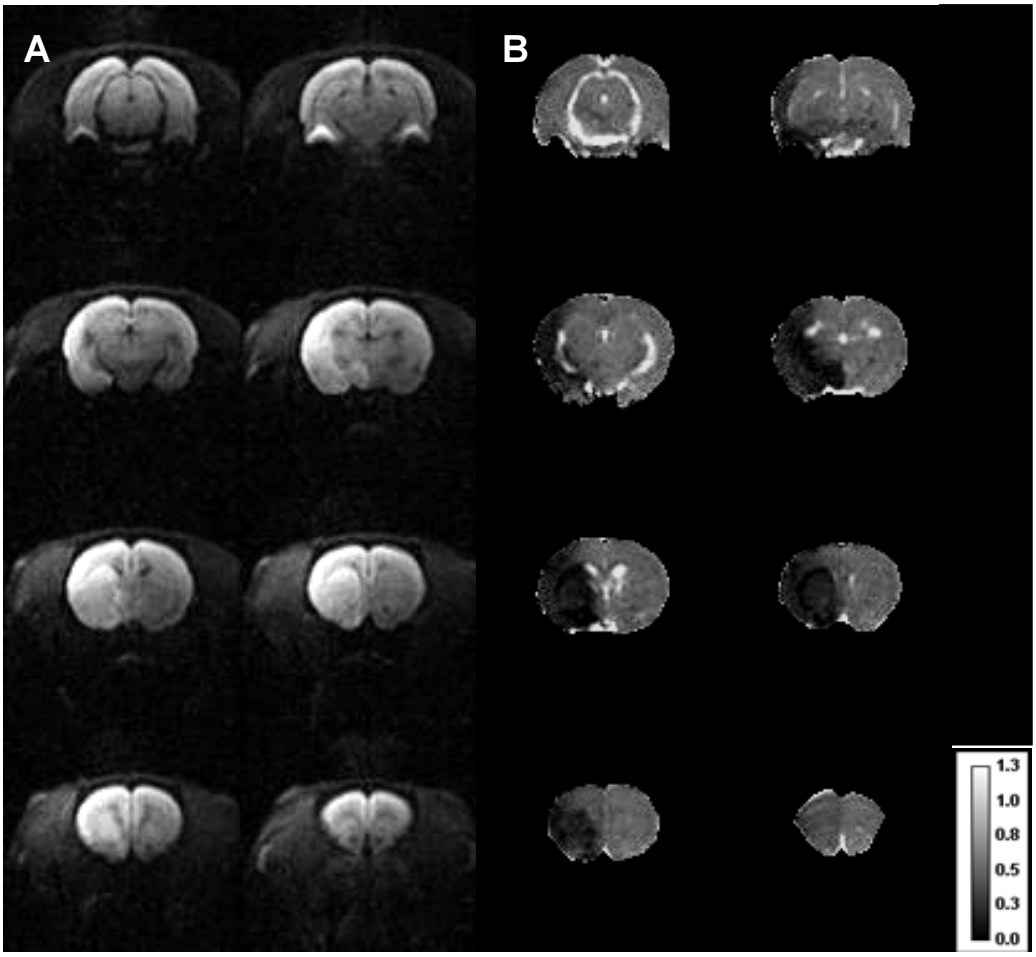

Figure 2.5: Diffusion-weighted images and corresponding ADC maps
A. DWI images of eight coronal slices from a rat brain 2.5 h following intraluminal filament model of permanent MCAO (pMCAO) and B. Equivalent ADC maps. The ischaemic damage appears bright on the DWI images and dark on acute ADC maps. ADC values expressed as x10-3 mm2/sec

2.5.4 Arterial spin labelling

2.5.4.1 Technical Specifications

Non-invasive quantitative CBF was carried out on coronal slices within the MCA territory during ischaemia, and immediately following reperfusion for Chapter 5, using a form of pseudo-continuous ASL based on a train of adiabatic inversion pulses (Moffat *et al* 2005). The sequence employs a spin-echo echo-planar-imaging (EPI) imaging module (TE 20 ms, TR 7000 ms, matrix 96 x 96, FOV 25 x 25 mm^2, slice thickness 1.5 mm, 16 averages, 4 shots) preceded by 50 hyperbolic secant inversion pulses in a 3 second train. The time taken to generate data for a single slice is approximately 5 minutes. In addition to this, a T_1-weighted image (scan time 10 minutes for the whole brain) was performed to allow quantification of CBF in mL per 100 g per minute.

2.5.4.2 Post-processing

CBF maps were generated for each of the 6 contiguous slices throughout the brain. Raw datasets were processed ImageJ software. Quantification of the CBF images was performed with use of methods described. The labelled CASL images were first subtracted from the averaged control images (subtracted CASL) and then divided by the signal intensity to generate a relative CBF map. Fully quantitative CBF maps were generated by dividing the relative CBF map by the T_1 values generated from the T_1 map (Figure 2.6). A perfusion deficit map can then be generated from the quantitative CBF map by applying a relevant threshold (e.g. 57% reduction of the mean contralateral hemisphere excluding the ventricles

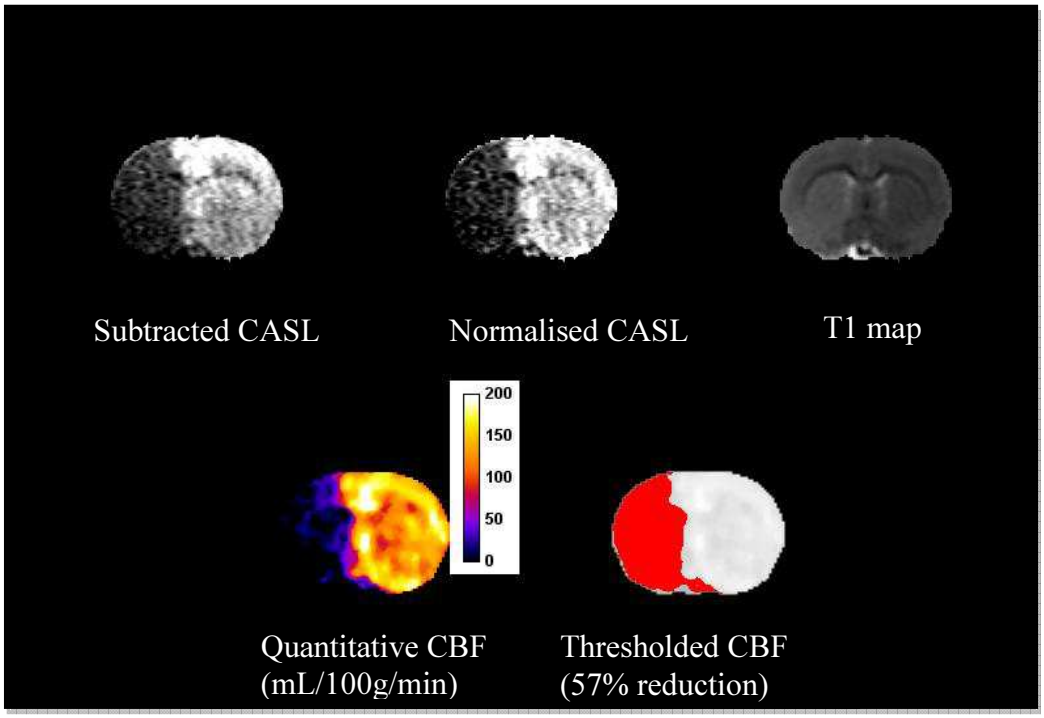

Figure 2.6: ASL Images and the corresponding T1 map generated from a rat 1 h following intraluminal filament-induced MCAO

2.5.5 T2-weighted scanning

In Chapter 5 and 6 infarct volume was determined using MRI RARE (rapid acquisition with refocused echoes) T_2 weighted imaging. T_2 weighted imaging can be reliably used to identify ischaemic brain tissue 12 to 24 hours following stroke but during the critical period of 6-12 hours, this method does not adequately assess the severity and extent of ischaemia (Baird and Warach 1998).In acute stroke, the changes in blood flow and tissue swelling which occur are associated with very subtle signal changes in T_2 images. Areas of injured tissue produce higher signal intensity than normal brain tissue allowing the infarct to be clearly distinguished.

A coronal RARE T_2 sequence (effective TE: 46.8 ms, TR: 5000 s; in plane resolution of 97 um; 16 slices of 0.75 mm thickness) was used for T_2-derived final infarct measurements. ImageJ was used to separate the images (8 slices are displayed in Figure 2.7) and the hyperintense region that represented the infarct was manually delineated using the freehand function. Measurement of individual images gave the infarct areas in millimetres squared, and infarct volume was calculated by adding up the 16 areas and multiplying by the slice thickness (0.75 mm). The area of the contralateral and ipsilateral hemisphere on each slice was also measured. The volumes of the contralateral and ipsilateral hemispheres were calculated by multiplying the total area across the 16 slices by the slice thickness (0.75mm). Total infarct volume was corrected for oedema using published equations which take compression of the contralateral hemisphere into account (Gerriets *et al* 2004), in addition to swelling of the ipsilateral hemisphere (Swanson *et al* 1990).

For the calculation of infarct volume corrected for swelling of the ipsilateral hemisphere the following equation was used:

$$\text{Corrected lesion volume} = \text{volume of contralateral hemisphere} - (\text{volume of ipsilateral hemisphere} - \text{lesion volume})$$

A correction factor which accounts for compression of the contralateral hemisphere is calculated by the following equation:

$$\text{Compression Factor} = (\text{ipsilateral volume} + \text{contralateral volume}) / (2 \times \text{contralateral volume})$$

To calculate infarct volume which is corrected for both ipsilateral swelling and contralateral compression, the following equation was used:

Infarct volume = corrected lesion volume x compression factor

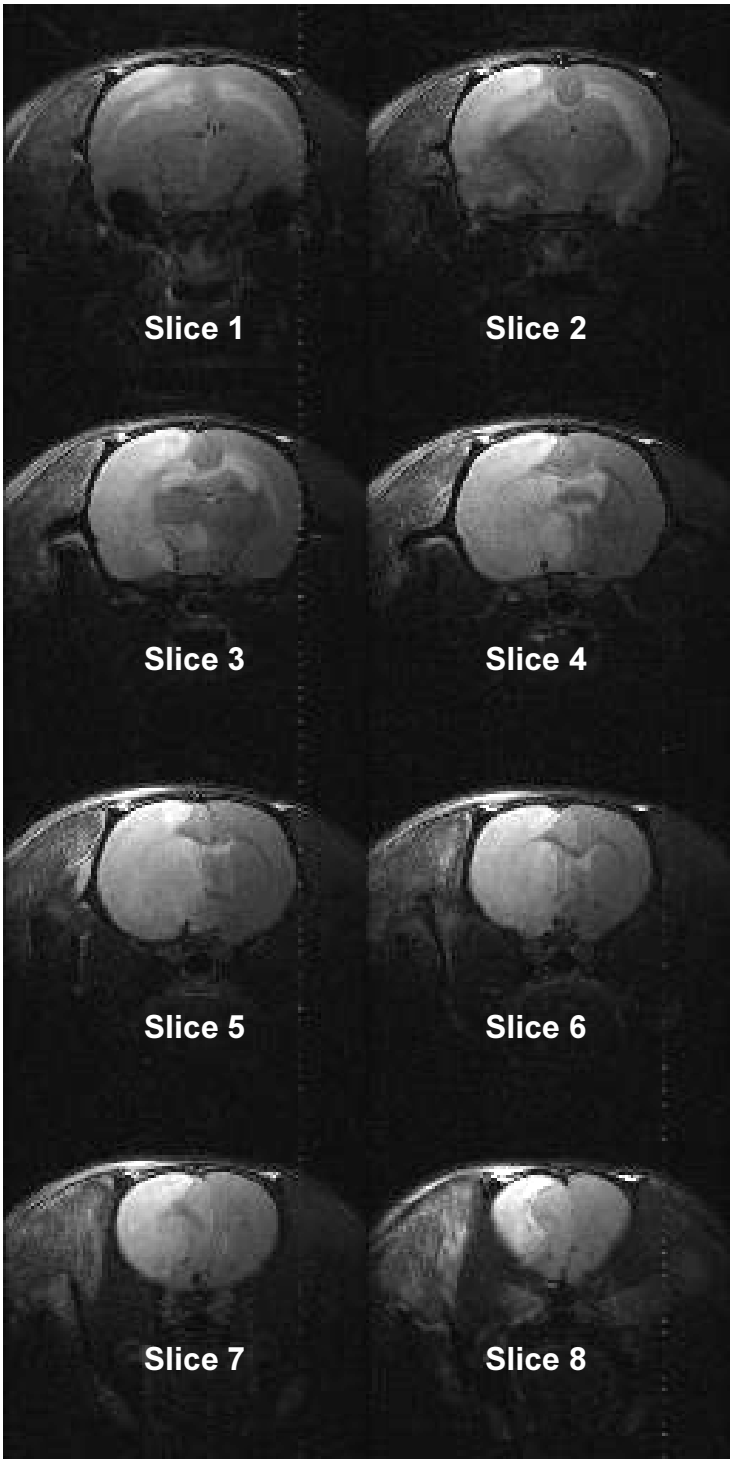

Figure 2.7: T2-weighted images of eight coronal slices (caudal to rostral) from a rat brain following intraluminal filament induced permanent MCAO at 24 hours post-ischaemia. Ischaemic damage appears bright on RARE T2 images

2.6 Measuring lipid peroxidation

Lipid peroxidation is a well established mechanism of cellular injury and is used as an indicator of oxidative stress in cells and tissues. Lipid peroxides are unstable and decompose to form a complex series of compounds including reactive carbonyl compounds. Polyunsaturated fatty acid peroxides generate 4-hydroxyalkenals (HAE) and malondialdehyde (MDA) which have been used as markers of lipid peroxidation and oxidative stress

2.6.1 4-HNE Immunohistochemistry

Immunohistochemistry for the detection of 4-Hydroxynonenal (4-HNE), which is a 4-hydroxyalkenal that has been used as an indicator of lipid peroxidation, was used in Chapter 4

Sections adjacent to those used in H&E staining were selected for immunohistochemical staining for a marker of lipid peroxidation produced by oxidative stress, 4-HNE. Sections were first dewaxed in Histoclear for a minimum of 30 minutes. Sections were then placed in citric acid (10mM, pH 6-6.2) and heated at full power in a microwave (800W) for 10 minutes. The sections were allowed to cool for 10 minutes followed before washing in running water for 5 minutes. To quench endogenous peroxidases, the sections were then immersed in 3% H2O2 in methanol solution for 20 minutes followed by two washes (2 x 5 minutes) in 50mM phosphate buffered saline (PBS, pH 7.4). Each brain section was then circled using a hydrophobic marker to help keep staining reagents localized on the tissue sections, reduce the volume needed per section and prevent mixing of reagents on the same slide. A blocking solution containing 5% bovine serum albumin and 10% normalised goat serum (Vector Laboratories) in 50mM PBS (pH 7.4) was applied to sections and incubated for 1 hour at room temperature to block non-specific surfaces. The monoclonal antibody for immunohistochemistry was specific for the 4-HNE adducted protein (4-Hydroxynonenal monoclonal antibody, Clone 198960, R&D systems). A dilution of 1:2000 of the 4-HNE primary antibody stock solution (100µg/ml) in the same blocking solution was chosen after several trial dilutions were tested. The

primary antibody was then applied to sections which were incubated overnight at 4°C. Sections were then washed in PBS (2 x 5 minutes).

Secondary antibody (biotinylated anti-mouse, BA-9200, Vector Laboratories) was made to a dilution of 1:100 in 50mM PBS (pH 7.4) and applied to each section for 1 hour before being washed in PBS (2 x 5 minutes). Sections were incubated in a streptavidin-biotinylated horseradish peroxidise complex (ABC Elite kit, Vector) for 1 hour. The sections were then washed in PBS and incubated in 3,3'-diaminobenzidine peroxidase substrate solution (DAB, Vector) for 3 minutes before being washed in running water. Finally, the sections were dehydrated in stages using graded alcohols (70%, 90%, and 100%), cleared in Histoclear, and mounted for light microscopic analysis. Two negative controls, with omission of either primary or secondary antibodies, were included in each immunohistochemistry protocol.

Sections were viewed under a light microscope. Cells that exhibited deep, intense staining compared to contralateral tissue were classed as Immunopositive for 4-HNE (Figure 2.8). Regions of immunopositivity were transcribed onto the same scale line diagrams as used in H&E infarct determination. Similarly the area of immunopositivity on each coronal section was calculated using Image J and the total volume using integration of the known distances between the coronal levels using stereotaxic endpoints of 13.20mm and 0.50mm.

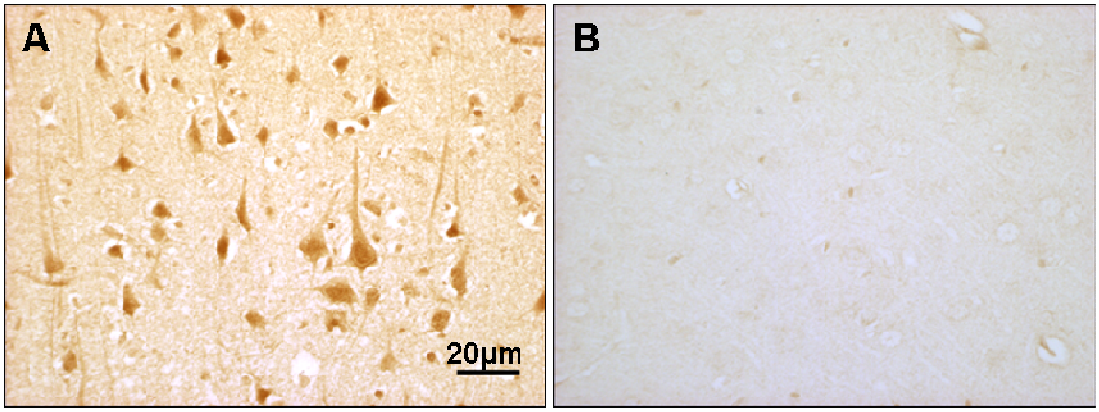

Figure 2.8: 4-HNE-immunopositivity analysis 24 h post MCAO. A) 4-HNE immunopositive cells had a staining distribution in core and peri-infarct areas. Staining was present within cell bodies and axons in grey and white matter B) Normal tissue exhibited faint staining in both cell bodies and axons and a low background contrast. Scale Bar = 20µm

2.6.2 Quantification of MDA and HAE

In Chapter 5 quantification of MDA and HAE in cerebral tissue was done using a colourimetric assay (LPO-586 Assay, OxisResearch), which is based on the reaction of the chromogenic reagent N-methyl-2-phenylindole (R1) with MDA and HAE. The reaction of MDA or HAE with N-methyl-2-phenylindole produces a stable chromophore which has a maximum absorbance at 586nm, which was measured in a spectrophotometer.

The brain was removed immediately and, using the sagittal slice from the Tri-Pilot T2 weighted scan as a guide, the section of the brain that was used for RARE T2 imaging defined-infarct volume analysis was dissected. The section was then divided into 4 ROIs. First the ipsilateral and contralateral hemispheres were separated and then subsequently divided into their respective cortex and total subcortical structures. Each ROI was transferred to a microfuge tube and snap frozen in liquid nitrogen and stored at -80°C to prevent loss of MDA and HAE and to prevent further oxidation in the sample. For each ROI, 100 mg tissue was weighed out and transferred to a fresh 2 ml microfuge tube. A titanium carbide ball was added to each tube along with 1ml of ice-cold 20mM PBS (pH 7.4) and 10 µl 0.5M butylated hydroxytoluene (BHT). The samples were then homogenised in a tissue lyser (3 x 20 seconds, 28 Hz) before being spun at in a microcentrifuge at 4°C (3000 x g, 10 minutes). The supernatant was then removed, being careful not to disturb the pellet in the bottom, and 200 µl samples were prepared in duplicate for each ROI and kept on ice. Standards of known MDA concentrations were then prepared. MDA itself is not stable as an aldehyde so the acetal, 1,1,3,3-Tetramethoxypropane (TMOP) was used to prepare the standards, which generates MDA during the acid incubation step. The TMOP stock was diluted to in deionised water prior to use to generate 200 µl of each of the standard concentrations listed in Table 2.3. To each of the ROI samples and standards 650 µl of diluted R1 (1:3, R1: diluent, ferric Iron in methanol) was added before gently vortexing. Next 150 µl of methanesulphonic acid was added and after vortexing, each tube was closed and incubated in a water bath at 45°C for 60 minutes. The samples were then removed from the water bath and centrifuged for 10 minutes at 15000 x g to produce a clear

supernatant. The supernatant was then transferred to a cuvette and the absorbance measured at 586 nm in a spectrophotometer.

Target concentration of standard in reaction mixture, μM	0	0.1	0.25	0.5	1	2	3	4
Volume of 20 μM standard to add (mL)	0	5	12.5	25	50	100	150	200
Volume of diH2O or buffer used for diluting or mixing sample to add (mL)	200	195	187.5	175	150	100	50	0

Table 2.3: Standard Curve Dilution Volumes for TMOP stock

2.7 Neurological Score

An 18 point composite neurological score was used to assess functional outcome in rats following MCAO in Chapter 5 (Garcia *et al* 1995). The test was conducted 4 days prior to induction of cerebral ischaemia for baseline assessment and then 23-24 hours post-MCAO to assess the neurological deficit present. This score comprises 6 neurological tests which assess spontaneous activity, symmetry in limb movement, forepaw outstretching, climbing ability, body proprioception and response to vibrissae touch, with each test scored with a maximum of 3 points. The scores from each test are added to give an overall neurological score, where the maximum score of 18 is achieved where there is no observable deficit and the minimum score of 3 indicates the most severely impaired animals (Table 2.4).

2.7.1 Spontaneous Activity

The rat was observed for a period of 5 minutes in its home cage with the cage top removed. The spontaneous activity of the rat was assessed by its ability to approach all four walls of the cage and was scored from 0 to 3. A score of 3 indicates that the rat moved around the cage, explored the environment and approached at least three walls of the cage. A score of 2 was given if the rat moved around in the cage but didn't approach all four walls, although it eventually reached at least one upper rim of the cage. A score of 1 indicates that the rat barely moved in the cage and didn't rise up on its hindlimbs to approach any of the cage walls and a score of 0 was given if the rat did not move at all during the observation period.

Test	Neurological Score			
	0	1	2	3
Spontaneous activity (in cage for 5 min)	No movement	Barely moves	Moves but does not approach at least three sides of cage	Moves and approaches at least three sides of cage
Symmetry of movements (four limbs)	Contralateral side: no movement	Contralateral side: slight movement	Contralateral side: moves slowly	Both sides: move symmetrically
Symmetry of forelimbs (outstretching while held by tail)	Contralateral side: no movement, no outreaching	Contralateral side: slight movement to outreach	Contralateral side: moves and outreaches less than right side	Symmetrical outreach
Climbing wall of wire cage	...	Fails to climb	Contralateral side is weak	Normal climbing
Reaction to touch on either side of trunk	...	No response on contralateral side	Weak response on contralateral side	Symmetrical response
Response to vibrissae touch	...	No response on contralateral side	Weak response on contralateral side	Symmetrical response

Table 2.4. The 18 point composite neurological score to test functional outcome in rats following middle cerebral artery occlusion**.** This neurological evaluation comprises 6 tests which are each given a score up to 3. The scores for each test are added to given an overall score of functional outcome, where the maximum score of 18 indicates no observable deficit and the minimum score of 3 indicates severe neurological impairment. Adapted from Garcia et al (1995).

2.7.2 Symmetry in the Movement of Four Limbs

Symmetry in the movement of the four limbs was assessed by suspending the rat in the air by holding the base of the tail. Scores were assigned as follows: a score of 3 was given if all four limbs extended symmetrically and scored 2 if the limbs on the contralateral side extended less or more slowly than those on the unaffected side. A score of 1 was assigned if limbs on the contralateral side showed minimal movement and 0, if the contralateral forelimb did not move at all.

2.7.3 Forepaw Outstretching

The rat was held by the base of the tail so that it had to walk along the surface of the table using its forelimbs only. The hindlimbs were kept in the air and symmetry in the outreaching of both forelimbs was observed. Scores indicate the following: 3, both forelimbs were outstretched, and the rat walked symmetrically on forepaws; 2, the contralateral forepaw outstretched less than the ipsilateral forepaw, and forepaw walking was impaired; 1, the contralateral forelimb exhibited minimal movement; and 0, the contralateral forelimb did not move at all.

2.7.4 Climbing

The rat was placed on wire grid and was then pulled off the wire by gripping the base of the tail and the strength of attachment was noted. A score of 3 was given if the rat climbed easily and gripped tightly to the wire. The rat scored 2 if the contralateral side was impaired while climbing or did not grip as hard as the ipsilateral side and a score of 1 indicates that the rat failed to climb or tended to circle instead of climbing.

2.7.5 Body Proprioception

The rat was sharply prodded with a blunt wooden pencil on each side of the body, and the reaction to the stimulus was observed. A score of ^{3} indicates that the rat reacted by turning head and was equally startled by the stimulus on both sides. A score of 2 was given if the rat reacted slowly to stimulus on the

contralateral side and a score of 1 if the rat did not respond to the stimulus at all on the contralateral side.

2.7.6 Response to Vibrissae Touch

A wooden pencil was brushed against the vibrissae on each side; the stick was moved toward the whiskers from the rear of the animal to avoid entering the visual fields. A score of 3 was assigned if the rat reacted by turning head or was equally startled by the stimulus on both sides. A score of 2 indicates that the rat reacted slowly to stimulus on the contralateral side and a score of 1 was given if there was no response to the stimulus on the contralateral side.

2.8 Glucose Tolerance Test

Glucose tolerance was assessed for a two hour period following an *i.p.* injection of 15 % glucose solution (10 ml/kg). Rats were fasted overnight (water available *ad libitum*) before commencing experiment. Rats were transferred from their cages into a heated box (26 ºC) to aid in vasodilation. Each animal was removed from the box and the medial aspect of each hind limb was shaved to expose the femoral vein and its distal branches. The area was then cleaned using alcohol wipes before a syringe needle was used to puncture the femoral vein. The drop of blood formed was analysed using the blood glucose system (Accu-Chek Aviva, Roche, Germany) to establish a baseline value for blood glucose (mmol/L). Each rat was then administered with 15 % glucose solution (*i.p.* 1 ml/100 g) and a timer started. Subsequent blood samples were collected by venupuncture at 10, 20, 30, 60 and 120 minutes post glucose load and immediately analysed using the blood glucose system. Between each measurement the rats were returned to the heated box to help maintain vasodilation. Only 3 samples were taken from each leg, one from each femoral vein and two from the distal branches of the vein to minimise damage and bruising to the vessels. The blood glucose system accuracy was checked using the appropriate control solutions at the start of each new pack of test strips.

2.9 Non-invasive blood pressure measurements

It is necessary to monitor systolic blood pressure in both the SHRSP and the WKY to ensure that the stroke-prone strain is indeed hypertensive compared to the normotensive control strain. The American Heart Association recommends indirect measurement of blood pressure to detect substantial group differences in systolic blood pressure (Kurtz et al, 2005). The tail cuff method of systolic blood pressure (BP) measurement is a non-invasive technique which was developed by the West of Scotland's Department of Clinical Physics and Bioengineering, based at the Southern General Hospital in Glasgow (Evans et al, 1994). This technique involves the placement of a cuff around the proximal end of the rat's tail which is then inflated with air until the point at which the pressure in the cuff matches that of the tail artery, resulting in a transient occlusion of the vessel. This leads to an absence of a pulse which is detected by a signal transducer, which is also located on the tail of the rat, at a more distal position than the tail cuff. The signal is relayed to a central monitoring system which is connected to a laptop (Dell, UK) which then displays the systolic blood pressure reading in mmHg and the cuff is then deflated. This technique is advantageous as it does not require catheterisation of an artery as required for direct methods of blood pressure measurement and has been validated against direct measures of blood pressure measurement (Feng et al, 2008). Furthermore, it allows BP measurements to be obtained in conscious animals without the influence of anaesthesia on BP, as is the case with invasive methods. However, there may be an element of stress associated with the mild restraint involved which will be reflected in the measurements obtained but this can be minimised by incorporating a thorough acclimatisation and training period into the regime.

2.9.1 Tail Cuff Apparatus

Prior to BP measurement, the animals must be pre-warmed to induce maximal vasodilatation of the tail artery. This is achieved by placing the animals in an insulated heat box (dimensions 37cm x 35cm x 40cm) (Figure 2.9). The upper surface of the box has a circular opening (diameter 7cm) to allow the box to be warmed to a temperature of 34oC using a hairdryer (Boots, UK). Once the

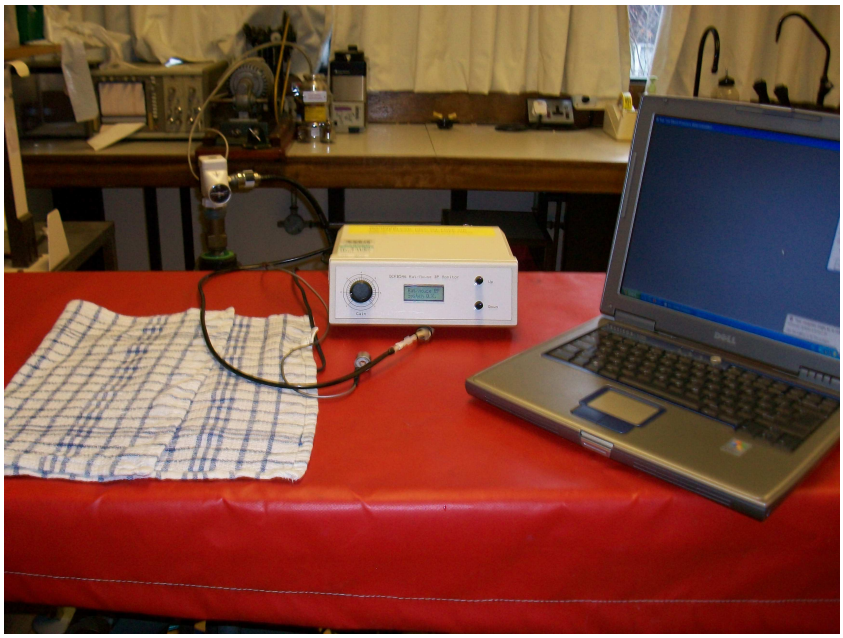

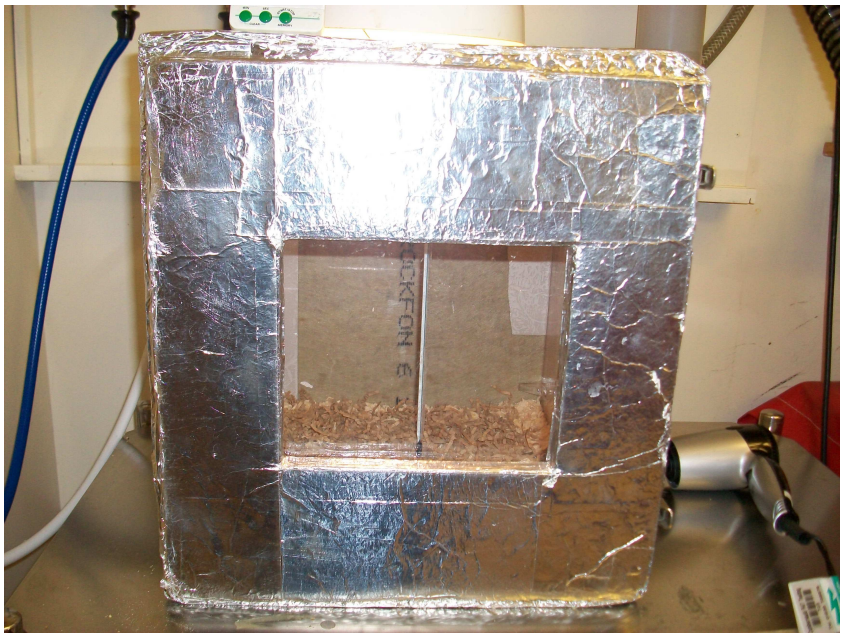

Figure 2.9: The tail cuff apparatus. The top image shows the central blood pressure monitoring system which is connected to a laptop, where the systolic blood pressure measurements are displayed and recorded. A heat mat and a towel are used to keep the rat warm and lightly restrain movement. The bottom image shows the heat box, which is pre-warmed to 34oC. The rat is placed in the box for 10-15 minutes to induce maximal vasodilation of the tail artery prior to blood pressure measurement.

desired temperature was reached it was maintained by positioning an angle poise lamp over the opening of the box and this was monitored using a thermometer situated on the inner wall of the chamber. The door on the front panel of the heat box allowed easy access to the rat in the chamber and the removable insulating tile on the door could be removed to observe the animal. Removal of the insulating tile and the angle poise lamp from the upper opening could be used to promote heat loss if the temperature rose above 35^{o}C.

The tail cuff was constructed by cutting the medial portion of a 5ml syringe (Plastipak, UK) to a length of 2cm. A length of latex tubing (length 6cm, width 1.5cm) was then inserted into the syringe. A 10 gauge catheter, cut to 4cm in length was inserted into the latex tubing and secured in place by tying 5-0 thread around the tubing. This had to be done meticulously as it was common for air to leak if the seal was not complete. The opposite end of the latex tubing was turned over to the outer face of the syringe and was secured using a plastic o-ring (1.7cm diameter) (Figure 2.10). The catheter was then connected to the central BP measurement system. The central monitoring system was also connected to a cylinder of medical air (BOC Gases, UK) via a hose, a laptop (Dell, UK) and a piezoceramic transducer (Figure 2.9).

2.9.2 Animal Training Procedure

All rats were subjected to a 2 day training period to acclimatise them to handling and the tail cuff apparatus. On day one of training each rat, were taken to the room where the tail cuff apparatus was set up, in their home cage. The rat was placed in the heat box with no heat applied and allowed to explore for 15 minutes. The animals were then handled for a period of 20 minutes and were allowed to explore the table where the tail cuff apparatus was set up. They were also wrapped in a towel to accustom them to mild restraint.

On day 2, the training procedure was as described for day 1 but the heat box had been heated to 34°C. Then the tail cuff and transducer (Figure 2.10) were positioned on the tail whilst the rat was being mildly restrained within a towel. After each day training the rats were rewarded with pumpkin seeds.

Figure 2.10: The tail cuff and transducer. The top image shows the tail cuff which is placed on the base of the tail and inflates and deflates in cycles. The bottom image shows the piezoceramic transducer which relays the blood pressure signal to the central blood pressure monitoring system.

2.9.3 Measurement Protocol

The tail cuff method was used to measure systolic blood pressure in WKY and SHRSP rats, between 1 and 3 days prior to induction of cerebral ischaemia. BP measurement was not performed on a Monday, as it had been found by a colleague that because the cages of the rats were cleaned out on this day that the animals tended to be more stressed (Emma Reid, personal communication).

Rats were placed in the pre-warmed heat box for 10-15 minutes and no longer than 20 minutes. Care was taken to regularly assess the temperature in the box by looking at the thermometer attached to the inner wall of the box. If the temperature was above 36^{o}C, then the front panel of the box was removed to aid heat loss. The front panel of the heat box also allowed the animals to be observed. The rats were deemed to be warm enough when there was very little spontaneous movement and the ears looked very pink.

At this stage the rat was removed from the box and swiftly wrapped in a towel with only the tail exposed. The rat was placed onto the heat mat to keep it warm and the tail cuff and the signal transducer were positioned on the tail (Figure 2.11). Once the rat was settled and was sitting on the heat mat, wrapped in the towel, with no need for restraint, then BP measurements were taken. The laptop was used to inflate and deflate the cuff in cycles to obtain measurements of systolic blood pressure. This was repeated until 8-10 consistent measurements of systolic blood pressure were acquired and the mean and standard deviation were then calculated. Only the most consistent measurements were used to calculate the mean systolic blood pressure for each animal. Measurements which were acquired when an animal was visibly stressed were excluded. After the tail cuff procedure, the rats were returned to their home cage and were rewarded with pumpkin seeds.

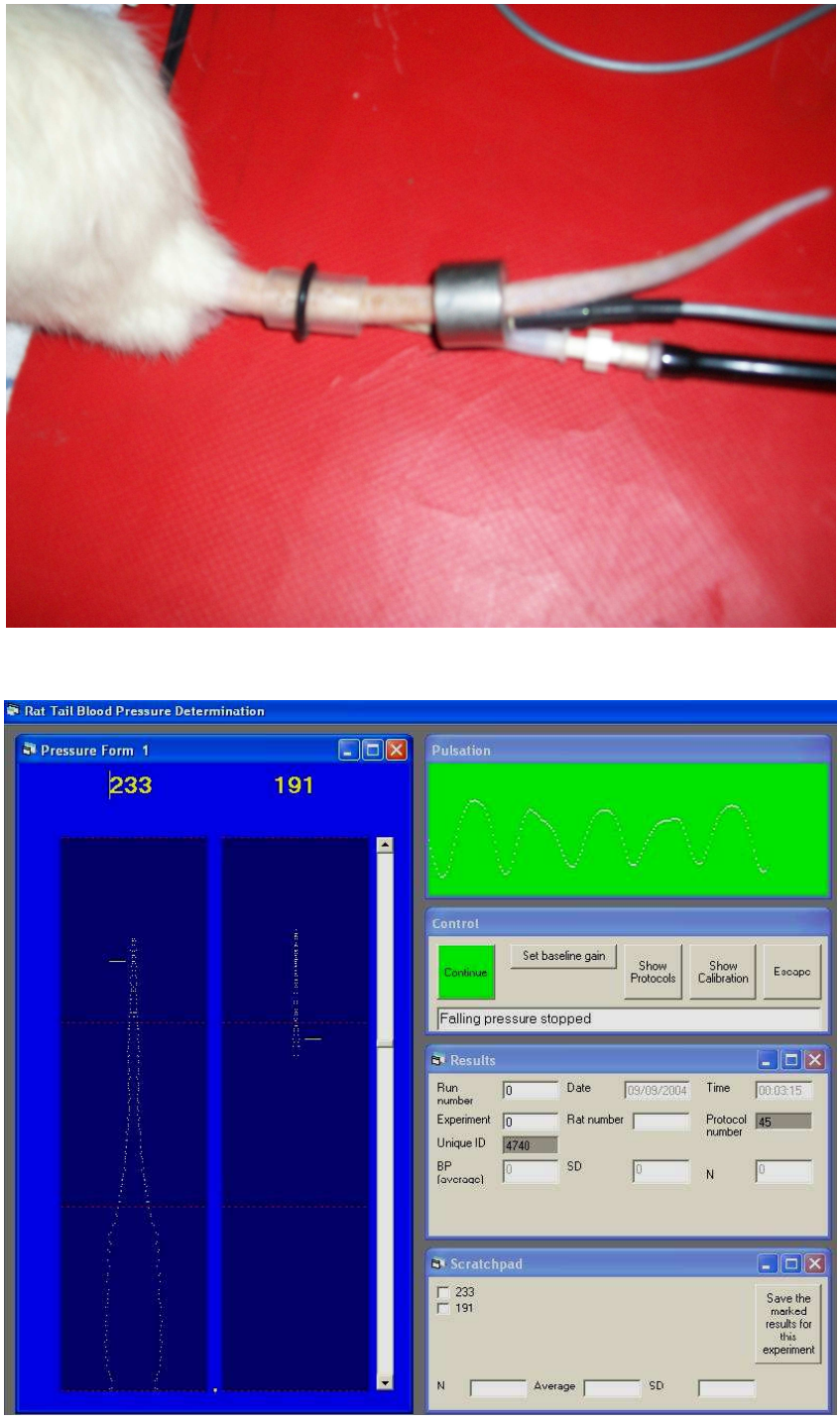

Figure 2.11: The tail cuff method of non-invasive blood pressure measurement. The top image illustrates the positioning of the tail cuff and the signal transducer on the tail of the rat, where the cuff is positioned at the base and the transducer is placed distal to the cuff. The bottom image shows the computer screen as displayed when blood pressure measurements are being recorded. The strength of the signal is shown in the green box in the top right hand corner of the display and the measurements are recorded in the box on the bottom right corner.

Chapter 3 - Optimisation of the animal models

3.1 Introduction

In this chapter data are presented for the purpose of characterising and optimising a number of rodent models for use in pre-clinical post stroke hyperglycaemia (PSH) experiments. The first aim was to set up a previously described model of insulin resistance and metabolic syndrome in the lab (Strahorn *et al* 2005). Secondly, to optimise a method of inducing acute hyperglycaemia in rats that led to a level of blood glucose that reflects what has been found in hyperglycaemic stroke patients in the GIST-UK clinical trial (Gray *et al* 2004b). Finally, compare two different models of middle cerebral artery occlusion (MCAO) to decide which one would be most appropriate for the planned studies.

3.1.1 Models of Hyperglycaemia

Hyperglycaemia has been widely studied in experimental stroke using a variety of rodent models. Intravenous streptozotocin administration has featured often in preclinical research to assess the effects of hyperglycaemia on cerebral ischaemia yet this is a model of type I diabetes which shares little in common with the mechanisms thought to be involved in PSH. Streptozotocin targets the insulin producing β cells of the pancreas leading to necrosis which in turn diminishes the capacity for insulin release (Szkudelski 2001). As a result of this loss of insulin production and release, the levels of glucose in the blood cannot be sufficiently controlled and this leads to sustained hyperglycaemia. Data included in a recent meta-analysis of studies using the streptozotocin injection model to investigate hyperglycaemia in experimental stroke showed blood glucose values were on average 25.2mmol/l (MacDougall and Muir 2010). Another method commonly used to investigate the impact of hyperglycaemia on experimental stroke relies on a bolus injection or an infusion of glucose either prior to, at the time of, or after MCAO. A variety of concentrations of glucose have been used in experimental stroke studies as well as different administration protocols. The plasma glucose values in hyperglycaemic animals using the glucose injection model were 23.4 mmol/l from the studies included in the recent meta-analysis (MacDougall and Muir 2010).

Clinically PSH rarely leads to blood glucose values above 16mmol/l (Gray *et al* 2007), which raises the question of how pertinent studies that use much higher levels of blood glucose are to the typical clinical scenario. Similarly as type II diabetes accounts for approximately 90% of all diagnosed cases of diabetes, the streptozotocin-induced hyperglycaemia model has little pathophysiological relevance to that seen most commonly in stroke patients. Developing a model that consistently produces clinically relevant blood glucose values for assessment of PSH is imperative for future experimental studies.

3.1.2 Rodent models of insulin resistance and metabolic syndrome

Approximately 56% of acute stroke patients who develop hyperglycaemia are subsequently diagnosed with insulin resistance which is known to manifest as impaired glucose tolerance, impaired fasting glucose or the "metabolic syndrome"(Gray *et al* 2004b; McCormick and Muir 2006). Previously spontaneously hypertensive stroke prone rats (SHRSP) fed on a 60% fructose diet, compared to their reference Wistar-Kyoto (WKY) strain, have been shown to develop insulin resistance, hypertension, elevated plasma triglyceride levels and reduced high density lipoprotein (HDL) cholesterol, all of which are features of the metabolic syndrome (Strahorn *et al* 2005). This model encompasses the majority of features of the metabolic syndrome which makes it an excellent model for investigating the role of insulin resistance and other co-morbidities in pre-clinical stroke research. The combination of a model of insulin resistance with and without acute clinically relevant hyperglycaemia following cerebral ischaemia offers an opportunity to investigate the effects of hyperglycaemia with and without insulin resistance and commonly occurring associated stroke co-morbidities.

3.1.3 Different models of MCA Occlusion

It is important to use a model of focal cerebral ischaemia that is suited to the research questions being posed. Subsequent studies in this thesis aim to use a model of middle cerebral artery occlusion (MCAO) to assess the expansion of the lesion and loss of penumbral tissue in the acute phase of ischaemic damage. The

intraluminal filament method of MCAO is known to produce substantial infarcts especially in the SHRSP and WKY strains. This arises from blocking the origin of the MCA leading to extensive damage in the caudate nucleus and other subcortical regions as well as a large proportion of the cortex. In-house studies of this MCAO model using diffusion weighted imaging and perfusion weighted imaging have shown that commonly almost the entire ipsilateral hemisphere can be considered ischaemically damaged with very little penumbra as defined by diffusion-perfusion mismatch even as early as 1 hour post occlusion in SHRSP rats. Such a large initial lesion could therefore restrict the ability to detect a detrimental influence of hyperglycaemia or other co-morbidities on infarct expansion due to a “ceiling effect” since maximal damage could already be achieved in the absence of raised blood glucose. Using a different model of focal cerebral ischaemia may allow for smaller initial lesions that have more potential to extend into the area of hypoperfusion, in turn perhaps unmasking any acceleratory effect of hyperglycaemia on penumbral loss and lesion expansion. Diathermy of the MCA distal to the origin has the potential to cause smaller cortical lesions which may lead to proportionally more penumbra than seen in the intraluminal filament model. It was important therefore to evaluate the amount of diffusion –perfusion mismatch defined penumbra in the acute time period following diathermy of the MCA and similarly to compare the size of the lesions and reproducibility of each model. This information could then be used to inform on the model that should be taken forward for future experimentation.

3.1.4 Study Aims

Study 1: Glucose tolerance test and lipid profile analysis

To establish the fructose fed SHRSP model in the lab by confirming the presence of insulin resistance compared to the reference WKY strain. Secondly to confirm the differences in the blood lipid profile between the fructose fed SHRSP and the WKY rat strains.

Study 2: Investigate normo- and hyperglycaemia after MCAO under isoflurane-induced anaesthesia

To ascertain a glucose dose that would induce clinically relevant levels of hyperglycaemia following MCAO using a single glucose load.

Study 3: Comparison of the intraluminal filament model and the distal diathermy model of MCAO occlusion

To investigate the most suitable model of permanent focal cerebral ischaemia for the proposed study; the intraluminal filament model or the distal diathermy model.

3.2 Materials and Methods

All experiments were carried out under licence from the Home Office and were subject to The Animals (Scientific Procedures) Act, 1986. For studies 1 and 2, male rats (9 weeks old) were obtained from breeding colonies of SHRSP and WKY within the Institute of Cardiovascular and Medical Sciences, University of Glasgow and allowed a one week acclimatisation period upon arrival. SHRSP were then fed on a 60% fructose diet for 2 weeks prior to any experimentation. WKY were fed on standard rat chow and both food and water were available *ad libitum* to both groups of animals. All experiments were conducted when rats were 12 weeks of age. Male Sprague-Dawley rats (250-300g, Harlan, Bicester, UK) were used in study 3 for comparison of the two MCAO occlusion models. This was due to limited supply of male WKY and SHRSP rats from the breeding colony.

3.2.1 Glucose tolerance test and lipid profile analysis (Study 1)

Fructose fed SHRSP (ffSHRSP, n=6) and WKY (n=7) rats were fasted overnight then weighed on the morning of the test. The rats were placed in a Perspex incubator set at 37°C for 20 minutes to allow for peripheral vasodilation. The hind limbs were then shaved and swabbed with alcohol so the femoral vein could be visualised. The glucose tolerance test was then performed as previously described in Chapter 2.8. Upon completion of the test rats were anaesthetised in a Perspex chamber using 5% isoflurane before being transferred to a facemask where anaesthesia was maintained at this concentration. An incision into the chest was made and the diaphragm cut away from the ribcage. The ribcage was then cut back towards the neck to expose the heart. Terminal blood samples were taken via cardiac puncture and these samples were spun in a centrifuge (3 min, 10000 rpm). The plasma was removed and immediately frozen and stored at -80°C. Once all the samples were collected insulin and lipid profile analysis was conducted on the plasma as described in Chapter 2.

3.2.2 Investigating normo- and hyperglycaemia after MCAO under isoflurane-induced anaesthesia (Study 2)

WKY rats were randomly assigned to either glucose (WKY + G, n = 6) or vehicle (WKY, n = 6) treatment groups. Fructose fed SHRSP rats were also randomly assigned to glucose (ffSHRSP + G, n = 6) or vehicle (ffSHRSP, n = 3) groups. Animals were fasted overnight prior to experimentation to improve reproducibility in baseline blood glucose values. Animals were anaesthetised with 5% isoflurane in a Perspex chamber and then orally intubated. They were then mechanically ventilated with 2.5% isoflurane in a nitrous oxide-oxygen mixture (70:30). Blood gases were maintained within the normal physiological range apart from increased PaO_2 due to the oxygen enriched mixture used to maintain physiological stability throughout the experiment. A rectal thermocouple provided continual monitoring of core body temperature that was maintained at 37°C±0.5°C. A polyethylene catheter (Portex: external diameter 0.96mm; internal diameter 0.58mm; 20cm long) was placed in the right femoral artery, to continuously monitor blood pressure and conduct blood gas analysis.

A single dose of a 15% glucose solution (in distilled water, 10ml/kg) was administered i.p. 10 minutes prior to occlusion of the MCA to WKY + G and ffSHRSP + G groups. Their respective control groups, (WKY and ffSHRSP) received vehicle (distilled water, 10ml/kg). This dose was selected based on results from the glucose tolerance test, as in conscious rats it lead to a peak blood glucose concentration of between 12 and 16 mmol/l, which was within the clinically relevant range in stroke patients.

After occlusion of the MCA, anaesthesia was maintained for 4 hours whilst arterial blood samples were taken for blood glucose analysis. Animals were then recovered before being perfuse fixed with 4% paraformaldyhyde 24 h post MCAO. The brains were removed and subjected to further tissue processing (Chapter 2.4.3) before being embedded in paraffin wax. Each brain was cut using a microtome into coronal sections (7 µm) at 8 predefined anatomical levels spanning the MCA territory. These sections were stained using haematoxylin and eosin as described in Chapter 2.4.4. The areas of ischaemic damage from these sections, identified using light microscopy (x 400), were transcribed onto

representative line diagrams before being scanned into Image J for infarct quantification as described in Chapter 2.4.5.

3.2.3 Comparison of the intraluminal filament and the distal diathermy models of middle cerebral artery occlusion (Study 3)

Male Sprague-Dawley rats (n=6) were initially anaesthetised with 5% inhaled isoflurane delivered in a nitrous oxide-oxygen mixture (70:30) in an induction chamber at room temperature. A surgical tracheotomy was performed and the animals were mechanically ventilated with 2.5% isoflurane in a nitrous oxide-oxygen mixture (70:30). A polyethylene catheter (Portex: external diameter 0.96mm; internal diameter 0.58mm; 20cm long) was placed in the right femoral artery, to continuously monitor blood pressure and conduct blood gas analysis. Blood gases were maintained within the normal physiological range apart from increased PaO_2 due to the oxygen enriched mixture used to maintain physiological stability throughout the experiment. A rectal thermocouple provided continual monitoring of core body temperature that was maintained at 37°C±0.5°C. Occlusion of the MCA was either induced using the intraluminal filament method (n=6) or the distal MCA diathermy model (n=6) both described previously in Chapter 2.3. Following MCA occlusion animals were maintained under anaesthesia for 4 hours. Animals were then immediately killed by overdose of anaesthesia. The brains were removed and transferred to a freezer (-18°C) for 20 minutes before being sectioned into 2mm thick coronal slices. These sections were then immersed in TTC at 37°C for 10-15 minutes as described in Chapter 2.4.6 and the areas and total volume of ischaemic injury were calculated in Image J.

One male Sprague-Dawley rat underwent MRI scanning to assess the amount of penumbral tissue created by the distal diathermy model of MCAO. Following MCA occlusion the rat was placed prone in a rat cradle and the head was restrained using tooth and ear bars to limit head movement. Body temperature was maintained for the duration of the scanning protocol using a closed circuit thermal jacket and was monitored by a rectal thermocouple. A linear surface receiver coil (2cm diameter) was placed above the head of the animal before

being transferred to the scanner, as described in Chapter 2.5.1. Diffusion-weighted imaging was performed to identify ischaemically damaged tissue in 8 coronal slices within the MCA territory using the sequence described in Chapter 2.5.3.1. Non-invasive quantitative cerebral blood flow measurements were carried out on 6 coronal slices, which were spatially identical to slices 2-7 acquired from DWI scans, using a form of pseudo-continuous arterial spin labelling based on a train of adiabatic inversion pulses (Moffat *et al* 2005). These scans take considerably longer to acquire than DWI images which prevents 8 coronal images being acquired within the time window available. The sequence is described in Chapter 2.5.4.1

3.2.4 Statistical analysis

Glucose tolerance data were plotted over time and the area under the curve was calculated. Data were analysed using a 2 way ANOVA and an unpaired Student's t-test, respectively. Blood glucose level data in Study 2 were analysed using a 2 way ANOVA with Bonferroni multiple comparisons post test. Infarct volume data were expressed as group means and analysed using a 1 way ANOVA with Bonferroni multiple comparisons post test. Data are expressed as mean ± standard deviation or as scatterplots with the mean indicated.

3.3 Results

3.3.1 Glucose tolerance test and lipid profile analysis (Study 1)

3.3.1.1 Body weights

As expected there was a significant difference between ffSHRSP and WKY rats in this study (ffSHRSP, 227.3±13.69 g; WKY, 258.7±13.27 g, p<0.001). This is a known characteristic of the SHRSP compared to age-matched WKY control rats (Ibrahim *et al* 2006; Strahorn *et al* 2005).

3.3.1.2 Glucose Tolerance test

The glucose tolerance test was performed on WKY and ffSHRSP rats. Initial blood glucose measurements taken prior to the glucose challenge were similar in both the WKY and ffSHRSP (WKY, 4.9±0.6 mmol/L; ffSHRSP, 6.0±1.5 mmol/L, p=0.06, Figure 3.1a). Following a single i.p. injection of 15% glucose (10ml/kg) the blood glucose level rose rapidly in both groups over the first 10 minutes, although the rate of increase was significantly higher in the ffSHRSP compared to WKY (WKY, 33.9±5.0 mmol/L/h; ffSHRSP, 44.0±6.7 mmol/L/h, p=0.009). The mean rate of increase diminished in both groups to a similar rate at 20 minutes post glucose administration (WKY, 12.3±4.5mmol/L/h; ffSHRSP, 18.1±12.7 mmol/L/h, p=0.28). Mean peak glucose was observed in both groups 20 minutes following the glucose challenge. The mean peak glucose reached in the ffSHRSP was significantly higher than that observed in the WKY group (ffSHRSP, 16.6±3.2 mmol/L; WKY, 12.6±1.0 mmol/L, p=0.01). This suggests that the ffSHRSP group are not responding as well to the challenge of glucose as the WKY group. At the 2 hour time point, blood glucose in both groups had returned to baseline values (WKY, 5.3±0.4; ffSHRSP, 5.9±0.5). The area under the curve data demonstrates that the ffSHRSP have a significantly greater blood glucose level over the 2 hour tolerance test compared to the WKY strain (ffSHRSP, 1051±79; WKY, 1308±238, p=0.02) indicating insulin resistance. There was a considerable amount of variability in the ffSHRSP group compared to the WKY group demonstrated in the difference in the size of the standard deviations.

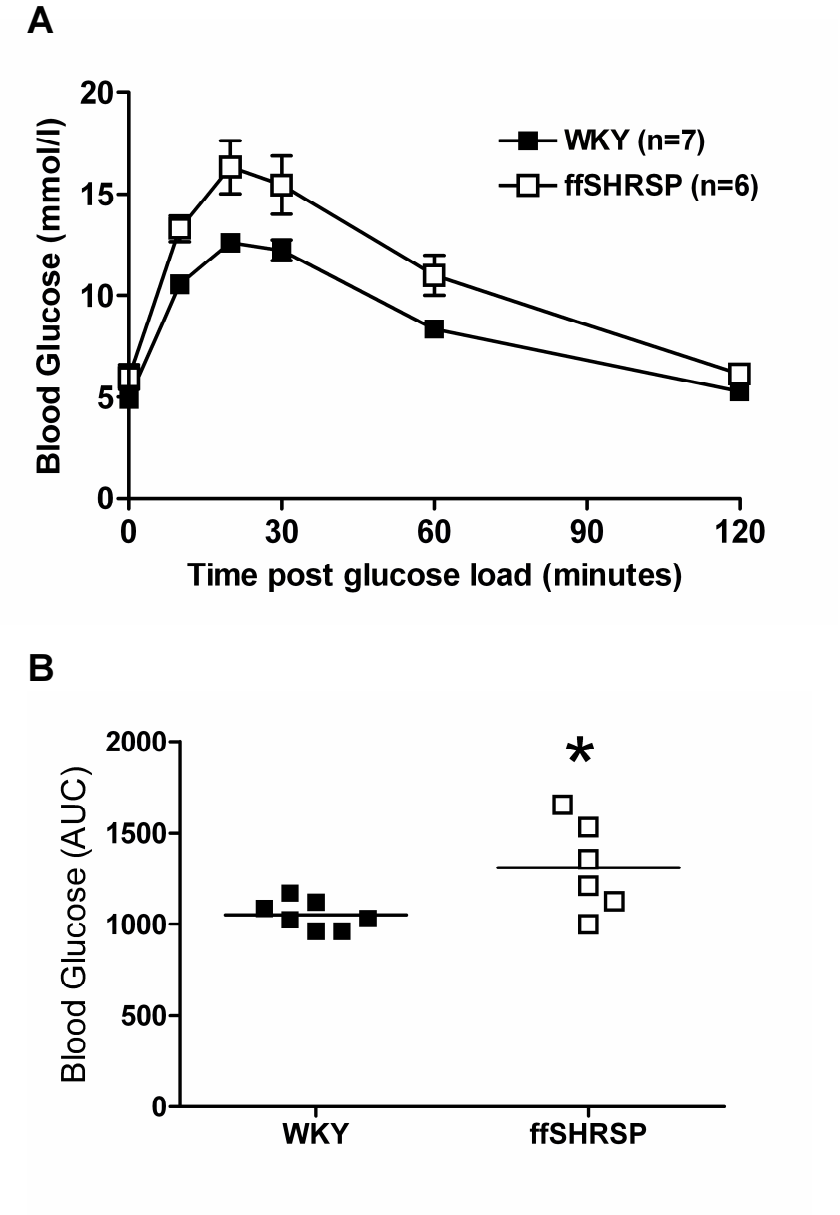

Figure 3.1: The blood glucose response to a glucose challenge in WKY and ffSHRSP rats, presented as the temporal profile (A) and area under the curve (B). The data in A) are expressed as mean ± standard deviation. The data in B) are expressed as AUC for each animal with the mean indicated and analysed using a unpaired t-test. * $P<0.05$.

3.3.1.3 Plasma insulin, lipid profile and adiposity

The ffSHRSP group demonstrated a number of differences in the plasma lipid profile compared with the WKY group (Table 3.1). The ffSHRSP had a significantly greater level of plasma triglycerides than the WKY strain ($p>0.0001$). The total and HDL cholesterol were both significantly lower in the ffSHRSP than in the WKY group ($p>0.001$). Interestingly the mean plasma insulin level was significantly increased in the ffSHRSP compared to the WKY group ($p=0.03$). Although the ffSHRSP rats were significantly lighter than the WKY rats they exhibited a higher adiposity index (% body fat).

	WKY (n=5)	ffSHRSP (n=5)
Adiposity (% body fat)	1.40± 0.29	2.40± 0.09**
Plasma triglycerides (mmol/l)	0.28± 0.04	0.65± 0.11***
Total cholesterol (mmol/l)	2.53±0.09	1.74± 0.11***
HDL cholesterol (mmol/l)	2.212±0.07	1.58±0.12***
Insulin(µg/l)	0.30± 0.07	0.46± 0.14*

Table 3.1 Features of the metabolic syndrome in WKY and ffSHRSP. Data are expressed as mean ± standard deviation. Analysed using a Student t-test; *, P<0.05; **, P<0.001; ***, P<0.0001 compared to WKY.

3.3.2 Investigating normo- and hyperglycaemia after MCAO under isoflurane-induced anaesthesia (Study 2)

3.3.2.1 Physiological variables

During surgical preparation animals in all groups were maintained within normal physiological limits (pCO_2, 35-45 mmHg; pH, 7.35-7.45; body temperature, 37.0 ±0.5°C) with the exception of pO_2 which was higher than normal due to the concentration of oxygen used to deliver the anaesthetic.

3.3.2.2 Blood glucose

Baseline blood glucose level was similar in all 4 groups. After administration of glucose to WKY + G and ffSHRSP + G groups, blood glucose level increased substantially compared to respective controls that received vehicle, reaching peak glucose between 20 and 30 minutes post glucose loading (Figure 3.2A). Peak glucose was similar in WKY + G (10.7±2.6 mmol/L) and ffSHRSP + G (11.6± 3.1 mmol/L, p=0.58). Blood glucose remained significantly higher in WKY + G compared with control up until 2 hours post glucose administration. However, although not statistically significant blood glucose remained above the level of the control WKY group at each subsequent time point. The ffSHRSP + G group again remained high throughout the experiment although only a number of time points reached statistical significance (20, 60, 240 minutes). From the area under the curve data (Figure 3.2B) generated from the temporal blood glucose plot, administration of glucose leads to an overall significant increase in blood glucose (WKY vs. WKY + G, 1488±48 vs. 2167±390, $p<0.05$; ffSHRSP vs. ffSHRSP + G, 1625±214 vs. 2542±581, $p<0.01$). There was no increase in blood glucose observed in either control group as a result of vehicle administration or induction of MCAO suggesting a lack of influence from these factors on glycaemic control in this particular time frame.

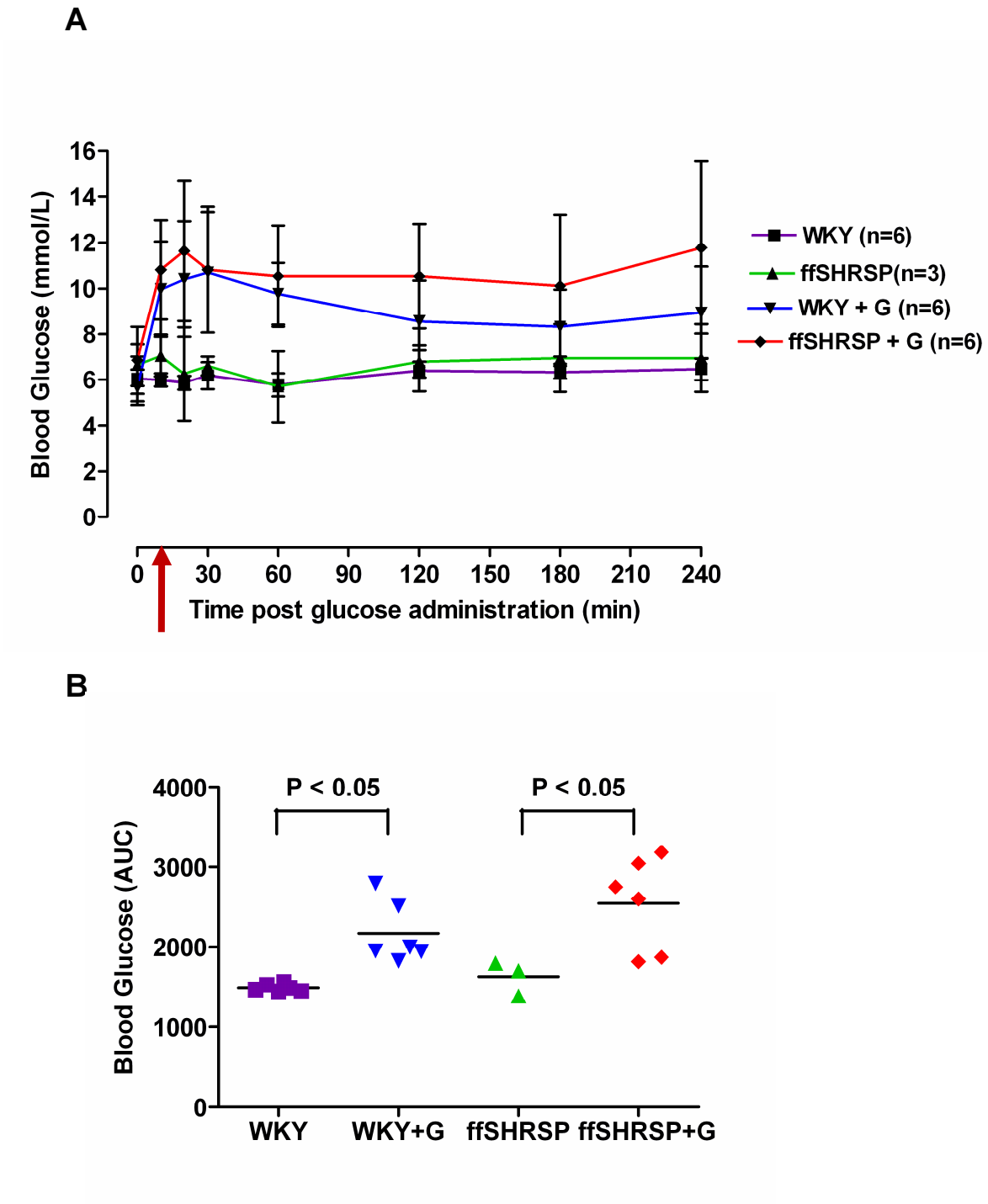

Figure 3.2: Acute hyperglycaemia in WKY and ffSHRSP. A) The temporal profile of blood glucose following glucose or vehicle administration. Red arrow indicates time of MCAO. Both ffSHRSP and WKY reached similar peak glucose values at 20 minutes post glucose loading. B) Plotting area under the curve shows that loading with glucose leads to a significant increase in blood glucose compared to vehicle treated animals. Data analysed using 1 way ANOVA with Bonferoni post test.

3.3.2.3 Infarct quantification

Quantitative histology indicated that infarct volume at 24 hours post MCAO using the intraluminal filament model was not significantly different between the glucose loaded WKYs and the vehicle treated WKY controls (Figure 3.3). Similarly there was no difference between the glucose treated ffSHRSP and the vehicle treated ffSHRSP controls. Most interestingly no difference was observed between the ffSHRSP and WKY vehicle treated animals. Upon examination of the line diagrams, from which the infarct volumes were calculated, it was obvious that the lesion sizes were extremely large encompassing the majority of the hemisphere (Figure 3.4).

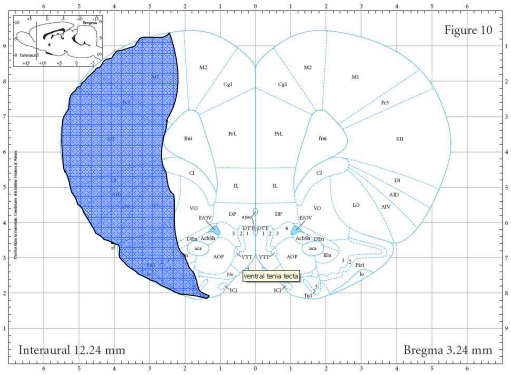

Level 1. Bregma = 3.24 mm

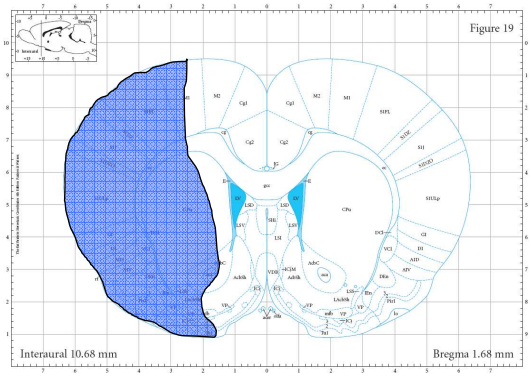

Level 2. Bregma = 1.68 mm

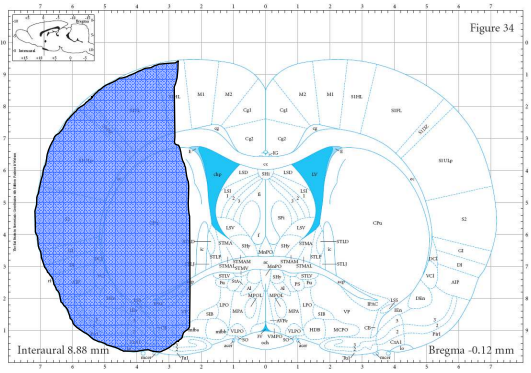

Level 3. Bregma = -0.12 mm

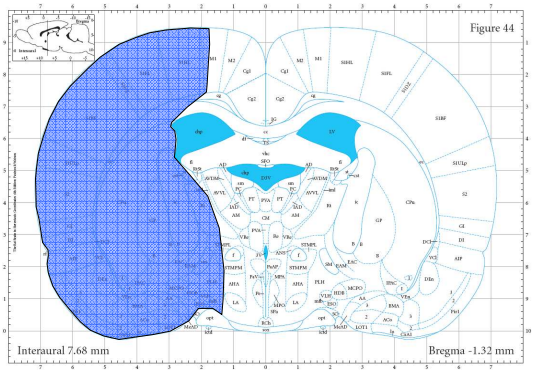

Level 4. Bregma = -1.32 mm

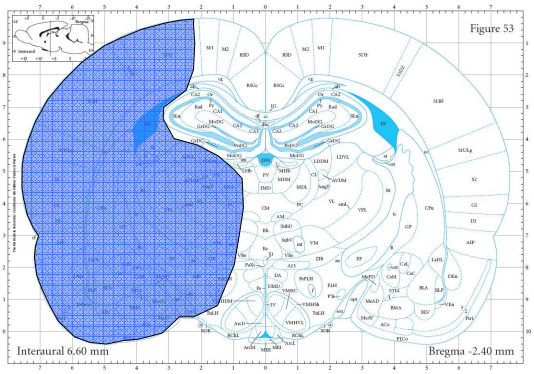

Level 5. Bregma = -2.40 mm

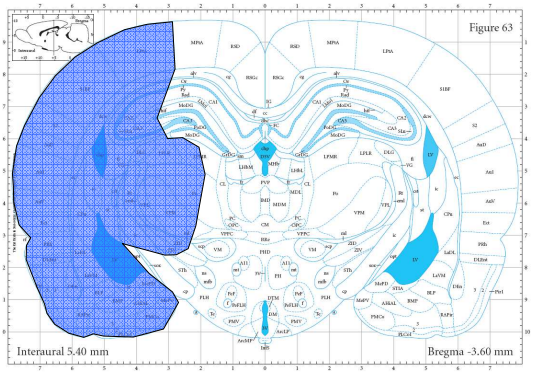

Level 6. Bregma = -3.60 mm

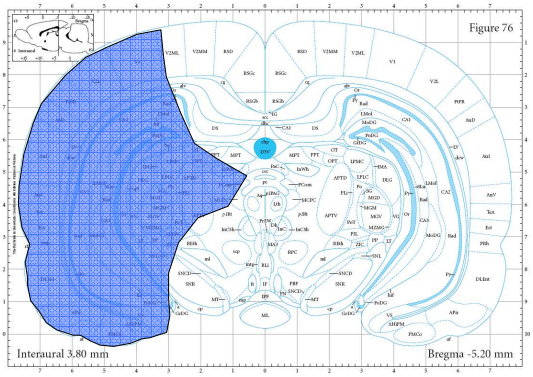

Level 7. Bregma = -5.20 mm

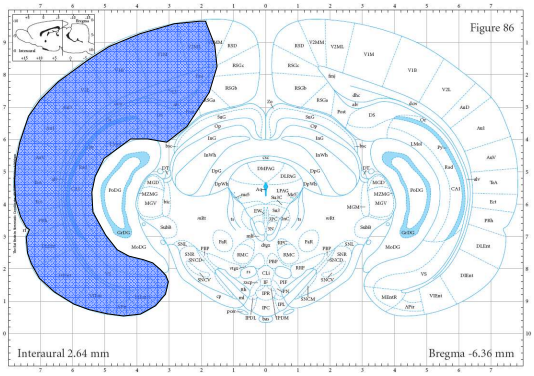

Level 8. Bregma = -6.36 mm

Figure 3.3: The infarct areas at 24h after intraluminal filament-induced MCAO in the median ffSHRSP rat. Line diagram (Paxinos and Watson, 2007) comprising 8 pre-determined coronal levels with the blue area representing ischaemic damage. ffSHRSP exhibit almost complete hemispheric lesion in all 8 levels.

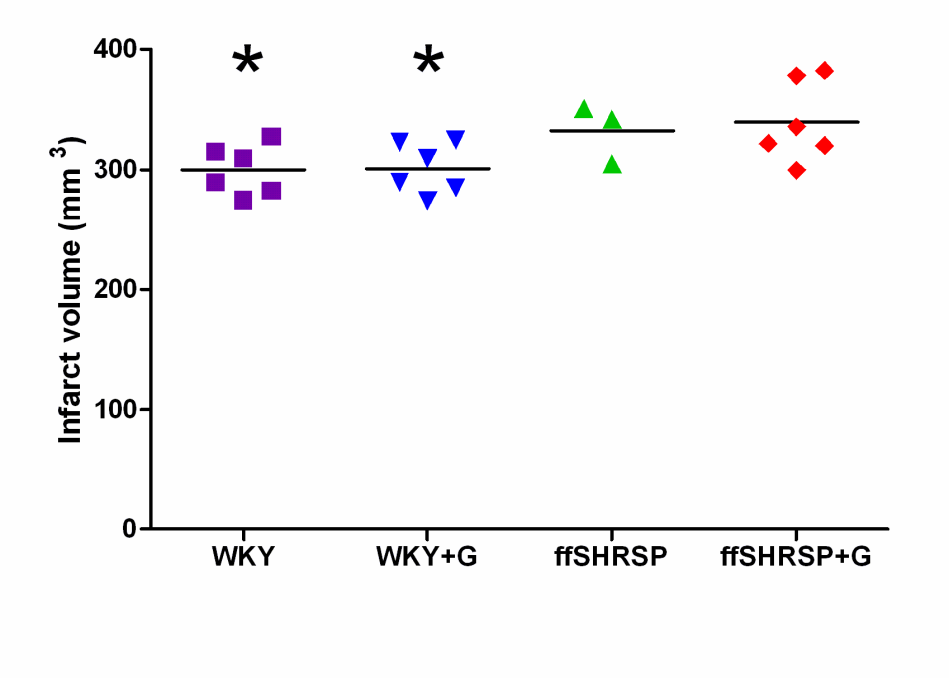

Figure 3.4: Infarct volumes at 24 hours post MCAO. There was no difference associated with glucose loading in WKY groups. Glucose had no effect on infarct size in ffSHRSP groups. Interestingly no statistically significant difference in infarct size between WKY and ffSHRSP was observed. Glucose loading in ffSHRSP caused a significant increase in infarct compared to both WKY treated with glucose and WKY treated with vehicle.
*, $P<0.05$ vs. ffSHRSP + G group.

3.3.3 Comparison of the intraluminal filament and the distal diathermy method of MCAO (Study 3)

3.3.3.1 Physiological variables

During surgical preparation Sprague Dawley rats in all groups were maintained within normal physiological limits (pCO_2, 35-45 mmHg; pH, 7.35-7.45; body temperature, 36.8-37.2°C) with the exception of pO_2 which was higher than normal due to the concentration of oxygen used to deliver the anaesthetic. There was however no difference in pO_2 between any of the groups.

3.3.3.2 Infarct quantification

There were notable differences in the extent of ischaemic damage in the intraluminal filament model compared to the distal diathermy occlusion model (Figure 3.5). Separating the lesion into cortical and subcortical regions (Figure 3.6), there was no statistically significant difference in cortical damage between the 2 models (diathermy, 46.1±18.5 mm^3; intraluminal filament, 61.3± 14.3 mm^3). In the intraluminal filament model the majority of the lesion was subcortical accounting for over 60% of the lesion (Figure 3.6). The distal diathermy occlusion of the MCA produced no subcortical damage in any of the 6 animals.

a)

Rostral

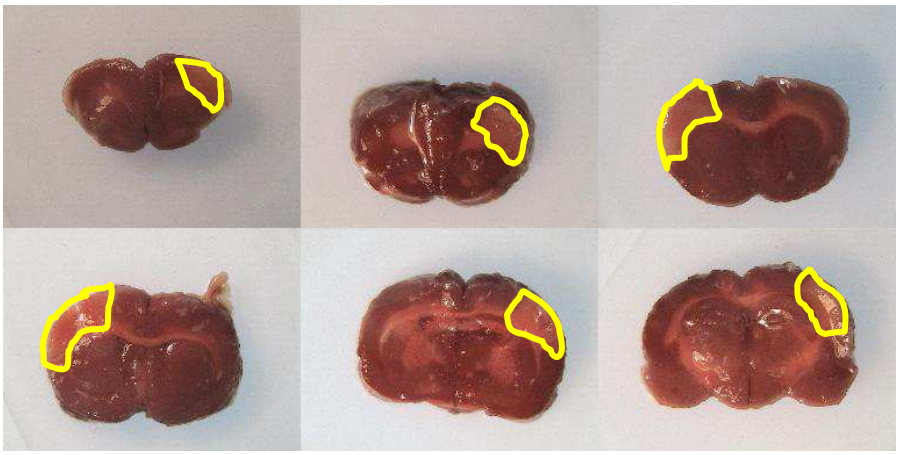

Caudal

b)

Rostral

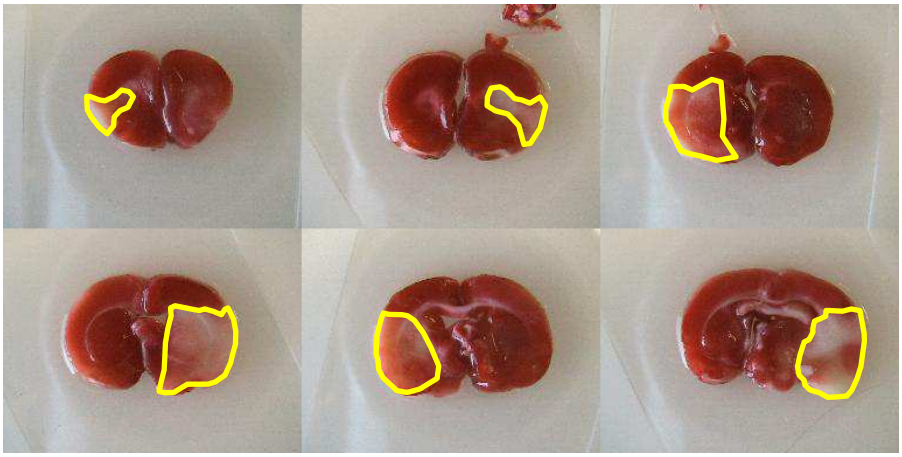

Caudal

Figure 3.5: Representative coronal TTC stained brain tissue following 4 hour permanent MCAO in Sprague Dawley by a) distal diathermy and b) intraluminal filament model. MCAO via distal diathermy occlusion results in ischaemic damage being confined to the cortex. A large volume of subcortical tissue damage is present using the intraluminal filament model.

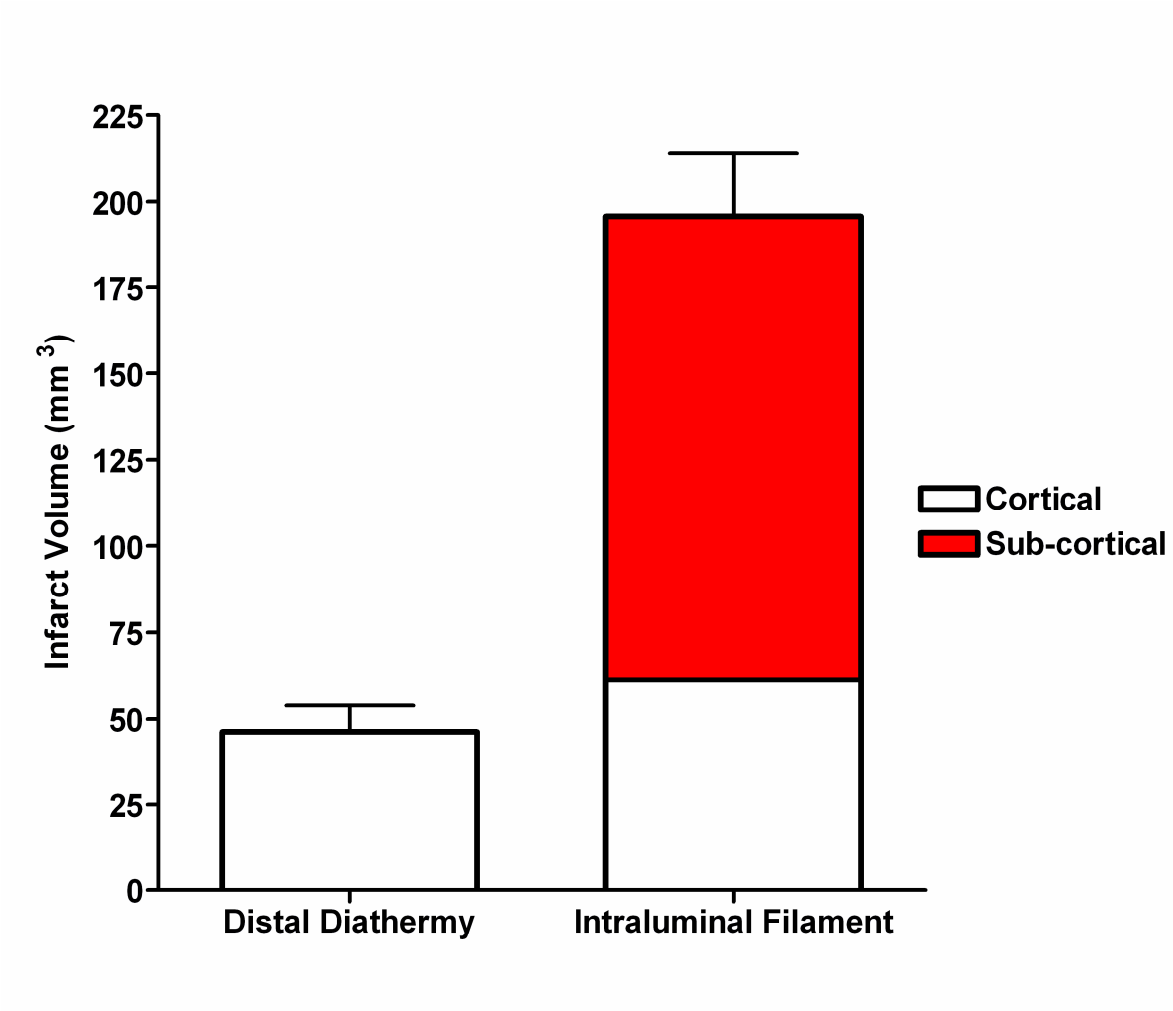

Figure 3.6: Infarct volume calculated from TTC stained coronal sections from Sprague Dawley rats that underwent MCAO by either the distal diathermy (n=6) or intraluminal filament model (n=6). Lesion size is significantly greater following intraluminal filament MCAO than distal diathermy occlusion. There is significant subcortical damage caused by intraluminal filament MCAO compared to none seen in the distal diathermy model. Data are displayed as mean ± standard deviation.

3.3.3.3 Identifying the penumbra

From the MRI images it is clear that at 1 hour post MCAO, there is a large volume of diffusion-perfusion mismatch defined penumbra tissue in the distal diathermy model (Figure 3.7). The perfusion deficit remained constant throughout the scanning period (Figure 3.8A). At subsequent time points the volume of DWI-PWI mismatch defined penumbra diminished from 40.5mm^3 to 20.7mm^3 as the ADC lesion expanded (Figure 3.8B). Even at 4 hours post MCAO there is substantial perfusion diffusion mismatch at the rostral caudal poles of the MCA territory suggesting the lesion would further expand to match the volume of the perfusion deficit.

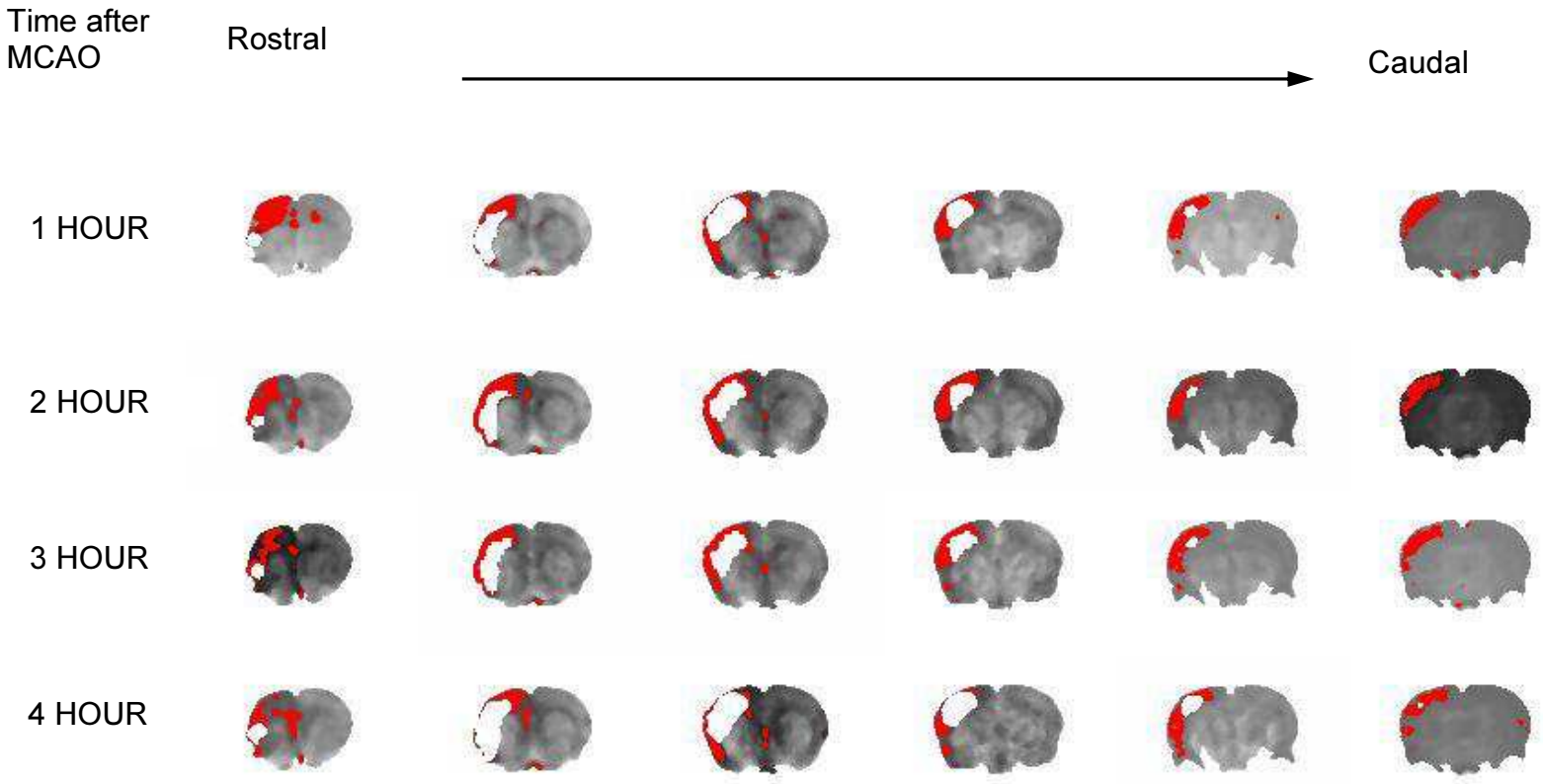

Figure 3.7: MRI DWI and PWI mismatch identifying suspected penumbra in a Sprague Dawley rat with a distal diathermy MCAO. Scans from 6 coronal slices are displayed at hourly intervals following stroke onset. Red areas depict the perfusion deficit and the white areas indicate ADC-defined lesion. Penumbra can be identified at all 4 hours post MCAO (remaining red regions). The DWI defined ischaemic damage or injury increases over time. The perfusion deficit remains relatively stable.

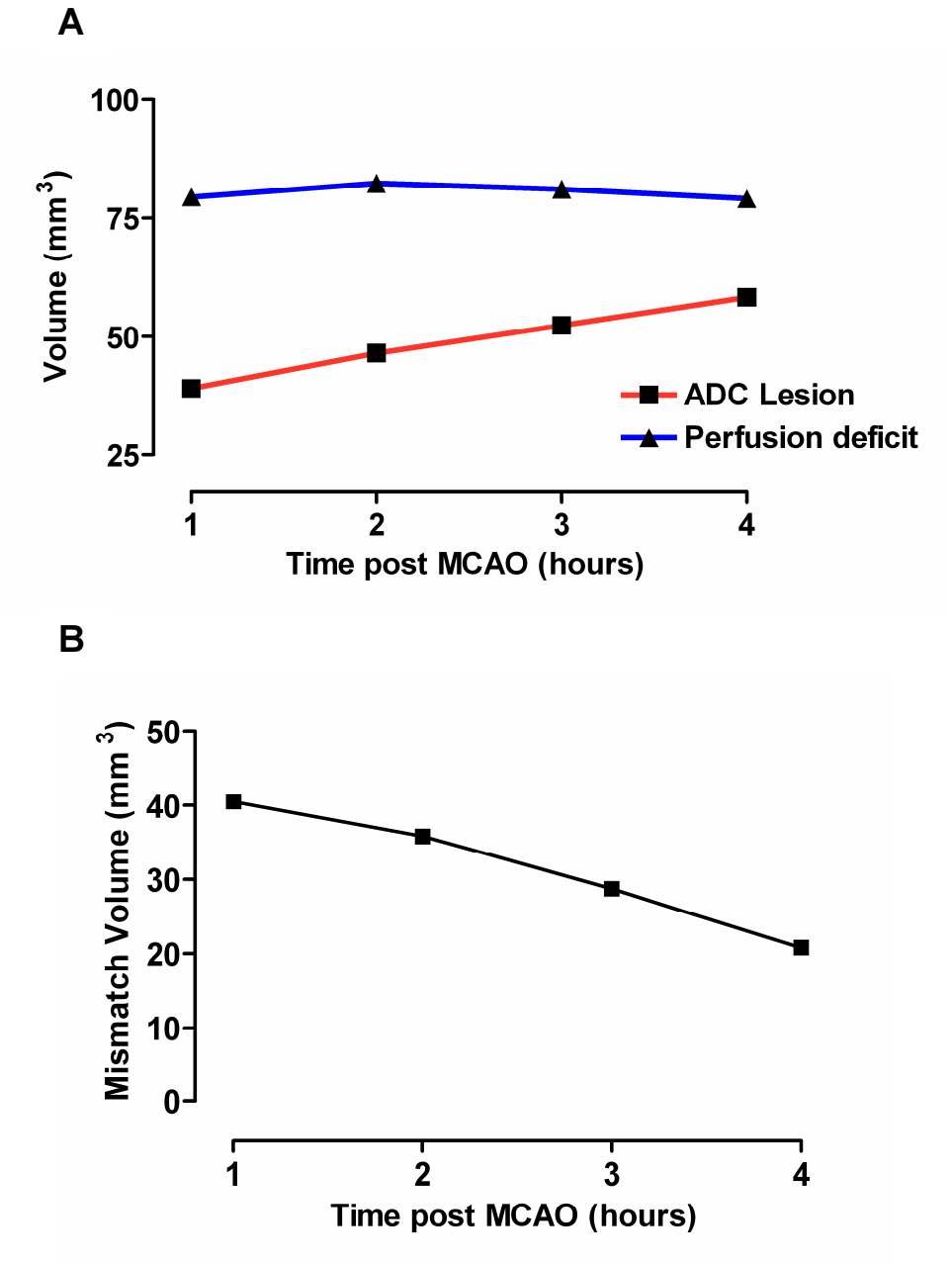

Figure 3.8: Lesion evolution and penumbral loss following MCAO by distal diathermy occlusion of the MCA. A) Illustrates the progression of DWI defined ischaemic damage over time (red line) and the PWI defined blood perfusion deficit (blue line). B) Shows the loss of DWI-PWI mismatch defined penumbral tissue as the ischaemic lesion develops.

3.4 Discussion

The preliminary experiments in this chapter were designed to optimise rodent models to be used in subsequent studies of post stroke hyperglycaemia. They confirm that the fructose fed SHRSP does exhibit insulin resistance as well as other features of the metabolic syndrome. They demonstrated that a single i.p. administration of 15% glucose solution induces clinically relevant levels of hyperglycaemia in both WKY and fructose fed SHRSP rats under anaesthesia which was suitably maintained during the acute period following MCAO. They highlight the neuroanatomically extensive lesions produced by the intraluminal filament model of MCAO as opposed to those produced by a distal MCAO using diathermy, and they indicate that the latter model of MCAO produces smaller, purely cortical lesions with a relatively large amount of assumed penumbral tissue.

3.4.1 Fructose fed SHRSP exhibit insulin resistance and other features of metabolic syndrome

The National Cholesterol Education Program (NCEP) set out criteria that stated at least 3 risk factors from hypertension, obesity, insulin resistance, hypertriglyceridaemia and low HDL cholesterol must be present for diagnosis of metabolic syndrome in humans. SHRSP rats fed on a 60% fructose diet for two weeks display hypertension, impaired glucose tolerance, dyslipidaemia (reduced HDL cholesterol and increase plasma triglycerides), hyperinsulinaemia as well as an increased adiposity index compared to the WKY strain thus making it an appropriate model for investigating the metabolic syndrome. Previously this model was only shown to elicit impaired glucose tolerance without hyperinsulinaemia (Strahorn *et al* 2005). This suggested impaired glucose tolerance was primarily due to impairments in glucose-stimulated insulin secretion rather than a decreased sensitivity to insulin. It is well established that the accumulation of triglycerides and other lipid derived intermediates in the ß-cells of the pancreas is directly linked to impairment in insulin secretion (Schaffer 2003; Zhou and Grill 1995). Interestingly since hyperinsulinaemia has been observed in the fructose fed SHRSP model of metabolic syndrome it addresses both decreased sensitivity to insulin and impaired glucose-stimulated

insulin release that together are responsible for impaired glucose tolerance in humans.

When the fructose feeding model was developed, feeding both WKY and SHRSP rats on the 60% fructose diet was investigated (Strahorn *et al* 2005). It was observed that feeding WKY rats on the fructose rich diet failed to alter tolerance to glucose, producing a similar temporal profile and area under the curve to that observed in both WKY and SHRSP rats on standard chow diet. This was also observed in our lab on a small subset of animals, confirming that only the SHRSP after 2 weeks feeding is sensitive to fructose-induced impaired glucose tolerance.

The data collected from both the glucose tolerance test and from the terminal blood samples replicated what was reported by Strahorn et al (2005) with similar results for glucose tolerance, plasma triglycerides and both total and HDL cholesterol. However previously it had not been shown in this model that the fructose fed SHRSP exhibits elevated plasma insulin levels compared to WKY rats.

3.4.2 Other models of insulin resistance and metabolic syndrome

The fructose fed SHRSP model of insulin resistance is a variation on the commonly used spontaneously hypertensive rat (SHR) which has been shown to exhibit insulin resistance in both skeletal muscle (Hulman *et al* 1993) and isolated adipocytes (Reaven *et al* 1989) without additional feeding with fructose. In SHRSP rats I was unable to demonstrate these differences in vivo without the addition of a fructose feeding protocol. This is perhaps a sensitivity issue of the glucose tolerance test compared to the euglycaemia hyperinsulinaemia clamp technique used by Hulman et al (1993) on the SHR. Similarly the results from isolated adipocytes may not reflect what is seen in vivo, or the contribution of reduced insulin sensitivity in fat tissue may not lead to a measurable effect in vivo. More recently a sucrose feeding protocol has been used in SHR rats, which reflects the need for fructose feeding that we observed (Pagliassotti *et al* 1994). However the sucrose fed SHR was recently reviewed and showed that although an impairment in glucose tolerance was observed this model failed to significantly increase plasma insulin or triglycerides or show a difference in total

cholesterol compared to control animals (Oron-Herman *et al* 2008). This study also addressed the primarily diet-induced model of metabolic syndrome using Sprague Dawley rats which has been frequently used with a variety of feeding protocol durations. One study using male Sprague Dawley rats found that a 66% fructose feeding regime for 8 weeks led to increased fasting blood glucose, plasma insulin and triglycerides compared to controls (D'Angelo *et al* 2005). This reflects aspects of my findings although no differences in fasting blood glucose were observed in the WKY or fructose fed SHRSP in the current study. Similarly D'Angelo et al (2005) were unable to produce an increase in blood pressure which had been seen previously in Sprague Dawley rats having been fed a high fructose diet for 2 weeks (Hwang *et al* 1987) and also after feeding for 7 weeks (Oron-Herman *et al* 2008).

The main driving force currently for studies of metabolic syndrome and insulin resistance is the obesity epidemic that faces the western world. Prior to the experiments reported in this chapter consideration was given to the obese Zucker rat. In this rat a missense mutation in the leptin receptor causes hyperphagia, hyperlipidaemia, hyperinsulinaemia and obesity compared to the lean Zucker rat (Phillips *et al* 1996; Takaya *et al* 1996; Zucker and Zucker 1961). The insulin resistance exhibited by the obese Zucker rat is well characterised (Boulange *et al* 1981; Ionescu *et al* 1985; Penicaud *et al* 1987) and has been used widely as a model of metabolic syndrome. Hypertension has also been observed in a number of studies (Kim *et al* 1994; Zemel *et al* 1990; Zemel *et al* 1992)which, similar to the model employed in this study, meets the criteria set out for the human metabolic syndrome. Although the Zucker represents an excellent model for studying insulin resistance in cerebral ischaemia using the proposed PSH protocol, there are a few pragmatic issues that prevent the use of this model for our planned studies. The main issue relates to the size of the obese Zucker rat. The obese Zucker rats, at 10 weeks of age, weigh around 650g which is 3 times the size of the SHRSP rats that are currently used in our lab. As future experimentation will be investigating the acute evolution of damage using MR imaging this size becomes a significant limitation. The rat cradle we have for the MRI scanner is not big enough to accommodate a rat of that size. This would also pose problems for maintenance of body temperature as the water jacket

would not fit correctly. For this reason there was no possibility, using the equipment available, that acute imaging studies could be done on Zucker rats.

3.4.3 Hyperglycaemia was maintained in both WKY and fructose fed SHRSP after bolus injection of glucose

The dose of glucose used in conscious fructose fed SHRSP and WKY rats by Strahorn et al (2005) produced a level of hyperglycaemia in the current study between 12 and 16 mmol/L. Often studies have used levels of extremely high blood glucose levels from around 16 mmol/l to in excess of 27 mmol/l to study hyperglycaemia in cerebral ischaemia (Bomont and MacKenzie 1995; de Courten-Myers *et al* 1988; Ginsberg *et al* 1987; Gisselsson *et al* 1999; Huang *et al* 1998; Kawai *et al* 1998; Li *et al* 1998; Wei *et al* 2003; Yura *et al* 1986). The GIST-UK trial of stroke patients reported admission blood glucose concentrations of between 6.0 and 16.6 mmol/l (Gray *et al* 2004a). This suggests that, in conscious WKY and fructose fed SHRSP rats, the blood glucose values obtained from a single i.p. 15% glucose (10ml/kg) injection produce more clinically relevant levels of hyperglycaemia for studying PSH than the many studies that have resorted to much higher blood glucose levels. The 15% glucose (10ml/kg) dose was therefore selected as the basis for producing clinically relevant hyperglycaemia whilst under anaesthesia.

The data from Study 2 show that a single bolus injection of glucose in both WKY and fructose fed SHRSP rats lead to significant increases in blood glucose levels compared to vehicle treated animals. A similar peak glucose level occurred in both WKY and fructose fed SHRSP rats under anaesthesia reaching between 10 and 12 mmol/L at 20 minutes after administration. This is lower than was observed in the conscious animals, which is perhaps due to an additive stress response from the procedure; handling the animals, blood sampling, and i.p. injections. Interestingly the major difference is that blood glucose concentration remains increased for longer, especially in the fructose fed SHRSP group. In a study using isolated rat islets of Langerhans it has been found that isoflurane can inhibit the release of insulin from the pancreas in response to a glucose challenge (Desborough *et al* 1993). This is also supported by a number of in vivo studies that show in both humans and rodents that blood glucose increases under

anaesthesia (Kofke *et al* 1987; Lattermann *et al* 2001). This could possibly explain why hyperglycaemia is prolonged. The control groups, receiving only vehicle, show no increase in blood glucose concentration over the 4 hours of anaesthesia. There is also no increase following the induction of cerebral ischaemia. This suggests firstly that isoflurane has no effect on basal glucose levels at these time points and secondly that the insult of precluding flow from the MCA causes no measureable hyperglycaemia at the acute time points that may be associated with a stress response. This is contradictory to what is proposed to be causing a prolonged increase in blood glucose. It is known that isoflurane alters energy metabolism in the brain, dampening glucose utilisation in a number of areas which perhaps explains why the hyperglycaemia is maintained for longer in animals receiving a glucose challenge.

3.4.4 Distal diathermy MCAO produces small lesions and large penumbra.

Inducing cerebral ischaemia in WKY or SHRSP rats using the intraluminal filament model of MCAO has been found previously in our lab to result in large lesions encompassing the majority of the ipsilateral hemisphere (Reid *et al* 2012). There are a number of concerns associated with the intraluminal filament method of MCAO for recovery studies in WKY and SHRSP rat strains. There is an increased possibility of mortality due to the severe ischaemic damage and associated cerebral oedema that causes intracranial pressure to rise in closed skull models such as the intraluminal filament model.

There was no significant difference in infarct volume at 24h between the WKY and fructose fed SHRSP rats in Study 2. This is surprising as it is well established that the SHRSP rat strain is more sensitive to experimental stroke compared to the reference WKY strain (Carswell *et al* 1999; Coyle and Jokelainen 1983; Marks *et al* 2001). Interestingly the studies that have demonstrated the increased sensitivity to experimental stroke used a distal MCA occlusion similar to the diathermy method of MCAO rather than the intraluminal filament method of permanent MCAO which was used in Study 2. A significant difference was seen between the ffSHRSP+G group and the WKY and WKY+G groups suggesting that the small *n* number in the SHRSP group may not have been enough to distinguish

between the infarct volumes. No difference was seen following the administration of glucose to either ffSHRSP or WKY rats compared to their respective vehicle treated controls which doesn't support the majority of the available literature (MacDougall and Muir 2010). However it is postulated that perhaps, especially in ffSHRSP groups, a ceiling effect applies in permanent intraluminal filament induced MCAO such that a maximal amount of damage is produced. As future studies aim to elucidate the detrimental effects of hyperglycaemia on lesion growth this model of cerebral ischaemia may be unsuitable. Moreover MRI studies in our lab using SHRSP and WKY having undergone permanent MCAO by intraluminal filament introduction have shown that very little penumbral tissue is present even at early time points as the lesion is already very large (McCabe *et al* 2009; Reid *et al* 2012) . The rate of penumbral loss is an important outcome measure for investigating post stroke hyperglycaemia in the acute period of ischaemic injury and therefore a model that exhibits a reasonable amount of penumbral tissue is more suited to the experimental design proposed for subsequent studies in this thesis. A recent study conducted in our lab showed that the intraluminal filament model of permanent MCAO only produced a small amount of DWI-PWI mismatch defined penumbra in the SHRSP and WKY strain (McCabe *et al* 2009; Reid *et al* 2012). Even in the outbred Sprague Dawley strain the intraluminal filament model exhibits large lesions with only a small proportion of DWI-PWI mismatch defined penumbra (Robertson *et al* 2011) The intraluminal filament method of MCAO can also disrupt the extracranial blood flow to the facial muscles responsible for mastication, due to the surgical occlusion of the external carotid artery, which can cause issues during animal recovery from surgery. This has proved problematic with regards to maintaining animal weight and poses more mortality problems with recovery for more than 24 hours.

As shown in this chapter the distal diathermy model of MCAO produces much smaller infarcts with all ischaemic tissue confined to the cortex. The need for a small craniectomy also helps prevent brain oedema from increasing intracranial pressure and hence helping reduce mortality. The MRI data collected suggests that there is substantial penumbra associated with this model and even though these data were collected from a Sprague Dawley rat, comparisons with the intraluminal filament show almost double the volume of penumbra using the

distal diathermy model of MCAO in this strain (Robertson *et al*). The draw back with diathermy models is the level of surgical skill required to occlude the MCA. This is far more technically demanding than the intraluminal filament model of MCAO and led to 2 surgical deaths out of a total of 7 animals subjected to distal diathermy occlusion compared to no surgical deaths in the intraluminal filament model.

3.4.5 Summary

Using the SHRSP fed on a fructose enriched diet for 2 weeks impaired glucose tolerance and induced hyperinsulinaemia, hypertriglyceridaemia, reduced HDL cholesterol and increase adiposity compared to the WKY control strain. In addition to the innate hypertension associated with the SHRSP strain this forms an appropriate model of metabolic syndrome for future studies.

A single bolus i.p. injection of 15% glucose (10ml/kg) produced clinically relevant levels of hyperglycaemia that was maintained following MCAO for the length of the acute time period of interest. This will be carried forward for future experimentation.

The distal diathermy model of MCAO produced smaller infarcts than permanent MCAO induced by intraluminal filament and produced a considerable amount of penumbral tissue at acute time points. This model will therefore be used for future studies investigating the effects of hyperglycaemia and insulin resistance on focal cerebral ischaemia.

Chapter 4 - Effect of hyperglycaemia on ADC-defined ischaemic lesion growth in rats with and without features of metabolic syndrome

4.1 Introduction

The experiments in this chapter were designed to determine the effects of clinically relevant levels of acute hyperglycaemia along with insulin resistance and cardiovascular co-morbidities on ischaemic damage following MCAO. The first aim of these experiments was to investigate the effect of hyperglycaemia, in the presence and absence of insulin resistance, on the early expansion of the ischaemic lesion and loss of penumbral tissue following permanent MCAO. The second aim was to establish whether hyperglycaemia, again with and without insulin resistance, caused any differences in infarct volume determined at 24 hours post MCAO. The mechanisms associated with hyperglycaemia induced damage following MCAO are still not well understood and many theories have been postulated (Lindsberg and Roine 2004). One potential mechanism for hyperglycaemia and insulin resistance mediated damage is thought to be via oxidative stress pathways; therefore the level of lipid peroxidation was assessed by immunohistochemistry using the lipid peroxidation marker 4-hydroxynonenal.

4.1.1 Post-Stroke Hyperglycaemia

The only definitive treatment for ischaemic stroke is the use of the clot busting drug rt-PA. The percentage of patients who are receiving this treatment is less than 10% (Cocho *et al* 2005; Molina and Saver 2005) and although this is starting to increase there is still scope for other possible interventions either as adjuncts or alternatives to rt-PA in acute stroke management. A primary focus of acute stroke care is the monitoring of physiological variables and dealing with potentially pathological changes in such variables has the potential to affect clinical outcome.

Post stroke hyperglycaemia (PSH) occurs in over 60% patients without a diagnosis of diabetes and in more than 90% of diabetic patients (Muir *et al* 2011). PSH is a predictor of poor outcome independent of age, stroke type or severity (Weir *et al* 1997). The consistent observation of poor outcome associated with PSH has led to guidelines recommending routine blood glucose monitoring, and intervention with insulin for hyperglycaemia (Adams *et al* 2007; 2008). However, there is currently no clinical evidence of benefit from insulin use, and recent

findings raise concerns about the safety of insulin use in predominantly non-diabetic acute populations with stroke (Gray *et al* 2007; McCormick *et al* 2010). GKI infusions were associated with an increase in infarct size in persistent occlusions and a high incidence of hypoglycaemia which is also detrimental to stroke outcome.

Around 56% of hyperglycaemic stroke patients are subsequently diagnosed with insulin resistance, manifesting as impaired glucose tolerance, impaired fasting glucose or the "metabolic syndrome," a phenotype comprising combinations of insulin resistance, hypertension, hypertriglyceridaemia and obesity that is a significant risk factor for cardiovascular disease (Gray *et al* 2004b; McCormick and Muir 2006). In light of the potential risk of hypoglycaemia with insulin regimes in stroke, it is important to question whether the harmful effects of acute hyperglycaemia pertain to all stroke patients, or whether they differ in those with and without pre-existing insulin resistance.

4.1.2 Pre-clinical research of PSH

Hyperglycaemia in focal cerebral ischaemia is widely accepted to increase infarct size in animal models (Berger and Hakim 1989; Bomont and MacKenzie 1995; Duverger and MacKenzie 1988; Huang *et al* 1996; Liu *et al* 2007; Nedergaard 1987; Nedergaard and Diemer 1987; Quast *et al* 1997; Slivka 1991). However the majority of preclinical studies fail to model PSH appropriately, providing little relevance to the clinical situation (MacDougall and Muir). Streptozotocin, which destroys the insulin producing beta cells of the pancreas, has been often used to induce hyperglycaemia even though this more closely models type-1 diabetes, which doesn't represent the general stroke population (Duverger and MacKenzie 1988; Huang *et al* 1996; Nedergaard 1987; Quast *et al* 1997). Glucose infusions models emulate PSH much better, however extremely high levels of blood glucose have been used, which are rarely seen clinically (Berger and Hakim 1989; Bomont and MacKenzie 1995; Liu *et al* 2007; Nedergaard and Diemer 1987; Slivka 1991). Moreover preclinical research on hyperglycaemia following focal cerebral ischaemia has not been studied using a model of insulin resistance common to the stroke population. This highlights a

need for better modelling of PSH in animal models so that clinical trials can be better informed.

The majority of the literature focuses on assessing infarct volume at 24 hours or 48 hours post MCAO. There are few studies that have focussed on the fate of the potentially salvageable penumbral tissue that is present in the acute stage of cerebral ischaemia. Evidence of hyperglycaemia-exacerbated damage at early time points would suggest that early management of PSH could be beneficial, potentially preventing or slowing the recruitment of the penumbra into the infarct. This early management could also benefit patients who are potentially eligible to receive rt-PA since many pre-clinical studies have shown more profound exacerbation of ischaemic damage in reperfusion models of cerebral ischaemia compared to permanent occlusions under hyperglycaemic conditions (MacDougall and Muir 2010).

A few studies have investigated the effects of hyperglycaemia at the acute time points of lesion evolution and penumbral loss, utilising MRI to assess ischaemic damage even at very early time points. Single slice or multi slice imaging has been used in the acute period at a single time point (Quast *et al* 1995; Quast *et al* 1997). Serial multi slice imaging is able to track the development of damage and this provides a more suitable method of tracking the ischaemic damage using a relevant PSH model (Huang *et al* 1996; Martin *et al* 2006; Quast *et al* 1995; Wei *et al* 1997; Wei and Quast 1998; Wei *et al* 2003; Wei *et al* 2004).

4.1.3 Oxidative stress associated with hyperglycaemia

The mechanisms by which hyperglycaemia exacerbates ischaemic damage are still not widely understood. In the context of chronic hyperglycaemia, as occurs in diabetes, a central event implicated in the development of disease-related complications is oxidative stress. It is thought that hyperglycaemia leads to diabetic tissue damage via 5 mechanisms that are all activated by the overproduction of reactive oxygen species (ROS) by mitochondria.

Hyperglycaemia can increase the production of ROS, such as superoxide(Muranyi and Li 2006). Moreover a simple glucose challenge in patients was shown to increase the production of ROS from leukocytes as well as increase the

expression of $p47^{phox}$, the key protein component in the formation of NADPH oxidase, the enzyme responsible for ROS production (Mohanty *et al* 2000).

One of the aims of this study was to examine whether hyperglycaemia-induced changes in ischaemic damage were associate with increased oxidative stress

4.1.4 Study Aims

1) To determine the effect of hyperglycaemia on early ischaemic lesion development using the MRI derived DWI-PWI mismatch in rats with and without insulin resistance and other cardiovascular co-morbidities.

2) To assess the effect of hyperglycaemia on final infarct volume determined 24 hours post MCAO in rats with and without insulin resistance and other cardiovascular co-morbidities.

3) To investigate the potential role of oxidative stress in hyperglycaemia induced damage, using the lipid peroxidation marker 4-hydroxynonenal (4-HNE), in rats with and without insulin resistance and other cardiovascular co-morbidities.

4.2 Materials and Methods

All experiments were carried out under licence from the Home Office and were subject to The Animals (Scientific Procedures) Act, 1986. 10 week old male rats were obtained from breeding colonies of SHRSP and WKY within the Institute of Cardiovascular and Medical Sciences, University of Glasgow. SHRSPs were fed on a 60% fructose diet for 2 weeks prior to any experimentation. WKYs were fed on standard rat chow and both food and water were available *ad libitum*. All experiments were conducted when rats were 12 weeks of age.

SHRSP rats fed the fructose-rich diet were randomly assigned to either fructose fed (ffSHRSP, n=10) or fructose fed plus acute hyperglycaemia (ffSHRSP + G, n=10) groups upon arrival at Biological Services from the breeding colony and were singly housed. WKY rats were randomly assigned upon arrival to either WKY (n=10) or WKY + G (n=10) groups and were also singly housed.

4.2.1 Blood pressure measurements

Systolic blood pressure was measured 1-3 days prior to induction of cerebral ischaemia in all animals, whilst conscious, using tail-cuff plethysmography as previously described in Chapter 2.9. The mean systolic blood pressure for each rat was calculated and the data were compiled to compare the mean systolic blood pressure for each group.

4.2.2 Surgical procedures

Rats fasted overnight, were anaesthetised initially with 5% inhaled isoflurane in an induction chamber and then orally intubated. Animals were artificially ventilated with 2.5% isoflurane delivered in a nitrous oxide-oxygen mixture (70:30). All rats were given an intraperitoneal injection of the anti-muscarinic drug atropine sulphate (0.4ml, 600µg/ml, Martindale Pharmaceuticals, UK). This was used to prevent the production of bronchial secretions that could potentially block the airway during the experiment.

A polyethylene catheter (Portex, external diameter 0.96 mm; internal diameter 0.58 mm; 70 cm long) was inserted into the right femoral artery, to continuously monitor blood pressure and conduct blood gas analysis

Blood sampling was done immediately after the catheter was in place and then each hour to ensure blood gases were maintained within the normal physiological range apart from increased PaO_2 due to the oxygen enriched mixture used to maintain physiological stability during surgery. A rectal thermocouple provided continual monitoring of core body temperature which was maintained at 37±0.5^{o}C using a heat lamp.

Permanent focal cerebral ischaemia was induced using the distal diathermy method, as previously described in Chapter 2.3.2, via a small craniectomy. Once the MCA was cauterized it was cut to confirm occlusion before placing haemostatic sponge (Spongostan) over the area and stitching with a 4-0 suture.

4.2.3 Induction of hyperglycaemia

A single dose of a 15% glucose solution (aqueous, 10ml/kg) was administered i.p. 10 minutes prior to occlusion of the MCA in WKY (WKY + G) and fructose fed SHRSP (ffSHRSP + G) rats. Their respective control groups (ffSHRSP & WKY) received the vehicle (distilled water, 10ml/kg).

4.2.4 MRI scanning protocol

Immediately following MCAO the ventral surfaces of the left and right hind limbs as well as the chest were shaved using an electric shaver. Electrode gel (Sigma) was applied to the shaved areas and ECG leads were placed on top and secured with tape. The rat was then disconnected from the ventilator and blood pressure transducer before being transferred to the MRI cradle where the intubation tube was reconnected to a ventilator to maintain anaesthesia.

The rat was secured in the cradle using tooth and ear bars to prevent head movement during scanning. Body temperature was maintained for the duration of the scanning protocol using a closed circuit thermal jacket and was monitored by a rectal thermocouple. The ECG leads were connected and a pressure sensor

was attached to the back of the rat to measure respiration. The blood pressure transducer was similarly reconnected to monitor blood pressure throughout the scanning protocol. A linear surface receiver coil (2cm diameter) was placed above the head of the animal before being transferred to the scanner described in Chapter 2.5.1.

Diffusion-weighted imaging was performed to identify ischaemically damaged tissue in 8 coronal slices within the MCA territory using the sequence described in Chapter 2.5.3.1. Scans were acquired at 1 hour post MCAO and then each subsequent hour for 4 hours. ADC maps were subsequently produced from post-processing of DWI images and in-house determined strain specific thresholds of tissue viability were applied to WKY ($\leq 0.61 \times 10^{-3} mm^2 sec^{-1}$) and ffSHRSP ($\leq 0.59 \times 10^{-3} mm^2 sec^{-1}$)

Non-invasive quantitative cerebral blood flow measurements were carried out on 6 coronal slices, that were spatially identical to slices 2-7 acquired from DWI scans, using a form of pseudo-continuous arterial spin labelling (cASL) based on a train of adiabatic inversion pulses (Moffat *et al* 2005). The sequence is described in Chapter 2.5.4.1. Similarly to DWI scans the cASL scans were obtained at 1, 2, 3 and 4 hours following MCAO.

Unfortunately due to technical difficulties with the cASL scans, CBF maps were not able to be generated for the majority of animals. Due to this the diffusion perfusion mismatch could not be calculated and so the progression of the DWI defined lesion was used as an alternative measure of the evolution of damage. The technical problems with the cASL were resolved which allowed CBF maps to be generated for 16 animals. This perfusion data has been included in section 4.3.7.

4.2.5 Animal recovery

At the end of the 4 hour scanning protocol, the rat and cradle were removed from the MRI scanner. Once the rectal thermocouple, ECG leads, respiration sensor and ear bars were removed, the ventilator and blood pressure transducer were disconnected and the animal was immediately transferred from the cradle to the operating theatre where the ventilator was reconnected. The isoflurane

concentration was reduced to 1% to start the recovery process. The femoral catheter was removed and the femoral artery was sealed by electrocoagulation. The site was then re-sutured and the anaesthesia was withdrawn. At this point the nitrous oxide-oxygen mixture was readjusted to a 50:50 ratio to aid recovery. Once the animal had started to breathe against the ventilator for a period of 5 minutes the ventilator was temporarily disconnected. If the animal continued to breathe unassisted for a period of 5 minutes the intubation tube was carefully removed and the rat was transferred to a facemask to continue the oxygen supplementation. Once motor function had began to return the animal was transferred to a recovery cage containing some bedding and sawdust from its previous cage and its own cardboard tube. Soft diet, containing softened normal rat chow, was placed in the cage and dry pellets and water were also available *ad libitum*. The general condition of the animals was assessed at least 3 times during recovery and this was recorded.

4.2.6 Infarct determination

Rats were transcardially perfusion-fixed with heparinised saline followed by 4% paraformaldehyde in PBS at 24 hours after MCAO. Tissue was dehydrated and processed through to paraffin wax blocks as described in Chapter 2.4.2. Infarct was assessed using haematoxylin and eosin stained coronal sections (7µm). Ischaemic tissue was quantified at 8 pre-determined levels spanning the MCA territory. Areas of damage were transcribed on to representative line diagrams to correct for brain swelling or processing (Osborne *et al* 1987). For volumetric assessment the areas of ischaemic damage were calculated using Image J and integrated with the known distance between each coronal level, using stereotaxic atlas co-ordinates (Paxinos & Watson, 1998) as described in detail in Chapter 2.4.5.

4.2.7 Immunohistochemistry

Sections adjacent to those used for infarct measurements were processed for immunohistochemistry with an antibody against the lipid peroxidation by-product 4-hydroxynonenal (4-HNE, Clone 198960, R&D systems) as described in Chapter 2.6.1. Light microscopy was used to transcribe the location of increased

4-HNE immunopositivity compared to contralateral tissue onto a separate set of line diagrams to those used for infarct measurements. Image J was used to determine the volume of 4-HNE staining for each animal. This analysis was performed blinded to group identity and the infarct volume data.

4.2.8 Randomisation, blinding and statistical analysis

Animals were allocated upon arrival from the breeding colony to normoglycaemic or hyperglycaemic groups and randomised by the toss of a coin. The investigator was blinded to animal identity during the analysis of ADC lesion, infarct and 4-HNE volumes. Blood glucose levels and ADC lesion volumes were assessed using a 2 way ANOVA repeated measures test with Bonferroni post test. Infarct and 4-HNE immunopositivity volumes were assessed using a 1 way ANOVA with Bonferroni post test. Data are expressed as mean ± standard deviation.

4.3 Results

4.3.1 ffSHRSP rats exhibited hypertension compared to the WKY strain

Non-invasive blood pressure measurements, obtained in the conscious state prior to induction of cerebral ischaemia, confirmed the known strain differences between SHRSP and WKY rats (Table 4.1). The ffSHRSP groups both exhibited substantially elevated systolic blood pressure compared to the WKY groups. There was also no difference between rats assigned to the vehicle treatment or glucose treatment groups for subsequent experiments in either WKY or ffSHRSP groups.

4.3.2 Physiological variables

The ffSHRSP groups weighed significantly less compared to the WKY groups (Table 4.1). This is consistent with previously reported differences between the SHRSP and WKY strain.

During anaesthesia ffSHRSP rats had significantly higher MABP than WKY rats, as reflected in the elevated conscious blood pressure exhibited by the ffSHRSP groups compared to the WKY groups. There was no difference in core body temperature, blood gas or pH measurements between any of the four groups (Table 4.1). The $PaCO_2$ and pH were maintained within normal physiological limits however the PaO_2 was elevated out with this due to the oxygen enriched mixture used to deliver the anaesthesia compared to the percentage oxygen present in air.

There was no mortality in any of the 4 groups following MCAO surgery. However there were 7 surgical deaths that occurred due to bleeding from the MCA whilst attempting to electocoagulate the vessel. This occurred in 3 WKY rats and 4 ffSHRSP rats.

	Prior to anaesthesia		During anesthesia				
Group	Weight (g)	Systolic BP (mmHg)	P_aO_2 (mmHg)	P_aCO_2 (mmHg)	pH	MABP (mmHg)	Temperature (°C)
WKY (n=10)	271 ± 16	123.6 ± 6.9	139.1 ± 17.4	38.2 ± 4.0	7.39 ± 0.05	93.4 ± 12.1	37.1 ± 0.5
WKY + G (n=10)	274 ± 15	122.7 ± 6.5	140.8 ± 17.3	39.9 ± 5.3	7.40 ± 0.06	96.1 ± 8.9	37.3 ± 0.5
ffSHRSP (n=10)	219 ± 13 **	177.9 ± 5.9**	136.5 ± 14.2	36.5 ± 2.4	7.40 ± 0.07	116.7 ± 13.5 **	37.2 ± 0.4
ffSHRSP+G (n=10)	225 ± 13 ##	183.3 ± 8.4 ##	134.2 ± 13.9	37.0 ± 2.1	7.41 ± 0.06	114.6 ± 10.2 ##	37.3 ± 0.6

Table 4.1: Physiological variables: Body weight measured on the day of MCAO; Systolic BP measure 3-5 days prior to MCAO; PaO2, PaCO2, pH measured at time of MCAO; MABP, Temperature (rectal) expressed as mean for anaesthesia period. **, P<0.001 vs. WKY; ##, P<0.001 vs. WKY + glucose. Data presented as mean ± standard deviation.

4.3.3 Glucose administration led to clinically relevant hyperglycaemia in both WKY and ffSHRSP

The baseline blood glucose measurements, taken just prior to i.p. glucose or i.p. vehicle administration, were not significantly different between vehicle and glucose treatment groups or between the WKY and ffSHRSP strains (Figure 4.1).

Following i.p. glucose administration in the ffSHRSP + G and WKY + G groups, blood glucose increased significantly (Figure 4.1). The mean peak blood glucose levels in both WKY+G and ffSHRSP + G groups recorded at 1 hour post MCAO were similar. In the WKY+G group blood glucose reduced slightly between 1 hour and 2 hours however still remained significantly elevated compared to the vehicle treated WKY group. The ffSHRSP + G group maintained the peak level of hyperglycaemia until a small decrease was observed at 3 hours and similarly 4 hours following MCAO compared to the ffSHRSP group. At all time points examined during the MR scanning period, blood glucose levels in the WKY+G and the ffSHRSP + G groups were significantly greater than in vehicle-treated controls. There was no change in blood glucose levels in either WKY or ffSHRSP groups following vehicle treatment. This suggests that stress hyperglycaemia following MCAO was not observed during the MRI scanning period.

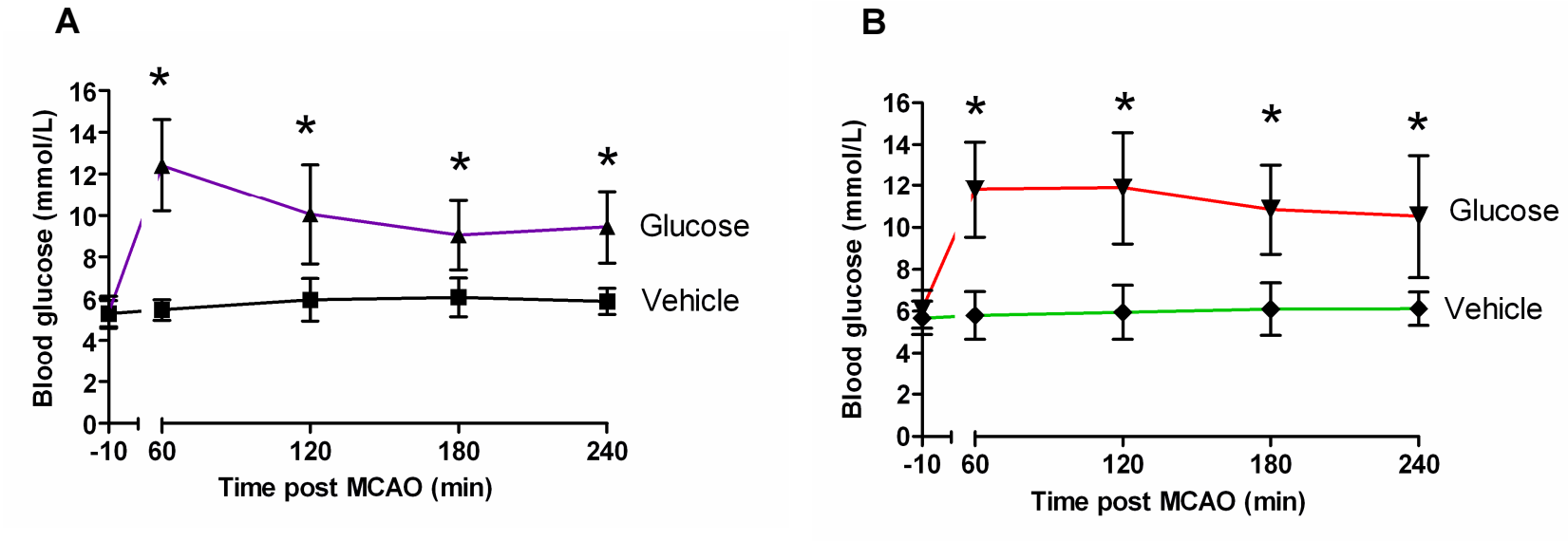

Figure 4.1: Blood glucose levels before and after MCAO in WKY (A) and ffSHRSP (B) rats. Glucose or vehicle was administered 10 mins before MCAO (-10). Peak levels measured in WKY and ffSHRSP rats after glucose administration were similar. In rats administered glucose, blood glucose levels remained elevated above the vehicle treated group for at least 4 hours after MCAO. Data analysed using a 2-way ANOVA, * $P < 0.001$ glucose versus vehicle. Data presented as mean ± standard deviation.

4.3.4 Hyperglycaemia accelerated the development of ischaemic injury in both WKY and ffSHRSP

Strain-specific ADC thresholds were applied to each of the hourly ADC maps obtained following MCAO to assess the acute evolution of ischaemic injury in each of the 4 experimental groups (Figure 4.2). From 1 hour to 4 hours post-MCAO the ADC-derived region of ischaemic damage expanded in WKY and ffSHRSP rats with and without glucose administration. At the earliest time point examined, 1 hour after MCAO, the mean ADC lesion was significantly larger in hyperglycaemic than in normoglycaemic WKY rats (Figure 4.3A) and the effect of hyperglycaemia was maintained over the subsequent 3 hours. The mean ADC lesion in hyperglycaemic ffSHRSP rats was larger than in normoglycaemic ffSHRSP at 1 hour after MCAO (Figure 4.3B) and the effect of hyperglycaemia on ADC lesion volume was maintained over subsequent time points in this strain. Thus, hyperglycaemia exacerbated early ischaemic brain damage in both normal rats and rats with features of metabolic syndrome.

The rate of ADC-derived lesion growth was significantly increased in both WKY + G and ffSHRSP + G compared to their respective vehicle treated control groups between 0 and 1 hour post MCAO (Figure 4.4). No further significant differences were observed at subsequent time points. This suggests that glucose dependant damage primarily occurs during the first hour following occlusion.

At 1 hour after MCAO the effect of hyperglycaemia on ADC lesion volume was similar in WKY and ffSHRSP rats causing a similar absolute increase in ischaemic damage (WKY, 50.8mm^3; ffSHRSP, 51.1mm^3; Table 4.2). Subsequently the difference between WKY and WKY + G groups increased further illustrating that hyperglycaemia was continuing to exacerbate ischaemic injury. However, the mean difference between the ffSHRSP groups did not change. Although a formal statistical analysis was not performed on these data they suggest that while hyperglycaemia exacerbated ischaemic damage in the first hour after MCAO in both ffSHRSP and WKY rats, its effect was less pronounced at later time points in ffSHRSP compared to WKY rats.

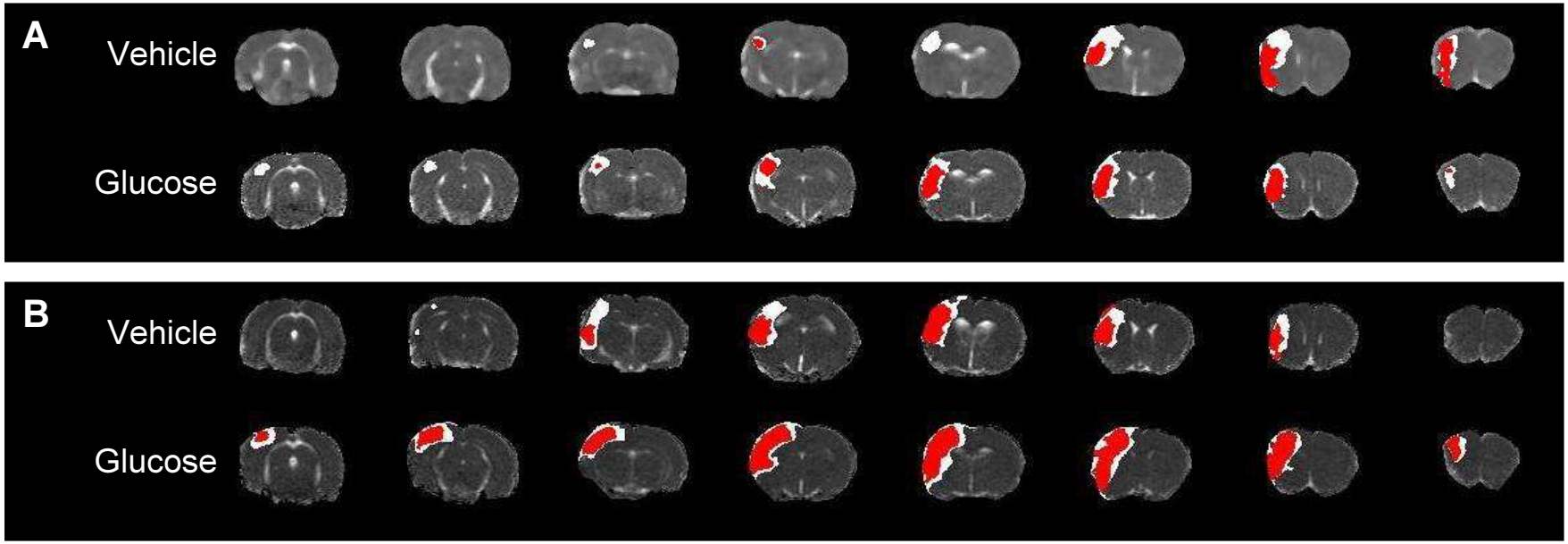

Figure 4.2: ADC-derived ischaemic injury in A) WKY and B) ffSHRSP rats following permanent MCAO both with and without glucose administration. Eight coronal slices from the median animal within each experimental group is displayed. The red areas represent the ischaemic injury at 1 hour post-MCAO whereas the white area represents the lesion at 4 hours post-MCAO. This highlights the spatial profile of the lesion and how it develops over the acute time period.

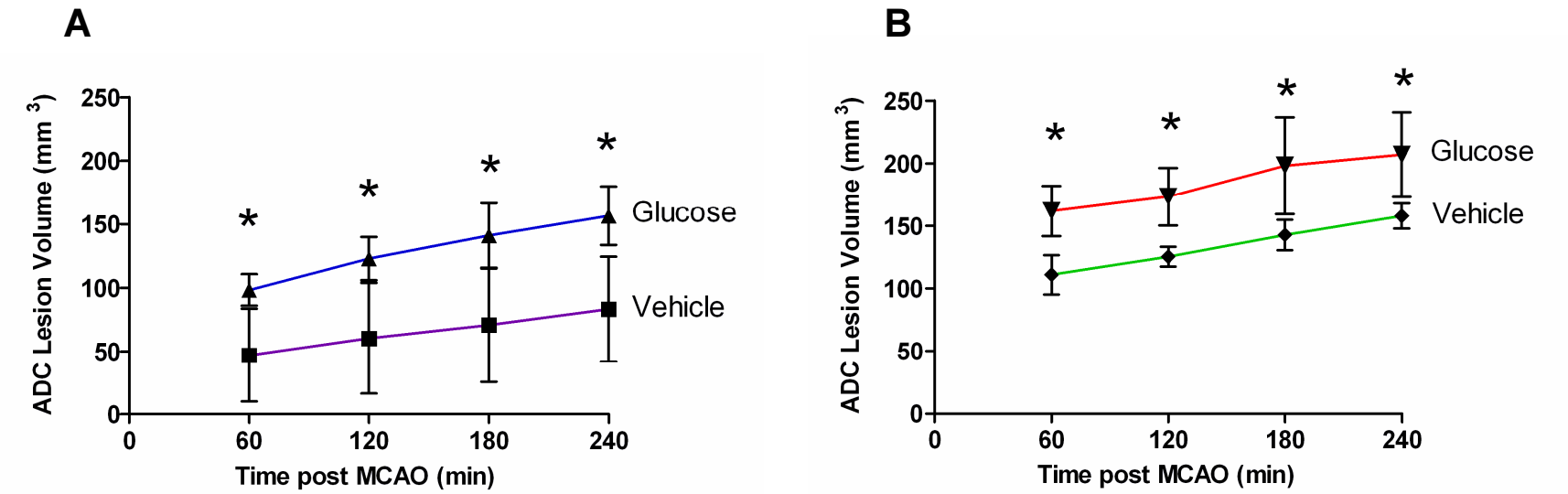

Figure 4.3: Volumetric analysis of ADC maps from 8 coronal slices 1-4 h after MCAO in WKY rats (A) and ffSHRSP rats (B). Hyperglycaemia exacerbated damage at all time points in both WKY and ffSHRSP rats. Data analysed using a 2-way ANOVA, *, $P<0.001$ compared with normoglycaemic vehicle-treated controls. Data presented as mean ± standard deviation.

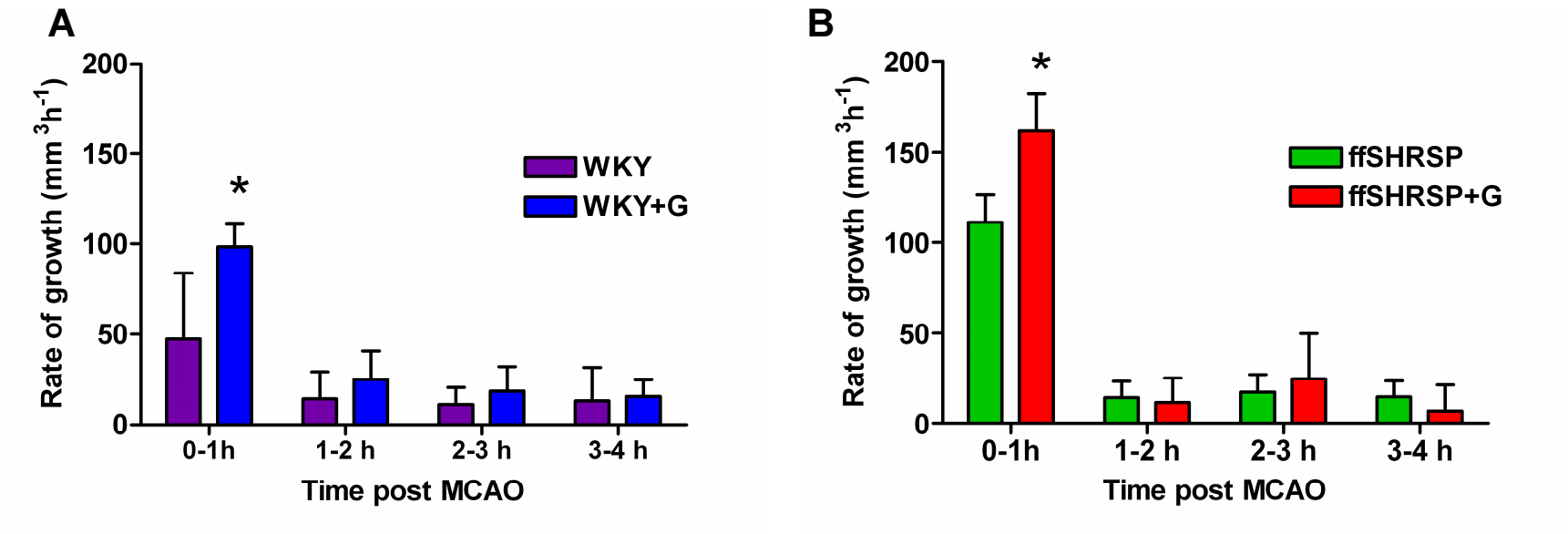

Figure 4.4: Rate of ADC lesion growth over each hour following MCAO in (A) WKY and WKY + G groups and (B) ffSHRSP and ffSHRSP + G groups. The rate was calculated from the volume of lesion growth occurring in each hour. Data analysed using a 2-way ANOVA, *, P<0.001 compared with normoglycaemic controls at that particular time point. Hyperglycaemic groups indicated by +G. Data presented as mean ± standard deviation

	Difference in mean volume of ischaemic damage between groups (mm^3)	
Time after MCAO (hours)	**WKY vs. WKY+G**	**ffSHRSP vs. ffSHRSP+G**
1	51	51
2	62	48
3	69	56
4	72	49

Table 4.2: Difference in infarct size between normo- and hyperglycaemic groups.

4.3.5 Hyperglycaemia increased infarct volume in WKY but not in ffSHRSP rats.

Infarct volume was significantly larger in hyperglycaemic WKY than in normoglycaemic WKY rats (Figure. 4.5A). The most pronounced differences were observed in sections at the rostral and caudal poles of the lesion (Figure. 4.5C). Infarct volume in hyperglycaemic ffSHRSP rats was not increased compared to normoglycaemic controls (Figure. 4.5B); the rostro-caudal distribution of the lesion being similar in both groups (Figure. 4.5D). Thus, hyperglycaemia in the early period after MCAO exacerbated infarct size at 24 hours only in rats lacking features of metabolic syndrome.

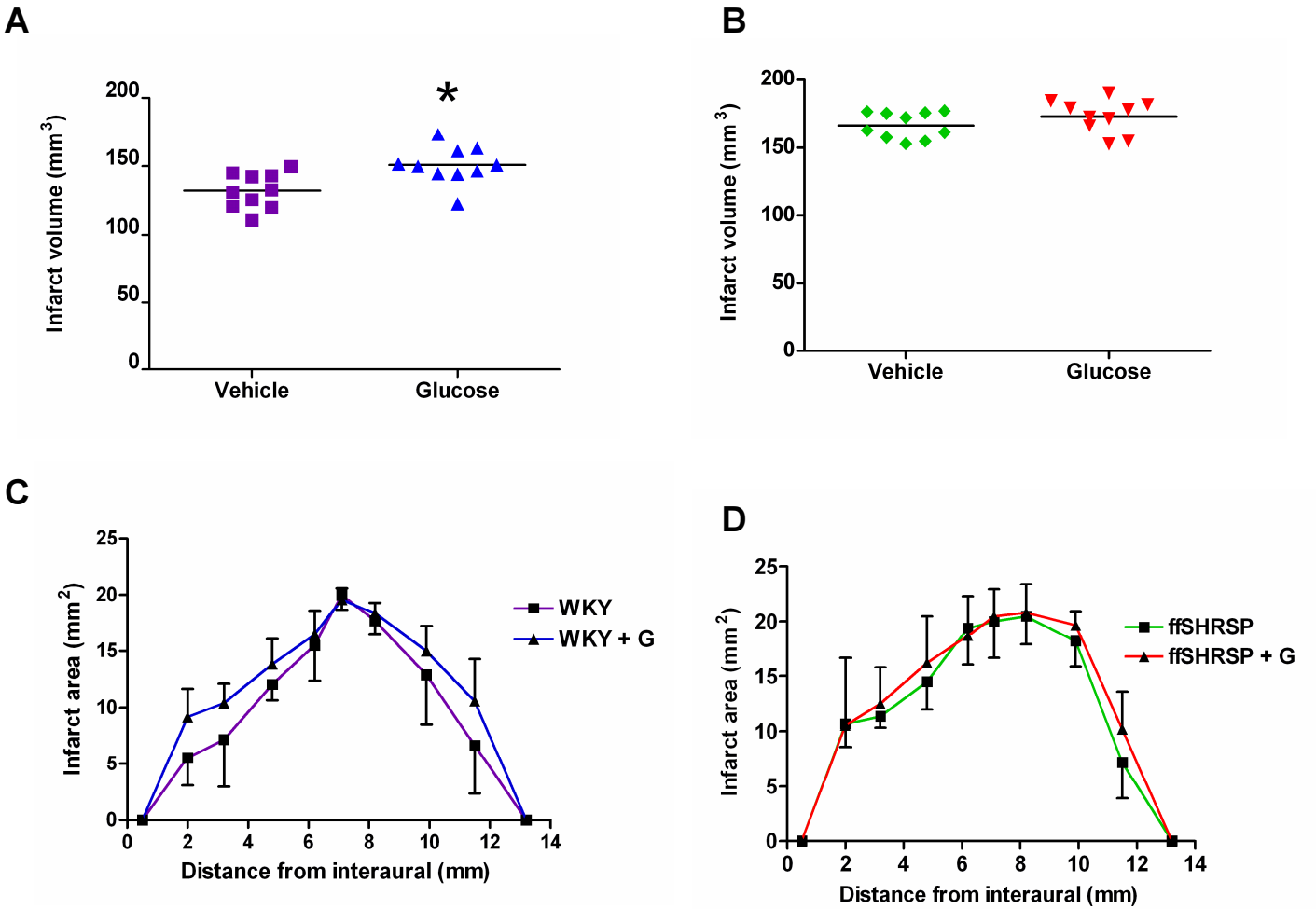

Figure 4.5: Volumetric analysis of cerebral infarction 24h after MCAO in WKY rats (A) and ffSHRSP rats (B) with and without glucose loading. The mean is illustrated by the horizontal bar. Data analysed using a 1-way ANOVA with Bonferoni post test.* P<0.001 glucose compared to vehicle administration. The rostro-caudal profile of the infarct is shown for WKY (C) and ffSHRSP (D). Hyperglycaemic groups indicated by +G. Data presented as mean ± standard deviation.

4.3.6 Hyperglycaemia exacerbated the extent of oxidative stress.

Compared to the contralateral hemisphere 4-HNE immunoreactivity was higher in ischaemically damaged tissue and peri-infarct regions. Intense staining for 4-HNE was observed in neurons and axons in both grey and white matter (Figure 4.6). Hyperglycaemia in WKY rats was associated with a greater volume of tissue exhibiting immunopositivity for 4-HNE (Figure 4.7a). In contrast, there was no significant difference in the volume of 4-HNE-positive tissue between ffSHRSP+G and the normoglycaemic ffSHRSP rats (Figure 4.7b). As these results mirrored the group differences observed for infarct volume, the volume of immunopositivity was expressed as a % of infarct volume (Figure. 4.7c, 4.7d). In both normo- and hyperglycaemic WKY rats, 4-HNE immunostaining occupied a smaller volume of tissue compared to the infarct in all animals. However, 4-HNE staining occupied a significantly greater proportion of tissue in hyperglycaemic WKY rats compared to controls indicating that hyperglycaemia was associated with greater lipid peroxidation. In ffSHRSP rats there were some animals in which 4-HNE staining occupied a greater volume of tissue than the infarct. There was no difference between normo- and hyperglycaemic ffSHRSP rats in the proportion of tissue occupied by 4-HNE staining indicating that hyperglycaemia was not associated with greater lipid peroxidation. The ffSHRSP rats had larger proportions of tissue occupied by 4-HNE staining compared to the WKY rats.

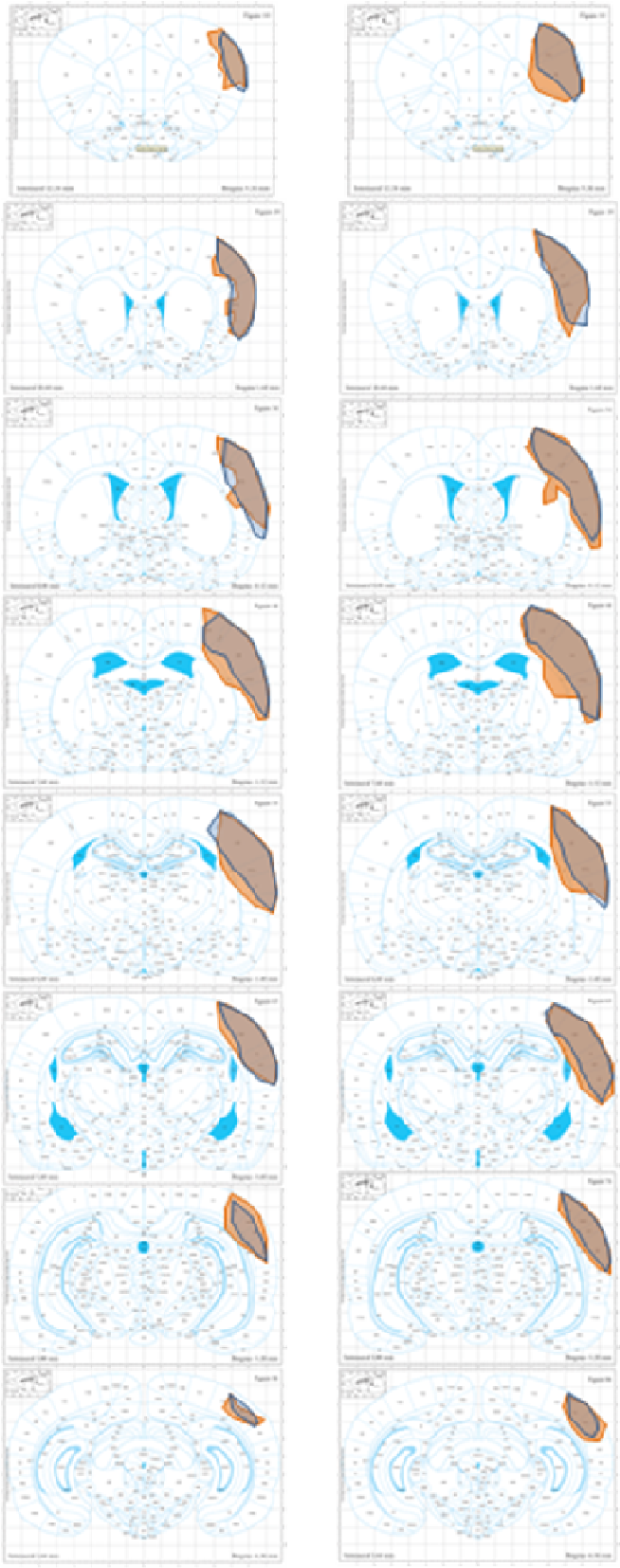

Figure 4.6: Line diagrams illustrating the distribution of immunostaining and infarct in a representative animal from (A) WKY and (B) WKY+G. The blue outlined areas indicated infarcted tisse and the orange outlined areas represent -HNE immunopositive tissue 24 h post MCAO

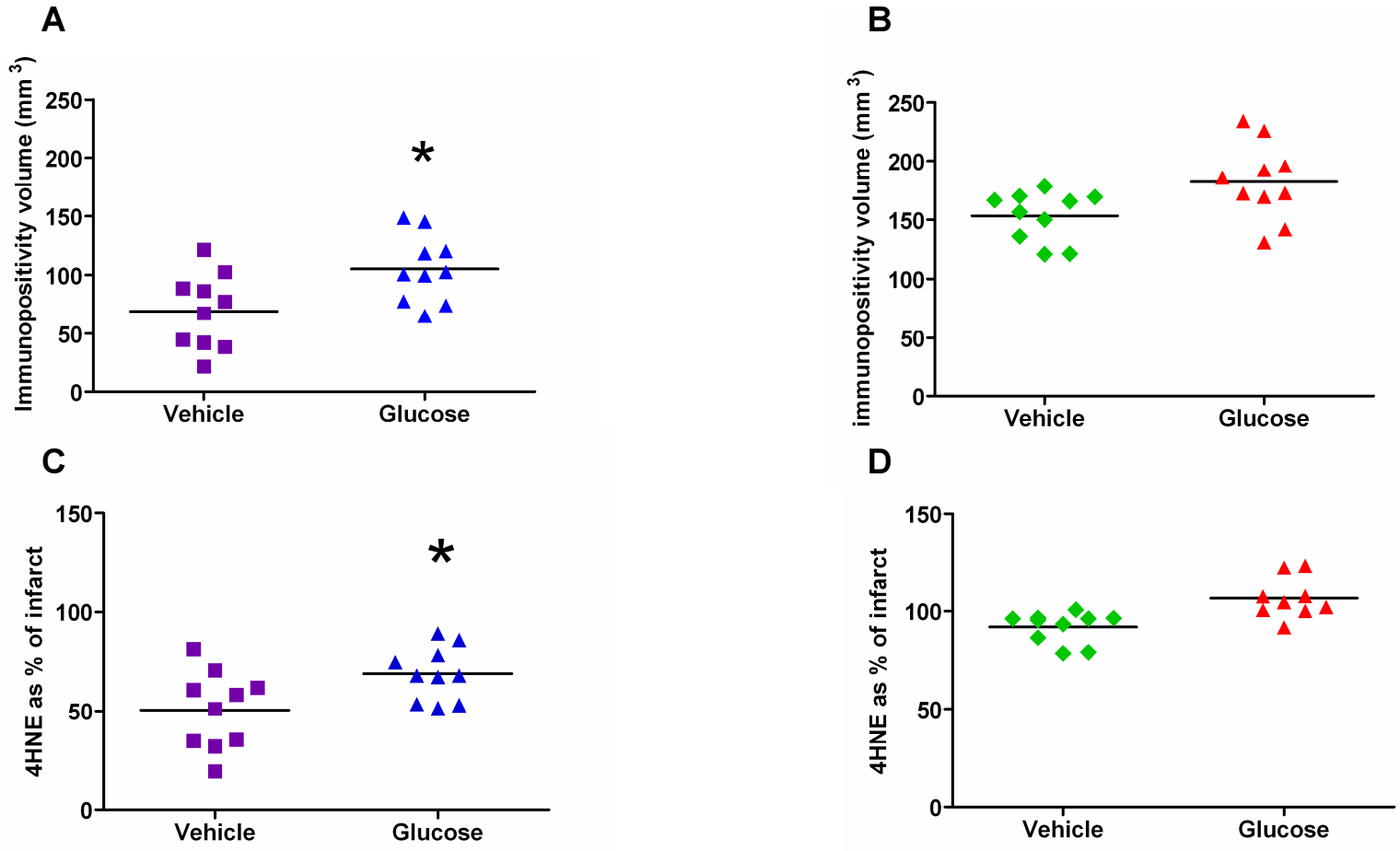

Figure 4.7: Volumetric analysis of 4-HNE immunopositivity 24 h post MCAO in both WKY (A) and ffSHRSP (B) with and without glucose loading. To confirm that the amount of immunopositivity wasn't just due to the size of the infarct 4-HNE staining was also expressed as a percentage of the infarct in both (C) WKY and (D) ffSHRSP with and without glucose loading.*, Data analysed using 1-way ANOVA with Bonferoni post test. P<0.001 compared to normoglycaemic controls

4.3.7 Hyperglycaemia exacerbated perfusion deficit in WKY but not ffSHRSP group

Due to the technical issues experienced with the cASL scanning protocol, it was not possible to generate cerebral blood flow maps for the majority of animals. However once this technical problem had been resolved the remaining animals were assessed for perfusion differences between groups (Figure 4.8).

The perfusion deficit at 1 hour post MCAO showed that there was a significantly larger volume of tissue with CBF below the threshold for tissue survival in the WKY + G group compared to the WKY group (Figure 4.9A). This suggests that hyperglycaemia in the WKY strain increased the perfusion deficit compared to the vehicle treated WKY group. This effect was not seen in the ffSHRSP groups where there was no increase in perfusion deficit as a result of glucose loading (Figure 4.9B).

There was no significant difference in contralateral CBF between WKY and WKY + G groups at any time point measured although a temporal decrease was observed in both groups (Figure 4.10). This suggests that although hyperglycaemia is potentially increasing the perfusion deficit, this isn't due to a global reduction in CBF compared to the vehicle treated WKY group.

The ffSHRSP and ffSHRSP + G groups had a significantly larger perfusion deficit than the WKY group at 1 hour post MCAO which is reflective of the volume of ischaemic injury derived from ADC maps. Interestingly the perfusion deficit increases in the ffSHRSP and the ffSHRSP +G over the 4 hours post MCAO whereas the perfusion deficit remains similar in the WKY and WKY + G groups over the duration of the MRI scanning protocol (Figure 4.11).

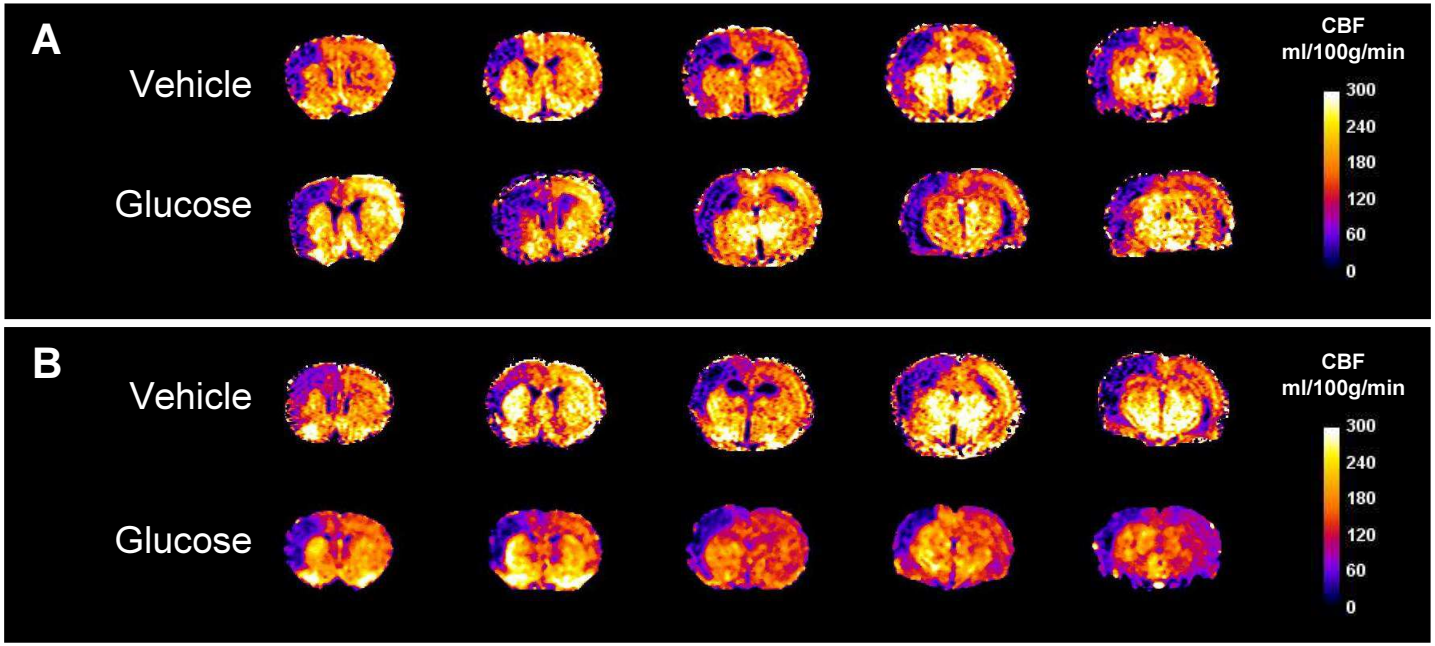

Figure 4.8: Quantitative CBF maps displaying hypoperfused tissue at 1 hour post-MCAO over 5 coronal slices in A) WKY and B) ffSHRSP with and without glucose administration. Darker regions represent areas of reduced blood flow which is predominantly found in the ipsilateral cortex as expected. The data shown are from the median animal in each group.

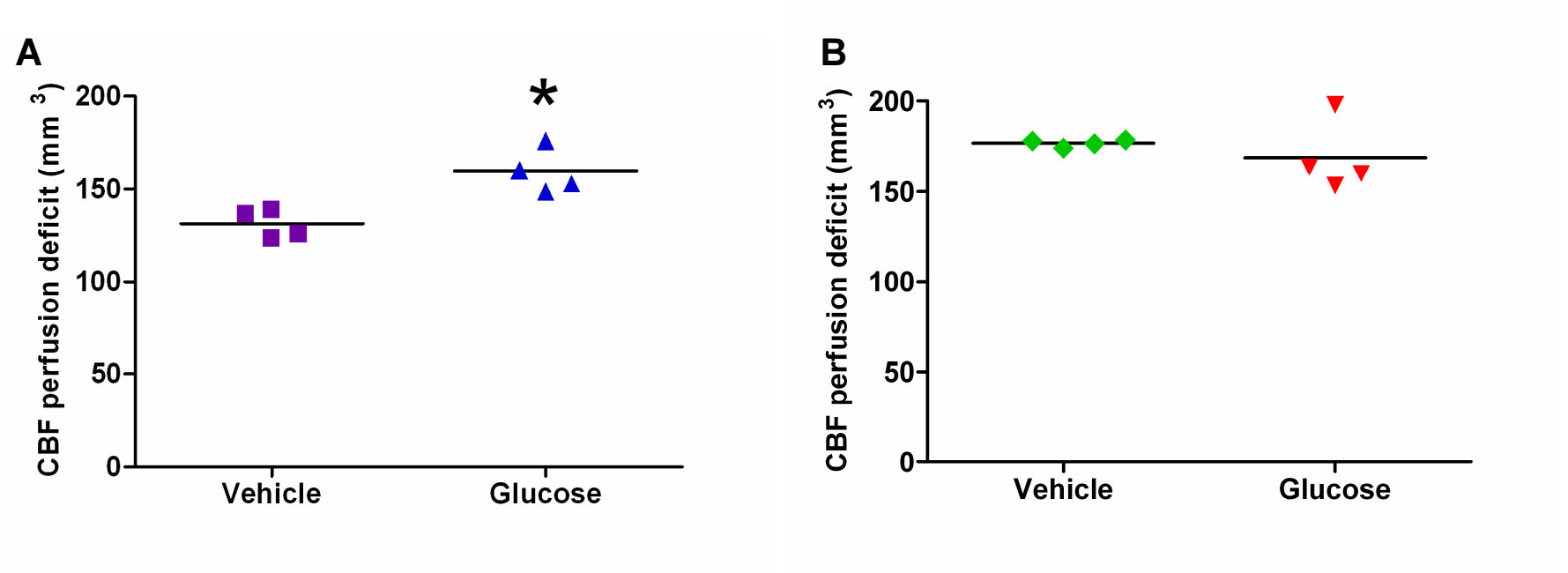

Figure 4.9: Volume of tissue 1 hour post MCAO exhibiting a perfusion deficit in (A) WKY and (B) ffSHRSP with and without glucose loading. Strain specific thresholds, which predict tissue that will become infarcted if not reperfused, were applied to CBF maps to quantify the perfusion deficit. Data presented as scatter plots with the means indicated. Data anaylsed with unpaired t-test. *, P>0.05 compared to vehicle treated control.

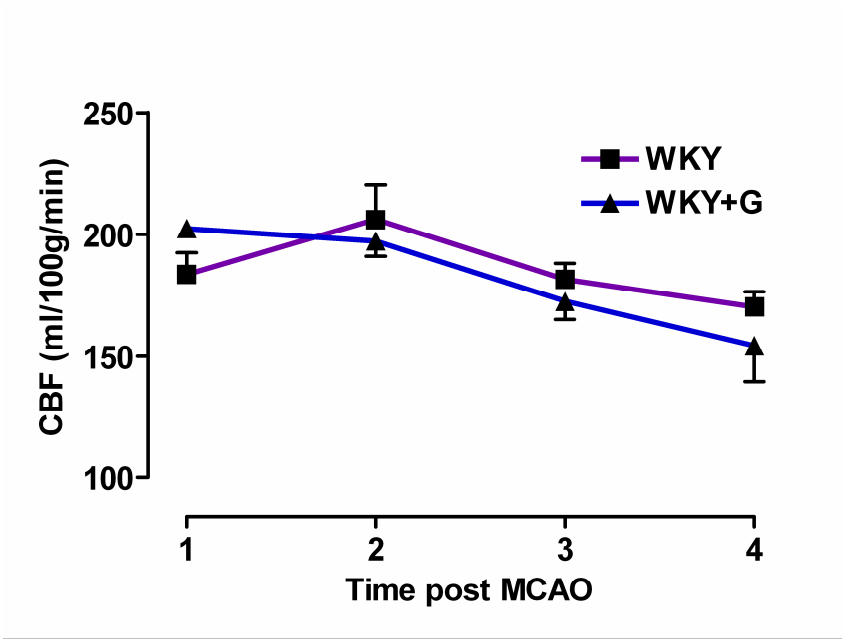

Figure 4.10: Mean contralateral CBF in WKY and WKY + G groups following permanent MCAO. No difference between the groups was seen at any measured time point. Data expressed as mean ± standard deviation.

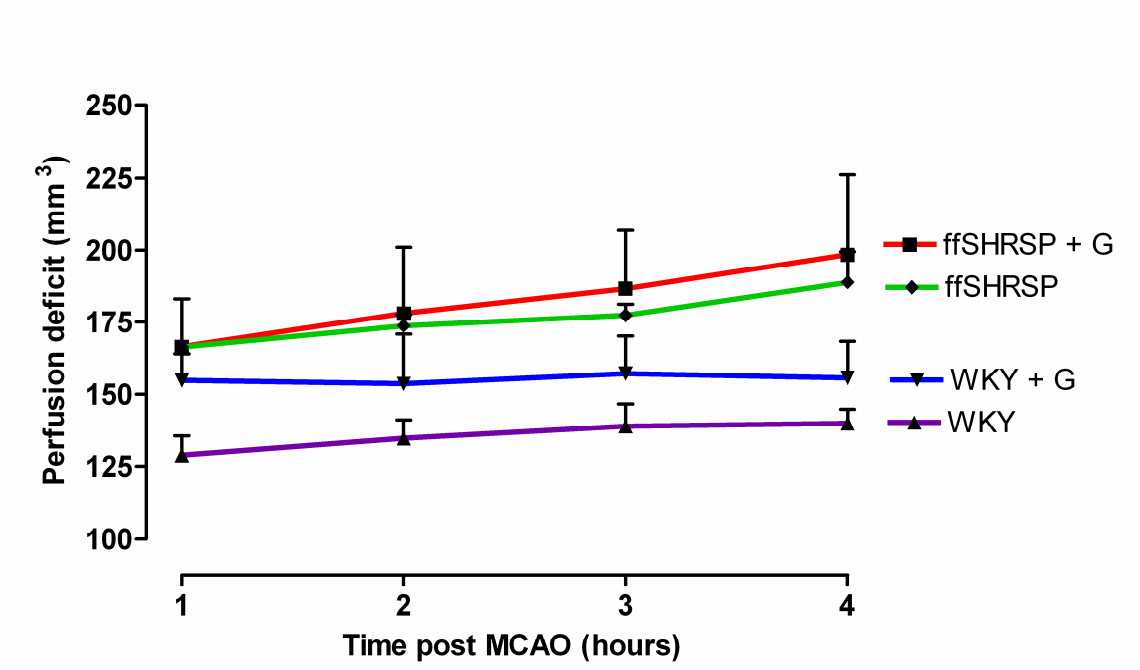

Figure 4.11: Temporal evolution of perfusion deficit, derived from CBF maps, WKY and ffSHRSP with and without glucose loading. Data presented as mean ± standard deviation.

4.4 Discussion

Previous studies of hyperglycaemia in animal models of ischaemia, while useful in establishing the principle that elevated blood glucose exacerbates brain damage, did not use models that reproduce features of typical human PSH; the majority used models of type I diabetes and very high concentrations (16 – 30 mmol/l) of blood glucose (MacDougall and Muir 2010). The current study modelled clinically relevant levels of blood glucose and also addressed the impact of moderate hyperglycaemia in the context of existing insulin resistance and hypertension.

4.4.1 Hyperglycaemia accelerates early lesion expansion in both WKY and ffSHRSP rats

The data demonstrate that moderate hyperglycaemia, present at the time of onset of focal cerebral ischaemia, markedly accelerates lesion growth over the first few hours. The effect of hyperglycaemia was pronounced as early as 1 hour after MCAO indicating the rapid nature of its detrimental actions in the ischaemic brain. This is consistent with data from a previous diffusion-weighted MRI study after permanent MCAO in rats(Huang *et al* 1996), although in the presence of substantially higher levels of blood glucose (~25 mmol/l) than those used in the present study (~12 mmol/l). Our data further demonstrate that clinically-relevant levels of hyperglycaemia accelerate lesion growth not only in normal rats but also in those with features of metabolic syndrome. The absolute increase in lesion size 1 hour post MCAO, attributable to the elevation in blood glucose, was very similar between the WKY and ffSHRSP rats. After the initial acceleration in growth the rate became consistent with that of the normoglycaemic groups for the remainder of the acute time frame. This suggests that to be able to improve the longevity of the penumbra the management of PSH needs to be very rapid.

The effect of hyperglycaemia on ischaemic lesion size at acute time points was proportionally greater in normal rats compared to those with features of metabolic syndrome. Thus, rats without co-morbidities commonly associated with stroke appear to be more susceptible to the detrimental effects of

hyperglycaemia. Acute lesion sizes in ffSHRSP rats were larger than those in WKY groups regardless of glycaemic profile, likely attributable to the known differences between SHRSP and WKY strains (McCabe *et al* 2009). We postulate that the lesser effect of hyperglycaemia in the metabolic syndrome group may be the result of a prevailing role for hypertension and poor collateral flow (Coyle and Heistad 1987) in exacerbating the evolution of damage in these animals such that there is less tissue at risk available to be influenced by hyperglycaemia in the acute phase. The pre-existence of metabolic syndrome components might already have induced an adverse metabolic state (e.g. increased oxidative stress) such that moderate hyperglycaemia could not significantly exacerbate what was already primed to be a larger infarct than that in the rats without the features of metabolic syndrome.

4.4.2 Hyperglycaemia exacerbates infarct size 24 hours post MCAO in WKY but not ffSHRSP

Moderate hyperglycaemia significantly increased infarct volume 24 hours post MCAO, but only in animals lacking features of metabolic syndrome. This suggests that there is a more profound effect in the absence of components of the metabolic syndrome. A systematic review of patient data reported that for stress hyperglycaemia, relative risks of mortality and poor functional outcome were increased in non-diabetic stroke patients, but not those with a diagnosis of diabetes(Capes *et al* 2001). It is possible that hyperglycaemia does not significantly influence the evolution of ischaemia in diabetic subjects, and that this review finding reflects the pathophysiological effects that are demonstrated in the present study, although it is possible that diabetic subjects numbers were too small to reliably detect a detrimental effect of hyperglycaemia.

Potentially any additional effect of hyperglycaemia on infarct size may have been masked by the extensive nature of the damage incurred in the ffSHRSP groups. The lesions were large encompassing the majority of the affected MCA territory downstream of the occlusion. It is possible that the level of damage in the ffSHRSP groups was close to maximal and therefore a ceiling effect may be present. This may explain why a significant difference was observed in the acute evolution of ischaemic damage between the glucose and vehicle treated ffSHRSP

groups but not at the 24 h time point used for infarct determination. The ceiling effect was the reason why the distal diathermy occlusion model was used instead of the more severe intraluminal filament model.

The clinical implication of our current findings could be that glycaemic control may be more important in acute stroke patients who do not have insulin resistance or other co-morbidities such as hypertension. However, although the effect of hyperglycaemia in ffSHRSP rats was less marked than in WKY, the former group incurred the largest infarcts. While glycaemic control might influence the early evolution of the infarct in patients with pre-existing metabolic syndrome, glycaemic control may be less beneficial since 24 hour infarct volume was not significantly exacerbated by acute PSH.

These comments can only be speculative since the clinical picture in stroke is more complex, and includes insulin treatment with its attendant risk of hypoglycaemia, the development of late rather than early hyperglycaemia, late complications of large infarction such as brain swelling and malignant oedema, and interaction with reperfusion therapies, none of which was modelled in the present study (McCormick *et al* 2010).

4.4.3 Possible mechanisms associated with hyperglycaemia dependent damage

Hyperglycaemia may be toxic to the ischaemic brain however the mechanism is not fully understood. In hypoperfused tissue at risk hyperglycaemia may contribute to the accumulation of lactate and intracellular acidosis as a result of increased anaerobic metabolism. In a rabbit model of stroke after 4 hours of permanent occlusion moderate hyperglycaemia (~11 mmol/l) caused a significant reduction in intracellular brain pH compared to controls (Anderson *et al* 1999). Acidosis may accelerate ischaemic injury and enhance production of free-radicals (Kagansky *et al* 2001; Siesjo *et al* 1996) leading to rises in intracellular calcium (OuYang *et al* 1994). Elevated intracellular calcium is a key component of glutamate-mediated excitotoxicity, which is a major pathological mechanism of ischaemic damage. This has been supported by a study that found

that elevated blood glucose led to a rise in extracellular glutamate in cerebral cortex after forebrain ischaemia (Li *et al* 2000).

Hyperglycaemia is known to be associated with inflammation and oxidative stress and is implicated in a number of mechanisms. Oxidative stress, primarily originating from release of superoxide from the mitochondria, is thought to be the unifying mechanism underlying the deleterious effects of chronic hyperglycaemia in complications, including neuropathy, associated with diabetes (Brownlee 2005; Tomlinson and Gardiner 2008). Superoxide radicals can cause direct damage to cells through lipid peroxidation, protein carbonylation and DNA damage. In the present study, enhanced oxidative stress after MCAO in hyperglycaemic rats was suggested by more widespread immunostaining for 4-HNE which may indicate the involvement of free radicals in acute hyperglycaemia. This supports previous findings that hyperglycaemia following cerebral ischaemia is able to increase production of superoxide. Using a global transient ischaemia model it was found that hyperglycaemia caused significant increase in superoxide production in the hippocampal CA1 neurons compared to normoglycaemic animals after 18 hours of recirculation, which preceded accelerated and enhanced neuronal death in the hippocampal CA1 area. (Muranyi and Li 2006). A 75g oral glucose challenge in humans has also been shown to cause an increase in superoxide generation in leukocytes by 140% above basal levels in addition to increasing production of the $p47^{phox}$ subunit of NADPH oxidase, which is responsible for superoxide generation (Mohanty *et al* 2000).

The proportion of tissue exhibiting 4-HNE immunopositivity was increased by hyperglycaemia in WKY but not in ffSHRSP rats in the present study. This preliminary evidence suggests that increased oxidative stress may contribute to the detrimental effect of hyperglycaemia in ischaemic brain in the absence but not presence of features of metabolic syndrome. However there are some limitations regarding the quantification of oxidative stress using immunohistochemistry. In this chapter areas of tissue, where staining for 4-HNE was present, were transcribed to line diagrams as a way of quantifying the level of oxidative stress in each animal. Obviously not every cell within these areas was stained and therefore this is a rather crude method of quantification. New advances in image analysis systems may provide the best way to analyse

immunostained sections rather than relying on a subjective method (Taylor & Levenson, 2006). These sytems are not economically viable for small laboratory needs and therefore subsequent studies in this thesis will move to a tissue assay for markers of lipid peroxidation and oxidative stress.

In addition to oxidative stress, the small amount of CBF data collected during this study indicates that hyperglycaemia may accelerate lesion expansion by increasing the perfusion deficit following MCAO. Interestingly, this hyperglycaemic effect was once again only seen in the WKY rats and hence suggests that hyperglycaemia can influence the CBF only in the absence of insulin resistance, hypertension and other features of the metabolic syndrome associated with the ffSHRSP model. Obviously the results from the perfusion data are underpowered in comparison to the other analyses conducted in this chapter but it is supported by some previous studies that show that administration of glucose to conscious rats can reduce regional CBF by 24% compared to normoglycaemic controls in the absence of cerebral ischaemia (Duckrow *et al* 1985; Duckrow *et al* 1987). This reduction is blood flow could not be explained purely by the increase in plasma osmolality as administration of mannitol, that lead to a similar osmolality observed following glucose administration, only reduced blood flow by 10%. This is also supported by a study conducted in cats that found after a 3 hour MCAO the hyperglycaemic animals suffered a 70% reduction in CBF compared to 34% in the normoglycaemic controls (Wagner *et al* 1992). It is known that ROS and free radicals can directly and indirectly act on cerebral blood vessels to alter vascular tone, which could potentially affect CBF. Superoxide, in high concentrations primarily causes vasoconstriction in the cerebral vasculature and this has been demonstrated in cerebral arteries using NADPH (Didion and Faraci 2002). Superoxide reacts with endothelial nitric oxide (NO), a potent vasodilator, at a rate 3 times faster than with superoxide dismutase (SOD). The inactivation of NO, by reacting with superoxide, results in the loss of the vasodilatory influence of NO on basal vascular tone causing vasoconstriction. The reaction of superoxide with NO leads to the production of the free radical peroxynitrite which may have its own effects on vascular tone. Interestingly a study has also highlighted the potential vasoconstrictory effects of superoxide on vascular smooth muscle independent of endothelial mediated mechanisms. Increasing superoxide levels have been shown

in vivo to contract basilar arteries, without endothelium, implying that superoxide may be able to directly contract cerebral arteries (Tosaka *et al* 2002). The ability of glucose to reduce cerebral perfusion could increase the volume of hypoperfused tissue and therefore lead to substantially larger infarcts and greater penumbral loss. Glucose-induced ROS can neutralise NO which can further reduce its availability for NO dependant vasodilation (Frank *et al* 2005). This loss of cerebrovascular reactivity pertains to chronic changes in glucose homeostasis and so the mechanism associated with this may not be conserved in acute hyperglycaemia. However from the results of this study it can be postulated that glucose may enhance ischaemic damage by oxidative stress and potentially increase the perfusion deficit associated with MCAO, and this may all be modulated by glucose-induced ROS.

4.4.4 Conclusions

Clinically relevant levels of hyperglycaemia have a rapid and profound detrimental effect on the early evolution of focal ischaemic brain damage in both the absence and presence of metabolic syndrome components. Despite this, infarct size at 24 hours post MCAO was increased only in the absence of these features. Therefore managing blood glucose levels as early as possible may benefit all hyperglycaemic stroke patients in the acute phase, but greater benefit is likely to be seen in those who do not have metabolic syndrome.

Mechanistically this study suggests an involvement of ROS under hyperglycaemic conditions in the absence of insulin resistance and other metabolic syndrome components. The potential involvement of oxidative stress in the detrimental effect of glucose is addressed in the subsequent chapter.

Chapter 5 - Increased superoxide generation in hyperglycaemia-induced ischaemic damage: Effects of SOD/catalase mimetic EUK-134

5.1 Introduction

Based on the findings in the previous chapter and the known role of superoxide in chronic hyperglycaemia associated pathologies, the experiments presented in this chapter were designed to investigate the role of oxidative stress in hyperglycaemia mediated damage following experimental stroke using the SOD/catalase mimetic EUK-134.

In the acute development of ischaemic damage following permanent MCAO, excitotoxicity and oxidative stress mechanisms are thought to be predominantly responsible for lesion expansion following bioenergetic failure (Chapter 1, Figure 1.7). Preclinical studies have implicated a role of superoxide in focal cerebral ischaemia using superoxide dismutase (SOD) knockout mice. In SOD2 knockouts, elevation of oxidative stress markers such as DNA fragmentation and mitochondrial cytochrome C were associated with increased infarct volume following permanent MCAO (Fujimura *et al* 1999; Murakami *et al* 1998).

The findings of Chapter 4 suggested that hyperglycaemia had increased free radical production, enhancing oxidative stress and lipid peroxidation in normal rats and therefore this was potentially the mechanism for hyperglycaemia-mediated damage in experimental stroke.

5.1.1 Hyperglycaemia mediated oxidative stress

In diabetes there are a number of associated complications, including neuropathies, which are thought to be mediated through increased flux through the polyol pathway, intracellular production of advanced glycation end products (AGEs), protein kinase C activation and increased hexosamine pathway activation (Brownlee 2005). Hyperglycaemia activates these 4 pathways via increased production of mitochondrial superoxide. Increased glycolysis results in higher NADH production which in turn results in increased electron transfer through the electron transport chain in the mitochondrion. This results in the accumulation of a number of intermediates, including ubisemiquinone which can transfer an electron to molecular oxygen to form superoxide. It has been shown in endothelial cells that 30mM glucose causes a 3 fold increase in reactive

oxygen species (ROS) production compared to 5mM glucose, and this increase is attenuated by overexpression of superoxide dismutase (Nishikawa *et al* 2000). Brownlee et al. claim that mitochondrial production of superoxide is the unifying mechanism of the 4 pathways leading to diabetic complications associated with hyperglycaemia, whereby superoxide partially inhibits the glycolytic pathway enzyme glyceraldehyde-3 phosphate dehydrogenase causing upstream accumulation of the substrates for the 4 pathways. PKC-dependent activation of NAD(P)H oxidase is also a significant source of superoxide. This evidence suggests that superoxide is likely to be involved in hyperglycaemia associated ischaemic damage. The role of superoxide in hyperglycaemic cerebral ischaemic damage is supported by the observations made in Chapter 4 regarding increased lipid peroxidation, which reflected increased infarct volume, in hyperglycaemic rats compared to normoglycaemic controls. It is known that acute hyperglycaemia can cause oxidative stress. In healthy human subjects using a glucose clamp test to increase plasma glucose to around 15mmol/L it was observed that circulating levels of nitrotyrosine, a marker of oxidative stress, were increased compared to subjects whose blood glucose was maintained at normal physiological levels (Marfella *et al* 2001). Nitrotyrosine is formed by nitrosylation of tyrosine residues by peroxynitrite, a free radical produced by the reaction of superoxide with nitric oxide. Vascular nitric oxide production is an important physiological response to induce vasodilation, inhibit platelet aggregation and leukocyte adhesion. Overproduction of superoxide can cause an imbalance between superoxide and nitric oxide leading to endothelial dysfunction and the formation of peroxynitrite. Inhibition of nitric oxide synthase with -nitro-arginine methyl ester (L-NAME) has been shown to reduce infarct volume in the streptozotozin diabetic rat model following transient MCAO (Quast *et al* 1995), and this is thought to be due to reductions in peroxynitrite formation.

Attenuating an increase in superoxide production to prevent possible downstream activation of damaging pathways, inactivation of critical enzymes and the further generation of free radicals could potentially reduce hyperglycaemia-associated ischaemic damage. It is thought that conventional antioxidants might not be appropriate because they neutralise ROS molecules on a one-to-one basis. The Superoxide dismutase (SOD)/catalase mimetic EUK-134

is a catalytic antioxidant that has been previously shown to reduce infarct volume by nearly 90% compared to controls in a rodent experimental stroke model (Baker *et al* 1998). EUK-134 mimics the actions of two enzymes, SOD and catalase which catalyses the neutralisation of superoxide to water and oxygen. EUK-134 is therefore able to target superoxide as its production is heightened both in response to ischaemia and furthermore to hyperglycaemia. This may be more appropriate than conventional antioxidants to neutralise this overproduction of ROS, which do so on a one-to-one basis. Affecting the overproduction of superoxide more successfully may uncover the mechanistic role in hyperglycaemic cerebral ischaemia.

5.1.2 Measuring the effects of EUK-134

In addition to exacerbation of infarct volume the studies in the previous chapter showed that lipid peroxidation, a marker of oxidative stress, was increased in the brains of hyperglycaemic rats compared to controls. It was therefore important to assess whether or not EUK-134 administration could reduce lipid peroxidation back to control levels and therefore determine the role of superoxide in hyperglycaemia mediated ischaemic damage. Lipid peroxides are unstable and decompose to form a complex series of compounds including reactive carbonyl compounds. Polyunsaturated fatty acid peroxides generate malondialdehyde (MDA) and 4-hydroxyalkenals, such as 4-Hydroxynonenal, upon decomposition. Measurement of MDA and 4-hydroxyalkenals has been used frequently as an indicator of lipid peroxidation. In this study tissue MDA levels were quantified in both cortical and subcortical structures for both the ipsilateral and contralateral hemispheres following experimental stroke.

To confirm that any effect associated with the administration of EUK-134 is as a result of a reduction in superoxide, circulating levels of the ROS were measured. Electron paramagnetic resonance (EPR) or electron spin resonance (ESR) spectroscopy is a technique for studying chemical species that have one or more unpaired electrons, such as the reactive oxygen species, superoxide. EPR works in a similar way to MRI although EPR is used to detect the transitions of unpaired electrons in an applied magnetic field, rather than H^+ in proton MRI. The unpaired electron, like a proton, has spin. When an external magnetic field is

applied, the paramagnetic electrons either orient in a direction parallel or antiparallel to the direction of the magnetic field. This creates two distinct energy levels for the unpaired electrons and allows them to be measured as they are driven between the two levels by applying microwave radiation. As superoxide is highly reactive, a spin probe, which reacts with superoxide, can be used to detect the levels of the ROS in blood samples. The spin probe, 1-hydroxy-3-carboxy-pyrrolidine (CPH) is oxidised to 3-carboxy-proxy by superoxide which yields an EPR spectra. Detection of circulating superoxide levels provided an indication of an effect of EUK-134 on the systemic level of superoxide.

5.1.3 Animal model

The previous Chapter adopted the ffSHRSP metabolic syndrome model and the control WKY strain for experimentation. Pragmatically, for the experiments described in this chapter, it was impossible to use the SHRSP or WKY rats due to supply issues from the University colony. Therefore the acute hyperglycaemia model was transferred to the Sprague-Dawley strain. However, this does not necessarily represent a limitation since, in preclinical stroke research, it is important to not focus studies solely on one particular model or strain. The predictability of pre-clinical research to clinical stroke is strengthened if results can be recreated in different models, strains and species.

5.1.4 Hypothesis

I hypothesised that pre-treatment with EUK-134 would attenuate the hyperglycaemia-associated ischaemic damage following MCAO and this would be reflected by a reduction in brain tissue lipid peroxidation, quantified by the marker malondialdehyde and circulating superoxide using EPR.

5.1.5 Study Aims

1) Establish if hyperglycaemia exacerbated infarct volume compared to normoglycaemia in Sprague-Dawley rats.

2) Investigate if EUK-134 was able to reduce the level of arterial superoxide compared to vehicle-treated animals.

3) Determine if EUK-134 could reduce infarct volume, and if this was associated with reduced lipid peroxidation, in both normoglycaemia and hyperglycaemic rats.

5.2 Methods

5.2.1 Animals

All experiments were carried out under licence from the Home Office and were subject to The Animals (Scientific Procedures) Act, 1986. Male Sprague Dawley rats (253±13 g, Harlan, Bicester, UK) were randomly assigned (see section 5.2.7) to one of 4 groups; Normoglycaemia (n=8), Hyperglycaemia (n=8), Normoglycaemia+EUK (n=8) or Hyperglycaemia+EUK (n=8)

5.2.2 Surgical procedures

Rats fasted overnight, were anaesthetised initially with 5% inhaled isoflurane in an induction chamber and then orally intubated. Animals were artificially ventilated with 2.5% isoflurane delivered in a nitrous oxide-oxygen mixture (70:30). All rats were given an intraperitoneal (i.p.) injection of the anti-muscarinic drug atropine sulphate (0.4ml, 600µg/ml, Martindale Pharmaceuticals, UK). This was used to prevent the production of bronchial secretions that could potentially block the airway during the experiment.

Polyethylene catheters (Portex, external diameter 0.96 mm; internal diameter 0.58 mm; 20 cm long) were inserted into the right femoral artery and the right femoral vein, for blood pressure/blood gas analysis and drug administration, respectively.

Blood sampling was done immediately after the catheter was in place and then each hour to ensure blood gases were maintained within the normal physiological range apart from increased PaO_2 due to the oxygen enriched mixture used to maintain physiological stability during surgery. A rectal thermocouple provided continual monitoring of core body temperature which was maintained at 37±0.5^{o}C using a heat lamp.

EUK-134 (2.5mg/kg in ~2ml saline, Cayman Chemicals) was infused intravenously at a rate of 0.6 ml per minute, 20 minutes prior to MCAO in Normoglycaemia+EUK and Hyperglycaemia+EUK groups. The dose was selected based on the solubility of the drug stated by the manufacturer

(http://www.caymanchem.com/pdfs/10006329.pdf) and a previous in vivo focal ischaemia study (Baker *et al* 1998). The Normoglycaemia and Hyperglycaemia groups were infused with vehicle (saline) of an equivalent volume. A single dose of a 15% glucose solution (aqueous, 10ml/kg) was administered i.p. 10 minutes prior to occlusion of the MCA to Hyperglycaemic and Hyperglycaemia+EUK groups. Their respective normoglycaemia control groups received vehicle (distilled water, 10ml/kg).

Permanent focal cerebral ischaemia was induced using the distal diathermy method, as previously described in Chapter 2.3.2, via a small craniectomy. Once the MCA was cauterized it was cut to confirm occlusion before placing haemostatic sponge (Spongostan, Ferrosan UK) over the area and stitching the wound closed with a 4-0 suture.

An arterial blood sample (475µl) was taken 2 hours post-MCAO and immediately deposited into a heparinised vacutainer and stored on ice. The blood was then processed for EPR analysis (see section 5.2.7)

5.2.3 Animal Recovery

After the 2 hour post-MCAO blood sample was taken the isoflurane concentration was reduced to 1% to start the recovery process. The femoral artery and vein catheters were removed and the entry hole in the artery and vein was sealed by electrocoagulation. The site was then re-sutured and the anaesthesia was withdrawn. At this point the nitrous oxide-oxygen mixture was readjusted to a 50:50 ratio to aid with recovery. Once the animal had started to breathe against the ventilator for a period of 5 minutes the ventilator was temporarily disconnected. If the animal continued to breathe unassisted for a period of 5 minutes the intubation tube was carefully removed and the rat was transferred to a facemask to continue the oxygen supplementation. Once motor function had began to return the animal was transferred to a recovery cage containing some bedding and sawdust from its previous cage and its own cardboard tube. Soft diet, containing softened normal rat chow, was placed in the cage and dry pellets and water were available ad libitum. The general condition of the animals was assessed at least 3 times a day during recovery and this was recorded.

5.2.4 Magnetic Resonance Imaging

Magnetic resonance imaging data were acquired on the system as described in Chapter 2.5.1. The rat was anaesthetised in a Perspex anaesthetic chamber with 5% isoflurane in a nitrous oxide-oxygen mixture (70-30) before being placed prone in the MRI cradle and attached to a face mask to continue delivery of anaesthetic at 2% isoflurane. The head was restrained using tooth and ear bars and body temperature was maintained for the duration of the scanning protocol using a closed circuit thermal jacket. Core body temperature was monitored by a rectal thermocouple. A linear surface receiver coil (2cm diameter) was placed above the head of the animal before being transferred to the scanner. A coronal RARE T2 sequence (effective TE: 46.8 ms, TR: 5000 s; in plane resolution of 97 um; 16 slices of 0.75 mm thickness) was acquired at 24 hours after stroke onset for infarct volume determination. ImageJ was used to separate the 16 images and the hyperintense region that represented the infarct was manually delineated using the freehand function. Measurement of individual images gave the infarct areas in millimetres squared, and infarct volume was calculated by summing the 16 areas and multiplying by the slice thickness (0.75 mm). The infarct was corrected for brain swelling as described in Chapter 2.5.5.

5.2.5 Neurological Scoring

An 18 point neurological score, as described in Chapter 2.7, was carried out ~23 hours post MCAO prior to the animal being scanned in the MRI for infarct determination.

5.2.6 Lipid peroxidation

At the end of the MRI scanning protocol the rat was removed from the cradle and transferred back to the operating theatre. Anaesthesia was increased to 5% isoflurane and 2 terminal blood samples (475 µl) were taken via cardiac puncture for EPR (see section 5.2.7). The brain was removed and the T2-defined region (encompassing all 16 slices) was dissected using the rostral-caudal positioning of the coronal T_2 scan for guidance. The cortex was removed and separated into ipsilateral and contralateral sections. This was also done with the subcortical

structures. These 4 regions were then processed for MDA and LPO analysis as described in Chapter 2.6.2. The quantity of MDA was corrected for the amount of protein in the sample using a BSA assay and standard curve.

5.2.7 Electron Paramagnetic Resonance (EPR)

The arterial blood samples collected at 2 hours and 24 hours post MCAO were incubated with 15µl CPH spin probe, mixed well and incubated at 37°C for 15 minutes. The sample was taken up into a 1ml syringe and the reaction between superoxide and CPH was stopped by immersing the sample in liquid nitrogen. The samples were then stored at -80°C until the EPR analysis was carried out. The EPR analysis was conducted by Jim McCulloch, chief technician in the Institute of Cardiovascular and Medical Sciences. Standards of known concentrations of CP were analysed alongside to obtain a standard curve. The concentration of CP in the blood samples was calculated from the standard curve as a measure of superoxide.

5.2.8 Randomisation, blinding and statistical analysis

To calculate the number of animals needed in each group a sample size calculation was conducted based on the changes in infarct volume, at 24 hours post MCAO, exhibited in WKY under hyperglycaemic conditions compared to normoglycaemic controls from Chapter 4 (Figure 5.1).

A

$$n = 1 + 2C\left(\frac{s}{d}\right)^2$$

B

	α	0.05	0.01
1-β	0.8	7.85	11.68
	0.9	10.51	14.88

Figure 5.1: Sample size calculation. A) Equation for sample size determination for continuous data where d = difference expected based on previous findings, s = standard deviation of group, C = constant derived from power and significance level. B) Table for determining C. α = significance level (95% or 99%), 1-β = Power (80% or 90%).

The difference in infarct volume observed between the WKY and WKY+G at 24 hours was 20 mm^3. The standard deviation for the WKY and WKY+G groups was 12.85 and 13.66 respectively. The sample size was based on an 80% power ($1-\beta = 0.8$) and a 95% significance level ($\alpha = 0.05$) and therefore the value for C was 7.85 according to Figure 5.1B. The sample size needed was calculated to be 7.8 animals in each group. In light of this 8 animals were assigned to each group.

Rats were assigned to 1 of the 4 groups using a randomisation plan generated at the beginning of the study (Table 5.1). I was blind to both the glucose administration and the EUK-134 administration. A colleague, who was in possession of the randomisation plan, presented me with the correct syringes at the time of drug administration. I was also blind to animal identity during the analysis of infarct volume and tissue MDA levels. Blood glucose levels were assessed using a 2 way ANOVA repeated measures test with Bonferroni post test. Infarct volume and MDA quantification were assessed using a 1 way ANOVA with Bonferroni post test. Neurological scores were assessed using a Kruskal-Wallis test with Dunn's multiple comparison post test. Data are expressed as mean ± standard deviation or as a scatter plot with the mean indicated.

A Randomization Plan

from

http://www.randomization.com

1	Normoglycaemia+EUK	17	Normoglycaemia+EUK
2	Hyperglycaemia	18	Normoglycaemia
3	Hyperglycaemia+EUK	19	Hyperglycaemia
4	Hyperglycaemia	20	Hyperglycaemia+EUK
5	Normoglycaemia	21	Hyperglycaemia
6	Normoglycaemia	22	Normoglycaemia+EUK
7	Normoglycaemia+EUK	23	Normoglycaemia
8	Hyperglycaemia+EUK	24	Hyperglycaemia+EUK
9	Hyperglycaemia+EUK	25	Hyperglycaemia+EUK
10	Normoglycaemia+EUK	26	Normoglycaemia+EUK
11	Normoglycaemia+EUK	27	Hyperglycaemia+EUK
12	Normoglycaemia	28	Normoglycaemia+EUK
13	Hyperglycaemia	29	Normoglycaemia
14	Hyperglycaemia	30	Normoglycaemia
15	Normoglycaemia	31	Hyperglycaemia
16	Hyperglycaemia+EUK	32	Hyperglycaemia

Table 5.1: Randomisation plan generated for the EUK-134 study with 8 animals in each of the 4 groups.

5.3 Results

5.3.1 Physiological variables

There was no difference in body weight between any of the 4 groups at the start of the study (Table 5.2). During anaesthesia there was no significant difference in the MABP, core body temperature, blood gases or pH measurements between any of the four groups (Table 5.2). The $PaCO_2$ and pH were maintained within normal physiological limits. However the PaO_2 was elevated out with this due to the oxygen enriched mixture used to deliver the anaesthesia.

There was no mortality in any of the 4 groups following MCAO surgery.

5.3.2 Glucose administration led to hyperglycaemia in Hyperglycaemia and Hyperglycaemia+EUK groups

The baseline blood glucose measurements, taken just prior to i.p. glucose or i.p. vehicle administration, were not significantly different between hyperglycaemia and normoglycaemia groups or between the vehicle and EUK-134 treatment groups (Figure 5.2).

Following i.p glucose administration to hyperglycaemia and hyperglycaemia+EUK groups, blood glucose increased significantly. The mean peak blood glucose levels in both hyperglycaemic groups recorded at 1 hour post MCAO were similar. The peak observed was higher than that previously observed in the WKY rats in Chapter 4 even though the same dose was used. There was no change in blood glucose levels in either the normoglycaemia or normoglycaemia+EUK groups following vehicle treatment.

	Prior to anaesthesia	During anaesthesia				
Group	Weight (g)	P_aO_2 (mmHg)	P_aCO_2 (mmHg)	pH	MABP (mmHg)	Temperature (°C)
Normoglycaemia (n=8)	243 ± 5	139.1 ± 39.4	38.2 ± 4.0	7.39 ± 0.05	93.4 ± 12.1	37.1 ± 0.5
Normoglycaemia+EUK (n=8)	251 ± 7	140.8 ± 27.3	39.9 ± 5.3	7.40 ± 0.06	93.3 ± 7.2	37.3 ± 0.5
Hyperglycaemia (n=8)	247 ± 7	136.5 ± 34.2	36.5 ± 2.4	7.40 ± 0.07	89.7 ± 13.5	37.2 ± 0.4
Hyperglycaemia+EUK (n=8)	248 ± 6	134.2 ± 44.9	37.0 ± 2.1	7.41 ± 0.06	93.2 ± 7.7	37.3 ± 0.6

Table 5.2: Physiological parameters of vehicle or EUK-134 treated hyperglycaemia and normoglycaemia groups. Body weight was measured immediately prior to anaesthesia. PaO2, PaCO2, pH, MABP and temperature were measured every 30 minutes and an average taken for the duration of anaesthesia. Data are presented as mean±SD, n=8 per group. MABP – mean arterial blood pressure

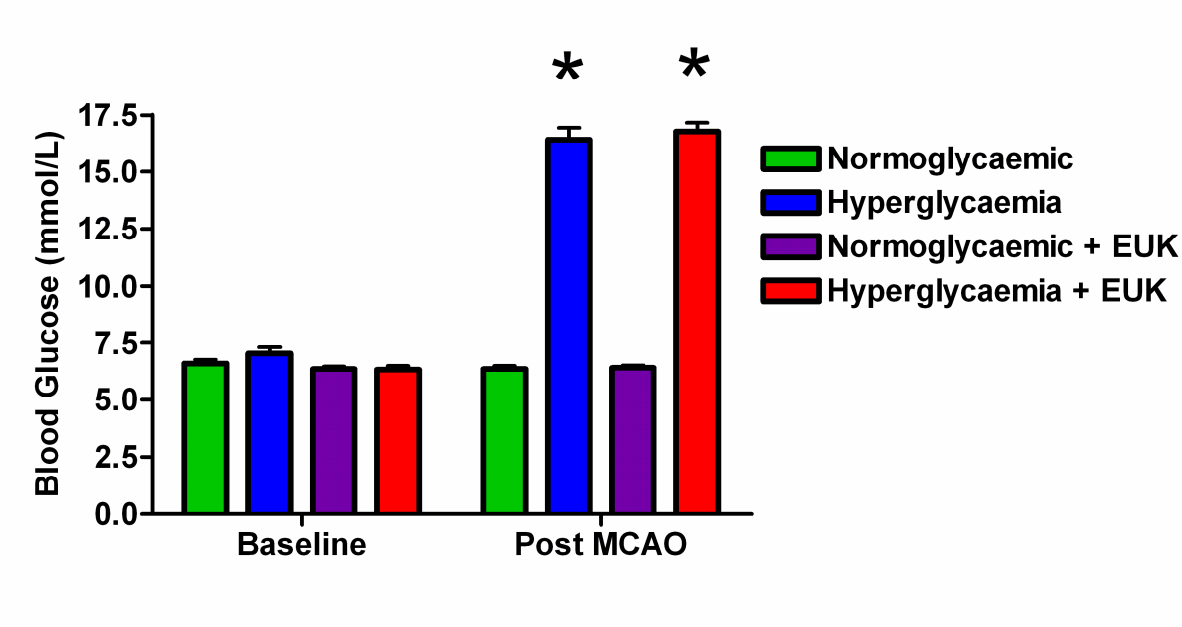

Figure 5.2: Blood glucose levels before and after glucose or vehicle administration. Peak levels measured in hyperglycaemia and hyperglycaemia+EUK groups after glucose administration were similar. There was no change in blood glucose following vehicle administration to normoglycaemia and normoglycaemia+EUK groups. Data analysed using 1 way ANOVA with Bonferoni post test. * $P<0.001$ compared to respective normoglycaemia controls.

5.3.3 Hyperglycaemia increased infarct volume irrespective of EUK-134 administration.

T2-derived infarct analysis showed that hyperglycaemic animals consistently exhibited ischaemic damage over a greater spatial profile than normoglycaemia animals (Figure 5.3). Infarct volumes were significantly larger in hyperglycaemic rats compared to normoglycaemic rats, which was consistent with the findings from Chapter 4(Figure 5.4). There was no significant difference between EUK-134 or vehicle treated normoglycaemia groups and similarly this was mirrored in the hyperglycaemia groups suggesting that EUK-134 was unable to reduce hyperglycaemia mediated damage following MCAO. Interestingly comparing the normoglycaemia group to the hyperglycaemia+EUK group, there was no significant difference between these groups.

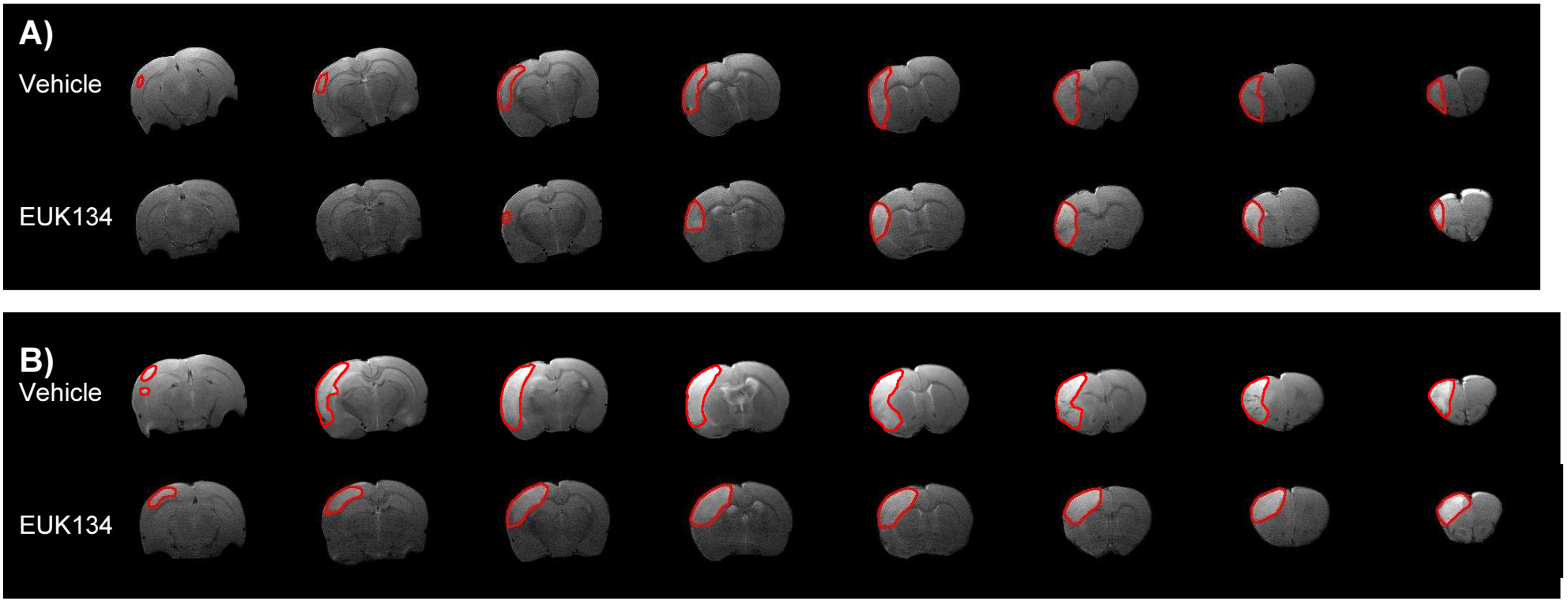

Figure 5.3: T2-derived infarcted tissue (circled red) in A) normoglycaemia and B) hyperglycaemia groups following permanent MCAO both with and without EUK-134 administration. The data presented are from the median animal within each experimental group.

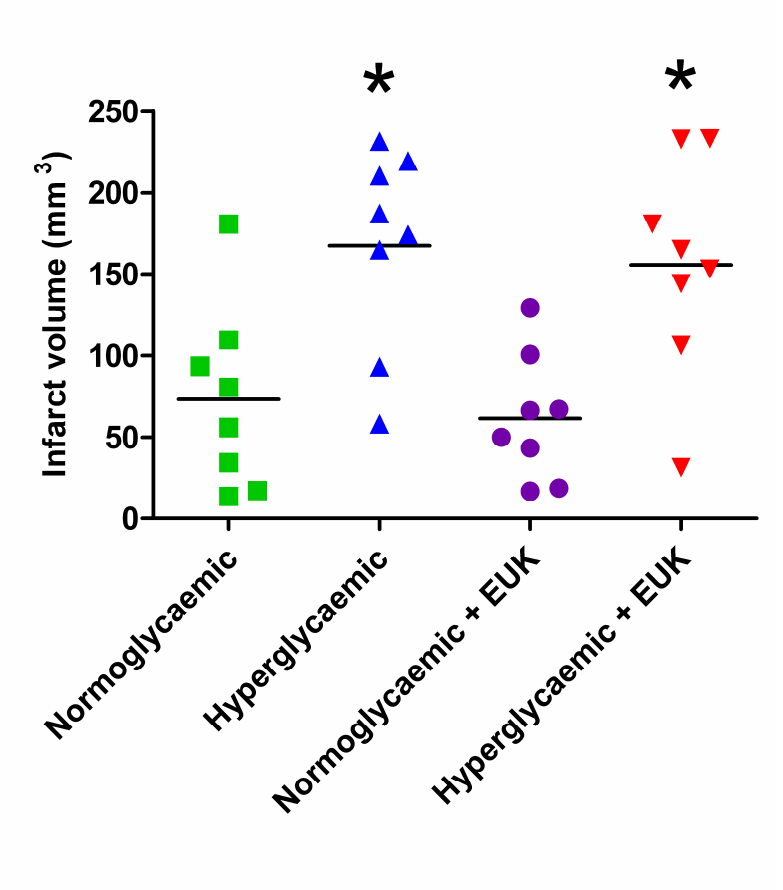

Figure 5.4: Volumetric analysis of cerebral infarction 24h after MCAO in normoglycaemia and hyperglycaemia groups both with and without EUK-134 administration. Data analysed using 1 way ANOVA with Bonferoni post test. * P<0.01 glucose compared to vehicle administration. Data presented as a scatterplot with mean indicated.

5.3.4 Neurological scores

The 18 point neurological score was conducted on all of the animals prior to experimentation (Figure 5.5). 31 animals were scored 18 out of 18 with one animal scoring 17. Following ischaemia all animals scored significantly worse than the baseline score. There was no difference between the EUK-134 and vehicle treated normoglycaemia groups (normoglycaemia, 11±2; normoglycaemia+EUK, 8±2) or hyperglycaemic groups (hyperglycaemia, 11±2; hyperglycaemia+EUK, 9±2).

The correlation between infarct volume and the neurological score was assessed in each of the 4 groups (Figure 5.6). The normoglycaemic group shows no obvious trend across the group as infarct volumes increase (Figure 5.6A). The hyperglycaemic group shows clustering around the higher infarct volumes but the lowest infarct volumes share the best neurological scores in the group (Figure 5.6B). The normoglycaemia+EUK group hints at a downward trend in neurological score with increasing infarct volume (Figure 5.6C), however the most convincing correlation exists in the hyperglycaemia+EUK group (R^2= 0.6, P=0.02, Figure 5.6D). Grouping all of the animals together there is a visible linear relationship between neurological score and infarct volume (R^2=0.5, P<0.001, Figure 5.7).

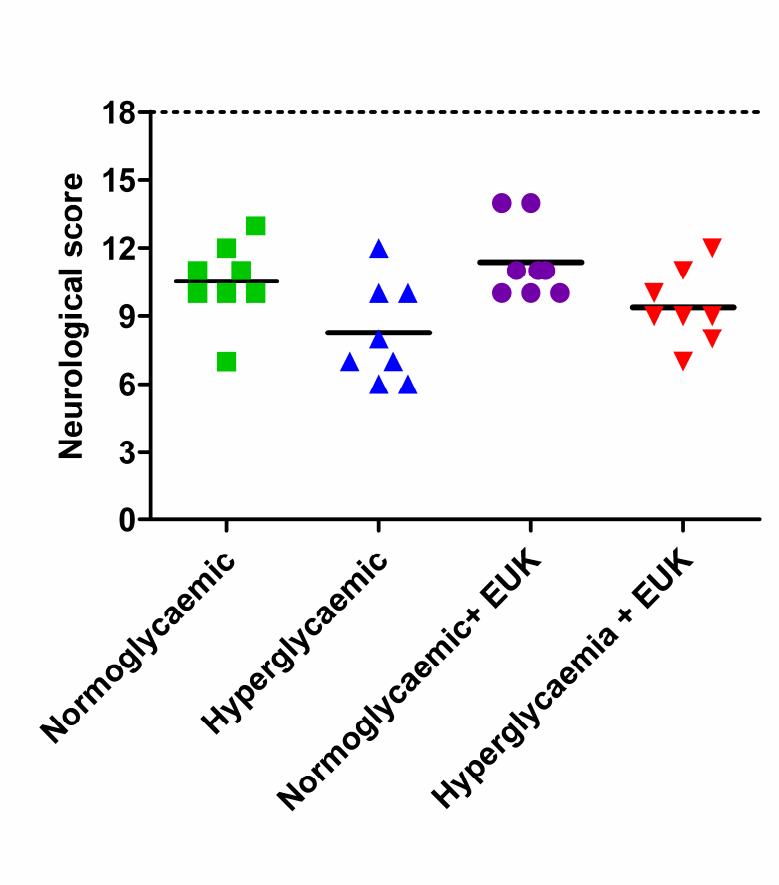

Figure 5.5: Neurological score ~23h after MCAO in normoglycaemia and hyperglycaemia groups following permanent MCAO both with and without EUK-134 administration. Prior to MCAO the baseline score for the rats was 18 in all groups. Data presented as scatterplot with mean indicated.

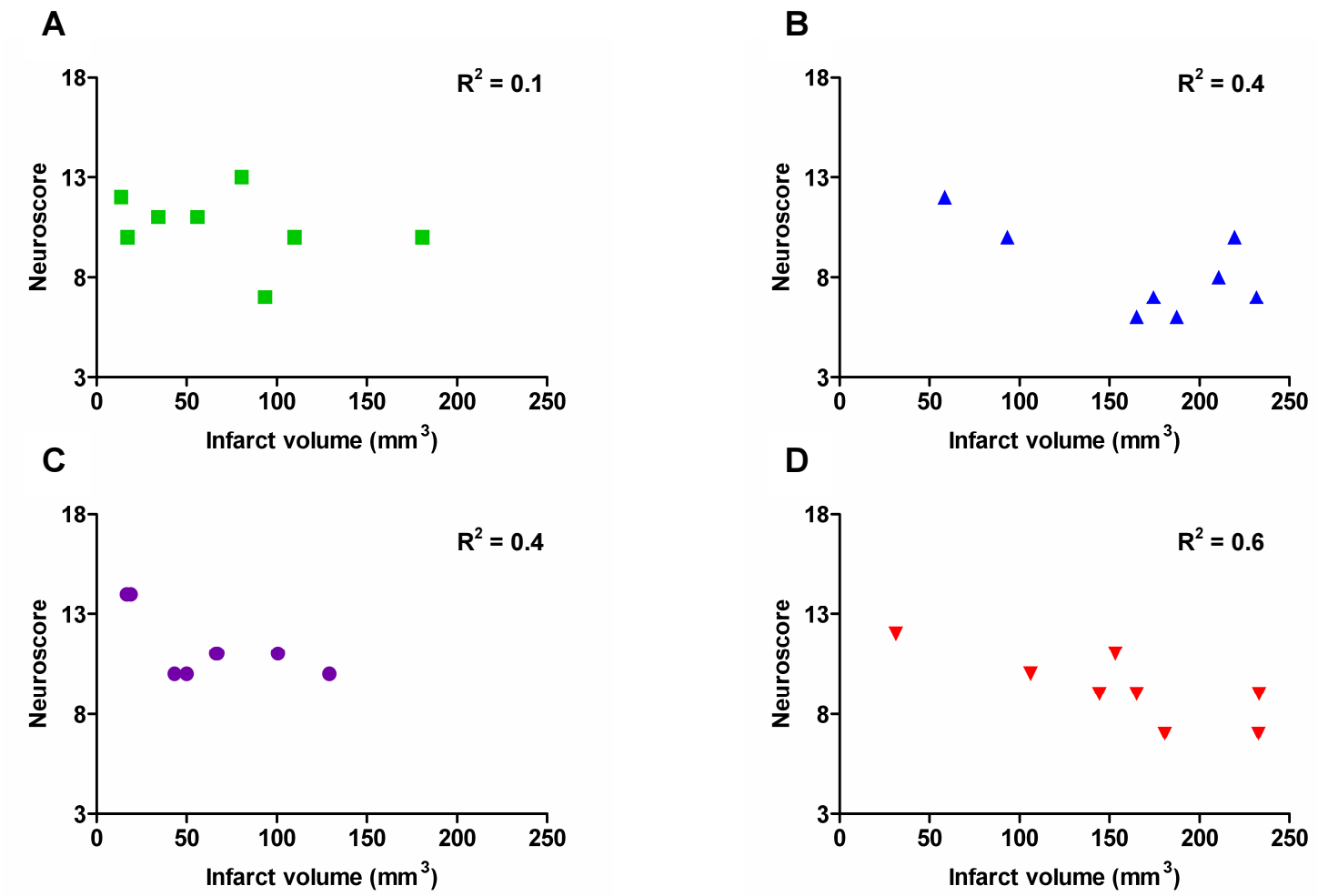

Figure 5.6: Correlation between level of infarct volume and 18 point neurological score in A) normoglycaemia and B) hyperglycaemia C) normoglycaemia+EUK and D) hyperglycaemia+EUK groups. A significant correlation was found in the hyperglycaemia+EUK group (R2= 0.6, P=0.02)

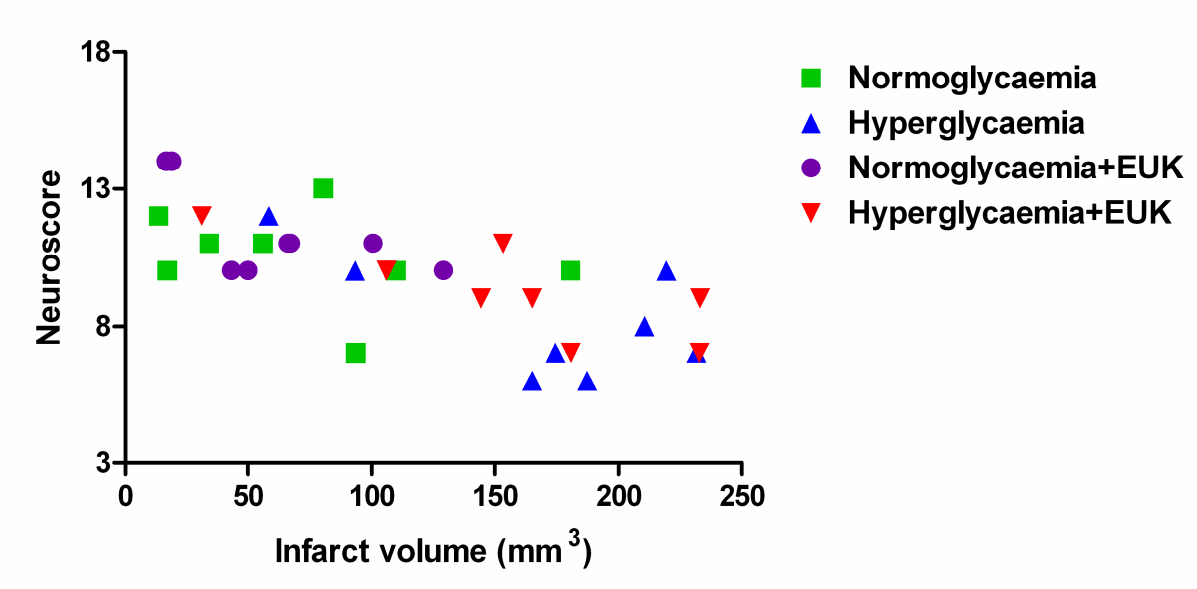

Figure 5.7: Correlation between neurological score and T2-derived infarct volume from all animals in the study. A significant correlation was found between the 18 point neurological score and infarct volume (r2 =0.5, P<0.001).

5.3.5 MDA was reduced by EUK-134 administration in normoglycaemia but not hyperglycaemia groups

Analysis of MDA levels in tissue homogenates from the infarct regions showed that following EUK-134 administration, the level of MDA in normoglycaemia animals was reduced in ipsilateral cortex compared to vehicle treated normoglycaemia animals (Figure 5.8A). This effect was however not observed in hyperglycaemic animals.

The level of MDA was not increased in hyperglycaemic animals compared to controls in the absence of EUK-134 suggesting that the effects of hyperglycaemia on infarct volume were not due to changes in lipid peroxidation. EUK-134 had no effect on MDA levels in the contralateral cortex, ipsilateral or contralateral subcortical ROIs (Figure 5.8 and 5.9).

5.3.6 MDA and infarct volume show little evidence of a correlation

The data collected for infarct volume and MDA analysis were compared to see if a correlation existed between the two measures (Figure 5.10). Looking at the graphs it is obvious that in each of the four groups there is no significant correlation between the level of MDA and the resulting infarct volume following MCAO. However grouping all of the animals together a weak association was established (R^2 = 0.191, P = 0.01, Figure 5.11). This suggests that independent of treatment ~20% of the infarct volume can be determined by the level of MDA.

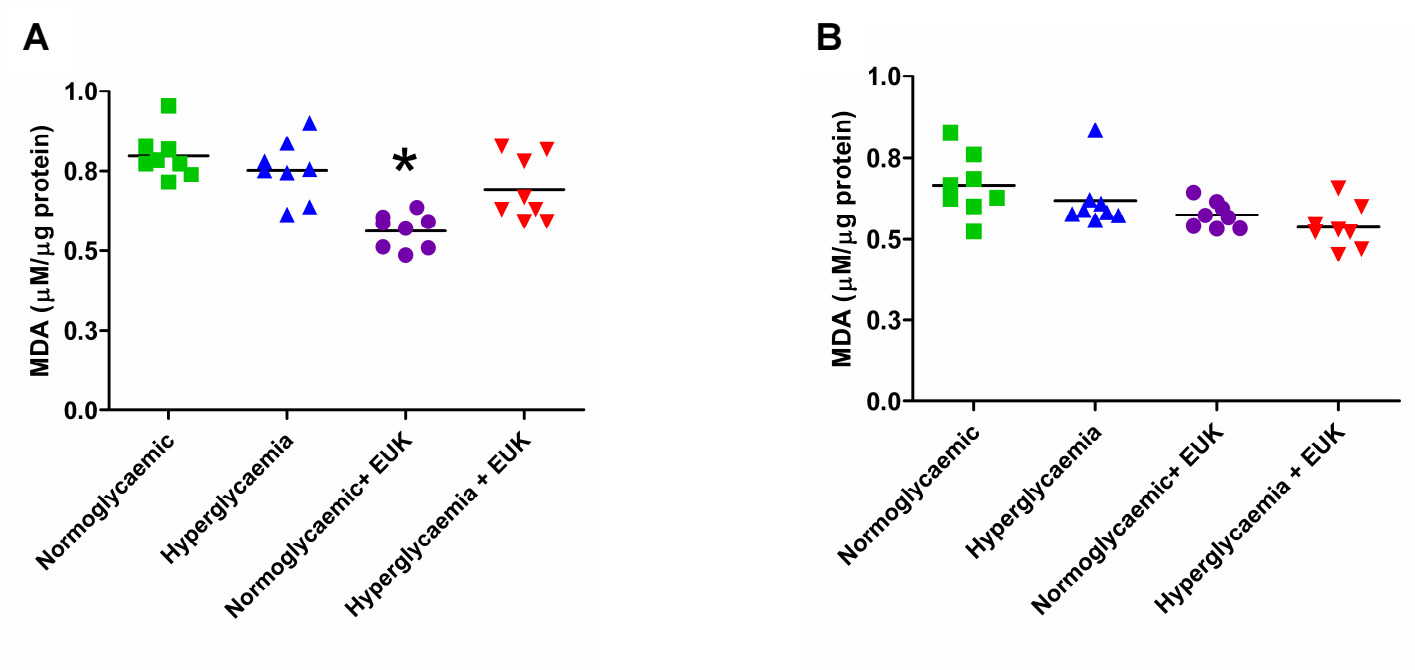

Figure 5.8: Levels of the lipid peroxidation marker, MDA, in A) ipsilateral and B) contralateral cortex 24 h post MCAO in normoglycaemia and hyperglycaemia groups both with and without EUK-134 administration. Data analysed using 1 way ANOVA with Bonferoni post test. *, P<0.01 compared to normoglycaemia group. Data presented as scatterplots with means indicated.

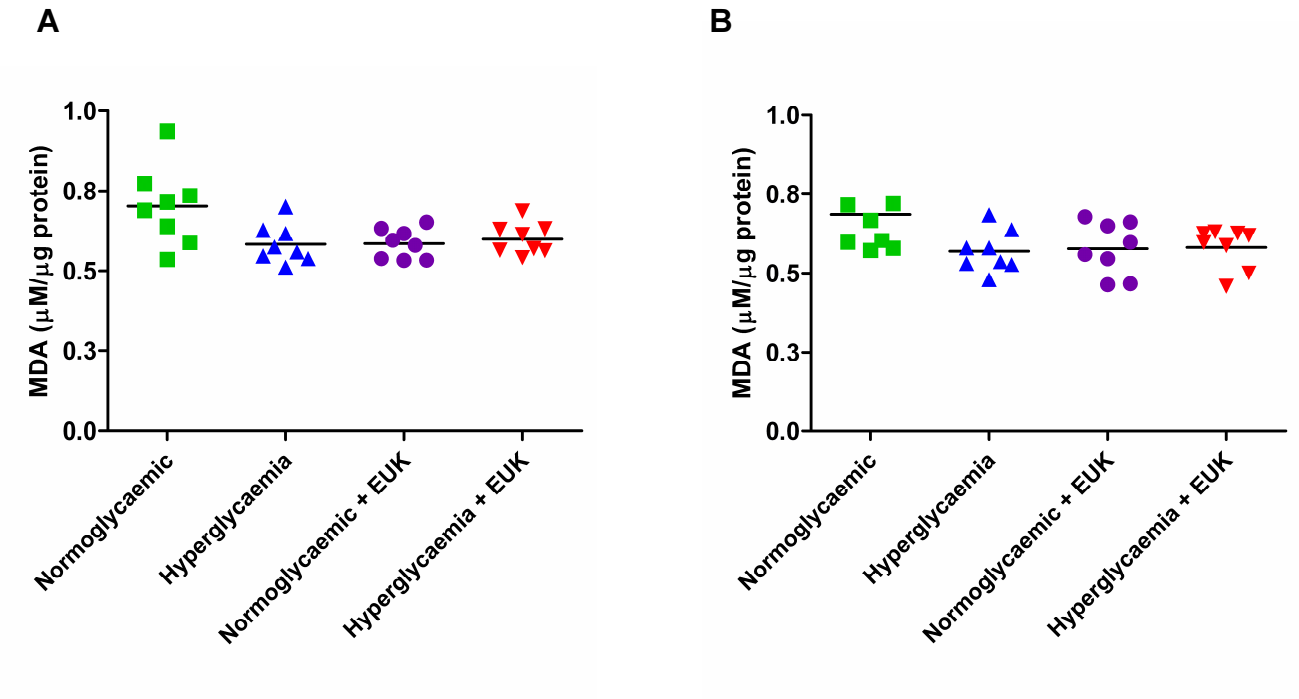

Figure 5.9: Levels of the lipid peroxidation marker, MDA, in A) ipsilateral and B) contralateral subcortical structures 24 h post MCAO in normoglycaemia and hyperglycaemia rats both with and without EUK-134 administration.

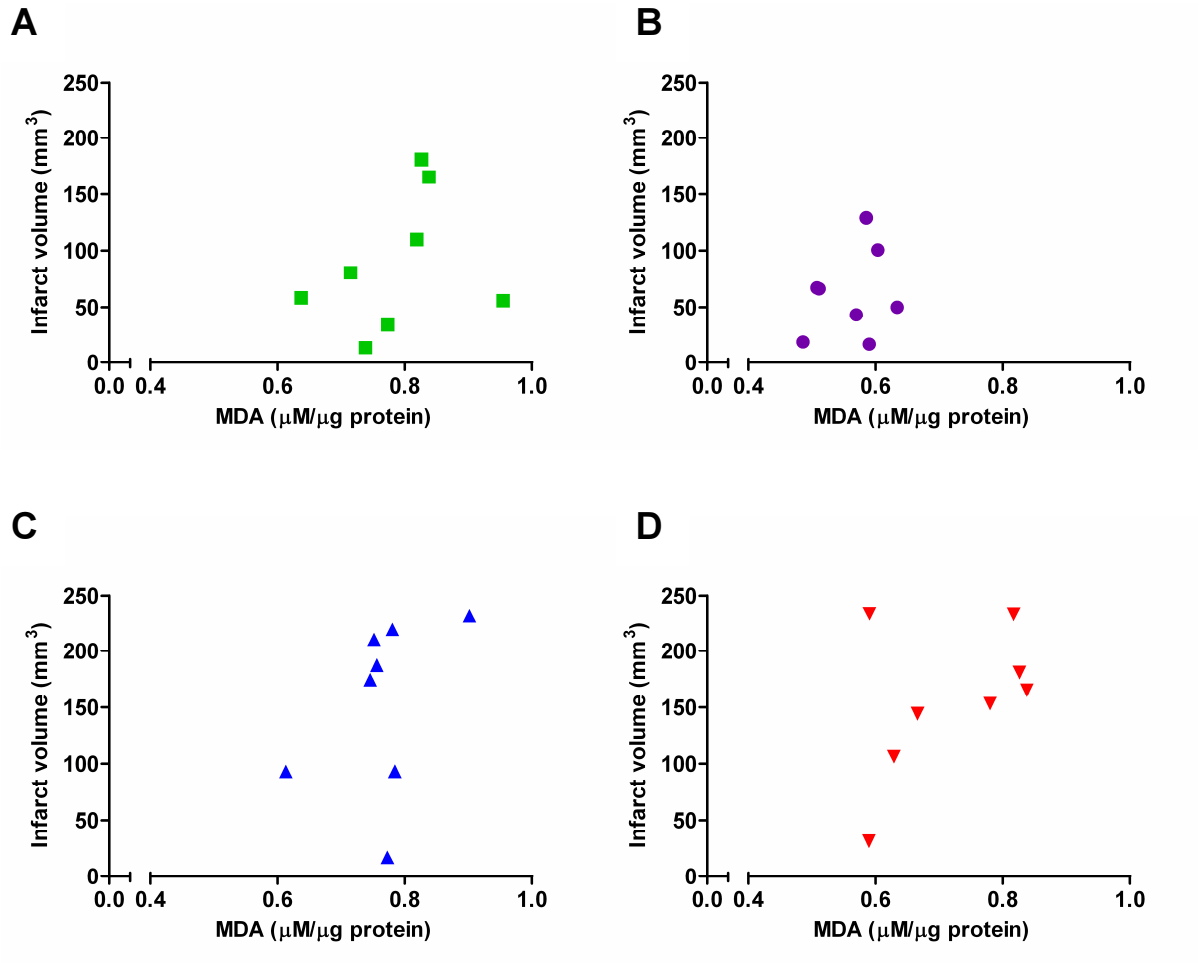

Figure 5.10: Correlation between level of MDA and T2-derived infarct volume in A) normoglycaemia and B) normoglycaemia+EUK C) hyperglycaemia and D) hyperglycaemia+EUK groups. No significant correlation was found in any of the 4 groups.

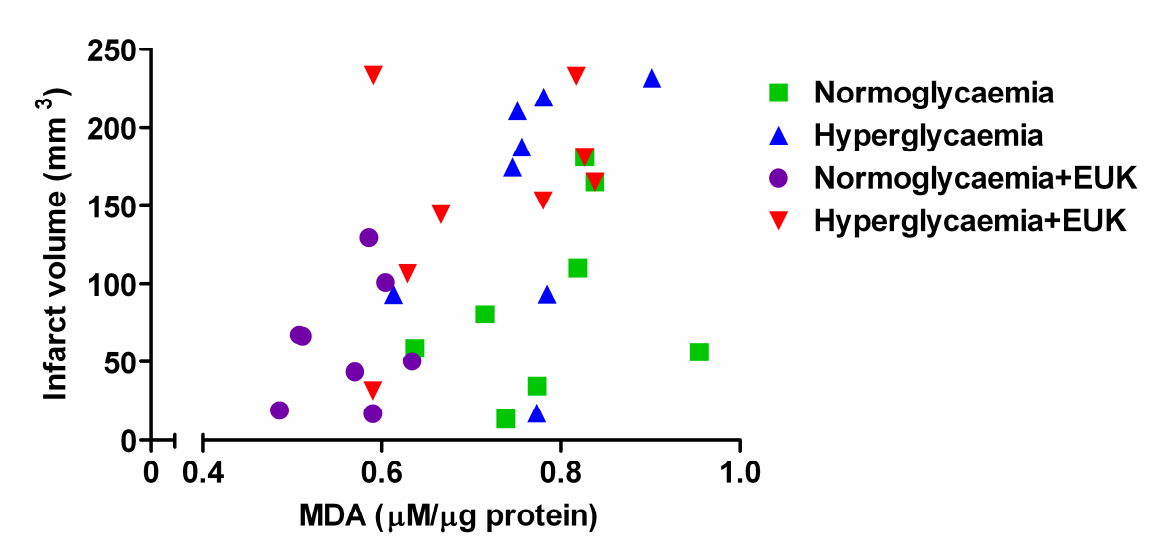

Figure 5.11: Correlation between level of MDA in ipsilateral cortex and T2-derived infarct volume from all animals in the study. A small but significant correlation (r2 = 0.191, P = 0.01) was found between the level of MDA and infarct volume.

5.3.7 Arterial superoxide levels were unchanged under hyperglycaemic conditions

No significant difference in CP concentration was found between the EUK-134 and vehicle treated hyperglycaemia or normoglycaemia groups in the 2 hour post MCAO blood samples. This suggests that hyperglycaemia is not exacerbating ischaemic injury at this time point via increased superoxide levels in the blood.

EUK-134 administration resulted in a decreasing trend of CP concentration in the arterial blood samples collected 2 hours post MCAO in both normoglycaemic and hyperglycaemic animals, compared to respective vehicle treated groups (Figure 5.12A). The administration of EUK-134 led to changes in the distribution of animals with regards to CP levels (Figure 5.12A). There is a significant, yet weak correlation between infarct volume and CP concentration 2 hours post MCAO in the EUK-134 treated groups (R^2 = 0.3, P = 0.04). This suggests that superoxide is weakly associated with final infarct.

At 24 hours post MCAO, arterial superoxide levels were significantly lower in all groups compared to 2 hours post MCAO (P<0.01, Figure 5.12B). The level of superoxide was again similar between the normoglycaemia and hyperglycaemia groups suggesting that systemic superoxide levels do not correlate with hyperglycaemia dependent damage.

To see if the levels of circulating superoxide 2 hours post MCAO predicted the extent of lipid peroxidation at 24 hours the data from both measures were compared (Figure 5.13). Visually there does not seem to be an obvious relationship between superoxide levels 2 hours post MCAO and the resulting level of malondialdehyde at 24 hours post MCAO. There was a statistically significant correlation, although the R^2 value was very low (r^2 = 0.2, P=0.02).

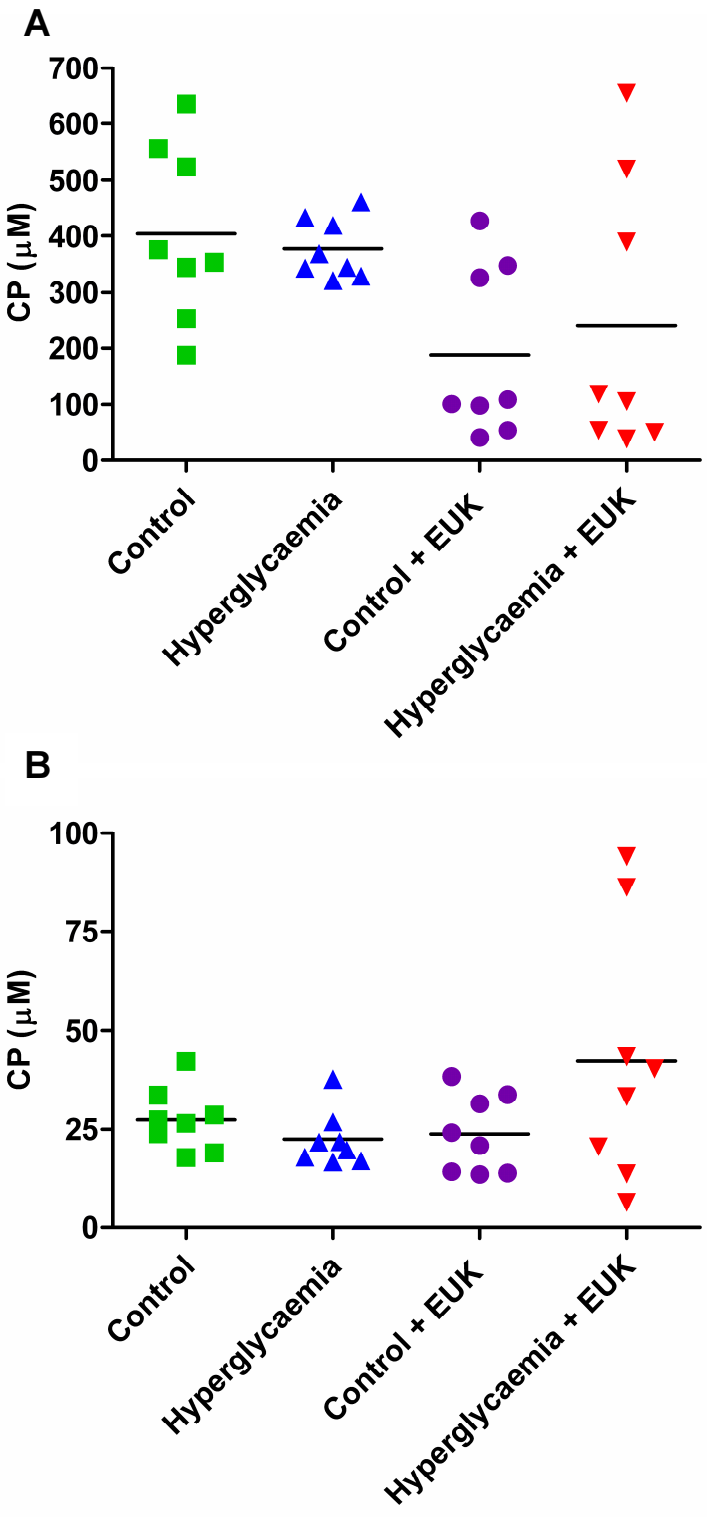

Figure 5.12: Level of CP produced by superoxide in arterial blood samples taken (A) 2 hours and (B) 24 hours post MCAO. Data expressed as scatter plots with mean for each group indicated.

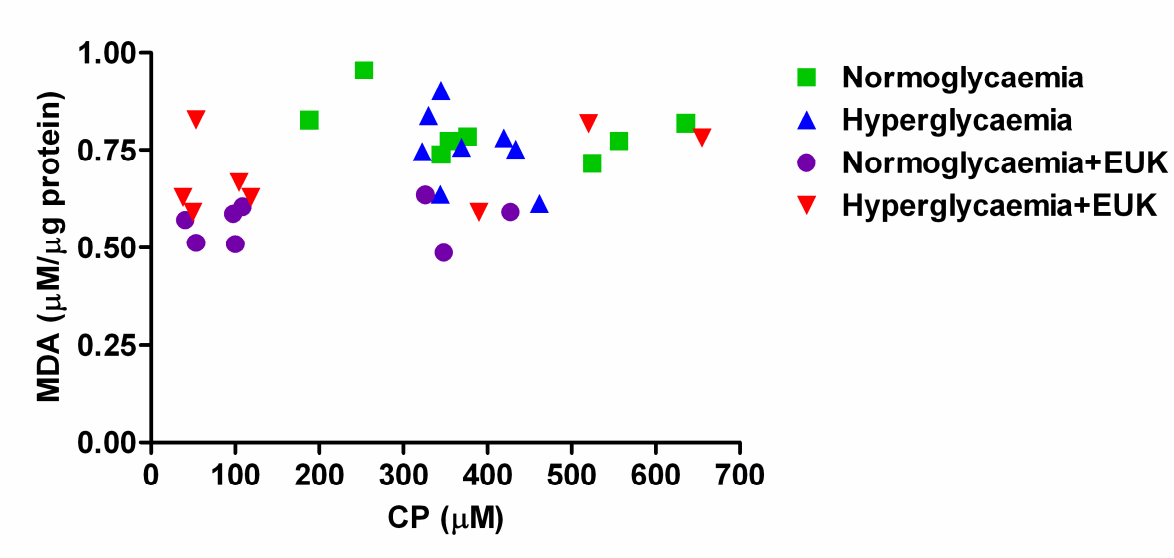

Figure 5.13: Correlation between level of CP (measure of superoxide) in blood and MDA in ipsilateral cortex from all animals in the study. A small but significant correlation was found between the level of CP and tissue MDA (r2 = 0.2, P=0.02).

5.4 Discussion

Many mechanisms by which hyperglycaemia can exacerbate ischaemic brain injury have been proposed using various animal models of stroke as well as clinical observations. However these mechanisms remain poorly understood. Oxidative stress, and the lipid peroxidation it can induce, has often been implicated in how glucose can injure the ischaemic brain which is supported by the data in Chapter 4 using a model of metabolic syndrome alongside a control strain. The current study has shown that hyperglycaemia also enhances ischaemic damage in the Sprague-Dawley strain of rat at 24 hours post-stroke confirming the findings of the previous study in WKY and SHRSP rat strains, and demonstrating that the detrimental effect of hyperglycaemia is not restricted to one particular model or one particular rat strain.

5.4.1 EUK-134 failed to reduce infarct volume in hyperglycaemic and normoglycaemic rats compared to vehicle treated controls.

The administration of the SOD/catalase mimetic, EUK-134 to both normoglycaemic and hyperglycaemic rats had no effect on the resulting infarct derived from T2-weighted MRI scans. Previously, using a permanent occlusion model in the rat, it was shown that using a 2.5mg/kg dose of EUK-134 administered intravenously in a single bolus dose three hours post occlusion infarct volume was attenuated compared to vehicle treated animals (Baker *et al* 1998). In that study EUK-134 reduced infarct by around 90% compared to controls and the remaining damage was comparable to the lesion size observed at 3 hours without treatment. This suggests that in the study conducted by Baker et al., EUK-134 was able to prevent any further damage from the time administered. The dose of EUK-134 used by Baker et al. was equivalent to the present study and EUK-134 was also administered in a single bolus intravenous injection. Experiments into renal nephrotoxicity using EUK-134 suggest that scavenging and dismutation of superoxide was effective at doses of 10-300μM whereas the present study only used a dose of 5μmoles/Kg (Samai *et al* 2007).

The dose used in the present study was selected based on the study by Baker et al (1998) and additionally from the solubility data provided on EUK-134. To successfully dissolve a greater dose would require a considerably larger volume of solvent which would far exceed recommended volumes for intravenous drug administration to rats.

The obvious difference between the studies is the administration time relating to the arterial occlusion. The present study was a proof of principle study to investigate the mechanism of hyperglycaemia mediated damage, rather than a neuroprotection study and therefore pre-treatment was selected on this basis. Baker et al (1998) administered EUK-134 3 hours post occlusion whereas in the present study EUK-134 was administered 20 minutes prior to occlusion and 10 minutes before glucose loading in the hyperglycaemia groups. The reason for a much earlier administration was to make sure that scavenging of superoxide could take place immediately following hyperglycaemia to hopefully maximise the effect. The study by Baker et al (1998) fails to state if measures were taken to prevent bias. For example, lack of blinding and randomisation can have substantial effects on outcome and may account for a proportion of the effect size observed (Macleod *et al* 2009).

5.4.2 Increased variability in infarct size in Sprague Dawley rats compared to WKY rats

Compared to the results gathered in Chapter 4 using ffSHRSP and WKY rats, there was a much greater variability in the infarct sizes using Sprague Dawley rats and in all groups. Some rats displayed very small lesions suggestive of an incomplete occlusion. However the MCA of each animal, irrespective of group, was electrocoagulated and then cut in a similar fashion which suggests that variation in the branching of the MCA or collateral supply from adjacent arterial territories may have resulted in a reduced volume of ischaemically damaged tissue. Various different types of MCA branching have been previously documented in Sprague-Dawley rats with varying frequencies of occurrence (Rubino and Young 1988). Collateral flow in the Sprague-Dawley strain is known to be better than the in- SHRSP strain which may account for a more variable occlusion size (Coyle 1986). Some groups have added varying durations of

bilateral- carotid artery clamping to reduce global CBF and therefore collateral flow in similar models of MCAO to reduce variability (Brint *et al* 1988; Chen *et al* 1986; Rubino and Young 1988). Rubino and colleagues (1988) found that in Sprague-Dawley rats no lesion was apparent in 38% and 43% of animals having undergone parietal or frontal branch MCAO respectively in addition to 30 minute bi-lateral occlusion of the ipsilateral and contralateral common carotid arteries. Another study showed that permanent ipsilateral common carotid occlusion in addition to distal MCAO produced reproducible infarcts in SHRSP rats but not in Fisher-344 or Wistar rats (Brint *et al* 1988). More reproducible infarcts were produced in a MCAO study where additional permanent ipsilateral common carotid occlusion was combined with 60 minutes of contralateral common carotid artery occlusion in Long Evans rats compared to single common carotid occlusion or MCAO alone (Chen *et al* 1986).

The model used for inducing focal cerebral ischaemia in the present study is perhaps not suitable for use in a normotensive strain of rat such as the Sprague Dawley due to the variability observed. Moving to either the 3 vessel occlusion model (Rubino and Young 1988) or the more widely used intraluminal filament model could potentially reduce the variability and increase the power of the experiment.

5.4.3 Hyperglycaemia dependant infarct exacerbation was not reflected by neurological score

No significant differences in neurological scores were seen between the hyperglycaemia and normoglycaemia groups or between the EUK-134 or vehicle treated groups. This suggests that hyperglycaemia does not worsen neurological scores in this study. However a correlation does exist between the volume of infarct and the resulting neurological score showing a relationship between the two outcome measures. The fact that the result obtained from the final infarct volume is not mirrored by the neurological score is perhaps due to the lack of sensitivity of the neurological score employed. PSH has been widely associated with worsening neurological deficit in patients (Baird *et al* 2003; Parsons *et al* 2002). Previously it has been shown that in a transient model of 60 minute MCAO, hyperglycaemia induced by streptozotocin worsened neurological scores

compared to controls using the Bederson (Bederson *et al* 1986b) scale (Kamada *et al* 2007). Motor function has been shown to be reduced in hyperglycaemic animals compared to normoglycaemic controls in a separate study (Warner *et al* 1995). The 18 point composite neurological score used in the present study incorporates many of the functional tests included in the Bederson Scale with numerous additions. This score has far more outputs with 15 possible outcomes (3-18) compared to the 4 grades in the Bederson Scale which may have made it more difficult to detect changes in the neurological function between the groups. Potentially the time at which the neurological score was carried out may have affected the results. The effect of the anaesthetic and the severity of the surgery might have influenced the result of the test rather than as a result of the ischaemic lesion.

The results from the neurological score are unable to add any significant information as no differences between the groups could be ascertained. The correlation between neurological score and infarct volume does give confidence that there is a degree of sensitivity in the neurological score however there are a number of limitations. Firstly the score could have been affected due to the leftover effect of anaesthesia and the surgery prior to conducting the neurological scoring. Similarly the sample size calculation conducted for this study was based on differences in infarct volume between normoglycaemic and hyperglycaemic WKY rats rather than on the neurological score which perhaps implies that the study was underpowered for this outcome measure.

5.4.4 EUK-134 reduced lipid peroxidation markers in ipsilateral cortex of normoglycaemia but not hyperglycaemia groups

In normoglycaemic animals the level of MDA was increased in the ipsilateral cortex compared to the other three regions of interest suggesting that as a result of MCAO the level of lipid peroxidation had increased in the region of tissue affected by the ischaemia. In normoglycaemia animals administered with EUK-134 the level of MDA in the ipsilateral cortex was reduced to the level of the other 3 regions of interest suggesting that EUK-134 had reduced the level of lipid peroxidation to the baseline level of the contralateral hemisphere. In the hyperglycaemia group the MDA level in ipsilateral cortex was again raised but

this was not attenuated by EUK-134 administration. This may suggest that EUK-134 is able to dampen the rise in superoxide production associated with cerebral ischaemia under normoglycaemic conditions, yet be overwhelmed at the current dose by the additional increase superoxide production that is associated with hyperglycaemia. EUK-134 has been shown to reduce lipid peroxidation in response to streptozotocin-induced oxidative damage in the brain and also reduce blood glucose to normoglycaemic levels (Bahramikia and Yazdanparast 2011). The pathophysiology between the streptozotocin model (model of type 1 diabetes) and glucose loading models of hyperglycaemia are very different and the mechanisms of damage between the two models are not conserved. Bahramikia et al (2011) used a dose of 20 mg/kg administered daily for three weeks by oral gavage. This is a chronic administration at a considerably higher dose than used in the present study or that used by Baker et al (1998) in the ischaemia model. The dose of EUK-134 selected for the present study was based on the accompanying data sheet which specified the solubility in saline and in line with the previous work on cerebral ischaemia (Baker *et al* 1998). For a higher dose to be achieved, the volume of vehicle would have been excessive for administration intravenously according to the Home Office guidelines.

The dose used in the present study was not sufficient to cause a reduction in lipid peroxidation in hyperglycaemic animals and perhaps a different multiple administration protocol may have increased the efficacy on oxidative stress. The weak correlation between infarct volume and the level of lipid peroxidation suggests that other mechanisms must be predominantly involved in driving infarct size.

5.4.5 Arterial blood superoxide levels were unchanged under hyperglycaemic conditions

A number of pathologies associated with diabetes, including neuropathy, are thought to occur in chronic hyperglycaemia through a variety of pathways (Tomlinson and Gardiner 2008). However the mechanisms responsible for these associate pathologies are thought to originate from the overproduction of superoxide from the mitochondria (Brownlee 2005). The results from the present study suggest that in acute hyperglycaemia this is not the case as superoxide

levels in hyperglycaemic animals remained consistent with normoglycaemic controls at 2 hours and 24 hours post MCAO. However, the level of superoxide in the blood may not reflect cerebral levels which may still have been affected. The measure of superoxide was primarily to confirm the potential action of EUK-134 to lower superoxide levels. The EUK-134 treated groups had a greater variation in the level of superoxide measured with a trend towards a reduction at 2 hours post MCAO compared to the vehicle treated groups. A number of the animals in both the hyperglycaemia + EUK and normoglycaemia + EUK groups possessed a similar level of superoxide to their respective vehicle treated groups, which might suggest a problem with the action or delivery of EUK-134 in these animals.

5.4.6 Conclusions

Although hyperglycaemia led to an increase in infarct volume the mechanism involved remains elusive. The SOD/catalase mimetic EUK-134 showed some efficacy in reducing systemic levels of superoxide and also reduced the level of lipid peroxidation as measured by MDA in normoglycaemia treated animals. However this drug had no effect on infarct volume and the level of lipid peroxidation correlated poorly with infarct volume suggesting mechanisms other than ROS damage are responsible for mediating hyperglycaemia dependant damage in permanent focal cerebral ischaemia.

Chapter 6 - Determining a T_2 threshold of abnormality from quantitative T_2 maps

6.1 Introduction

T_2 relaxation, which denotes contrast on T_2-weighted imaging, is the loss of transverse magnetisation between protons within a particular tissue as a result of spin-spin interactions (described in Chapter 1.3.5). When protons are subjected to a magnetic field, such as in an MRI scanner the magnetic moment of protons, or spin, precess around the axis of the magnetic field. The position of this precessional path is referred to as the phase of the proton. The application of electromagnetic radiation causes excitation of protons to a high energy state and leads to the synchronisation of spin precession. This state is known as spin coherence (Figure 6.1A). Phase coherence is gradually lost as energy is dissipated between protons, with some spins advancing and others falling behind on their precessional paths (Figure 6.1B).

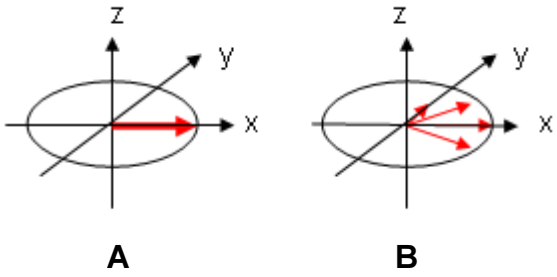

Figure 6.1: Diagrammatic representation of T2 relaxation. (A) Precessional paths are synchronised around the magnetic field (z) in the transverse plane (xy). (B) The precessional paths of protons are dephasing in the transverse plane (xy) around the magnetic field (z).

T_2 weighted imaging has been used to assess infarct volume non-invasively in a multitude of preclinical studies, including a number from our lab (Reid *et al* 2012; Robertson *et al* 2011) and in various clinical stroke studies (Parsons *et al* 2002; Simonsen *et al* 2002). The current imaging sequence that is used in our lab is a RARE T_2 weighted imaging sequence and can be reliably used to identify ischaemically damaged tissue 12 to 24 hours following stroke, although prior to this time point the T_2 signal changes are too subtle to assess the extent or severity of ischaemic damage(Baird and Warach 1998). Areas of injured tissue

produce higher signal intensity, reflecting a longer T_2 relaxation time, than in normal tissue, allowing the infarct to be delineated visually.

There are a number of limitations with the current RARE T_2 weighted scan used in our lab. The current sequence does not provide a quantitative measure of the T_2 relaxation times which prevents the comparative analysis of T_2 relaxation values for specific structures between subjects. In addition to this the RARE T_2 sequence is susceptible to signal drop off, most notably from the tissue situated at the greatest distance from the surface coil (Figure 6.2).

Figure 6.2: Coronal image acquired using RARE-T2 weighted MRI sequence. The red arrow indicates the direction of signal intensity loss which is visible on the image.

This lower signal intensity can make it more difficult to distinguish between potentially ischaemic tissue and normal tissue. Multi Spin-Multi Echo (MSME) T_2 weighted images enable the production of T_2 maps by using multiple echo times. This allows T_2 values to be calculated for each pixel regardless of the signal intensity, correcting for signal drop off. The lack of quantification in the current RARE T_2-weighted imaging means that the delineation of ischaemically damaged tissue must be done manually on the basis of visual differences in signal intensity, as the arbitrary values associated with contrast of the image can not be used to generate a biological threshold for normal and ischaemically damaged tissue. Inter- and intra-rater variability from manual delineation is a potential source of error in MRI imaging which has been previously examined (Ay *et al*

2008). Generating a T_2 threshold for abnormality should remove the inter- and intra-rater variability and hence make infarct determination more reliable. Although quantitative T_2 mapping has been used clinically (Siemonsen *et al* 2012), manual delineation has still been used to calculate infarct volume (Loubinoux *et al* 1997).

Thresholds of abnormality have been previously derived for both DWI (to detect ischaemic injury) and PWI (to define the perfusion deficit) for assessment of penumbra from PWI/DWI mismatch in a variety of preclinical studies (Kazemi *et al* 2004; Meng *et al* 2004; Reid *et al* 2012; Shen *et al* 2003). A number of experimental stroke studies have also used thresholds for quantitative T_2 mapping. A study in rats used TTC staining at 24 hours as a bench mark for infarct volume and a T_2 threshold of abnormality was calculated for the fast spin-echo pulse sequence employed. Using a statistical analysis programme the T_2 threshold was lowered until the number of pixels corresponded to the lesion size calculated from the TTC sections (Bardutzky *et al* 2007). The T_2 threshold of abnormality that Bardutzky et al derived was 77.9±3.6 ms and this was subsequently used for infarct determination. Another group found that T_2 relaxation times in the contralateral hemisphere varied depending on the tissue compartmentalisation from 55.8±2.2 ms in the thalamus to 66.0±0.9 ms in the striatum and therefore concluded that a threshold of abnormality for the entire brain could not be set (Loubinoux *et al* 1997). The specific sequence employed for T_2 quantification varies between scanners which means that inter-laboratory use of thresholds for T_2 may result in an error in quantification. It is therefore necessary to determine a threshold in each lab, for each sequence.

This chapter describes the iterative process of selecting a suitable threshold of abnormality which defines tissue with a longer T_2 relaxation than the threshold as infarct. The process for defining the T_2 threshold of abnormality is as follows:

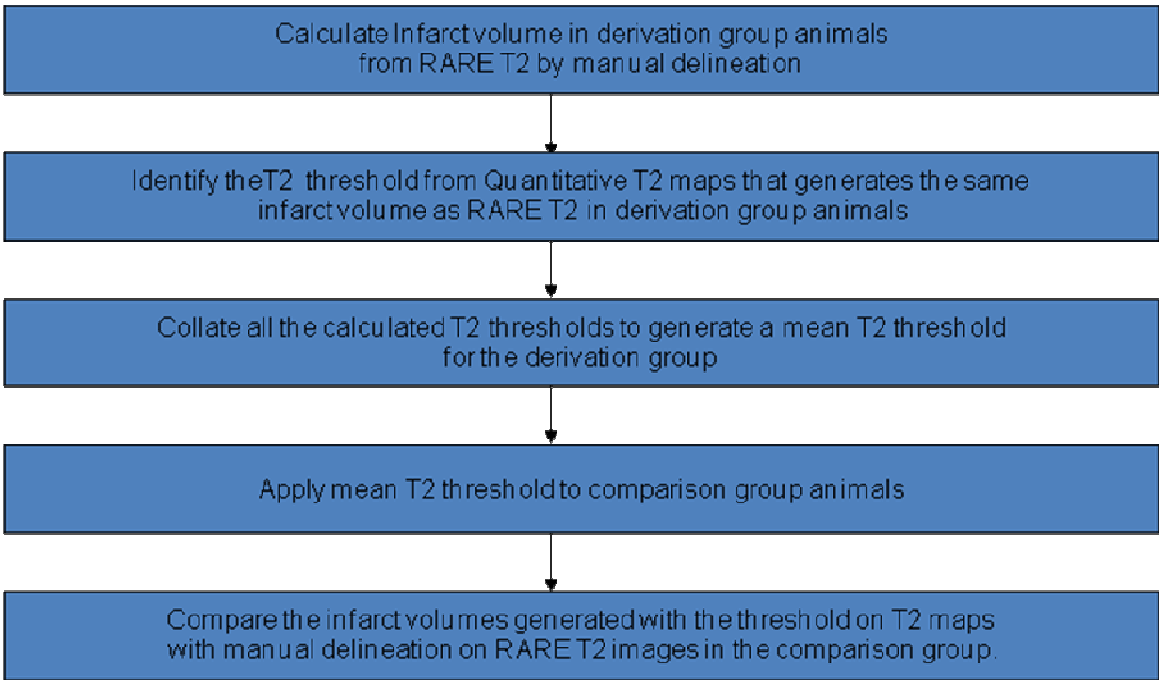

6.1.1 Study Aims

Using both quantitative mapping and RARE T_2 images acquired from Chapter 5, the aims of this chapter are:

1. Assess various T_2 relaxation thresholds to identify the most suitable for infarct determination by comparison with the current RARE T_2 sequence.

2. Apply the derived T_2 threshold to a separate group of animals to compare infarct volumes calculated from quantitative T_2 maps with RARE T_2.

3. Apply the derived threshold to a separate group of rats subjected to a different model of MCAO to elucidate the suitability of the threshold to another model.

6.2 Methods

6.2.1 MRI acquisition

Magnetic resonance imaging data were acquired on the system described in Chapter 2.5.1. A phased array 4 channel surface receiver coil was placed above the head of the animal before being transferred to the MRI scanner. A coronal RARE T_2 sequence (effective TE: 46.8 ms, TR: 5000 ms; in plane resolution of 97 um; 16 slices of 0.75 mm thickness) was acquired for manual infarct volume determination.

For automated infarct volume determination, using quantitative T_2 mapping, a coronal MSME T_2 sequence (effective TE 15ms, TR 9000 ms, number of echoes 16, matrix 96 x 96, FOV 25 x 25 mm^2, 8 slices of 1.5 mm thickness) was acquired. The MSME T_2 images were processed in Paravision 5 to generate quantitative T_2 maps.

The RARE T_2 scan acquires 16 slices compared to the MSME T_2 sequence which acquires 8. The thickness of the MSME T_2 imaging slices are twice the thickness of the RARE T_2 sequence slices. The geometry for the scans was identical to ensure the spatial profile used to calculate infarct volume were the same (Figure 6.3).

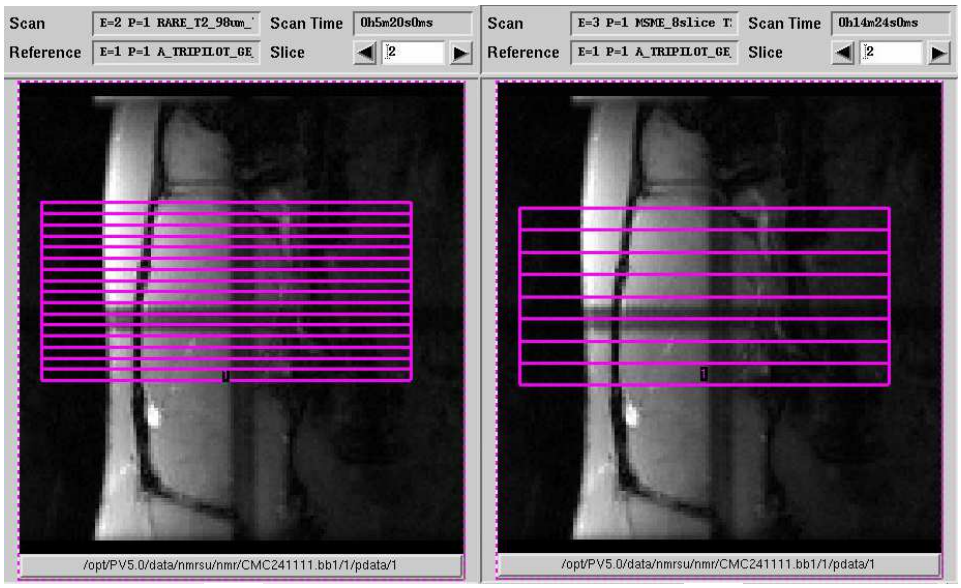

A B

Figure 6.3: Saggital Tripilot scan to set the geometry for A) RARE T2 weighted images and B) MSME T2 weighted images. Purple box indicates the region to be imaged with each slice represented. The geometry of the two scans is identical.

6.2.2 Group analysis

The T_2-weighted MRI data generated from the study in Chapter 5 were used to define a threshold of abnormality for the quantitative T_2 maps. The animals, all of which had undergone distal MCAO using diathermy, were split in two groups; the derivation group (n=17) and the comparison group (n=13). The derivation group was used to establish the mean T_2 relaxation threshold for determining infarct. The comparison group was used to assess how well the defined quantitative T_2 threshold correlates with the manually delineated volume from the RARE T_2 images.

The defined quantitative T_2 threshold was then applied to data acquired from animals that had undergone MCAO using the intraluminal filament method of focal cerebral ischaemia to assess its suitability in a different model of MCAO. These data were collected by Dr Chris McCabe and analysed by David Tarr.

6.2.3 Calculating Infarct volume in derivation group animals from RARE T_2 by manual delineation

ImageJ was used to separate the 16 images from the RARE T_2 weighted images and the hyperintense region that represented the infarct was manually delineated using the freehand function. Measurement of individual images gave the infarct areas in millimetres squared, and infarct volume was calculated by adding up the 16 areas and multiplying by the slice thickness (0.75 mm). This provided a reference for selecting the threshold on quantitative T_2 maps.

6.2.4 Identifying the T_2 threshold from Quantitative T_2 maps that generates the same infarct volume as RARE T_2 in derivation group animals

The absolute T_2 relaxation threshold for each animal in the derivation group was determined by applying a range of increasing threshold values (≥65 ms to ≥90 ms in increments of 1 ms) to the quantitative T_2 maps acquired 24 hours post-MCAO to generate T_2-derived lesion volume, for each threshold, across the 8 coronal slices. Each coronal slice was separated into ipsilateral and contralateral hemispheres and a histogram was drawn for each hemisphere based on the number of pixels within a range of T_2 relaxation times using ImageJ (1-201 ms, Figure 6.4).

The histogram data from each coronal slice were added together to produce a histogram for the entire imaged brain volume (Figure 6.5) and exported to Microsoft Excel where a macro was used to measure the lesion size at a range of thresholds based on the number of pixels at each T_2 relaxation time. The area of a pixel in the quantitative T_2 maps is 0.0678mm^2 allowing the number of pixels to be converted to an area and subsequently a volume by multiplying the total area by the slice thickness (1.5mm).

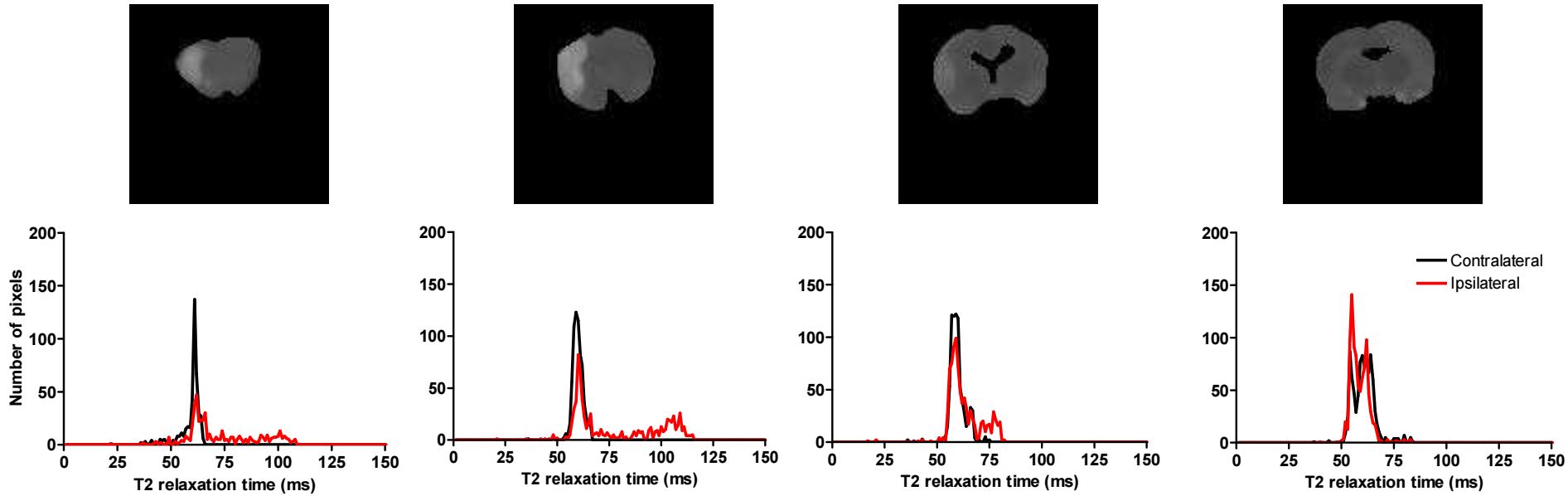

Figure 6.4: Coronal quantitative T2 maps generated from MSME T2 scans obtained 24 hours post MCAO, and corresponding histograms. Images and data are from 4 of the 8 coronal planes in one representative animal in the derivation group. Infarcted tissue in the ipsilateral hemisphere exhibits a higher T2 signal than normal tissue (images in top row). The corresponding histograms below each image illustrate the number of pixels from the quantitative T2 maps that correspond to a particular T2 relaxation time. The black line illustrates the contralateral hemisphere and the red line represents the ipsilateral hemisphere. Infarcted tissue has a longer relaxation time than normal tissue causing a shift to the right in the pixel distribution in the affected ipsilateral hemisphere.

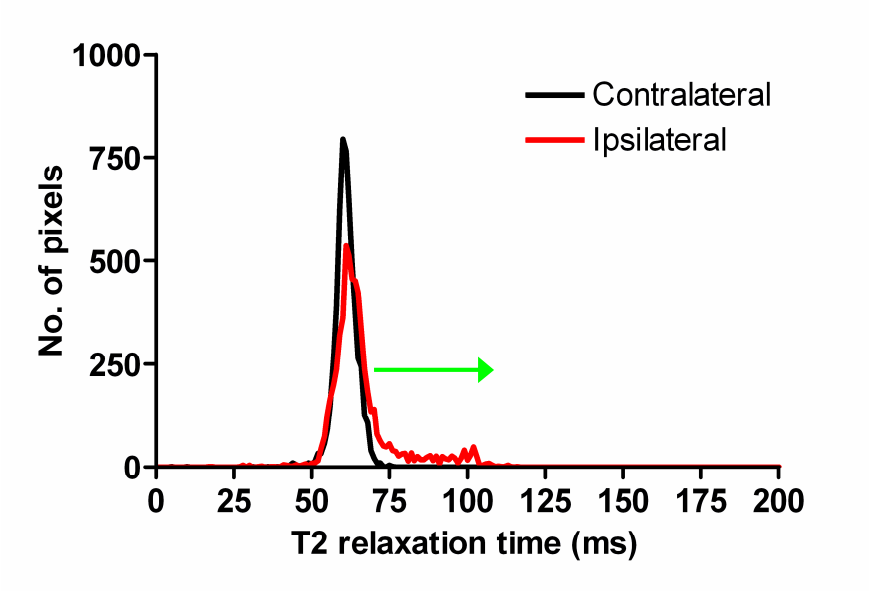

Figure 6.5: Example histogram for the imaged region of the brain generated from 8 coronal quantitative T2 maps from a representative animal of the derivation group. Very few pixels have a T2 relaxation time of <50 ms or >110 ms. The 1-201ms range is suitable to include the majority of pixels. The shift in the ipsilateral peak to the right (highlighted in green) shows the range of T2 relaxation times that potentially relate to infarct.

6.2.5 Collating all the calculated T_2 thresholds to generate a mean T_2 threshold for the derivation group

Once the T_2 threshold for each animal within the derivation group had been selected the data was graphed together. The mean T_2 threshold for the group was then calculated. This mean T_2 threshold was then tested in the comparison group.

6.2.6 Applying the mean T_2 threshold to comparison group animals

The quantitative T_2 maps for each animal in the comparison group were independently analysed. Using ImageJ the mean T_2 threshold value from the derivation group was applied to each of the 8 coronal slices acquired for each animal. The resulting area on each coronal slice corresponding to the threshold defined infarct was measured using the polygon tool. The areas from the 8 acquired coronal levels were then added together and multiplied by the slice thickness (1.5 mm).

6.2.7 Compare the infarct volumes generated with the threshold on T_2 maps with manual delineation on RARE T_2 images in the comparison group.

The infarct volume calculated using the threshold on quantitative T_2 maps was then formally compared to the manual delineation method using a Bland-Altman plot, which describes the bias (difference) between the two methods of infarct determination, in animals in the comparison group.

6.2.8 Reproducibility

Mean contralateral T_2 values were measured from quantitative T_2 maps to ascertain how consistent the T_2 values were between subjects and between coronal slices. If the contralateral values varied significantly then an absolute T_2 threshold would not be appropriate and a percentage increase in T_2 relaxation time would have to be derived.

Since the T_2 threshold for infarction is based on the manual delineation of ischaemically damaged tissue (defined as hyperintense regions) visible in RARE T_2 images, assessment of intra-rater reproducibility is important. A large error in the reproducibility of the manual delineation method of infarct quantification could lead to an error in the derivation of the T_2 threshold. Manual delineation of the infarct in both the derivation and the comparison group was conducted twice two weeks apart and blinded to the subject identification. The mean, standard deviation and coefficient of variance were calculated for each animal. The coefficient of variance is useful in determining the variation as it represents a measure relative to the mean rather than an absolute value. This is important as the infarct sizes are varied within the groups.

6.3 Threshold Derivation

6.3.1 T_2 relaxation in the hemisphere contralateral to MCAO is consistent throughout the derivation group

The mean T_2 relaxation value for each of the 8 coronal slices from quantitative T_2 maps was determined in each of the brains within the derivation group Table 6.1). The contralateral value of T_2 relaxation was consistent between each of the coronal levels analysed and also between brains. The mean value of T_2 relaxation for the contralateral hemisphere was 62.3±1.3 ms. The range of T_2 relaxation time thresholds, which will be assessed to identify the T_2 threshold of abnormality, will increase in increments of 1 ms. The standard deviation from contralateral T_2 is close to 1 ms which is an acceptable level of variation based on the thresholds to be tested. The reproducibility of T_2 relaxation between subjects gives confidence that an absolute T_2 threshold of abnormality can be derived, rather than calculating a percentage increase in T_2 compared to contralateral T_2 values.

Subject	Contralateral T_2 relaxation time for each coronal image (ms)								Mean	SD
	Slice 1	Slice 2	Slice 3	Slice 4	Slice 5	Slice 6	Slice 7	Slice 8		
DV1	62.8	65.1	60.6	64.8	61.6	60.9	61.2	61.1	62.2	1.7
DV2	64.4	65.9	61.2	61.8	62.8	62.7	63.9	65.3	63.5	1.6
DV3	63.8	64.4	60.7	63.4	63.2	63.2	62.4	63.2	63.0	1.0
DV4	64.0	64.2	62.4	61.5	62.5	62.4	62.5	64.4	63.0	1.0
DV5	62.0	63.3	61.9	61.3	61.8	62.5	61.9	62.3	62.1	0.6
DV6	62.2	62.1	60.0	61.6	61.9	61.7	62.0	64.6	62.0	1.2
DV7	61.0	61.0	60.8	60.4	61.1	60.8	60.5	61.7	60.9	0.4
DV8	62.6	62.4	61.1	61.2	62.1	61.5	61.3	61.1	61.7	0.6
DV9	63.5	63.1	62.0	62.2	62.0	62.6	62.7	65.0	62.9	0.9
DV10	60.7	60.1	60.8	60.9	60.0	60.5	60.2	60.1	60.4	0.3
DV11	65.7	65.1	64.0	62.7	62.2	63.9	62.5	63.7	63.7	1.1
DV12	63.2	62.0	61.3	61.3	61.9	62.4	60.9	62.2	61.9	0.7
DV13	62.3	60.8	62.4	61.5	62.0	61.5	60.9	62.5	61.7	0.6
DV14	64.0	63.0	61.0	61.2	62.2	62.1	62.6	64.1	62.5	1.1
DV15	64.0	64.7	62.6	63.2	63.1	62.2	62.1	61.4	62.9	1.0
DV16	61.5	61.5	62.9	61.8	62.1	62.1	61.8	64.1	62.2	0.8

Table 6.1: Contralateral hemisphere T_2 relaxation times calculated form quantitative T_2 maps in all animals from the derivation group. SD = standard deviation, ms = millisecond.

6.3.2 Intra-rater variation in the manual delineation of infarcts from RARE T_2-weighted images

Manual delineation of the infarct in both the derivation group (Table 6.2) and the comparison group (Table 6.3) was conducted twice and the variability was assessed (Figure 6.6). In the derivation group the variability was low with a coefficient of variation across the group of 6.9%. This was similar to that found in the comparison group which generated a coefficient of variation of 4.6%. The intra-observer variation found in both the derivation group and the comparison group is similar to the coefficient of variation found using a similar method for infarct determination on CT imaging (van der Worp *et al* 2001). The Bland-Altman scatterplots (Figure 6.5) show that in both groups there was only a very small bias (difference) between the repeat measurements of infarct volume.

Animal	Infarct volume measurement (mm^3)			Standard Deviation (mm^3)	Coefficient of variation (%)
	1	2	Mean		
DV1	63.1	62.2	62.7	0.6	1.0
DV2	18.5	22.8	20.7	3.0	14.7
DV3	51.3	50.1	50.7	0.8	1.7
DV4	47.5	65	56.3	12.4	22.0
DV5	39.5	34.2	36.9	3.7	10.2
DV6	120.8	118.4	119.6	1.7	1.4
DV7	88.5	77.9	83.2	7.5	9.0
DV8	131.2	149.9	140.6	13.2	9.4
DV9	19.7	18.4	19.1	0.9	4.8
DV10	75.7	68.6	72.2	5.0	7.0
DV11	301.4	285.3	293.4	11.4	3.9
DV12	120.5	115.7	118.1	3.4	2.9
DV13	197.3	180.1	188.7	12.2	6.4
DV14	125.4	142.1	133.8	11.8	8.8
DV15	167.9	159.1	163.5	6.2	3.8
DV16	182.7	175.7	179.2	4.9	2.8

Table 6.2: Intra-rater infarct volume assessment using manual delineation of RARE T_2 imaging in the derivation group.

Animal	Infarct volume measurement (mm^3)			Standard Deviation (mm^3)	Coefficient of variation (%)
	1	2	Mean		
COM1	18.4	17.9	18.2	0.4	1.9
COM2	117.1	120.3	118.7	2.3	1.9
COM3	60.1	58.2	59.2	1.3	2.3
COM4	210.3	195.9	203.1	10.2	5.0
COM5	236.1	224.7	230.4	8.1	3.5
COM6	194.3	174.2	184.3	14.2	7.7
COM7	215.1	230.4	222.8	10.8	4.9
COM8	195.1	179.9	187.5	10.7	5.7
COM9	175.1	168.4	171.8	4.7	2.8
COM10	45.3	50.1	47.7	3.4	7.1
COM11	43.1	38.8	41.0	3.0	7.4
COM12	175.3	190.1	182.7	10.5	5.7
COM13	177.4	188.3	182.9	7.7	4.2

Table 6.3: Intra-rater infarct volume assessment using manual delineation of RARE T_2 imaging in the comparison group.

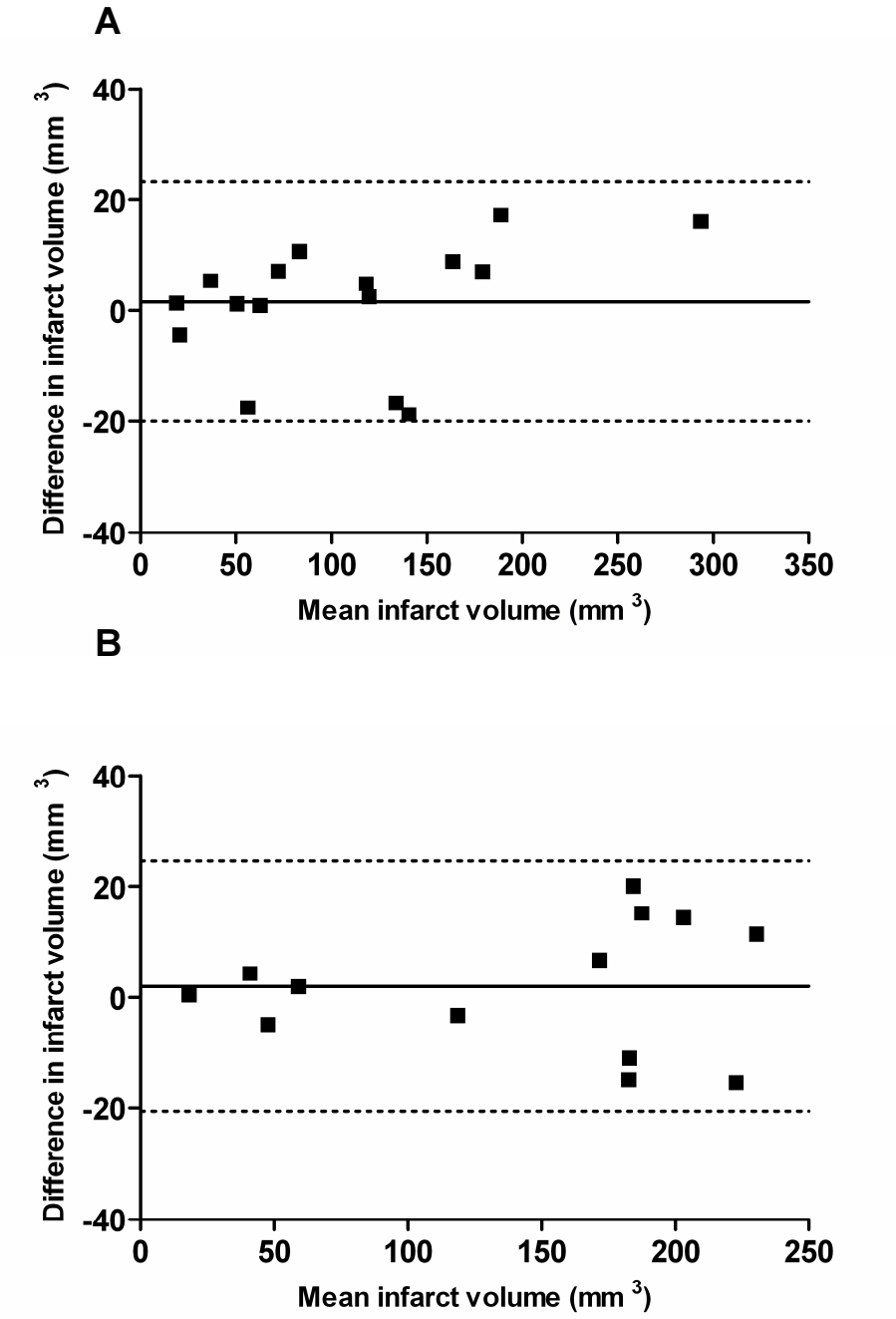

Figure 6.6: Scatterplots according to Bland and Altman presenting the intraobserver variability of the manual delineation method of infarct volume calculation from RARE T2 images within A) the derivation group (n=16) and B) the comparison group (n=13). Each point represents one animal in the group. Mean difference (bias) indicated by the solid line with 95% confidence limits (mean±1.96SD) indicated by the dotted lines.

6.3.3 Identifying the T_2 threshold from Quantitative T_2 maps that generates the same infarct volume as RARE T_2 in derivation group animals

Infarct volume was manually delineated from RARE T_2 weighted images for each animal in the derivation group. The quantitative T_2 maps for each animal in the derivation group were then analysed individually. T_2 thresholds of 65ms – 90 ms increasing in increments of 1 ms were applied and the infarct volume for each threshold was generated. This volume was based on the number of pixels lying above each threshold multiplied by the known volume of a pixel on the quantitative T_2 maps. The threshold that generated the same volume of infarct as that manually delineated from RARE T_2 images was selected (Table 6.4).

Threshold (ms)	Infarct Volume (mm^3)
65	505.7
66	478.5
67	455.1
68	434.0
69	417.3
70	401.4
71	388.2
72	377.5
73	369.0
74	361.1
75	351.6
76	344.1
77	337.2
78	330.2
79	324.4
80	319.1
81	313.1
82	306.5
83	299.9
84	293.6
85	288.7
86	282.8
87	276.2
88	269.9
89	262.4
90	255.3

Infarct Volume (RARE T_2): 301.4 mm^3

Table 6.4: Range of thresholds applied to quantitative T_2 maps with resulting infarct volume described. The threshold that produced the infarct volume most similar to the manually delineated infarct from RARE T_2 images was selected (highlighted in red)

The T_2 threshold for the majority of the derivation animals could not be defined within the range of thresholds calculated (65-90 ms) (Table 6.5).

Threshold (ms)	Infarct Volume (mm^3
65	268.49
66	242.86
67	218.76
68	195.67
69	176.96
70	162.62
71	150.72
72	141.2
73	132.21
74	125.90
75	121.23
76	116.96
77	112.28
78	107.1
79	103.1
80	99.0
81	94.7
82	91.3
83	88.6
84	84.4
85	82.1
86	78.9
87	76.4
88	73.5
89	71.3
90	68.7

Infarct Volume (RARE T_2): 19.7 mm^3

Table 6.5: Range of thresholds applied to quantitative T_2 maps with resulting infarct volume described. The upper limit of the threshold range was not sufficient to calculate the threshold that produced an infarct volume most similar to the manually delineated infarct from RARE T_2 images.

Out of the 16 animals in the derivation group, only 8 had a T_2 threshold that fell within the range of thresholds applied to the quantitative T_2 maps (Figure 6.7). The threshold range was based on the mean T_2 values from ROIs representing infarct calculated from the quantitative T_2 maps and from visual observations of the whole hemisphere histograms (Figure 6.8). The minimum T_2 relaxation time for infarct was calculated as 75.1±4.2 ms with the maximum T_2 relaxation time being 126.6±12.8 ms. These values suggest that a threshold of 90 ms, the upper limit of the threshold range applied, would underestimate the infarct volume as it would not include the values from 75-90 ms which potentially represent ischaemically damaged tissue.

Visual inspection of the quantitative raw T_2 maps highlights that the ventricles have a high signal intensity which lies above the upper limit of the T_2 relaxation threshold range (Figure 6.8). This means that the ventricles will be incorporated into the final infarct volume so that the infarct volume at each threshold within the applied range (65ms – 90ms) is overestimated.

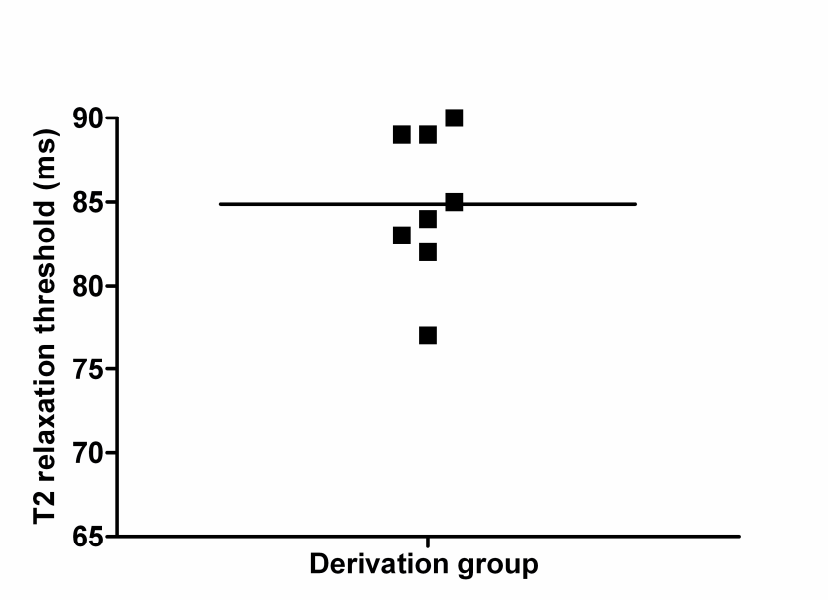

Figure 6.7: Graphical representation of the T2 threshold which produced a similar infarct volume to the manual delineation method of RARE T2 images. Only 8 of the 16 animals had a T2 threshold that fell within the range applied. Mean indicated by a solid line.

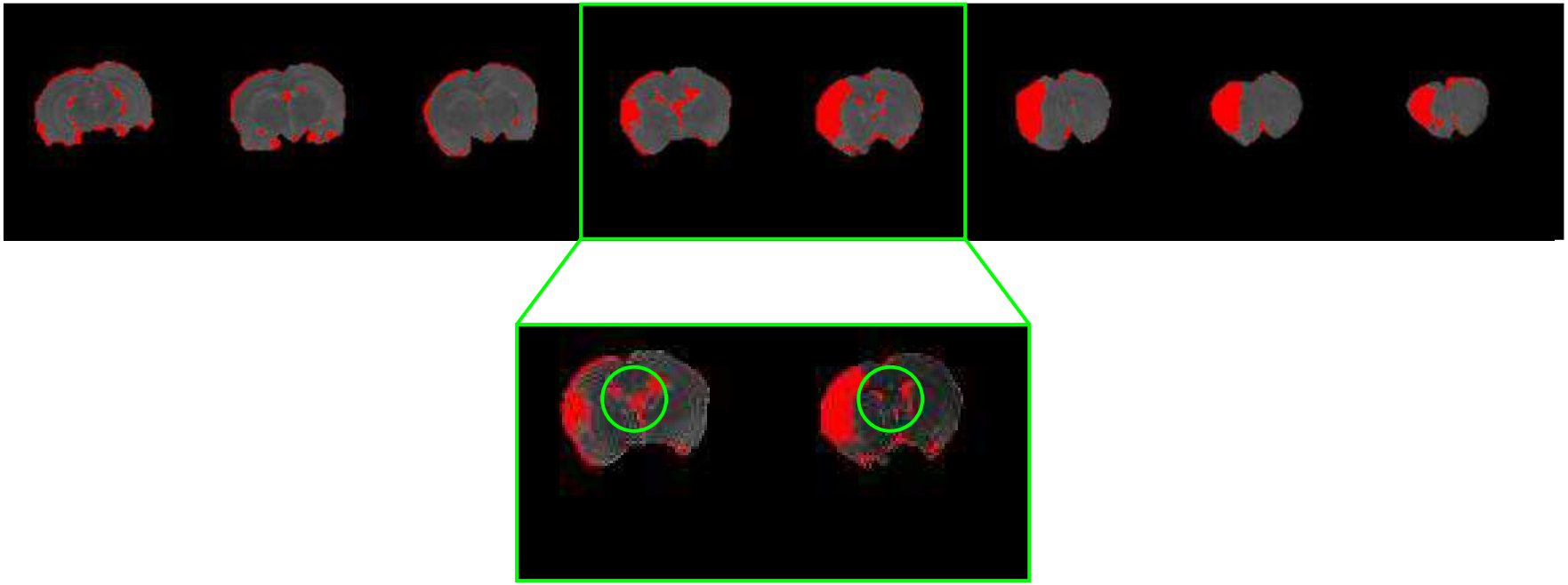

Figure 6.8: Representative quantitative T2 maps from an animal in the derivation group with an applied threshold (red). It can be seen that the ventricles are incorporated into the derived infarct (circled green).

6.3.4 Image processing steps to improve the T_2 threshold

The quantitative T_2 maps from each of the brains in the derivation group were modified to remove the ventricles from the images (Figure 6.9). This was done in both the ipsilateral and contralateral hemispheres by manually delineating the ventricles on the T_2 maps and deleting them from the image.

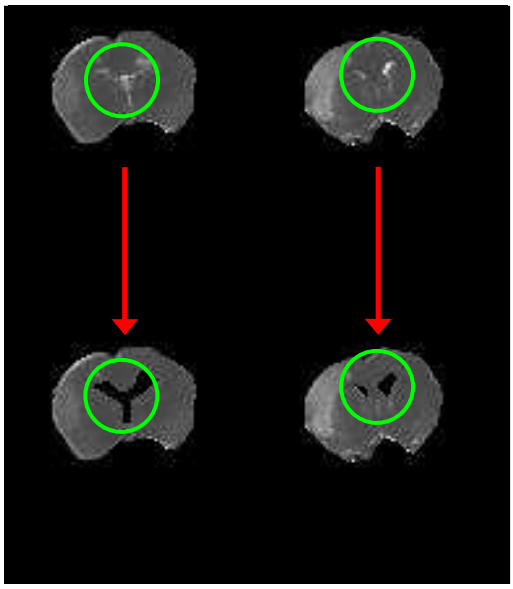

Figure 6.9: Coronal quantitative T2 maps before and after the removal of the ventricles (circled green).

New histogram data were calculated for the modified T_2 maps and the T_2 thresholds (65ms – 90ms) were reapplied to ascertain which threshold produced the most similar infarct volume to that calculated by manual delineation of RARE T_2 images. This was carried out on each animal of the derivation group to get an animal specific threshold before a group threshold was calculated.

Out of the 16 animals in the derivation group, 12 animals had a T_2 threshold that fell within the range of thresholds applied to the quantitative T_2 maps which is an improvement from the initial calculation (Figure 6.10). This highlights the involvement of the ventricles in the infarct defined by the threshold.

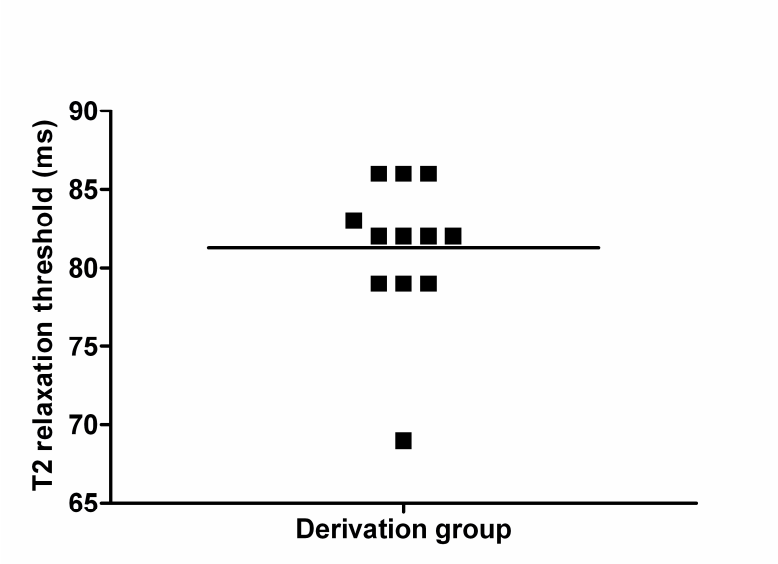

Figure 6.10: Graphical representation of the T2 threshold which produced a similar infarct volume to the manual delineation method of RARE T2 images. Only 12 of the 16 animals had a T2 threshold that fell within the range applied. Mean indicated by a solid line.

As there were still a number of animals whose T_2 threshold could not be determined using the T_2 threshold range applied, this suggested that another potential source of error, causing the infarct volume to be overestimated at a particular threshold, was present in the images. The modified quantitative T_2 maps were visually inspected to ascertain whether or not an inherent overestimation existed of infarct volume. It was obvious that there was a noticeable amount of noise around the brain incorporated in to the infarct (Figure 6.11). This noise, like the ventricles, will cause an overestimation of infarct volume at a given T_2 relaxation threshold.

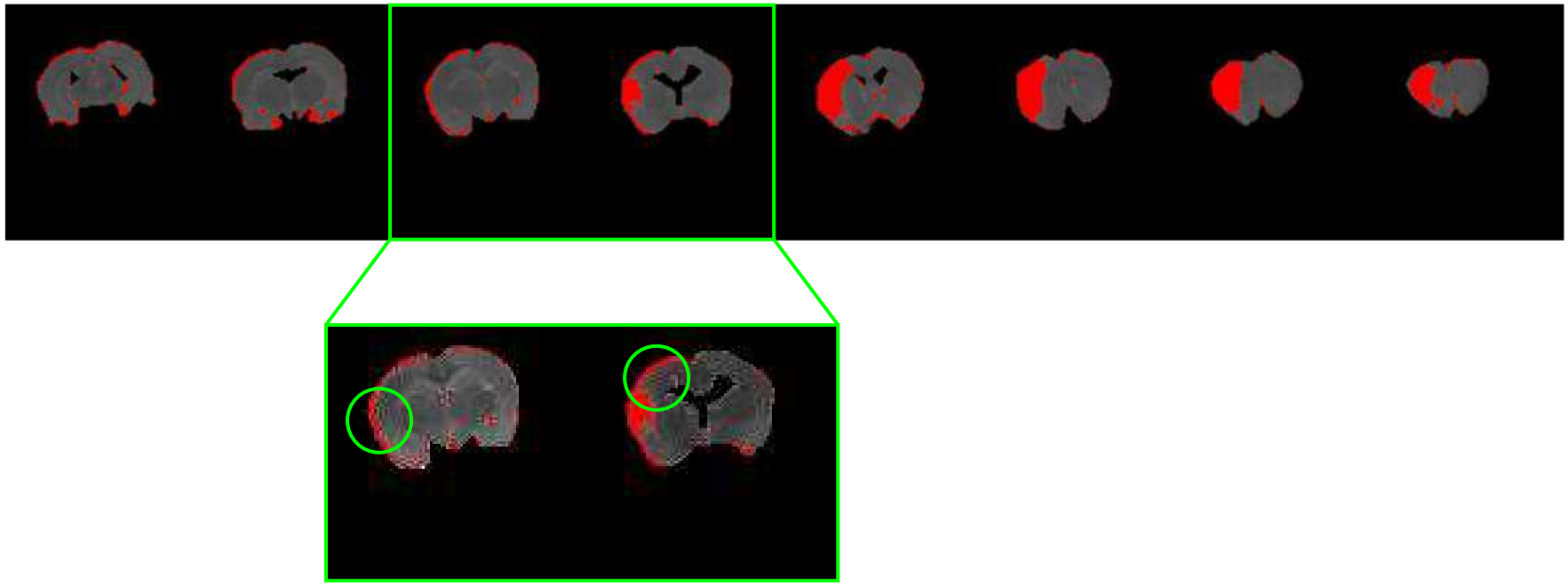

Figure 6.11: Representative quantitative T2 maps from an animal in the derivation group with an applied threshold (red). It can be seen that there is areas of noise around the outside of the coronal brain sections (circled in green) that is incorporated into the derived infarct.

ImageJ allows you to apply a median filter to an image. This filter helps smooth out any noise pixels by taking the median value of each surrounding pixel and applying the median to that pixel. The quantitative T_2 maps previously modified by manually removing the ventricles were subjected to a 1.0 pixel median filter (Figure 6.12). This was done to each of the 8 coronal slices for each brain within the derivation group.

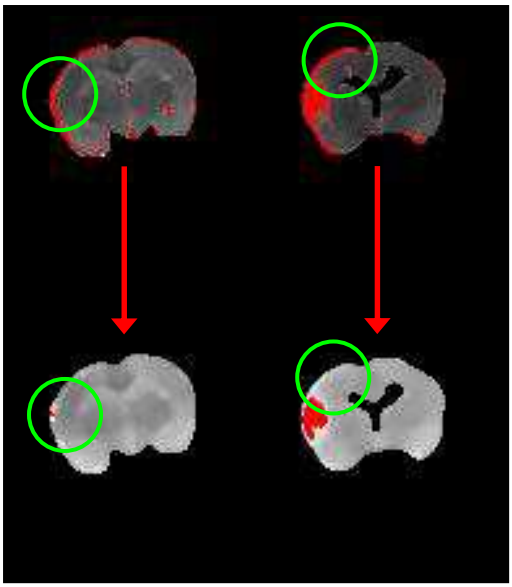

Figure 6.12: Coronal quantitative T2 maps before and after the application of a 1.0 pixel median filter. The noise previously observed (top row of images, circled green) has been removed by the filter (bottom row of images, circled green).

New histogram data was calculated for the modified T_2 maps once the median filter had been applied. The T_2 thresholds (65ms – 90ms) were reapplied to each T_2 map to ascertain which threshold produced the most similar infarct volume to that calculated by manual delineation of RARE T_2 images. This was carried out on each animal of the derivation group to get an animal specific threshold before a group threshold was calculated.

6.3.5 Collating all the calculated T_2 thresholds to generate a mean T_2 threshold for the derivation group

The data from the derivation group was collated to calculate a mean T_2 threshold for the group (Figure 6.13). Out of the 16 animals in the derivation group, all 16 animals had a T_2 threshold that fell within the range of thresholds applied to the quantitative T_2 maps.

The mean T_2 threshold calculated for the derivation group was 76.0±2.9 ms. The thresholds from each animal are quite comparable, although the standard deviation is around 3 times larger than that seen when calculating contralateral T_2 relaxation. Compared to the previous attempts at selecting a T_2 threshold the variability is much smaller between animals which suggests the amount of error present is lower. The 76 ms threshold also gave good spatial conformity with the manually delineated RARE T_2 images which is obviously as important as generating the correct volume for infarct quantification (Figure 6.14).

The images also highlight the infarct is spatial distinct from the ventricles. This means that it is possible to apply the threshold to images that have not been modified (had ventricles manually removed) and calculate infarct, visually discriminating between what is obviously ventricle/CSF signal and what represents infarct.

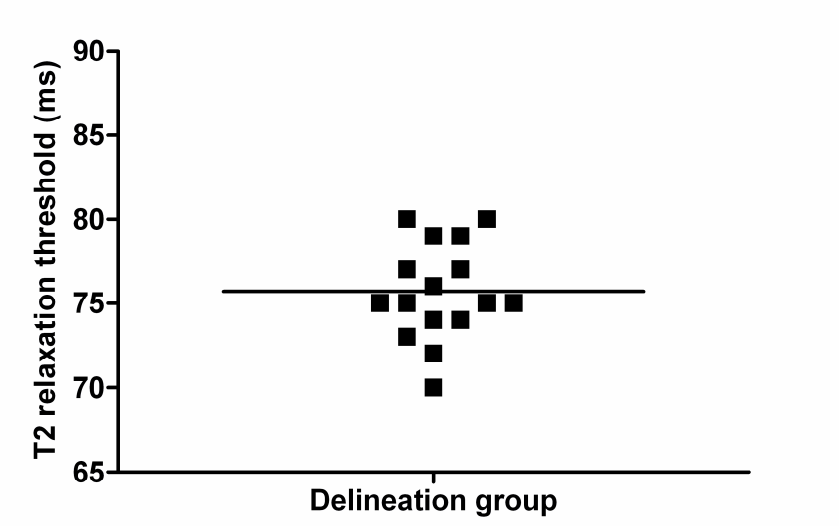

Figure 6.13: Graphical representation of the T2 threshold which produced a similar infarct volume to the manual delineation method of RARE T2 images. All 16 of the 16 animals had a T2 threshold that fell within the range applied. The mean T2 threshold is indicated by a solid line.

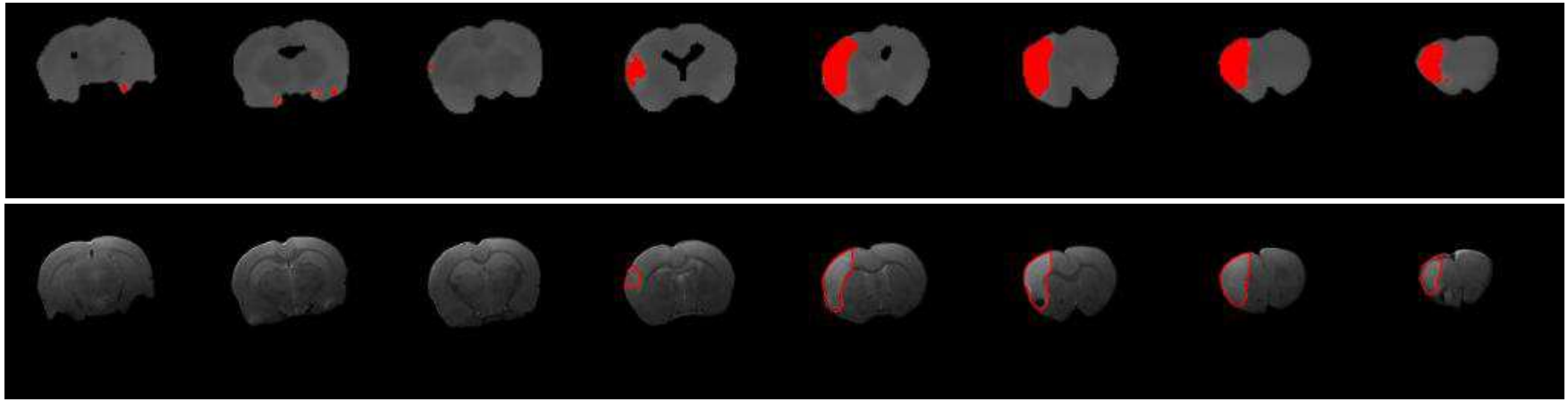

Figure 6.14: Representative quantitative T2 maps from an animal in the derivation group with the 76ms threshold applied (top row, filled red) and corresponding RARE T2 weighted coronal images with the manual delineation of the infarct superimposed (bottom row, circled red). The images show the infarct defined by the 76ms threshold shares good spatial conformity with the manual delineation method.

6.3.6 Applying the mean T_2 threshold to comparison group animals

The mean T_2 threshold from the derivation group needed to be tested in a separate group of animals to confirm its suitability. The comparison group (n=13) all had infarcts calculated from the RARE T_2 images by manual delineation. The quantitative T_2 maps for each animal of the comparison group were opened in ImageJ and subjected to the 1.0 pixel median filter to remove any unwanted noise from the images. Each coronal slice had the 76 ms threshold applied and the resulting area of infarct defined by the threshold was measured.

The two methods for infarct determination were compared (Figure 6.15). The 76ms threshold produces similar infarct volumes, generally overestimating slightly compared to the manual delineation method. The Bland-Altman plot confirmed the 76 ms threshold overestimated infarct volume by 7.5±12.5 mm^3 compared with the manual delineation of RARE T_2 images (Figure 6.16).

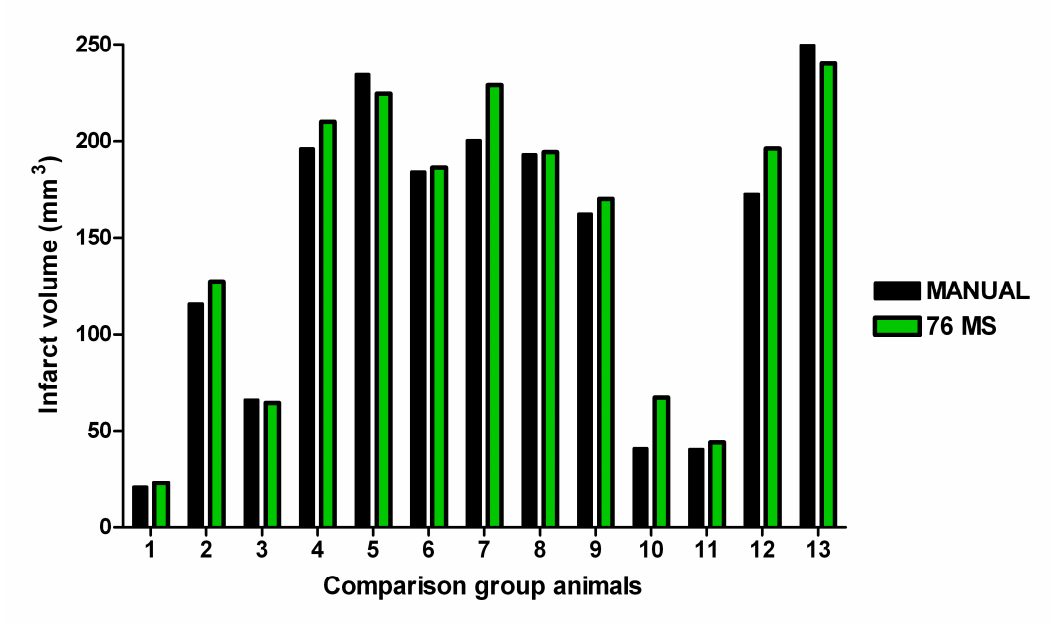

Figure 6.15: Comparison of infarct volume derived from manual delineation (black) and the quantitative T2 maps (green), using the calculated 76 ms threshold, in the comparison group.

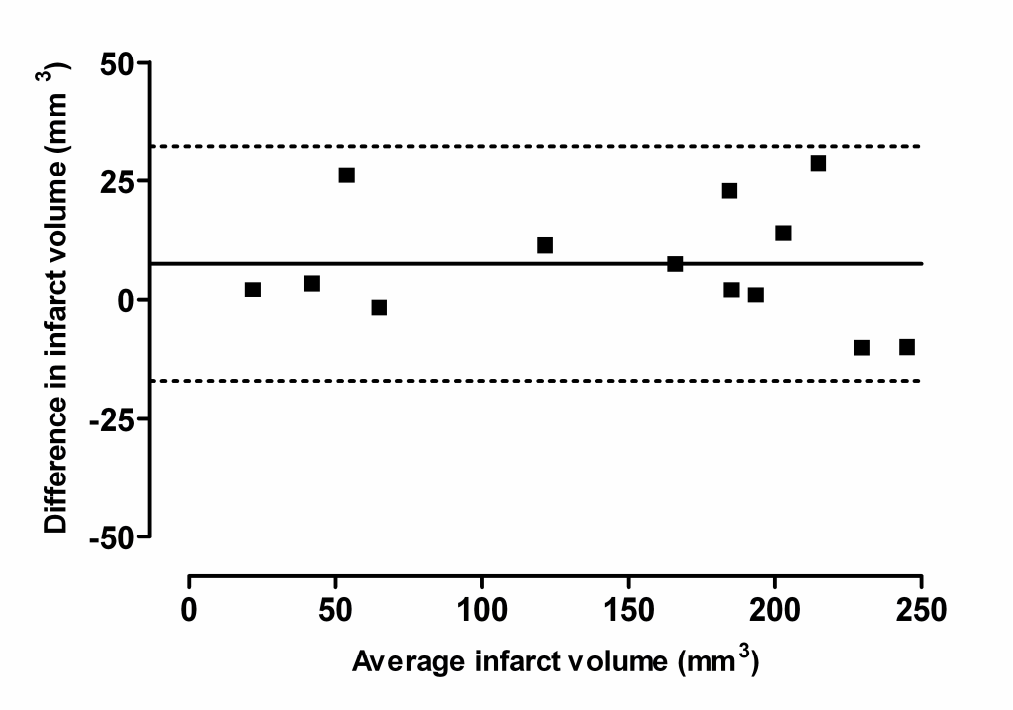

Figure 6.16: Bland-Altman plot comparing the 2 methods of infarct quantification. Each point represents and animal in the comparison group. Solid line indicates the bias, dotted lines indicate 95% limit of agreement.

6.3.7 Application of threshold of abnormality from quantitative T_2-maps for the intraluminal filament model of MCAO

It was important to ascertain whether or not the derived threshold would generate similar infarct volumes from quantitative T_2 maps compared to T_2 images in animals that had under gone MCAO using the intraluminal filament model. Confirming the suitability of this threshold will allow it to be used for ILF studies. However if it fails to reproduce the result then a new threshold would have to be derived for this model.

The 76ms threshold was applied to 14 male Sprague-Dawley rats and the threshold defined infarct was determined. The 76ms threshold-defined infarct encompasses the ventricles which interfere more with the infarct volume determination in this model of MCAO due to the increase in infarct volume and proximity of the lesion to the ventricles (Figure 6.17). This made it impossible to use this threshold to generate an accurate calculation of infarct based on this T_2 threshold.

The CSF that is present in the ventricles in known to have a very long T_2 relaxation time in the region of 2000ms. In theory an upper threshold limit could potentially delineate the infarct tissue from the CSF in the ventricles.

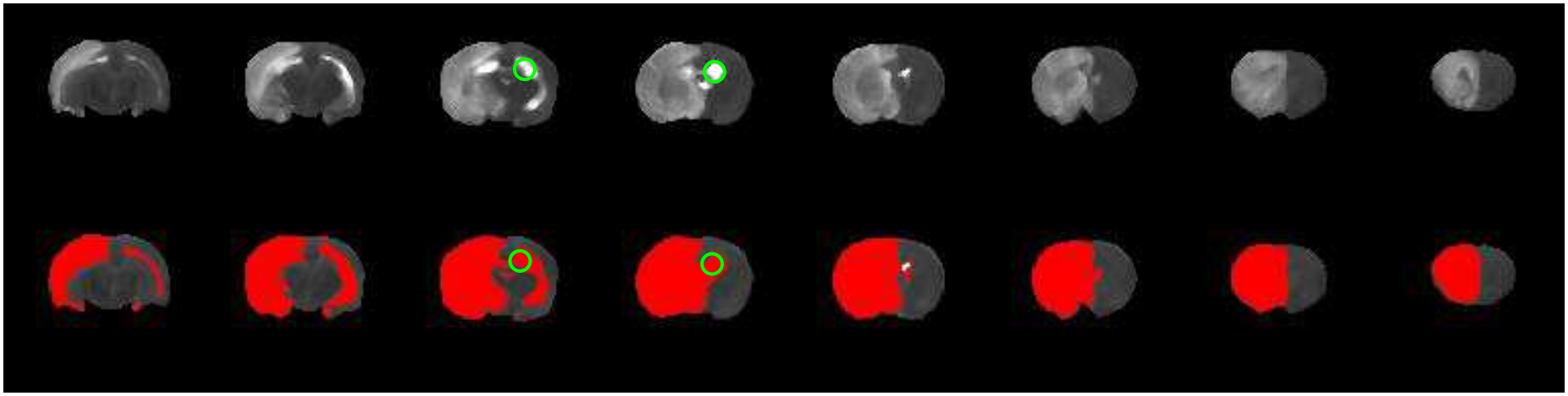

Figure 6.17: Quantitative T2 maps from a representative animal (A) and with the 76 ms threshold applied indicating infarction (red) (B). Green circles indicated examples of ventricles in the contralateral hemisphere that have a T2 value above the 76 ms threshold of abnormality and are consequently included in the threshold-defined infarct.

T_2 values were obtained for ROIs within the ipsilateral and contralateral ventricles to assess the mean, minimum and maximum T_2 values associated with the CSF. Similarly ROIs associated with infarct were measured to ascertain whether or not these regions could be separated based on their respective T_2 relaxation times (Figure 6.18).

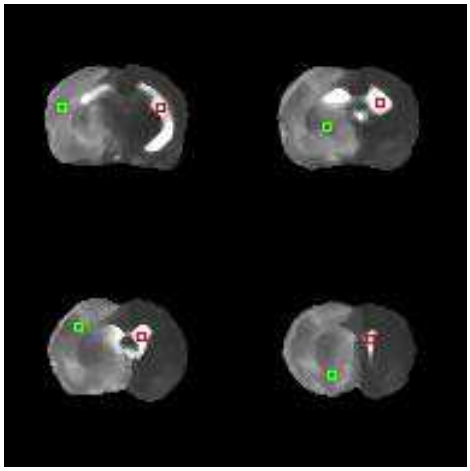

Figure 6.18: Quantitative T2 maps illustrating the ROIs used for ipsilateral and contralateral ventricle measurement (red square) and infarct T2 measurement (green square).

The mean T_2 for infarct was 107.5±5.9ms with a mean minimum T_2 value of 85.8±7.8ms and a mean maximum value of 136.1±11.9ms from all of the regions measured. The mean T_2 relaxation obtained from ROIs associated with the ventricles was 219.9±48.4ms with a mean minimum T_2 value of 148.0±43.6ms and a mean maximum value of 304.5±82.2ms from all of the regions measured.

The 76ms threshold was then applied to the quantitative T_2 maps with an upper T_2 relaxation time of 147ms which equates to the mean maximum T_2 value for infarct plus one standard deviation as calculated from the ROI measurements (Figure 6.19). This threshold range for infarct volume improved the delineation between ventricles and infarct, especially in areas where the ventricles are of a substantial size, rostral to the hippocampus. However in more caudal slices the lateral ventricles still become incorporated in to the threshold defined infarct. The border zone of the ventricles tends to be incorporated into the 76-147ms threshold which equates to a measurable area and inherent error with the threshold for quantitative T_2 maps.

The threshold range was compared to the manually delineated volume from T_2 images (Figure 6.20). Generally, from the comparison it seemed that this threshold overestimated the infarct volume compared to the manual delineation method. A Bland-Altman plot highlighted that the difference between the methods became larger as the average infarct volume became larger (Figure 6.21A). This difference between the methods was therefore expressed as a percentage which showed that the bias between the two methods was 18.5±10.5% (Figure 6.21B).

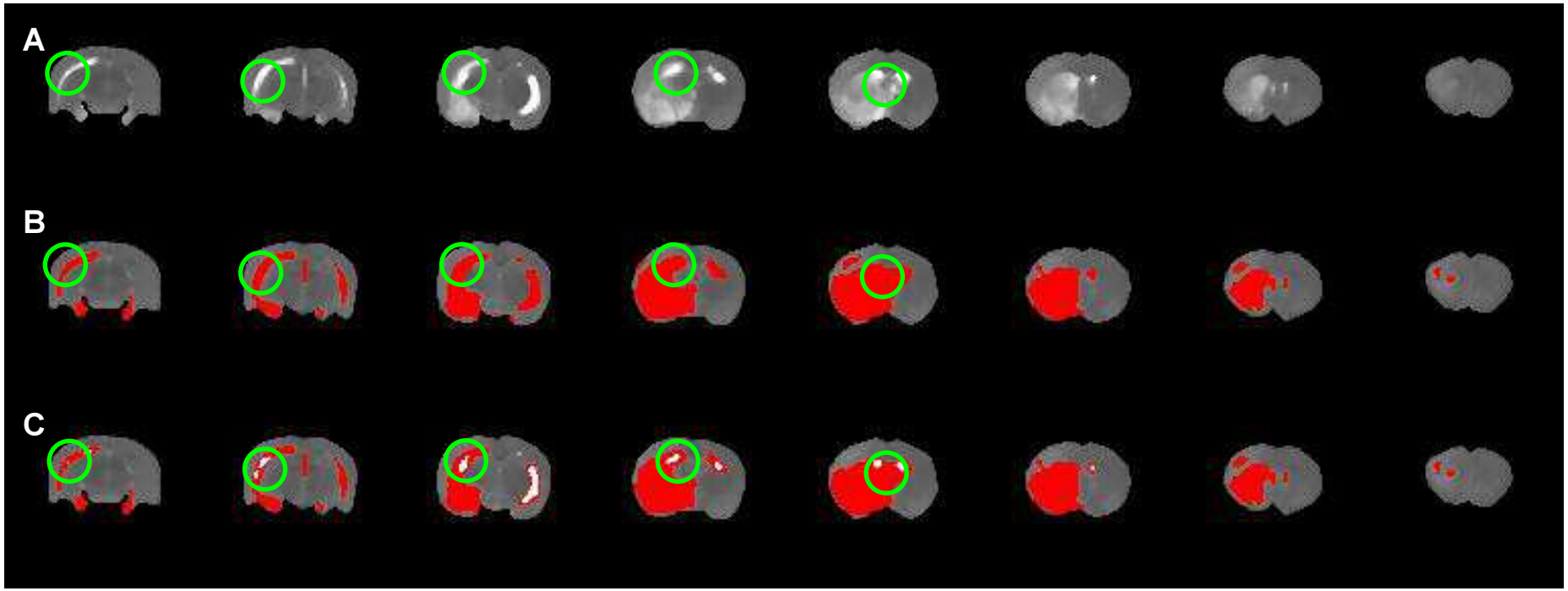

Figure 6.19: Quantitative T2 maps (A) with 76 ms threshold (B) and 76-147 ms threshold range applied (C). The 76-146 ms range provides a more accurate estimation of infarct volume as the ventricles are now not completely included in the threshold-determined infarct. However it can be seen that there is still considerable areas of threshold-determined infarct surrounding the ventricles which is not infarct.

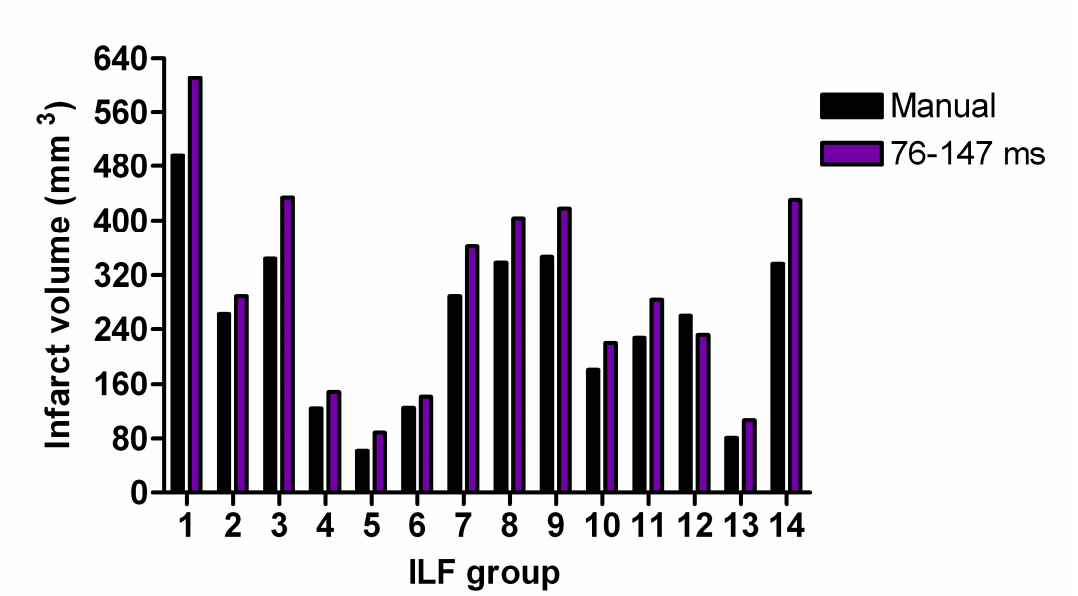

Figure 6.20: Comparison of infarct volume derived from manual delineation (black) and the quantitative T2 maps using the calculated 76-147 ms threshold (purple) in the intraluminal filament (ILF) group.

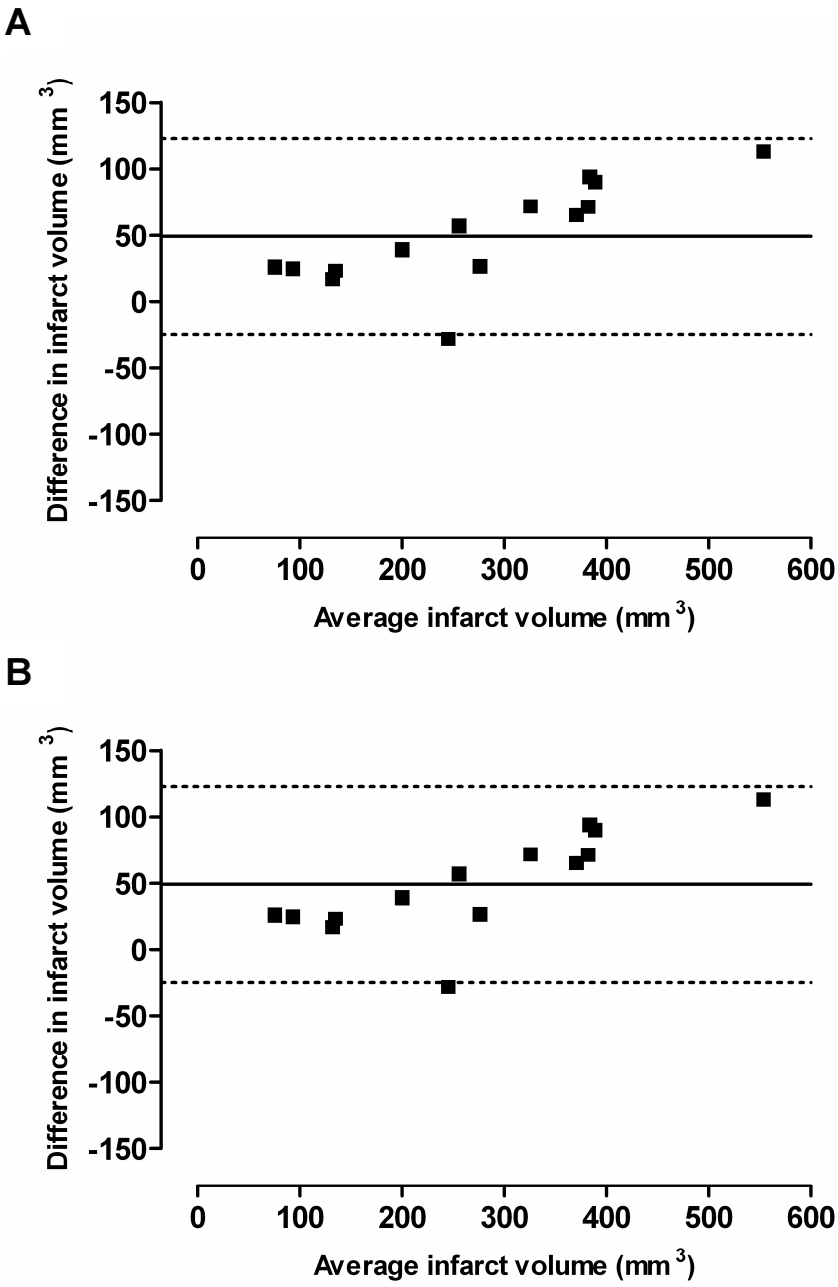

Figure 6.21: Bland-Altman plots comparing the 2 methods of infarct quantification. A) Comparison based on absolute difference in infarct volume between methods. Solid line indicates the bias, dotted lines indicate 95% limit of agreement. B) Comparison based on % difference in infarct volume between methods. Solid line indicates the bias, dotted lines indicate 95% limit of agreement.

6.4 Discussion

This study is the first to derive a T_2 relaxation threshold of abnormality for the quantitative T_2 map derived from an MSME T_2 weighted sequence in animals subjected to MCAO using the distal diathermy occlusion model. An in-house T_2 relaxation threshold was established for the Sprague Dawley strain based on the final infarct volume at 24 hours post MCAO using the RARE T_2 weighted imaging that has been previously used to for final infarct quantification (Reid *et al* 2012; Robertson *et al* 2011). The mean calculated threshold was then applied to a separate group of animals and compared once again to the RARE T_2 weighted imaging to confirm its utility.

6.4.1 A threshold for abnormality was successfully derived for the distal diathermy model of MCAO 24 hours post MCAO

The use of histograms to plot the number of pixels relating to specific T_2 relaxation times for the entire hemisphere led to substantial overestimation of the T_2 threshold for the quantitative T_2 maps due to the inclusion of the ventricles within the hemisphere. This was highlighted in the Bland-Altman plot which showed that the bias between the manual delineation and the threshold derived infarct was around 40 mm^3. Manually removing the ventricles reduced the threshold of abnormality to 85 ms which in turn reduced the bias to around 30 mm^3, although this is still a considerable bias between the two methods. Applying a filter helped smooth the images by removing pixels from around the periphery of the image which obviously did not form part of the ischaemic damage. This reduced the threshold to 76 ms and this resulted in a similar infarct volume between the manual delineation and the threshold defined infarct confirmed by a bias of -4 mm^3 calculated from the Bland-Altman plot. Good spatial correlation was observed using this threshold.

The spatial separation between the ventricles and the ischaemically damaged tissue in the distal diathermy MCAO model means that no prior alteration, i.e. manually removing the ventricles from the image, is needed when applying the threshold. A median filter is however still required to remove erroneous pixels. This is common practice within our lab for acute ischaemic damage

quantification on ADC maps and perfusion deficit measurement on quantitative CBF maps.

6.4.2 T_2 threshold only valid for experimental setup from which it was derived

The 76 ms threshold relates only to the specific sequence and equipment set up that is used in our lab. This is because magnetic field strength can affect T_2 relaxation time. It has been shown that in rats, an increase in magnetic field strength from 4T to 11.6T led to a shortening of T_2 relaxation of water in all brain structures measured (de Graaf *et al* 2006). Interestingly a study using a 4.7T MRI scanner derived a T_2 threshold against TTC staining at 24 hours and calculated the threshold to be 77.9±3.6 ms which is quite similar to that calculated in this study. This perhaps highlights that field strength is not the only factor that can significantly affect T_2 relaxation and hence the threshold of abnormality.

The time at which the MSME imaging was conducted in relation to occlusion time is important and this T_2 relaxation threshold of 76 ms can only be used for images acquired 24 hours post MCAO. From 0-12 hours post MCAO it is known that the changes in T_2 values are insignificant and can not be used to reliably detect ischaemic damage unlike ADC maps generated from DWI (Baird and Warach 1998). Similarly lengthening the time post-stroke also invalidates this threshold due to pseudonormalisation of T_2 relaxation with time (Verheul *et al* 1992). T_2 defined lesion volume can be visualised from as early as 5 hours, although it is severely underestimated compared to DWI defined ischaemic damage, with peak lesion volume occurring around 24 to 48 hours following permanent MCAO (Verheul *et al* 1992). This lesion volume then diminishes to almost half the peak volume after a week post MCAO due to the reduction in cellular water content as brain oedema resolves. This highlights the potential error that may be incurred if using this threshold even 48 hours post MCAO, as small but significant changes in the threshold of abnormality might be present.

Strain differences could also potentially influence the T_2 threshold of abnormality as similar differences have been found in thresholds of abnormality

for both ADC and for CBF. The ADC threshold for Sprague Dawley rats has been reported as a 30% reduction in ADC compared to the contralateral hemisphere to predict final infarct volume (Foley *et al*; Shen *et al* 2003), whereas in the WKY and SHRSP strains this has been calculated as 21% and 23% respectively (Reid *et al* 2012). CBF thresholds also differ with strain and a lower threshold of 23ml/100g/min has been calculated for WKY rats (Reid *et al* 2012) compared to 30ml/100g/min in Sprague Dawley rats (Shen *et al* 2003). Differences between SHRSP and the WKY control strain were also found between the CBF thresholds (Reid *et al* 2012).

These factors all highlight the importance of deriving a threshold for the specific MRI scanner, stroke model, strain and time post onset of ischaemia to achieve the most accurate and reliable threshold for determining final infarct volume using quantitative T_2 mapping.

6.4.3 Application of threshold to ILF MCAO model was unsuccessful

The T_2 threshold derived from animals that underwent MCAO using the distal diathermy model did not successfully calculate the infarct volume in animals subjected to the ILF model of MCAO. The close proximity of the much larger infarcts to the ventricles in the ILF model of MCAO made it impossible to demarcate ischaemically damaged tissue from the CSF-containing ventricles. CSF is known to have a T_2 relaxation of approximately 2000 ms which prompted the calculation of an upper threshold limit of 147 ms which equates to the mean maximum T_2 value for infarct over a number of voxels plus one standard deviation. The current MSME T_2 weighted sequence produces mean T_2 values of around 220 ms for CSF which is far lower than expected. The mean minimum value for CSF was calculated to be 148±48 ms which highlights potential crossover of T_2 values between the CSF and the infarct tissue. This was clear on the quantitative T_2 maps which exhibited considerable areas of tissue around the proximity of the ventricles and particularly the lateral ventricles that were included in the lesion determined by the 76-147 ms threshold. The Bland-Altman plots confirmed this error showing a 20% bias between the manual delineation and the threshold derived ischaemic damage.

The current sequence for the MSME T_2 weighted imaging does not give a true reading of CSF T_2 relaxation. The current upper threshold cannot successfully differentiate between infarct and CSF which inevitably leads to error in infarct volume quantification. Potentially the resolution of the MSME T_2-weighted images is not sufficient to visualise the border. The relatively large voxel size compared to the RARE T_2-weighted images mean that the pixels at the border between parenchymal tissue and CSF are influenced by signal from both with regards to T_2 relaxation. This would mean that normal parenchymal tissue, with a relatively short T_2 relaxation time, could display a longer T_2 due to the inclusion of CSF signal and vice versa. The MSME T_2 sequence acquires images based on the geometry and matrix size of the DWI and PWI sequences so that direct comparisons can be made on a pixel by pixel basis. The resolution of these scans is limited due to the time it takes to acquire a higher resolution image. This means that currently there is no option to increase the resolution of the MSME T_2 sequence. Similarly the sequence may need fine tuning to improve the differentiation between tissue and CSF. This would create a significant distinction, based on T_2, between the infarct and CSF which is not currently achieved with the available sequence.

The main problem with T_2-weighted imaging sequences is that aqueous solutions, including CSF have a long T_2 relaxation time. As ischaemically damaged tissue has an increased T_2 relaxation time the measurement of purely damaged tissue is difficult. Removing the CSF signal from the images would reduce the inherent error caused by this. Manually removing the ventricles from each image is not a solution as this requires manually distinguishing the ventricles from infarct, which leads to investigator error that the T_2 threshold of abnormality set out to eliminate.

A potential method for defining infarct volume using a quantitative T_2 map is by using cluster image analyses of ADC and T_2 maps where the ADC versus T_2 values from the contralateral hemisphere are plotted to generate a two-dimensional cluster scatterplot (Jiang *et al* 1997). The cluster associated with cerebrospinal fluid, with its characteristic high ADC values, are distinct from parenchymal tissue and ischaemically damaged tissue which enable these pixels to be excluded from the T_2 analysis. This prevents any operator error and image modification based on visual differences in signal intensity. Jiang et al (1997)

also defined the threshold of abnormality based on the mean T_2 values of the parenchymal tissue cluster excluding the pixels associated with CSF. Normal pixels were defined as mean T_2 ± 2 SD. A 2-dimensional cluster plot was then generated for the ipsilateral hemisphere and pixels lying outwith the defined normal cluster were classed as abnormal, representing the ischaemic lesion, and the normal pixels were defined using mean ADC ± 1.5 SD and mean T_2 ± 2 SD. Once the normal tissue cluster was defined, the two-dimensional cluster scatterplot from the coronal section of brain was then generated, and the abnormal pixels were defined as pixels outside the normal cluster. The numbers of normal and abnormal pixels were calculated within the ipsilateral hemisphere which can be used to calculate lesion area on a coronal slice and lesion volume based on slice thickness. This method must be conducted on DWI images and T_2 maps that share identical geometry, matrix size and field of view so that pixels in both images refer to the same anatomical location to allow pixels representing CSF to be discarded.

Another potential solution is to employ a different form of T_2-weighted MRI that is able to distinguish between CSF and parenchymal tissue. Fluid Attenuated Inversion Recovery (FLAIR) imaging is a T_2 weighted imaging technique that can potentially improve the detection of ischaemically damaged tissue. The technique suppresses the signal generated by CSF yet retains the increased intensity consistent with infarct (Hajnal *et al* 1992a; Hajnal *et al* 1992b). FLAIR imaging techniques are used clinically (Brant-Zawadzki *et al* 1996; Hjort *et al* 2008; Israeli *et al* 2011), and although less accurate than DWI, FLAIR imaging has be shown to detect early ischemic lesions better than T_2-weigted imaging (FLAIR, 91%; T_2-weighted, 71% detected)(van Everdingen *et al* 1998). Adaptations of the FLAIR technique have been achieved to help reduce the acquisition time and increase the number of slices that can be imaged as initial sequences were taking too long a time to acquire, to be clinically useful [give an idea of how long](Simonson *et al* 1996). In preclinical stroke research very few studies have adopted this technique (Taoka *et al* 2004) although a number of studies looking at tumour development in rats have done so (Jahnke *et al* 2009; Soussain *et al* 2007). FLAIR imaging sequence development for infarct quantification in rats would significantly benefit preclinical studies by reducing

both the error in infarct determination caused by the inclusion of ventricles and CSF and the post-image processing to remove the CSF signal.

6.5 Conclusions

Quantitative T_2 mapping allows comparison of T_2 relaxation times on a pixel by pixel basis. Utilising a threshold for abnormality can remove the intra- and inter investigator error inherent with the manual delineation of ischaemic damage from RARE T_2-weighted images. A threshold of 76 ms can accurately determine infarct volume in the distal diathermy method of MCAO but not in the intraluminal filament model. Interference from CSF signal is a problem with the current MSME T_2-weighted sequence and some fine tuning is required. Acquisition of both DWI and MSME T_2 scans is recommended to attempt to exclude pixels corresponding to CSF which will reduce the error associated with the CSF signal.

Chapter 7 - General Discussion

The studies presented in this thesis have demonstrated that acute hyperglycaemia, at clinically relevant levels, is detrimental to both early ischaemic lesion evolution and final infarct volume in animals lacking stroke co-morbidities such as hypertension and insulin resistance. Oxidative stress has been implicated in hyperglycaemia-associated ischaemic damage and in diabetic complications. However the studies in this thesis suggest that oxidative stress is not the primary mechanism to exacerbate damage attributable to acute hyperglycaemia following permanent MCAO.

In this chapter the findings of this thesis will be put into clinical context to discuss how these results can inform the clinical situation and what the current treatment options and guidelines are for hyperglycaemic stroke patients. The studies conducted in this thesis represented one of the first attempts to model clinically relevant hyperglycaemia in animals with and without features of the metabolic syndrome. Based on the findings of thesis, the direction of future work utilising clinically relevant models will be discussed. Before that I will start by discussing some of the issues surrounding the conduct of preclinical stroke studies that have been raised within the stroke research community in recent years.

7.1 Animal models in preclinical stroke research

In experimental stroke research it is important to bear in mind that animals are used to model pathophysiological processes but they cannot model stroke as a disease. The reliance on one particular model of focal cerebral ischaemia or one particular model of hyperglycaemia may lead to a biased preclinical opinion that does not translate to the clinical situation. The knowledge that over 7,000 studies examining the neuroprotective effects of more than 1,000 therapeutic interventions have been published (O'Collins *et al* 2006), yet only one successful pharmacological treatment has been successfully translated from bench to bedside highlights the importance of generating a broad preclinical picture with the use of many animal models and species.

Selection of the most suitable models to investigate PSH was deemed important for the work reported in this thesis as the majority of the previous literature

investigating hyperglycaemia in focal ischaemia models used the streptozotocin, type-1 diabetes model or glucose infusion/injection models which lead to extremely high blood glucose. The levels of hyperglycaemia previously investigated do not represent those observed in the majority of the hyperglycaemic stroke population. The acute hyperglycaemia model used throughout this thesis consistently produced clinically relevant levels of hyperglycaemia based on the range of glucose values included in the GIST-UK (Gray *et al* 2007) and the SELESTIAL trial (McCormick *et al* 2010). Interestingly however, different rat strains may require the glucose dosing to be altered. The Sprague-Dawley rats used in Chapter 5 had a higher baseline blood glucose compared to the WKY and SHRSP rats after an overnight fast. This also meant that dosing with glucose led to higher blood glucose levels in the Sprague-Dawley strain than in the WKY and SHRSP strains. This observation was surprising as in conscious Sprague-Dawley rats the baseline blood glucose level after an overnight fast are very similar to both the WKY and SHRSP strains. Currently in our lab, different strains of rat are being tested for baseline blood glucose values after overnight fasting and peak glucose after 50% glucose solution injection to select the most clinically relevant and reproducible strain for future investigations (Roy, unpublished 2012).

The studies presented in Chapter 4 are one of the first to investigate the role of acute hyperglycaemia in a model of metabolic syndrome following permanent MCAO. There were a number of models available for studies of this type at the outset, however the fructose fed SHRSP and WKY control strain were preferred. A lot of information on the studies previously conducted in the SHRSP model was available having been used frequently over the past few years (Strahorn *et al* 2005). The results demonstrate that hyperglycaemia did not increase infarct volume in the ffSHRSP compared to the WKY strain and this could be a result of a number of factors. Potentially the role of other co-morbidities could outweigh the additional effect of high blood glucose on ischaemic damage. The SHRSP is a well established model of hypertension which is the main phenotype of this strain. The SHRSP also lack sufficient collateral blood supply which is thought to increase their susceptibility to larger infarcts. Other models exist that do not have such a strong association with one particular risk factor associated with the metabolic syndrome. The Zucker rat is a well established model of insulin

resistance and obesity that develops its phenotype due to a mutation in the leptin receptor, which results in the rats overeating. This strain of rat was considered at the outset of the thesis, however Zucker rats were deemed unsuitable for acute imaging studies due to the physical limitations of the MRI scanner equipment. The cradle and physiological monitoring equipment is unable to accommodate a rat the size of an adult obese Zucker (>500g compared to ~270g for WKY and Sprague Dawley). Numerous high fructose feeding protocols (D'Angelo *et al* 2005; de Moura *et al* 2009; Hwang *et al* 1987; Oron-Herman *et al* 2008), and high fat feeding protocols(Buettner *et al* 2006; Deutsch *et al* 2009) in a variety of rat strains have been proposed and have shown similar phenotypes, encompassing insulin resistance, hyperinsulinaemia and hypertriglyceridaemia after fructose feeding, and additionally obesity in high fat feeding. These models are limited by the period of time it takes to induce an insulin resistant or metabolic syndrome phenotype, with many protocols lasting 10 weeks. However such chronic diet modification in these models may induce more clinically relevant changes in pathophysiology compared to the ffSHRSP which has such a relatively short (2 weeks) period of diet modification. Although one model of metabolic syndrome was selected for the studies presented in this thesis, the pathophysiology between the available models no doubt varies between the Zucker rat and the ffSHRSP rat and this should be borne in mind when considering the conclusions made from studies of only one model.

The studies presented in Chapters 4 and 5 highlight the challenges posed when studying models of focal cerebral ischaemia. Using WKY and SHRSP rats and the distal diathermy method of MCAO, the infarct volume at 24 hours was highly reproducible within each strain. However there was significant variability in final infarct volume when the distal diathermy model was used in Sprague-Dawley rats. Increasing the variability in turn means that larger group sizes are needed to achieve the same experimental power and this is associated with ethical, economic and pragmatic considerations. In addition to variability in infarct size, the extent of the ischaemic damage is also potentially an issue, especially when investigating factors which may increase infarct volume. In Chapter 4 using the SHRSP the lack of hyperglycaemia-mediated ischaemic damage could potentially be due to a ceiling effect such that the maximum extent of damage was reached. Effectively this could mean that any additional effect of

hyperglycaemia on infarct size is being masked as the infarct cannot grow any larger due solely to the physical size of the brain tissue available. The ILF model of MCAO was initially considered for the work in this thesis and in Chapter 3 was shown to cause extensive damage in the SHRSP strain. This model was therefore dropped in favour of the distal diathermy model to try and avoid such a ceiling effect on ischaemic damage. The distal diathermy model of MCAO has its limitations with regards to the mechanism of occlusion. The need for a craniectomy means it is far more surgically invasive and an open skull does not mimic the clinical situation. However the use of the ILF model of MCAO or embolic models suffer themselves from variability caused by incomplete occlusion. Embolic models are useful for investigating synergistic effects of agents with rt-PA. However generally they produce far less reproducible lesions than the ILF or electrocoagulation models of MCAO due to clot instability and location of the occluding embolus (Dinapoli *et al* 2006). Understanding the limitations of each MCAO model available is crucial in the selection of the most appropriate model for a particular experiment.

Rats are the most commonly used species used in experimental stroke due to the similarity of the cerebrovasculature to humans as both possess a circle of Willis. The use of specific inbred strains also improves reproducibility in infarct volume and other outcome measures. Furthermore the cost of purchasing and maintaining rats is relatively low compared to larger mammals and their use in preclinical research is thought to be more socially acceptable (Sicard and Fisher 2009). However, there are a number of limitations associated with using rats to model human stroke. Rodents possess small lissencephalic brains which are not directly comparable with the large gyrencephalic brains of humans. Additionally, rats only have a small proportion of subcortical white matter which makes it difficult to study ischaemic damage of white matter or to model lacunar infarction (Carmichael 2005). Rodents are capable of rapidly recovering from behavioural deficits induced by cerebral ischaemia, unlike in humans, which makes it difficult to investigate a number of neurological deficits (Sicard and Fisher 2009). More suitable species with regards to cerebral macrostructure include dogs, pigs and non-human primates as these possess large gyrencephalic brains with similar proportions of grey and white matter to humans (Howells *et al* 2010). These species difference should be taken into account in model

selection depending on the outcome measures that are to be investigated rather than focusing solely on rodents, especially for more longitudinal behavioural studies.

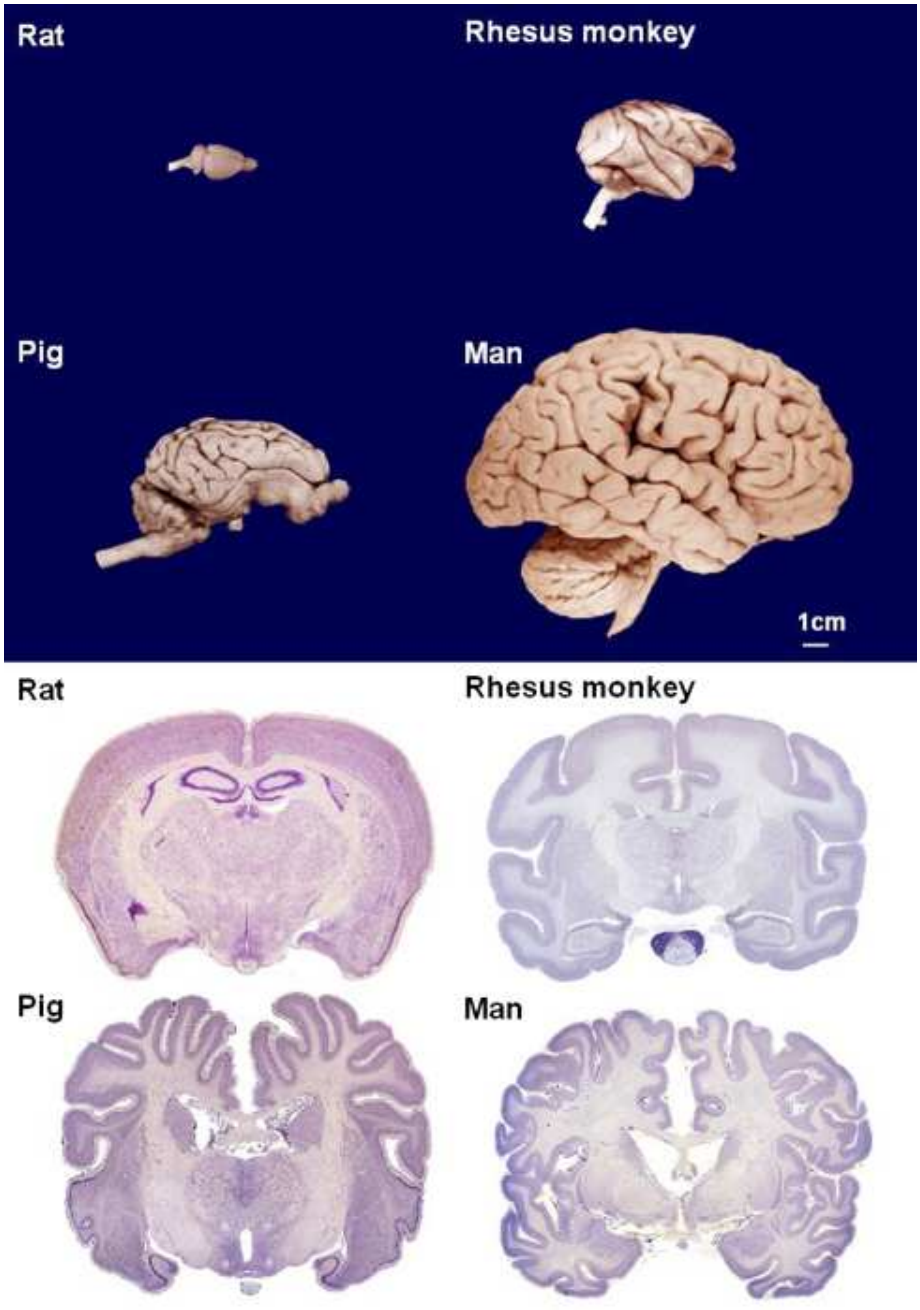

Figure 7.1: Brain size and gyral complexity in mammal species. Reproduced from Howells et al. (2010).

7.2 Study design in preclinical stroke research

Suboptimal study design in preclinical studies may also contribute to the poor translation from bench to bedside in stroke research. Only a minority of preclinical studies reporting neuroprotective effects of pharmacological agents have reported randomised treatment allocation and blinding of investigators (van der Worp *et al* 2005). A previous meta-epidemiological study examined a number of meta-analyses of experimental stroke studies and showed that those studies that failed to blind the investigator to the induction of ischaemia reported greater treatment effects than those that were blinded (Crossley *et al* 2008). Analysis of the publications that supported the efficacy of NXY-059 showed that at least half of the reported 44% improvement in outcome could be attributed to experimental bias (Macleod *et al* 2008). This was primarily as a result of the failure to randomise experimental group allocation and lack of blinding of investigators to the treatment and assessment of outcome.

The methodology employed in this thesis aimed to minimise the experimental bias often present in preclinical stroke studies. The recommendations set out by the Stroke Therapy Academic Industry Roundtable (STAIR 1999) were taken into account for studies presented in Chapter 4 and Chapter 5. In Chapter 5, sample size calculations were employed, based on the differences in infarct volume between normoglycaemic and hyperglycaemic WKY rats to inform the number of animals required to investigate the effects of hyperglycaemia in Sprague-Dawley rats. Animal group allocation in Chapter 4 was done with the flip of a coin for the WKY and SHRSP strains. In Chapter 5 a randomisation plan was used. I was blinded to the animal identity during the analysis in all experimental chapters. However, in Chapter 4 there were limitations that may have led to a degree of bias. Firstly, although the WKY and SHRSP rats look identical in their appearance, the WKY rats are larger than their age-matched SHRSP counterparts. This means it was obvious which strain of rat was being used at any given time. The induction of hyperglycaemia was also not blinded in Chapter 4. This should have been blinded, even though frequent blood sampling for blood glucose analysis during the conduct of individual experiments confirms either glucose or vehicle administration almost immediately. In Chapter 5 I was blinded to the administration of both glucose and EUK-134. Neurological scoring was

blinded to EUK-134 but again the glucose administration was known due to previous blood sampling which may have led to a degree of bias in what is already a subjective assessment. Finally in Chapter 5, the infarct measurements from RARE T_2-weighted images were thought to include error due to the manual delineation of the infarct based on increased signal intensity. The development of a threshold of abnormality for infarct volume calculations from T2 maps will reduce inherent inter- and intra-investigator error when using this MRI technique. However, as discussed in that Chapter this approach is not without limitations.

The measures taken in this thesis to remove experimental bias are extremely important, especially for informing potential clinical trial design. All preclinical studies should be designed based on the guidelines set out for clinical trials and explicitly state the measures put in place to reduce experimental bias in the results. The use of a multitude of models is also important to gain a broader sense of the mechanisms involved which may advise management of PSH patients in the future.

7.3 Hyperglycaemia mediated ischaemic damage: Role of oxidative stress

The brain is particularly vulnerable to oxidative stress due to its high polyunsaturated fatty acid content, low antioxidant capacity, and insufficient neuronal cell repair activity (Traystman *et al* 1991). From the data presented in this thesis the role of oxidative stress in hyperglycaemia-mediated ischaemic damage remains unclear. The data presented in Chapter 4 suggested that under hyperglycaemic conditions WKY at 24 hours post MCAO had significantly larger infarcts than normoglycaemic WKY rats. Similarly hyperglycaemic WKY rats experienced a greater extent of lipid peroxidation compared to their normoglycaemic counterparts following permanent MCAO. This data suggested that hyperglycaemia associated ischaemic damage was mediated via oxidative stress. However this was not replicated in Sprague-Dawley rats (data in Chapter 5) where no difference in the level of the lipid peroxidation marker, MDA, was found in any of the brain regions analysed. This did not reflect the difference in infarct volume where in Sprague-Dawley hyperglycaemia exacerbated infarct

volume at 24 hours post MCAO, similar to the differences seen in WKY rats. There are a number of limitations with the oxidative stress data. One of which is that in Chapter 4 only one marker of lipid peroxidation was used. This was due to a shortage of tissue available for immunohistological staining. In Chapter 5, although only MDA was quantified the level of circulating superoxide ions was measured. The EPR protocol had its limitations. Most notably was the incubation time with the spin probe CPH. Preliminary experiments were undertaken to select the optimum incubation time which was found to be 15 minutes. However the majority of the samples taken at 2 hours were off the scale when measured. This meant that the samples had to be diluted and refrozen before analysis. It is unclear what the effect of diluting the samples and the different dilutions that had to be used had on the results.

The results from this thesis suggest that oxidative stress following permanent MCAO is not a major facilitator of hyperglycaemia-induced ischaemic damage. Furthermore, the proof of concept study described in Chapter 5 did not provide evidence that a drug which reduces oxidative stress could attenuate the detrimental effect of hyperglycaemia on the extent of ischaemic damage. However, the role of oxidative stress in reperfusion injury has been indicated in a number of studies (del Zoppo 2006; Schaller 2005; Traystman *et al* 1991). The ability of ROS to enter reperfused brain regions after recanalisation may provide a larger volume of tissue to cause injury to compared to the moderately hypoperfused, relatively small penumbra present following permanent MCAO.

7.4 Management of post stroke hyperglycaemia

One of the overall aims of this thesis was to inform future clinical trials design to assess whether patients may benefit from blood glucose lowering treatments. Co-ordinated stroke unit care is of proven benefit with studies demonstrating that stroke unit care reduces mortality and dependency (Candelise *et al* 2007; Collaboration 2007; Terent *et al* 2009). Rigorous physiological monitoring could therefore benefit patients in the acute phase of stroke and could potentially extend the time window in which reperfusion therapies could be used.

American and European guidelines regarding the management of PSH advise for active treatment of hyperglycaemia, although the criteria for the use of insulin as a treatment vary. European Stroke Initiative guidelines advise intervention if blood glucose exceeds 10 mmol/L, and the American Stroke Association advise a threshold of 11 mmol/L (Adams *et al* 2007). In a survey across 22 countries, the mean threshold of blood glucose concentration for intervention was found to be 10.6 mmol/L but ranged from 7.4 to 14.0 mmol/L in different countries (Thomassen *et al* 2003). In this thesis the blood glucose level induced for hyperglycaemia in rats was ~12 mmol/L which meets the criteria for both the American and European guidelines. The findings presented in the thesis demonstrate that hyperglycaemia at the time of onset of focal cerebral ischaemia exacerbates both the acute development of the ischaemic lesion and the final volume of infarct determined at 24 hours, at least in animals lacking co-morbidities such as hypertension or insulin resistance. The detrimental effect of hyperglycaemia was found not to be confined to one strain of rat, having been demonstrated in both WKY and Sprague-Dawley rats. Therefore, since infarct volume was not increased in hyperglycaemic ffSHRSP rats compared to normoglycaemic ffSHRSP rats (modelling aspects of the metabolic syndrome) the results are consistent with the suggestion that patients who lack co-morbidities, such as insulin resistance and hyperlipidaemia, may respond more favourably to management of blood glucose. This is in line with clinical data which has shown that PSH led to worse clinical outcomes compared to normoglycaemia in non-diabetic populations (Scott *et al* 1999; Williams *et al* 2002).

The lack of clinical evidence for the benefit of the vigorous management of glucose in acute stroke patients questions the usefulness of interventions using insulin. The GIST-UK trial was the first large clinical trial of blood glucose modulation in acute stroke. Insulin administration, as a GKI infusion, had no significant effect on mortality within 90 days or prevalence of severe disability at 90 days compared to patients who received saline only (Gray *et al* 2007). The heterogeneous population presented by acute stroke patients may mask the beneficial effects of interventions to lower blood glucose. The GIST-UK trial did not discriminate patients based on diabetic or impaired glucose tolerance status unless insulin was already prescribed (Gray *et al* 2007). From the results presented in this thesis, it would suggest that patients who may not have

benefitted from reducing blood glucose (i.e. those with the features modelled by the ffSHRSP rat) were included in the trial.

7.5 Future investigation of post stroke hyperglycaemia

The clinical picture in acute ischaemic stroke is more complex than the processes modelled in this thesis and therefore conclusions about the role of hyperglycaemia and in turn its management in patients must be qualified. The studies conducted had a number of limitations and additional experimental studies will be required to inform more effective management of patients. Insulin treatment was not investigated and so the effectiveness of glucose lowering treatments in models of acute hyperglycaemia, in the presence and absence or insulin resistance and other co-morbidities, remain to be elucidated as does the associated risk of hypoglycaemia with insulin treatment. It will be interesting to see whether hypoglycaemia develops similarly in different rat models. Hyperglycaemia can develop later, often in the first 24-48 hours following stroke, while I only investigated the effects of high blood glucose at the time of stroke. The complications of large infarcts, brain swelling and malignant oedema were similarly not modelled in this thesis and these could be important factors when selecting patients for treatment of hyperglycaemia. Another important consideration is the interaction of hyperglycaemia with reperfusion therapies. Future preclinical evaluation of PSH needs to focus on the use of glucose lowering agents in models of acute hyperglycaemia and also in models of insulin resistance and metabolic syndrome to confirm whether or not insulin can improve outcome measures. The synergistic effects of hyperglycaemia and rt-PA need to be investigated, again in the presence and absence of co-morbidities. Utilising embolic models of MCAO and the transient ILF model of MCAO provide a good basis for investigating these processes. This thesis focussed on clinically relevant levels of hyperglycaemia, informed by the GIST-UK trial rather than the extremely high blood glucose levels achieved in the majority of preclinical work. Including mild, moderate and severe hyperglycaemia may elucidate different mechanisms that could be upregulated at different thresholds of hyperglycaemia.

7.6 Conclusions

The studies presented in this thesis have highlighted that acute hyperglycaemia increases the rate of ischaemic lesion growth and final infarct volume in rats lacking insulin resistance and associated cardiovascular co-morbidities. The mechanism by which hyperglycaemia exacerbates ischaemic damage remains elusive. Oxidative stress may be involved, although from the investigations conducted in this thesis this is not a primary mechanism of hyperglycaemia associated ischaemic damage following permanent MCAO. This thesis has highlighted the need to use clinically relevant models of PSH, with regards to the level of hyperglycaemia and the pathophysiology associated with it, and future investigations in to PSH should continue to utilise such models.

References

Abe T, Sugihara H, Nawa H, Shigemoto R, Mizuno N, Nakanishi S (1992) Molecular characterization of a novel metabotropic glutamate receptor mGluR5 coupled to inositol phosphate/Ca2+ signal transduction. *J Biol Chem* 267:13361-8.

Adams HP, Jr., Brott TG, Furlan AJ, Gomez CR, Grotta J, Helgason CM, Kwiatkowski T, Lyden PD, Marler JR, Torner J, Feinberg W, Mayberg M, Thies W (1996) Guidelines for thrombolytic therapy for acute stroke: a supplement to the guidelines for the management of patients with acute ischemic stroke. A statement for healthcare professionals from a Special Writing Group of the Stroke Council, American Heart Association. *Circulation* 94:1167-74.

Adams HP, Jr., del Zoppo G, Alberts MJ, Bhatt DL, Brass L, Furlan A, Grubb RL, Higashida RT, Jauch EC, Kidwell C, Lyden PD, Morgenstern LB, Qureshi AI, Rosenwasser RH, Scott PA, Wijdicks EF (2007) Guidelines for the early management of adults with ischemic stroke: a guideline from the American Heart Association/American Stroke Association Stroke Council, Clinical Cardiology Council, Cardiovascular Radiology and Intervention Council, and the Atherosclerotic Peripheral Vascular Disease and Quality of Care Outcomes in Research Interdisciplinary Working Groups: The American Academy of Neurology affirms the value of this guideline as an educational tool for neurologists. *Circulation* 115:e478-534.

Albers GW, Thijs VN, Wechsler L, Kemp S, Schlaug G, Skalabrin E, Bammer R, Kakuda W, Lansberg MG, Shuaib A, Coplin W, Hamilton S, Moseley M, Marks MP (2006) Magnetic resonance imaging profiles predict clinical response to early reperfusion: the diffusion and perfusion imaging evaluation for understanding stroke evolution (DEFUSE) study. *Ann Neurol* 60:508-17.

Anderson RE, Tan WK, Martin HS, Meyer FB (1999) Effects of glucose and PaO2 modulation on cortical intracellular acidosis, NADH redox state, and infarction in the ischemic penumbra. *Stroke* 30:160-70.

Aramori I, Nakanishi S (1992) Signal transduction and pharmacological characteristics of a metabotropic glutamate receptor, mGluR1, in transfected CHO cells. *Neuron* 8:757-65.

Asahi M, Wang X, Mori T, Sumii T, Jung JC, Moskowitz MA, Fini ME, Lo EH (2001) Effects of matrix metalloproteinase-9 gene knock-out on the proteolysis of blood-brain barrier and white matter components after cerebral ischemia. *J Neurosci* 21:7724-32.

Astrup J, Symon L, Branston NM, Lassen NA (1977) Cortical evoked potential and extracellular K+ and H+ at critical levels of brain ischemia. *Stroke* 8:51-7.

Ay H, Arsava EM, Vangel M, Oner B, Zhu M, Wu O, Singhal A, Koroshetz WJ, Sorensen AG (2008) Interexaminer difference in infarct volume measurements on MRI: a source of variance in stroke research. *Stroke* 39:1171-6.

Bahramikia S, Yazdanparast R (2011) EUK-8 and EUK-134 reduce serum glucose and lipids and ameliorate streptozotocin-induced oxidative damage in the pancreas, liver, kidneys, and brain tissues of diabetic rats. *Medicinal Chemistry Research*:1-9.

Baird AE, Warach S (1998) Magnetic resonance imaging of acute stroke. *J Cereb Blood Flow Metab* 18:583-609.

Baird TA, Parsons MW, Phanh T, Butcher KS, Desmond PM, Tress BM, Colman PG, Chambers BR, Davis SM (2003) Persistent poststroke hyperglycemia is

independently associated with infarct expansion and worse clinical outcome. *Stroke* 34:2208-14.

Baker K, Marcus CB, Huffman K, Kruk H, Malfroy B, Doctrow SR (1998) Synthetic combined superoxide dismutase/catalase mimetics are protective as a delayed treatment in a rat stroke model: a key role for reactive oxygen species in ischemic brain injury. *J Pharmacol Exp Ther* 284:215-21.

Bardutzky J, Shen Q, Henninger N, Schwab S, Duong TQ, Fisher M (2007) Characterizing tissue fate after transient cerebral ischemia of varying duration using quantitative diffusion and perfusion imaging. *Stroke* 38:1336-44.

Baron JC (1999) Mapping the ischaemic penumbra with PET: implications for acute stroke treatment. *Cerebrovasc Dis* 9:193-201.

Barone FC, Arvin B, White RF, Miller A, Webb CL, Willette RN, Lysko PG, Feuerstein GZ (1997) Tumor necrosis factor-alpha. A mediator of focal ischemic brain injury. *Stroke* 28:1233-44.

Bederson JB, Pitts LH, Germano SM, Nishimura MC, Davis RL, Bartkowski HM (1986a) Evaluation of 2,3,5-triphenyltetrazolium chloride as a stain for detection and quantification of experimental cerebral infarction in rats. *Stroke* 17:1304-8.

Bederson JB, Pitts LH, Tsuji M, Nishimura MC, Davis RL, Bartkowski H (1986b) Rat middle cerebral artery occlusion: evaluation of the model and development of a neurologic examination. *Stroke* 17:472-6.

Berger L, Hakim AM (1989) Nimodipine prevents hyperglycemia-induced cerebral acidosis in middle cerebral artery occluded rats. *J Cereb Blood Flow Metab* 9:58-64.

Berthiaume N, Zinker BA (2002) Metabolic responses in a model of insulin resistance: comparison between oral glucose and meal tolerance tests. *Metabolism* 51:595-8.

Bomont L, MacKenzie ET (1995) Neuroprotection after focal cerebral ischaemia in hyperglycaemic and diabetic rats. *Neurosci Lett* 197:53-6.

Boulange A, Planche E, de Gasquet P (1981) Onset and development of hypertriglyceridemia in the Zucker rat (fa/fa). *Metabolism* 30:1045-52.

Branston NM, Symon L, Crockard HA, Pasztor E (1974) Relationship between the cortical evoked potential and local cortical blood flow following acute middle cerebral artery occlusion in the baboon. *Exp Neurol* 45:195-208.

Branston NM, Strong AJ, Symon L (1977) Extracellular potassium activity, evoked potential and tissue blood flow. Relationships during progressive ischaemia in baboon cerebral cortex. *J Neurol Sci* 32:305-21.

Brant-Zawadzki M, Atkinson D, Detrick M, Bradley WG, Scidmore G (1996) Fluid-attenuated inversion recovery (FLAIR) for assessment of cerebral infarction. Initial clinical experience in 50 patients. *Stroke* 27:1187-91.

Brint S, Jacewicz M, Kiessling M, Tanabe J, Pulsinelli W (1988) Focal brain ischemia in the rat: methods for reproducible neocortical infarction using tandem occlusion of the distal middle cerebral and ipsilateral common carotid arteries. *J Cereb Blood Flow Metab* 8:474-85.

Brouns R, De Deyn PP (2009) The complexity of neurobiological processes in acute ischemic stroke. *Clin Neurol Neurosurg* 111:483-95.

Brownlee M (2001) Biochemistry and molecular cell biology of diabetic complications. *Nature* 414:813-20.

Brownlee M (2005) The pathobiology of diabetic complications: a unifying mechanism. *Diabetes* 54:1615-25.

Bruce AJ, Boling W, Kindy MS, Peschon J, Kraemer PJ, Carpenter MK, Holtsberg FW, Mattson MP (1996) Altered neuronal and microglial responses to excitotoxic and ischemic brain injury in mice lacking TNF receptors. *Nat Med* 2:788-94.

Bruno A, Levine SR, Frankel MR, Brott TG, Lin Y, Tilley BC, Lyden PD, Broderick JP, Kwiatkowski TG, Fineberg SE (2002) Admission glucose level and clinical outcomes in the NINDS rt-PA Stroke Trial. *Neurology* 59:669-74.

Buettner R, Parhofer KG, Woenckhaus M, Wrede CE, Kunz-Schughart LA, Scholmerich J, Bollheimer LC (2006) Defining high-fat-diet rat models: metabolic and molecular effects of different fat types. *J Mol Endocrinol* 36:485-501.

Butcher KS, Parsons M, MacGregor L, Barber PA, Chalk J, Bladin C, Levi C, Kimber T, Schultz D, Fink J, Tress B, Donnan G, Davis S (2005) Refining the perfusion-diffusion mismatch hypothesis. *Stroke* 36:1153-9.

Campbell BC, Purushotham A, Christensen S, Desmond PM, Nagakane Y, Parsons MW, Lansberg MG, Mlynash M, Straka M, De Silva DA, Olivot JM, Bammer R, Albers GW, Donnan GA, Davis SM (2012) The infarct core is well represented by the acute diffusion lesion: sustained reversal is infrequent. *J Cereb Blood Flow Metab* 32:50-6.

Candelise L, Gattinoni M, Bersano A, Micieli G, Sterzi R, Morabito A (2007) Stroke-unit care for acute stroke patients: an observational follow-up study. *Lancet* 369:299-305.

Capes SE, Hunt D, Malmberg K, Pathak P, Gerstein HC (2001) Stress hyperglycemia and prognosis of stroke in nondiabetic and diabetic patients: a systematic overview. *Stroke* 32:2426-32.

Carmichael ST (2005) Rodent models of focal stroke: size, mechanism, and purpose. *NeuroRx* 2:396-409.

Carswell HV, Anderson NH, Clark JS, Graham D, Jeffs B, Dominiczak AF, Macrae IM (1999) Genetic and gender influences on sensitivity to focal cerebral ischemia in the stroke-prone spontaneously hypertensive rat. *Hypertension* 33:681-5.

Cenci MA, Whishaw IQ, Schallert T (2002) Animal models of neurological deficits: how relevant is the rat? *Nat Rev Neurosci* 3:574-9.

Chalela JA, Alsop DC, Gonzalez-Atavales JB, Maldjian JA, Kasner SE, Detre JA (2000) Magnetic resonance perfusion imaging in acute ischemic stroke using continuous arterial spin labeling. *Stroke* 31:680-7.

Chan PH, Kawase M, Murakami K, Chen SF, Li Y, Calagui B, Reola L, Carlson E, Epstein CJ (1998) Overexpression of SOD1 in transgenic rats protects vulnerable neurons against ischemic damage after global cerebral ischemia and reperfusion. *J Neurosci* 18:8292-9.

Chen RL, Balami JS, Esiri MM, Chen LK, Buchan AM (2010) Ischemic stroke in the elderly: an overview of evidence. *Nat Rev Neurol* 6:256-65.

Chen ST, Hsu CY, Hogan EL, Maricq H, Balentine JD (1986) A model of focal ischemic stroke in the rat: reproducible extensive cortical infarction. *Stroke* 17:738-43.

Chen ZL, Strickland S (1997) Neuronal death in the hippocampus is promoted by plasmin-catalyzed degradation of laminin. *Cell* 91:917-25.

Chew W, Kucharczyk J, Moseley M, Derugin N, Norman D (1991) Hyperglycemia augments ischemic brain injury: in vivo MR imaging/spectroscopic study with nicardipine in cats with occluded middle cerebral arteries. *AJNR Am J Neuroradiol* 12:603-9.

Christensen H (2005) Insular lesions and hyperglycemia in acute stroke revisited. *Stroke* 36:229-30; author reply -30.

Cocho D, Belvis R, Marti-Fabregas J, Molina-Porcel L, Diaz-Manera J, Aleu A, Pagonabarraga J, Garcia-Bargo D, Mauri A, Marti-Vilalta JL (2005) Reasons for exclusion from thrombolytic therapy following acute ischemic stroke. *Neurology* 64:719-20.

Collaboration SUT (2007) Organised inpatient (stroke unit) care for stroke. *Cochrane Database Syst Rev*:CD000197.

Connolly ES, Jr., Winfree CJ, Springer TA, Naka Y, Liao H, Yan SD, Stern DM, Solomon RA, Gutierrez-Ramos JC, Pinsky DJ (1996) Cerebral protection in homozygous null ICAM-1 mice after middle cerebral artery occlusion. Role of neutrophil adhesion in the pathogenesis of stroke. *J Clin Invest* 97:209-16.

Coyle P, Jokelainen PT (1983) Differential outcome to middle cerebral artery occlusion in spontaneously hypertensive stroke-prone rats (SHRSP) and Wistar Kyoto (WKY) rats. *Stroke* 14:605-11.

Coyle P (1986) Different susceptibilities to cerebral infarction in spontaneously hypertensive (SHR) and normotensive Sprague-Dawley rats. *Stroke* 17:520-5.

Coyle P, Heistad DD (1987) Blood flow through cerebral collateral vessels one month after middle cerebral artery occlusion. *Stroke* 18:407-11.

Crossley NA, Sena E, Goehler J, Horn J, van der Worp B, Bath PM, Macleod M, Dirnagl U (2008) Empirical evidence of bias in the design of experimental stroke studies: a metaepidemiologic approach. *Stroke* 39:929-34.

D'Angelo G, Elmarakby AA, Pollock DM, Stepp DW (2005) Fructose feeding increases insulin resistance but not blood pressure in Sprague-Dawley rats. *Hypertension* 46:806-11.

Dandona P, James IM, Newbury PA, Woollard ML, Beckett AG (1978) Cerebral blood flow in diabetes mellitus: evidence of abnormal cerebrovascular reactivity. *Br Med J* 2:325-6.

Davis SM, Donnan GA, Parsons MW, Levi C, Butcher KS, Peeters A, Barber PA, Bladin C, De Silva DA, Byrnes G, Chalk JB, Fink JN, Kimber TE, Schultz D, Hand PJ, Frayne J, Hankey G, Muir K, Gerraty R, Tress BM, Desmond PM (2008) Effects of alteplase beyond 3 h after stroke in the Echoplanar Imaging Thrombolytic Evaluation Trial (EPITHET): a placebo-controlled randomised trial. *Lancet Neurol* 7:299-309.

de Courten-Myers G, Myers RE, Schoolfield L (1988) Hyperglycemia enlarges infarct size in cerebrovascular occlusion in cats. *Stroke* 19:623-30.

de Courten-Myers GM, Kleinholz M, Wagner KR, Myers RE (1989) Fatal strokes in hyperglycemic cats. *Stroke* 20:1707-15.

de Courten-Myers GM, Kleinholz M, Wagner KR, Myers RE (1994) Normoglycemia (not hypoglycemia) optimizes outcome from middle cerebral artery occlusion. *J Cereb Blood Flow Metab* 14:227-36.

de Graaf RA, Brown PB, McIntyre S, Nixon TW, Behar KL, Rothman DL (2006) High magnetic field water and metabolite proton T1 and T2 relaxation in rat brain in vivo. *Magn Reson Med* 56:386-94.

de Moura RF, Ribeiro C, de Oliveira JA, Stevanato E, de Mello MA (2009) Metabolic syndrome signs in Wistar rats submitted to different high-fructose ingestion protocols. *Br J Nutr* 101:1178-84.

del Zoppo GJ, Schmid-Schonbein GW, Mori E, Copeland BR, Chang CM (1991) Polymorphonuclear leukocytes occlude capillaries following middle cerebral artery occlusion and reperfusion in baboons. *Stroke* 22:1276-83.

del Zoppo GJ (2006) Stroke and neurovascular protection. *N Engl J Med* 354:553-5.

Desborough JP, Jones PM, Persaud SJ, Landon MJ, Howell SL (1993) Isoflurane inhibits insulin secretion from isolated rat pancreatic islets of Langerhans. *Br J Anaesth* 71:873-6.

Deutsch C, Portik-Dobos V, Smith AD, Ergul A, Dorrance AM (2009) Diet-induced obesity causes cerebral vessel remodeling and increases the damage caused by ischemic stroke. *Microvasc Res* 78:100-6.

Didion SP, Faraci FM (2002) Effects of NADH and NADPH on superoxide levels and cerebral vascular tone. *Am J Physiol Heart Circ Physiol* 282:H688-95.

Dinapoli VA, Rosen CL, Nagamine T, Crocco T (2006) Selective MCA occlusion: a precise embolic stroke model. *J Neurosci Methods* 154:233-8.

Dirnagl U, Iadecola C, Moskowitz MA (1999) Pathobiology of ischaemic stroke: an integrated view. *Trends Neurosci* 22:391-7.

Donnan GA, Fisher M, Macleod M, Davis SM (2008) Stroke. *Lancet* 371:1612-23.

Dreier JP, Major S, Manning A, Woitzik J, Drenckhahn C, Steinbrink J, Tolias C, Oliveira-Ferreira AI, Fabricius M, Hartings JA, Vajkoczy P, Lauritzen M, Dirnagl U, Bohner G, Strong AJ (2009) Cortical spreading ischaemia is a novel process involved in ischaemic damage in patients with aneurysmal subarachnoid haemorrhage. *Brain* 132:1866-81.

Duckrow RB, Beard DC, Brennan RW (1985) Regional cerebral blood flow decreases during hyperglycemia. *Ann Neurol* 17:267-72.

Duckrow RB, Beard DC, Brennan RW (1987) Regional cerebral blood flow decreases during chronic and acute hyperglycemia. *Stroke* 18:52-8.

Dugan LL, Choi DW (1994) Excitotoxicity, free radicals, and cell membrane changes. *Ann Neurol* 35 Suppl:S17-21.

Duverger D, MacKenzie ET (1988) The quantification of cerebral infarction following focal ischemia in the rat: influence of strain, arterial pressure, blood glucose concentration, and age. *J Cereb Blood Flow Metab* 8:449-61.

Ebinger M, De Silva DA, Christensen S, Parsons MW, Markus R, Donnan GA, Davis SM (2009) Imaging the penumbra - strategies to detect tissue at risk after ischemic stroke. *J Clin Neurosci* 16:178-87.

Fabricius M, Fuhr S, Bhatia R, Boutelle M, Hashemi P, Strong AJ, Lauritzen M (2006) Cortical spreading depression and peri-infarct depolarization in acutely injured human cerebral cortex. *Brain* 129:778-90.

Foley LM, Hitchens TK, Barbe B, Zhang F, Ho C, Rao GR, Nemoto EM (2011) Quantitative Temporal Profiles of Penumbra and Infarction During Permanent Middle Cerebral Artery Occlusion in Rats. *Transl Stroke Res* 1:220-9.

Forster C, Clark HB, Ross ME, Iadecola C (1999) Inducible nitric oxide synthase expression in human cerebral infarcts. *Acta Neuropathol* 97:215-20.

Frank GD, Eguchi S, Motley ED (2005) The role of reactive oxygen species in insulin signaling in the vasculature. *Antioxid Redox Signal* 7:1053-61.

Fujimura M, Morita-Fujimura Y, Kawase M, Copin JC, Calagui B, Epstein CJ, Chan PH (1999) Manganese superoxide dismutase mediates the early release of mitochondrial cytochrome C and subsequent DNA fragmentation after permanent focal cerebral ischemia in mice. *J Neurosci* 19:3414-22.

Furukawa K, Fu W, Li Y, Witke W, Kwiatkowski DJ, Mattson MP (1997) The actin-severing protein gelsolin modulates calcium channel and NMDA receptor activities and vulnerability to excitotoxicity in hippocampal neurons. *J Neurosci* 17:8178-86.

Garcia JH, Wagner S, Liu KF, Hu XJ (1995) Neurological deficit and extent of neuronal necrosis attributable to middle cerebral artery occlusion in rats. Statistical validation. *Stroke* 26:627-34; discussion 35.

Gerriets T, Stolz E, Walberer M, Muller C, Kluge A, Bachmann A, Fisher M, Kaps M, Bachmann G (2004) Noninvasive quantification of brain edema and the space-occupying effect in rat stroke models using magnetic resonance imaging. *Stroke* 35:566-71.

Ginsberg MD, Prado R, Dietrich WD, Busto R, Watson BD (1987) Hyperglycemia reduces the extent of cerebral infarction in rats. *Stroke* 18:570-4.

Gisselsson L, Smith ML, Siesjo BK (1999) Hyperglycemia and focal brain ischemia. *J Cereb Blood Flow Metab* 19:288-97.

Giulian D, Li J, Leara B, Keenen C (1994) Phagocytic microglia release cytokines and cytotoxins that regulate the survival of astrocytes and neurons in culture. *Neurochem Int* 25:227-33.

Gray CS, Hildreth AJ, Alberti GK, O'Connell JE (2004a) Poststroke hyperglycemia: natural history and immediate management. *Stroke* 35:122-6.

Gray CS, Scott JF, French JM, Alberti KG, O'Connell JE (2004b) Prevalence and prediction of unrecognised diabetes mellitus and impaired glucose tolerance following acute stroke. *Age Ageing* 33:71-7.

Gray CS, Hildreth AJ, Sandercock PA, O'Connell JE, Johnston DE, Cartlidge NE, Bamford JM, James OF, Alberti KG (2007) Glucose-potassium-insulin infusions in the management of post-stroke hyperglycaemia: the UK Glucose Insulin in Stroke Trial (GIST-UK). *Lancet Neurol* 6:397-406.

Green DR, Reed JC (1998) Mitochondria and apoptosis. *Science* 281:1309-12.

Griesdale DE, de Souza RJ, van Dam RM, Heyland DK, Cook DJ, Malhotra A, Dhaliwal R, Henderson WR, Chittock DR, Finfer S, Talmor D (2009) Intensive insulin therapy and mortality among critically ill patients: a meta-analysis including NICE-SUGAR study data. *CMAJ* 180:821-7.

Guadagno JV, Warburton EA, Aigbirhio FI, Smielewski P, Fryer TD, Harding S, Price CJ, Gillard JH, Carpenter TA, Baron JC (2004) Does the acute diffusion-

weighted imaging lesion represent penumbra as well as core? A combined quantitative PET/MRI voxel-based study. *J Cereb Blood Flow Metab* 24:1249-54.

Hacke W, Kaste M, Fieschi C, Toni D, Lesaffre E, von Kummer R, Boysen G, Bluhmki E, Hoxter G, Mahagne MH, et al. (1995) Intravenous thrombolysis with recombinant tissue plasminogen activator for acute hemispheric stroke. The European Cooperative Acute Stroke Study (ECASS). *JAMA* 274:1017-25.

Hacke W, Kaste M, Fieschi C, von Kummer R, Davalos A, Meier D, Larrue V, Bluhmki E, Davis S, Donnan G, Schneider D, Diez-Tejedor E, Trouillas P (1998) Randomised double-blind placebo-controlled trial of thrombolytic therapy with intravenous alteplase in acute ischaemic stroke (ECASS II). Second European-Australasian Acute Stroke Study Investigators. *Lancet* 352:1245-51.

Hacke W, Albers G, Al-Rawi Y, Bogousslavsky J, Davalos A, Eliasziw M, Fischer M, Furlan A, Kaste M, Lees KR, Soehngen M, Warach S (2005) The Desmoteplase in Acute Ischemic Stroke Trial (DIAS): a phase II MRI-based 9-hour window acute stroke thrombolysis trial with intravenous desmoteplase. *Stroke* 36:66-73.

Hacke W, Kaste M, Bluhmki E, Brozman M, Davalos A, Guidetti D, Larrue V, Lees KR, Medeghri Z, Machnig T, Schneider D, von Kummer R, Wahlgren N, Toni D (2008) Thrombolysis with alteplase 3 to 4.5 hours after acute ischemic stroke. *N Engl J Med* 359:1317-29.

Hajnal JV, Bryant DJ, Kasuboski L, Pattany PM, De Coene B, Lewis PD, Pennock JM, Oatridge A, Young IR, Bydder GM (1992a) Use of fluid attenuated inversion recovery (FLAIR) pulse sequences in MRI of the brain. *J Comput Assist Tomogr* 16:841-4.

Hajnal JV, De Coene B, Lewis PD, Baudouin CJ, Cowan FM, Pennock JM, Young IR, Bydder GM (1992b) High signal regions in normal white matter shown by

heavily T2-weighted CSF nulled IR sequences. *J Comput Assist Tomogr* 16:506-13.

Hamilton MG, Tranmer BI, Auer RN (1995) Insulin reduction of cerebral infarction due to transient focal ischemia. *J Neurosurg* 82:262-8.

Hasegawa Y, Fisher M, Latour LL, Dardzinski BJ, Sotak CH (1994) MRI diffusion mapping of reversible and irreversible ischemic injury in focal brain ischemia. *Neurology* 44:1484-90.

Heiss WD, Grond M, Thiel A, von Stockhausen HM, Rudolf J, Ghaemi M, Lottgen J, Stenzel C, Pawlik G (1998) Tissue at risk of infarction rescued by early reperfusion: a positron emission tomography study in systemic recombinant tissue plasminogen activator thrombolysis of acute stroke. *J Cereb Blood Flow Metab* 18:1298-307.

Heiss WD (2003) Best measure of ischemic penumbra: positron emission tomography. *Stroke* 34:2534-5.

Hjort N, Wu O, Ashkanian M, Solling C, Mouridsen K, Christensen S, Gyldensted C, Andersen G, Ostergaard L (2008) MRI detection of early blood-brain barrier disruption: parenchymal enhancement predicts focal hemorrhagic transformation after thrombolysis. *Stroke* 39:1025-8.

Hossmann KA (1996) Periinfarct depolarizations. *Cerebrovasc Brain Metab Rev* 8:195-208.

Howells DW, Porritt MJ, Rewell SS, O'Collins V, Sena ES, van der Worp HB, Traystman RJ, Macleod MR (2010) Different strokes for different folks: the rich diversity of animal models of focal cerebral ischemia. *J Cereb Blood Flow Metab* 30:1412-31.

Huang NC, Wei J, Quast MJ (1996) A comparison of the early development of ischemic brain damage in normoglycemic and hyperglycemic rats using magnetic resonance imaging. *Exp Brain Res* 109:33-42.

Huang NC, Yongbi MN, Helpern JA (1998) The influence of preischemic hyperglycemia on acute changes in brain water ADCw following focal ischemia in rats. *Brain Res* 788:137-43.

Hudgins WR, Garcia JH (1970) Transorbital approach to the middle cerebral artery of the squirrel monkey: a technique for experimental cerebral infarction applicable to ultrastructural studies. *Stroke* 1:107-11.

Hulman S, Falkner B, Freyvogel N (1993) Insulin resistance in the conscious spontaneously hypertensive rat: euglycemic hyperinsulinemic clamp study. *Metabolism* 42:14-8.

Hunter AJ, Green AR, Cross AJ (1995) Animal models of acute ischaemic stroke: can they predict clinically successful neuroprotective drugs? *Trends Pharmacol Sci* 16:123-8.

Hwang IS, Ho H, Hoffman BB, Reaven GM (1987) Fructose-induced insulin resistance and hypertension in rats. *Hypertension* 10:512-6.

Ibrahim J, McGee A, Graham D, McGrath JC, Dominiczak AF (2006) Sex-specific differences in cerebral arterial myogenic tone in hypertensive and normotensive rats. *Am J Physiol Heart Circ Physiol* 290:H1081-9.

Ionescu E, Sauter JF, Jeanrenaud B (1985) Abnormal oral glucose tolerance in genetically obese (fa/fa) rats. *Am J Physiol* 248:E500-6.

Israeli D, Tanne D, Daniels D, Last D, Shneor R, Guez D, Landau E, Roth Y, Ocherashvilli A, Bakon M, Hoffman C, Weinberg A, Volk T, Mardor Y (2011) The application of MRI for depiction of subtle blood brain barrier disruption in stroke. *Int J Biol Sci* 7:1-8.

Jahnke K, Muldoon LL, Varallyay CG, Lewin SJ, Brown RD, Kraemer DF, Soussain C, Neuwelt EA (2009) Efficacy and MRI of rituximab and methotrexate treatment in a nude rat model of CNS lymphoma. *Neuro Oncol* 11:503-13.

Jian Liu K, Rosenberg GA (2005) Matrix metalloproteinases and free radicals in cerebral ischemia. *Free Radic Biol Med* 39:71-80.

Jiang Q, Chopp M, Zhang ZG, Knight RA, Jacobs M, Windham JP, Peck D, Ewing JR, Welch KM (1997) The temporal evolution of MRI tissue signatures after transient middle cerebral artery occlusion in rat. *J Neurol Sci* 145:15-23.

Junod A, Lambert AE, Stauffacher W, Renold AE (1969) Diabetogenic action of streptozotocin: relationship of dose to metabolic response. *J Clin Invest* 48:2129-39.

Kagansky N, Levy S, Knobler H (2001) The role of hyperglycemia in acute stroke. *Arch Neurol* 58:1209-12.

Kamada H, Yu F, Nito C, Chan PH (2007) Influence of hyperglycemia on oxidative stress and matrix metalloproteinase-9 activation after focal cerebral ischemia/reperfusion in rats: relation to blood-brain barrier dysfunction. *Stroke* 38:1044-9.

Karunanayake EH, Hearse DJ, Mellows G (1974) The synthesis of [14C] streptozotocin and its distribution and excretion in the rat. *Biochem J* 142:673-83.

Kawai N, Keep RF, Betz AL, Nagao S (1998) Hyperglycemia induces progressive changes in the cerebral microvasculature and blood-brain barrier transport during focal cerebral ischemia. *Acta Neurochir Suppl* 71:219-21.

Kazemi M, Silva MD, Li F, Fisher M, Sotak CH (2004) Investigation of techniques to quantify in vivo lesion volume based on comparison of water apparent diffusion coefficient (ADC) maps with histology in focal cerebral ischemia of rats. *Magn Reson Imaging* 22:653-9.

Kidwell CS, Saver JL, Mattiello J, Starkman S, Vinuela F, Duckwiler G, Gobin YP, Jahan R, Vespa P, Kalafut M, Alger JR (2000) Thrombolytic reversal of acute human cerebral ischemic injury shown by diffusion/perfusion magnetic resonance imaging. *Ann Neurol* 47:462-9.

Kim JH, Snider T, Abel M, Zemel MB (1994) Hypertension in young, healthy Zucker obese rats is not responsive to reduced salt intake. *J Nutr* 124:713-6.

Kittaka M, Wang L, Sun N, Schreiber SS, Seeds NW, Fisher M, Zlokovic BV (1996) Brain capillary tissue plasminogen activator in a diabetes stroke model. *Stroke* 27:712-9.

Kofke WA, Hawkins RA, Davis DW, Biebuyck JF (1987) Comparison of the effects of volatile anesthetics on brain glucose metabolism in rats. *Anesthesiology* 66:810-3.

Koizumi J, Yoshida Y, Nakazawa T, Ooneda G (1986) Experimental studies of ischemic brain edema. 1. A new experimental model of cerebral embolism in rats in which recirculation can be introduced in the ischemic area. *Jpn J Stroke* 8:1-8.

Lattermann R, Schricker T, Wachter U, Georgieff M, Goertz A (2001) Understanding the mechanisms by which isoflurane modifies the hyperglycemic response to surgery. *Anesthesia and Analgesia* 93:121-7.

Leist M, Nicotera P (1998) Apoptosis, excitotoxicity, and neuropathology. *Exp Cell Res* 239:183-201.

Li PA, Gisselsson L, Keuker J, Vogel J, Smith ML, Kuschinsky W, Siesjo BK (1998) Hyperglycemia-exaggerated ischemic brain damage following 30 min of middle cerebral artery occlusion is not due to capillary obstruction. *Brain Res* 804:36-44.

Li PA, Shuaib A, Miyashita H, He QP, Siesjo BK, Warner DS (2000) Hyperglycemia enhances extracellular glutamate accumulation in rats subjected to forebrain ischemia. *Stroke* 31:183-92.

Like AA, Rossini AA (1976) Streptozotocin-induced pancreatic insulitis: new model of diabetes mellitus. *Science* 193:415-7.

Lin B, Ginsberg MD, Busto R (1998) Hyperglycemic exacerbation of neuronal damage following forebrain ischemia: microglial, astrocytic and endothelial alterations. *Acta Neuropathol* 96:610-20.

Lindsay S, Liu TH, Xu JA, Marshall PA, Thompson JK, Parks DA, Freeman BA, Hsu CY, Beckman JS (1991) Role of xanthine dehydrogenase and oxidase in focal cerebral ischemic injury to rat. *Am J Physiol* 261:H2051-7.

Lindsberg PJ, Roine RO (2004) Hyperglycemia in acute stroke. *Stroke* 35:363-4.

Lipton P (1999) Ischemic cell death in brain neurons. *Physiol Rev* 79:1431-568.

Liu L, Wang Z, Wang X, Song L, Chen H, Bemeur C, Ste-Marie L, Montgomery J (2007) Comparison of two rat models of cerebral ischemia under hyperglycemic conditions. *Microsurgery* 27:258-62.

Longa EZ, Weinstein PR, Carlson S, Cummins R (1989) Reversible middle cerebral artery occlusion without craniectomy in rats. *Stroke* 20:84-91.

Loubinoux I, Volk A, Borredon J, Guirimand S, Tiffon B, Seylaz J, Meric P (1997) Spreading of vasogenic edema and cytotoxic edema assessed by quantitative diffusion and T2 magnetic resonance imaging. *Stroke* 28:419-26; discussion 26-7.

MacDougall NJ, Muir KW (2010) Hyperglycaemia and infarct size in animal models of middle cerebral artery occlusion: systematic review and meta-analysis. *J Cereb Blood Flow Metab* 31:807-18.

Mackay J, Mensah GA. (2004). *The atlas of heart disease and stroke*: World Health Organization, 112pp.

Macleod MR, van der Worp HB, Sena ES, Howells DW, Dirnagl U, Donnan GA (2008) Evidence for the efficacy of NXY-059 in experimental focal cerebral ischaemia is confounded by study quality. *Stroke* 39:2824-9.

Macleod MR, Fisher M, O'Collins V, Sena ES, Dirnagl U, Bath PM, Buchan A, van der Worp HB, Traystman R, Minematsu K, Donnan GA, Howells DW (2009) Good laboratory practice: preventing introduction of bias at the bench. *Stroke* 40:e50-2.

Malmberg K, Ryden L, Efendic S, Herlitz J, Nicol P, Waldenstrom A, Wedel H, Welin L (1995) Randomized trial of insulin-glucose infusion followed by subcutaneous insulin treatment in diabetic patients with acute myocardial

infarction (DIGAMI study): effects on mortality at 1 year. *J Am Coll Cardiol* 26:57-65.

Malmberg K, Ryden L, Wedel H, Birkeland K, Bootsma A, Dickstein K, Efendic S, Fisher M, Hamsten A, Herlitz J, Hildebrandt P, MacLeod K, Laakso M, Torp-Pedersen C, Waldenstrom A (2005) Intense metabolic control by means of insulin in patients with diabetes mellitus and acute myocardial infarction (DIGAMI 2): effects on mortality and morbidity. *Eur Heart J* 26:650-61.

Management ESIRfS (2008) Guidelines for management of ischaemic stroke and transient ischaemic attack 2008. *Cerebrovasc Dis* 25:457-507.

Marfella R, Quagliaro L, Nappo F, Ceriello A, Giugliano D (2001) Acute hyperglycemia induces an oxidative stress in healthy subjects. *J Clin Invest* 108:635-6.

Marks L, Carswell HV, Peters EE, Graham DI, Patterson J, Dominiczak AF, Macrae IM (2001) Characterization of the microglial response to cerebral ischemia in the stroke-prone spontaneously hypertensive rat. *Hypertension* 38:116-22.

Martin A, Rojas S, Chamorro A, Falcon C, Bargallo N, Planas AM (2006) Why does acute hyperglycemia worsen the outcome of transient focal cerebral ischemia? Role of corticosteroids, inflammation, and protein O-glycosylation. *Stroke* 37:1288-95.

Martin RL, Lloyd HG, Cowan AI (1994) The early events of oxygen and glucose deprivation: setting the scene for neuronal death? *Trends Neurosci* 17:251-7.

McAuley MA (1995) Rodent models of focal ischemia. *Cerebrovasc Brain Metab Rev* 7:153-80.

McCabe C, Gallagher L, Gsell W, Graham D, Dominiczak AF, Macrae IM (2009) Differences in the evolution of the ischemic penumbra in stroke-prone spontaneously hypertensive and Wistar-Kyoto rats. *Stroke* 40:3864-8.

McCormick M, Muir KW (2006) Prevalence of impaired glucose metabolism and metabolic syndrome in non-diabetic patients with acute post-stroke hyperglycaemia. *Cerebrovasc Dis* 21:1.

McCormick M, Hadley D, McLean JR, Macfarlane JA, Condon B, Muir KW (2010) Randomized, controlled trial of insulin for acute poststroke hyperglycemia. *Ann Neurol* 67:570-8.

Meng X, Fisher M, Shen Q, Sotak CH, Duong TQ (2004) Characterizing the diffusion/perfusion mismatch in experimental focal cerebral ischemia. *Ann Neurol* 55:207-12.

Mhairi Macrae I (1992) New models of focal cerebral ischaemia. *Br J Clin Pharmacol* 34:302-8.

Mies G, Iijima T, Hossmann KA (1993) Correlation between peri-infarct DC shifts and ischaemic neuronal damage in rat. *Neuroreport* 4:709-11.

Minematsu K, Li L, Sotak CH, Davis MA, Fisher M (1992) Reversible focal ischemic injury demonstrated by diffusion-weighted magnetic resonance imaging in rats. *Stroke* 23:1304-10; discussion 10-1.

Moffat BA, Chenevert TL, Hall DE, Rehemtulla A, Ross BD (2005) Continuous arterial spin labeling using a train of adiabatic inversion pulses. *J Magn Reson Imaging* 21:290-6.

Mohanty P, Hamouda W, Garg R, Aljada A, Ghanim H, Dandona P (2000) Glucose challenge stimulates reactive oxygen species (ROS) generation by leucocytes. *J Clin Endocrinol Metab* 85:2970-3.

Molina CA, Saver JL (2005) Extending reperfusion therapy for acute ischemic stroke: emerging pharmacological, mechanical, and imaging strategies. *Stroke* 36:2311-20.

Moreton FC, McCormick M, Muir KW (2007) Insular cortex hypoperfusion and acute phase blood glucose after stroke: a CT perfusion study. *Stroke* 38:407-10.

Moseley ME, Cohen Y, Mintorovitch J, Chileuitt L, Shimizu H, Kucharczyk J, Wendland MF, Weinstein PR (1990a) Early detection of regional cerebral ischemia in cats: comparison of diffusion- and T2-weighted MRI and spectroscopy. *Magn Reson Med* 14:330-46.

Moseley ME, Kucharczyk J, Mintorovitch J, Cohen Y, Kurhanewicz J, Derugin N, Asgari H, Norman D (1990b) Diffusion-weighted MR imaging of acute stroke: correlation with T2-weighted and magnetic susceptibility-enhanced MR imaging in cats. *AJNR Am J Neuroradiol* 11:423-9.

Muir KW (2002) Heterogeneity of stroke pathophysiology and neuroprotective clinical trial design. *Stroke* 33:1545-50.

Muir KW, Santosh C (2005) Imaging of acute stroke and transient ischaemic attack. *J Neurol Neurosurg Psychiatry* 76 Suppl 3:iii19-iii28.

Muir KW, McCormick M, Baird T, Ali M (2011) Prevalence, Predictors and Prognosis of Post-Stroke Hyperglycaemia in Acute Stroke Trials: Individual Patient Data Pooled Analysis from the Virtual International Stroke Trials Archive (VISTA). *Cerebrovascular Diseases Extra* 1:11.

Murakami K, Kondo T, Kawase M, Li Y, Sato S, Chen SF, Chan PH (1998) Mitochondrial susceptibility to oxidative stress exacerbates cerebral infarction that follows permanent focal cerebral ischemia in mutant mice with manganese superoxide dismutase deficiency. *J Neurosci* 18:205-13.

Muralikrishna Adibhatla R, Hatcher JF (2006) Phospholipase A2, reactive oxygen species, and lipid peroxidation in cerebral ischemia. *Free Radic Biol Med* 40:376-87.

Muranyi M, Li PA (2006) Hyperglycemia increases superoxide production in the CA1 pyramidal neurons after global cerebral ischemia. *Neurosci Lett* 393:119-21.

Murros K, Fogelholm R, Kettunen S, Vuorela AL, Valve J (1992) Blood glucose, glycosylated haemoglobin, and outcome of ischemic brain infarction. *J Neurol Sci* 111:59-64.

Namura S, Zhu J, Fink K, Endres M, Srinivasan A, Tomaselli KJ, Yuan J, Moskowitz MA (1998) Activation and cleavage of caspase-3 in apoptosis induced by experimental cerebral ischemia. *J Neurosci* 18:3659-68.

Nedergaard M (1987) Transient focal ischemia in hyperglycemic rats is associated with increased cerebral infarction. *Brain Res* 408:79-85.

Nedergaard M, Diemer NH (1987) Focal ischemia of the rat brain, with special reference to the influence of plasma glucose concentration. *Acta Neuropathol* 73:131-7.

NINDS (1995) Tissue plasminogen activator for acute ischemic stroke. The National Institute of Neurological Disorders and Stroke rt-PA Stroke Study Group. *N Engl J Med* 333:1581-7.

Nishikawa T, Edelstein D, Du XL, Yamagishi S, Matsumura T, Kaneda Y, Yorek MA, Beebe D, Oates PJ, Hammes HP, Giardino I, Brownlee M (2000) Normalizing mitochondrial superoxide production blocks three pathways of hyperglycaemic damage. *Nature* 404:787-90.

Nogawa S, Zhang F, Ross ME, Iadecola C (1997) Cyclo-oxygenase-2 gene expression in neurons contributes to ischemic brain damage. *J Neurosci* 17:2746-55.

O'Collins VE, Macleod MR, Donnan GA, Horky LL, van der Worp BH, Howells DW (2006) 1,026 experimental treatments in acute stroke. *Ann Neurol* 59:467-77.

O'Neill PA, Davies I, Fullerton KJ, Bennett D (1991) Stress hormone and blood glucose response following acute stroke in the elderly. *Stroke* 22:842-7.

Oron-Herman M, Kamari Y, Grossman E, Yeger G, Peleg E, Shabtay Z, Shamiss A, Sharabi Y (2008) Metabolic syndrome: comparison of the two commonly used animal models. *Am J Hypertens* 21:1018-22.

Osborne KA, Shigeno T, Balarsky AM, Ford I, Mcculloch J, Teasdale GM, Graham DI (1987) Quantitative Assessment of Early Brain-Damage in a Rat Model of Focal Cerebral-Ischemia. *Journal of Neurology Neurosurgery and Psychiatry* 50:402-10.

OuYang YB, Mellergard P, Kristian T, Kristianova V, Siesjo BK (1994) Influence of acid-base changes on the intracellular calcium concentration of neurons in primary culture. *Exp Brain Res* 101:265-71.

Pacher P, Beckman JS, Liaudet L (2007) Nitric oxide and peroxynitrite in health and disease. *Physiol Rev* 87:315-424.

Pagliassotti MJ, Shahrokhi KA, Moscarello M (1994) Involvement of liver and skeletal muscle in sucrose-induced insulin resistance: dose-response studies. *Am J Physiol* 266:R1637-44.

Parsons MW, Barber PA, Desmond PM, Baird TA, Darby DG, Byrnes G, Tress BM, Davis SM (2002) Acute hyperglycemia adversely affects stroke outcome: a magnetic resonance imaging and spectroscopy study. *Ann Neurol* 52:20-8.

Parsons MW, Pepper EM, Bateman GA, Wang Y, Levi CR (2007) Identification of the penumbra and infarct core on hyperacute noncontrast and perfusion CT. *Neurology* 68:730-6.

Paxinos G, Watson C. (1998). *The rat brain in stereotaxic coordinates*. 4th ed. London: Academic Press.

Penicaud L, Ferre P, Terretaz J, Kinebanyan MF, Leturque A, Dore E, Girard J, Jeanrenaud B, Picon L (1987) Development of obesity in Zucker rats. Early insulin resistance in muscles but normal sensitivity in white adipose tissue. *Diabetes* 36:626-31.

Phillips MS, Liu Q, Hammond HA, Dugan V, Hey PJ, Caskey CJ, Hess JF (1996) Leptin receptor missense mutation in the fatty Zucker rat. *Nat Genet* 13:18-9.

Quast MJ, Wei J, Huang NC (1995) Nitric oxide synthase inhibitor NG-nitro-L-arginine methyl ester decreases ischemic damage in reversible focal cerebral ischemia in hyperglycemic rats. *Brain Res* 677:204-12.

Quast MJ, Wei J, Huang NC, Brunder DG, Sell SL, Gonzalez JM, Hillman GR, Kent TA (1997) Perfusion deficit parallels exacerbation of cerebral ischemia/reperfusion injury in hyperglycemic rats. *J Cereb Blood Flow Metab* 17:553-9.

Rakieten N, Rakieten ML, Nadkarni MR (1963) Studies on the diabetogenic action of streptozotocin (NSC-37917). *Cancer Chemother Rep* 29:91-8.

Reaven GM, Chang H, Hoffman BB, Azhar S (1989) Resistance to insulin-stimulated glucose uptake in adipocytes isolated from spontaneously hypertensive rats. *Diabetes* 38:1155-60.

Reid E, Graham D, Lopez-Gonzalez MR, Holmes WM, Macrae IM, McCabe C (2012) Penumbra detection using PWI/DWI mismatch MRI in a rat stroke model with and without comorbidity: comparison of methods. *J Cereb Blood Flow Metab*.

Ribo M, Molina CA, Delgado P, Rubiera M, Delgado-Mederos R, Rovira A, Munuera J, Alvarez-Sabin J (2007) Hyperglycemia during ischemia rapidly accelerates brain damage in stroke patients treated with tPA. *J Cereb Blood Flow Metab* 27:1616-22.

Richard Green A, Odergren T, Ashwood T (2003) Animal models of stroke: do they have value for discovering neuroprotective agents? *Trends in Pharmacological Sciences* 24:402-8.

Robertson CA, McCabe C, Gallagher L, Lopez-Gonzalez Mdel R, Holmes WM, Condon B, Muir KW, Santosh C, Macrae IM (2011) Stroke penumbra defined by an MRI-based oxygen challenge technique: 1. Validation using [14C]2-deoxyglucose autoradiography. *J Cereb Blood Flow Metab* 31:1778-87.

Rothwell NJ, Hopkins SJ (1995) Cytokines and the nervous system II: Actions and mechanisms of action. *Trends Neurosci* 18:130-6.

Rothwell PM, Coull AJ, Silver LE, Fairhead JF, Giles MF, Lovelock CE, Redgrave JNE, Bull LM, Welch SJV, Cuthbertson FC, Binney LE, Gutnikov SA, Anslow P,

Banning AP, Mant D, Mehta Z (2005) Population-based study of event-rate, incidence, case fatality, and mortality for all acute vascular events in all arterial territories (Oxford Vascular Study). *The Lancet* 366:1773-83.

Rubino GJ, Young W (1988) Ischemic cortical lesions after permanent occlusion of individual middle cerebral artery branches in rats. *Stroke* 19:870-7.

Russell JC, Proctor SD (2006) Small animal models of cardiovascular disease: tools for the study of the roles of metabolic syndrome, dyslipidemia, and atherosclerosis. *Cardiovasc Pathol* 15:318-30.

Saita K, Chen M, Spratt NJ, Porritt MJ, Liberatore GT, Read SJ, Levi CR, Donnan GA, Ackermann U, Tochon-Danguy HJ, Sachinidis JI, Howells DW (2004) Imaging the ischemic penumbra with 18F-fluoromisonidazole in a rat model of ischemic stroke. *Stroke* 35:975-80.

Samai M, Sharpe MA, Gard PR, Chatterjee PK (2007) Comparison of the effects of the superoxide dismutase mimetics EUK-134 and tempol on paraquat-induced nephrotoxicity. *Free Radic Biol Med* 43:528-34.

Saver JL, Albers GW, Dunn B, Johnston KC, Fisher M (2009) Stroke Therapy Academic Industry Roundtable (STAIR) recommendations for extended window acute stroke therapy trials. *Stroke* 40:2594-600.

Savitz SI, Fisher M (2007) Future of neuroprotection for acute stroke: in the aftermath of the SAINT trials. *Ann Neurol* 61:396-402.

Schaffer JE (2003) Lipotoxicity: when tissues overeat. *Curr Opin Lipidol* 14:281-7.

Schaller B (2005) Prospects for the future: the role of free radicals in the treatment of stroke. *Free Radic Biol Med* 38:411-25.

Schellinger PD, Fiebach JB, Hacke W (2003) Imaging-based decision making in thrombolytic therapy for ischemic stroke: present status. *Stroke* 34:575-83.

Schielke GP, Yang GY, Shivers BD, Betz AL (1998) Reduced ischemic brain injury in interleukin-1 beta converting enzyme-deficient mice. *J Cereb Blood Flow Metab* 18:180-5.

Schilling M, Besselmann M, Leonhard C, Mueller M, Ringelstein EB, Kiefer R (2003) Microglial activation precedes and predominates over macrophage infiltration in transient focal cerebral ischemia: a study in green fluorescent protein transgenic bone marrow chimeric mice. *Exp Neurol* 183:25-33.

Schlaug G, Benfield A, Baird AE, Siewert B, Lovblad KO, Parker RA, Edelman RR, Warach S (1999) The ischemic penumbra: operationally defined by diffusion and perfusion MRI. *Neurology* 53:1528-37.

Scott JF, Robinson GM, French JM, O'Connell JE, Alberti KG, Gray CS (1999) Prevalence of admission hyperglycaemia across clinical subtypes of acute stroke. *Lancet* 353:376-7.

Shen Q, Meng X, Fisher M, Sotak CH, Duong TQ (2003) Pixel-by-pixel spatiotemporal progression of focal ischemia derived using quantitative perfusion and diffusion imaging. *J Cereb Blood Flow Metab* 23:1479-88.

Shimizu-Sasamata M, Bosque-Hamilton P, Huang PL, Moskowitz MA, Lo EH (1998) Attenuated neurotransmitter release and spreading depression-like depolarizations after focal ischemia in mutant mice with disrupted type I nitric oxide synthase gene. *J Neurosci* 18:9564-71.

Sicard KM, Fisher M (2009) Animal models of focal brain ischemia. *Exp Transl Stroke Med* 1:7.

Siemonsen S, Lobel U, Sedlacik J, Forkert ND, Mouridsen K, Ostergaard L, Thomalla G, Fiehler J (2012) Elevated T2-values in MRI of stroke patients shortly after symptom onset do not predict irreversible tissue infarction. *Brain* 135:1981-9.

Siesjo BK, Katsura KI, Kristian T, Li PA, Siesjo P (1996) Molecular mechanisms of acidosis-mediated damage. *Acta Neurochir Suppl* 66:8-14.

Simonsen CZ, Rohl L, Vestergaard-Poulsen P, Gyldensted C, Andersen G, Ostergaard L (2002) Final infarct size after acute stroke: prediction with flow heterogeneity. *Radiology* 225:269-75.

Simonson TM, Magnotta VA, Ehrhardt JC, Crosby DL, Fisher DJ, Yuh WT (1996) Echo-planar FLAIR imaging in evaluation of intracranial lesions. *Radiographics* 16:575-84.

Slivka AP (1991) Hypertension and hyperglycemia in experimental stroke. *Brain Res* 562:66-70.

Soussain C, Muldoon LL, Varallyay C, Jahnke K, DePaula L, Neuwelt EA (2007) Characterization and magnetic resonance imaging of a rat model of human B-cell central nervous system lymphoma. *Clin Cancer Res* 13:2504-11.

STAIR (1999) Recommendations for standards regarding preclinical neuroprotective and restorative drug development. *Stroke* 30:2752-8.

Strahorn P, Graham D, Charchar FJ, Sattar N, McBride MW, Dominiczak AF (2005) Genetic determinants of metabolic syndrome components in the stroke-prone spontaneously hypertensive rat. *J Hypertens* 23:2179-86.

Sudlow CL, Warlow CP (1997) Comparable studies of the incidence of stroke and its pathological types: results from an international collaboration. International Stroke Incidence Collaboration. *Stroke* 28:491-9.

Swanson RA, Morton MT, Tsao-Wu G, Savalos RA, Davidson C, Sharp FR (1990) A semiautomated method for measuring brain infarct volume. *J Cereb Blood Flow Metab* 10:290-3.

Symon L, Pasztor E, Branston NM (1974) The distribution and density of reduced cerebral blood flow following acute middle cerebral artery occlusion: an experimental study by the technique of hydrogen clearance in baboons. *Stroke* 5:355-64.

Szkudelski T (2001) The mechanism of alloxan and streptozotocin action in B cells of the rat pancreas. *Physiol Res* 50:537-46.

Takaya K, Ogawa Y, Isse N, Okazaki T, Satoh N, Masuzaki H, Mori K, Tamura N, Hosoda K, Nakao K (1996) Molecular cloning of rat leptin receptor isoform complementary DNAs--identification of a missense mutation in Zucker fatty (fa/fa) rats. *Biochem Biophys Res Commun* 225:75-83.

Tan JC, Dillon WP, Liu S, Adler F, Smith WS, Wintermark M (2007) Systematic comparison of perfusion-CT and CT-angiography in acute stroke patients. *Ann Neurol* 61:533-43.

Tanne D, Kasner SE, Demchuk AM, Koren-Morag N, Hanson S, Grond M, Levine SR (2002) Markers of increased risk of intracerebral hemorrhage after intravenous

recombinant tissue plasminogen activator therapy for acute ischemic stroke in clinical practice: the Multicenter rt-PA Stroke Survey. *Circulation* 105:1679-85.

Taoka T, Fujioka M, Matsuo Y, Notoya M, Iwasaki S, Fukusumi A, Nakagawa H, Sakamoto M, Kichikawa K, Ohishi H (2004) Signal characteristics of FLAIR related to water content: comparison with conventional spin echo imaging in infarcted rat brain. *Magn Reson Imaging* 22:221-7.

Taylor JM, Crack PJ (2004) Impact of oxidative stress on neuronal survival. *Clin Exp Pharmacol Physiol* 31:397-406.

Terent A, Asplund K, Farahmand B, Henriksson KM, Norrving B, Stegmayr B, Wester PO, Asberg KH, Asberg S (2009) Stroke unit care revisited: who benefits the most? A cohort study of 105,043 patients in Riks-Stroke, the Swedish Stroke Register. *J Neurol Neurosurg Psychiatry* 80:881-7.

Thomassen L, Brainin M, Demarin V, Grond M, Toni D, Venables GS (2003) Acute stroke treatment in Europe: a questionnaire-based survey on behalf of the EFNS Task Force on acute neurological stroke care. *Eur J Neurol* 10:199-204.

Tomlinson DR, Gardiner NJ (2008) Diabetic neuropathies: components of etiology. *J Peripher Nerv Syst* 13:112-21.

Tosaka M, Hashiba Y, Saito N, Imai H, Shimizu T, Sasaki T (2002) Contractile responses to reactive oxygen species in the canine basilar artery in vitro: selective inhibitory effect of MCI-186, a new hydroxyl radical scavenger. *Acta Neurochir (Wien)* 144:1305-10; discussion 10.

Tracey F, Stout RW (1994) Hyperglycemia in the acute phase of stroke and stress response. *Stroke* 25:524-5.

Traystman RJ, Kirsch JR, Koehler RC (1991) Oxygen radical mechanisms of brain injury following ischemia and reperfusion. *J Appl Physiol* 71:1185-95.

van den Berghe G, Wouters P, Weekers F, Verwaest C, Bruyninckx F, Schetz M, Vlasselaers D, Ferdinande P, Lauwers P, Bouillon R (2001) Intensive insulin therapy in the critically ill patients. *N Engl J Med* 345:1359-67.

Van den Berghe G, Wilmer A, Hermans G, Meersseman W, Wouters PJ, Milants I, Van Wijngaerden E, Bobbaers H, Bouillon R (2006) Intensive insulin therapy in the medical ICU. *N Engl J Med* 354:449-61.

van der Worp HB, Claus SP, Bar PR, Ramos LM, Algra A, van Gijn J, Kappelle LJ (2001) Reproducibility of measurements of cerebral infarct volume on CT scans. *Stroke* 32:424-30.

van der Worp HB, de Haan P, Morrema E, Kalkman CJ (2005) Methodological quality of animal studies on neuroprotection in focal cerebral ischaemia. *J Neurol* 252:1108-14.

van Everdingen KJ, van der Grond J, Kappelle LJ, Ramos LM, Mali WP (1998) Diffusion-weighted magnetic resonance imaging in acute stroke. *Stroke* 29:1783-90.

Verheul HB, Berkelbach van der Sprenkel JW, Tulleken CA, Tamminga KS, Nicolay K (1992) Temporal evolution of focal cerebral ischemia in the rat assessed by T2-weighted and diffusion-weighted magnetic resonance imaging. *Brain Topogr* 5:171-6.

Wagner KR, Kleinholz M, de Courten-Myers GM, Myers RE (1992) Hyperglycemic versus normoglycemic stroke: topography of brain metabolites, intracellular pH, and infarct size. *J Cereb Blood Flow Metab* 12:213-22.

Wang P, Chen H, Qin H, Sankarapandi S, Becher MW, Wong PC, Zweier JL (1998) Overexpression of human copper, zinc-superoxide dismutase (SOD1) prevents postischemic injury. *Proc Natl Acad Sci U S A* 95:4556-60.

Warlow C, Sudlow C, Dennis M, Wardlaw J, Sandercock P (2003) Stroke. *Lancet* 362:1211-24.

Warner DS, Todd MM, Dexter F, Ludwig P, McAllister AM (1995) Temporal thresholds for hyperglycemia-augmented ischemic brain damage in rats. *Stroke* 26:655-60.

Wei J, Huang NC, Quast MJ (1997) Hydroxyl radical formation in hyperglycemic rats during middle cerebral artery occlusion/reperfusion. *Free Radic Biol Med* 23:986-95.

Wei J, Quast MJ (1998) Effect of nitric oxide synthase inhibitor on a hyperglycemic rat model of reversible focal ischemia: detection of excitatory amino acids release and hydroxyl radical formation. *Brain Res* 791:146-56.

Wei J, Cohen DM, Quast MJ (2003) Effects of 2-deoxy-d-glucose on focal cerebral ischemia in hyperglycemic rats. *J Cereb Blood Flow Metab* 23:556-64.

Wei JN, Wang QC, Liu GF, Ezell EL, Quast MJ (2004) Reduction of brain injury by antithrombotic agent acutobin after middle cerebral artery ischemia/reperfusion in the hyperglycemic rat. *Brain Res* 1022:234-43.

Weir CJ, Murray GD, Dyker AG, Lees KR (1997) Is hyperglycaemia an independent predictor of poor outcome after acute stroke? Results of a long-term follow up study. *BMJ* 314:1303-6.

Williams LS, Rotich J, Qi R, Fineberg N, Espay A, Bruno A, Fineberg SE, Tierney WR (2002) Effects of admission hyperglycemia on mortality and costs in acute ischemic stroke. *Neurology* 59:67-71.

Yamasaki Y, Matsuo Y, Matsuura N, Onodera H, Itoyama Y, Kogure K (1995) Transient increase of cytokine-induced neutrophil chemoattractant, a member of the interleukin-8 family, in ischemic brain areas after focal ischemia in rats. *Stroke* 26:318-22; discussion 22-3.

Yonas H, Jungreis C (1995) Xenon CT cerebral blood flow: past, present, and future. *AJNR Am J Neuroradiol* 16:219-20.

Yoneda Y, Tokui K, Hanihara T, Kitagaki H, Tabuchi M, Mori E (1999) Diffusion-weighted magnetic resonance imaging: detection of ischemic injury 39 minutes after onset in a stroke patient. *Ann Neurol* 45:794-7.

Yura S, Sako K, Aizawa S, Suzuki N, Yonemasu Y, Kojima M (1986) [The effect of hyperglycemia on ischemic brain damage: relevance to the local cerebral blood flow]. *No To Shinkei* 38:1117-25.

Zaman AG, Helft G, Worthley SG, Badimon JJ (2000) The role of plaque rupture and thrombosis in coronary artery disease. *Atherosclerosis* 149:251-66.

Zaro-Weber O, Moeller-Hartmann W, Heiss WD, Sobesky J (2009) The performance of MRI-based cerebral blood flow measurements in acute and subacute stroke compared with 15O-water positron emission tomography: identification of penumbral flow. *Stroke* 40:2413-21.

Zasslow MA, Pearl RG, Shuer LM, Steinberg GK, Lieberson RE, Larson CP, Jr. (1989) Hyperglycemia decreases acute neuronal ischemic changes after middle cerebral artery occlusion in cats. *Stroke* 20:519-23.

Zemel MB, Sowers JR, Shehin S, Walsh MF, Levy J (1990) Impaired calcium metabolism associated with hypertension in Zucker obese rats. *Metabolism* 39:704-8.

Zemel MB, Peuler JD, Sowers JR, Simpson L (1992) Hypertension in insulin-resistant Zucker obese rats is independent of sympathetic neural support. *Am J Physiol* 262:E368-71.

Zhang ZG, Chopp M, Zaloga C, Pollock JS, Forstermann U (1993) Cerebral endothelial nitric oxide synthase expression after focal cerebral ischemia in rats. *Stroke* 24:2016-21; discussion 21-2.

Zhou YP, Grill V (1995) Long term exposure to fatty acids and ketones inhibits B-cell functions in human pancreatic islets of Langerhans. *J Clin Endocrinol Metab* 80:1584-90.

Zhu CZ, Auer RN (2004) Optimal blood glucose levels while using insulin to minimize the size of infarction in focal cerebral ischemia. *J Neurosurg* 101:664-8.

Zucker LM, Zucker TF (1961) Fatty—a new mutation in the rat. *Journal of Heredity* 52:4.